The Seismic Structure Under the Central Midland Valley from Refraction Measurements

By

MUSTAFA AMER SOLA

B.Sc. University of Libya, 1970

M.Phil. University of East Anglia, 1974

Thesis submitted in fulfilment of the degree of Doctor of Philosophy (by research) in the Faculty of Science, Geology Department, Glasgow University.

MAY 1985

CONTENTS

CONTENTS

CONTENTS

FIGURES

TABLES

ACKNOWLEDGEMENTS

I wish to record my thanks to my Supervisor, Dr. D. W. Powell, for his guidance, continued advice and help during the execution of this project.

Thanks to the head of the Geology Department, Professor B. E. Leake, with whose permission this work was carried out. I am grateful also to Dr. J. Hall for the help and useful discussion at various stages of the work, and Mr. B. Doody and Mr. K. Davidson.

Thanks to Mr. G. Gordon for building the FM recorders and maintenance.

Additional help and assistance in the field are also supplied by Mr. R. Morrison and his staff, particularly Messrs. R. T. Cumberland, E. Spires, J. Gallagher, K. Roberts, D. MacLean and R. MacDonald.

Thanks also goes to Global Seismology Unit of the I.G.S. for their assistance and use of replay equipment and making the field tapes of LOWNET available.

I am grateful to the quarry owners and managers of Tamsloup, Kaimes, Craigpark, Medrox, Cairngryffe, Douglasmuir, Loanhead and the Headless Cross Open Cast. The N.C.B. site engineer, Mr. D. Todd; Rechie Ltd. Blasting Co. for their assistance and patience and all the land owners and tenants for granting access to their land.

I also thank Miss D. McCracken and Miss F. Brennan for their accurate efficient typing of this thesis.

I thank all members of my family for their moral support.

The financial support of the Libyan people is well appreciated.

SUMMARY

The geology of the Midland Valley is outlined with special reference to the Central Coalfield and its sub-Carboniferous foundation within which, previous interpretations propose, lies a dense, magnetic, body near Bathgate. Seismic velocity structures within (LOWNET), across (LISPB) and south of (SUSP) the Midland Valley are shown together with existing data on velocities in local rocks of Carboniferous age. The purpose of the present seismic refraction study is defined and its reliance on commercial quarry operations and their suitability are discussed. The recording playback systems developed in the Department during this survey, their utilisation and accuracy in determining travel times are described.

The measured travel time profiles are used first to derive velocity depth profiles and correlated with geological formations (Carboniferous to Lower Palaeozoic) known at outcrop within the region. An unseen crystalline basement is deduced probable at 4 to 5 km depth. This is the a_o LISPB refractor. Its velocity and associated delays are assessed using all available data. Ray traced models have been used both across Bathgate and on parts of the LISPB line where steep structures are shown to contravene TIME-TERM/PLUS-MINUS assumptions. The structure on a_o is described and discussed in terms of two delay components with different velocities attributed to post-Lower Old Red Sandstone and pre-Upper Old Red Sandstone strata. The seismic delays on a_o are used to 'strip' the Bouguer gravity to a Regional Gravity map from which further conclusions are drawn.

The data tables, cross-sections with reduced T-X graphs and the geological maps showing the recording sites, with the reduced record sections are included in the Appendices.

CHAPTER I

INTRODUCTION (GEOLOGY OF THE MIDLAND VALLEY AND PREVIOUS GEOPHYSICAL WORK)

1.1 Introduction

The relatively lowland region between the Grampian Highlands and the Southern Uplands is physiographically the MIDLAND VALLEY.

Geologically it is an 80 km wide graben-like structure between north east trending boundary faults (Highland Boundary and Southern Upland Faults).

Within it the principal outcrops are of Carboniferous and Old Red Sandstone strata. Beyond it Dalradian and Lower Palaeozoic rocks dominate. (Figure 1.1).

The Upper Palaeozoic sediments and volcanics within the valley range up to several kilometres in thickness. There are, on the other hand, Silurian inliers, horsts and/or anticlines towards the Southern Upland Faults margins. Ordovician rocks outcrop along the Highland Boundary Fault within the Highland Border series and towards the Southern Upland Fault near Girvan. In the latter area, beneath a mid-Ordovician unconformity, these rocks are members of an ophiolite suite. Crystalline rocks also occur as (1) minor post Lower Old Red Sandstone intrusions (2) a Lower Old Red Sandstone granodiorite pluton (3) clasts in Palaeozoic conglomerates and Upper Palaeozoic volcanic vents.

A summary of previous geophysical work, gravity and magnetic field interpretations is presented, along with results of the seismological studies in the Midland Valley.

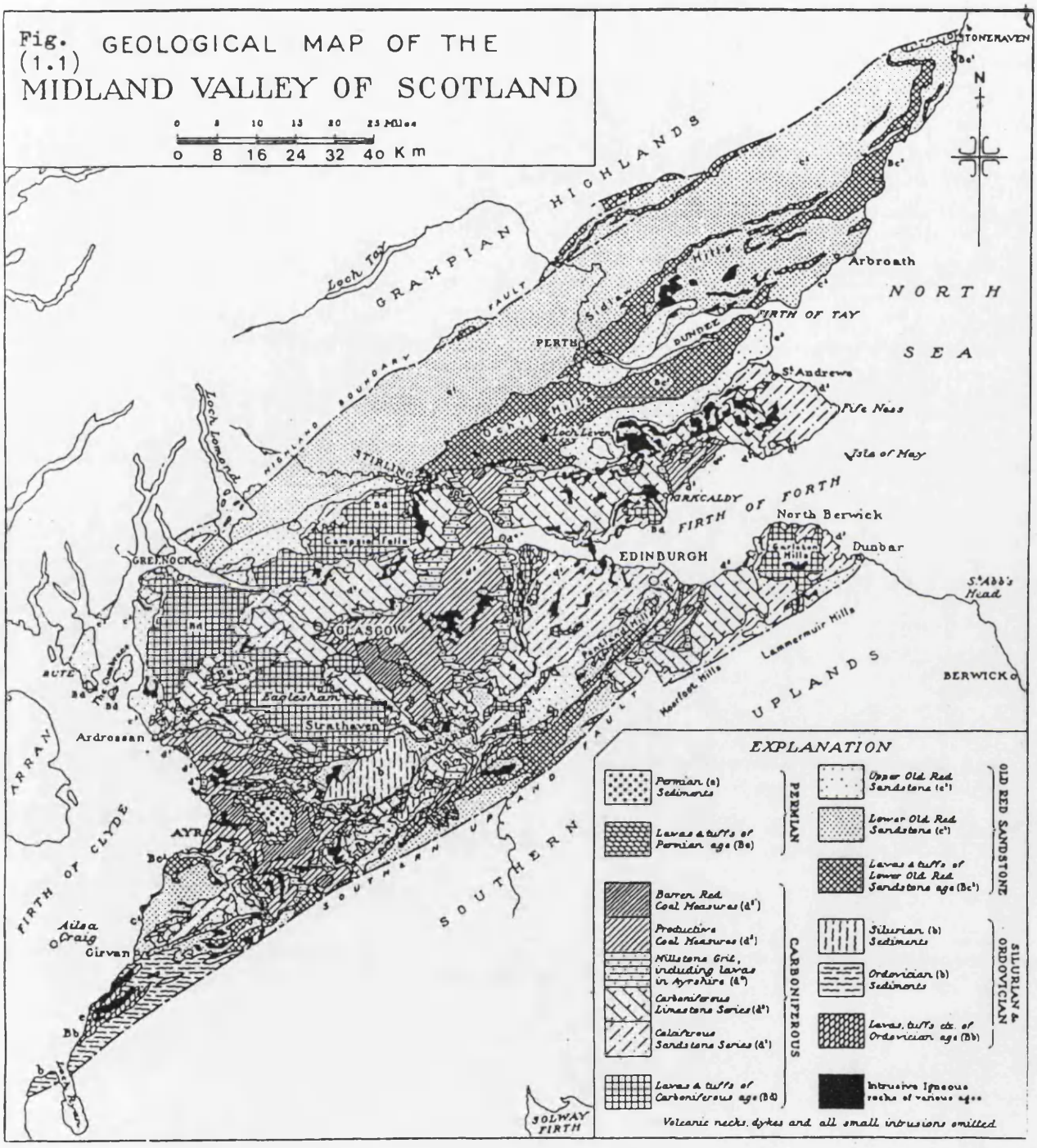

(After MacGregor and MacGregor, 1948)

1.2. Geological Succession (Table 1.1)

To the tabulation of the succession following as in MacGregor and MacGregor (1948) have been added maximum formation thicknessess and physical properties. More information on thicknessess is given in this chapter and also on geological sections in Appendix 2. Seismic velocities are detailed in CH. 3.

The following subsections of 1.2 outline, in stratigraphic sequence, those aspects of the geology which bear on the problem studied in this thesis.

1.2.1 Quaternary Deposits

These are thickest, about 100 m, as sands and gravels filling former river channels. One follows the Lower Forth and deposits of this kind may contribute to the delay times associated with some of the shotpoint sites (e.g. Methil). None of the land shot/receiver points are sited on such a channel.

Boulder clay is the most widespread and the most consolidated of these deposits. Its thickness rarely exceeds 10 m i.e. differential delays due to it are unlikely to exceed 0.01 sec.

Peat occurs in several areas e.g. south west of Falkirk towards Cumbernauld. Such an area has been avoided for seismic measurement because of the high background noise levels encountered on it.

1.2.2 Tertiary Dykes

North/north west trending dolerites, typically 10 m wide dykes found only to the west of the main area studied.

ERA	SYSTEM	DIVISION LITHOSTRATIGRAPHICS				MAXIMUM THICKNESS (metre)	PHYSICAL PROPERTIES (see esp. fig. 3.5)	CONTEMPORANEOUS IGNEOUS	INTRUSIVE IGNEOUS ROCKS	LITHOLOGIES
Quaternary	Recent + Pleistocene	Unconformity				206	G = 2.00			peat, sand, gravel, boulder clay
Tertiary									dolerite dykes	dykes, granite dolerite
Upper Palaeozoic	Permian	Mauchline sandstone			e	750	G = 2.44 - 2.68 v = 3.00	lavas and tuffs	volcanic necks and plugs	sandstone, basal volcanics
	Carboniferous	Unconformity								
		Coal Measures	Upper coal measures		dc3	1050	G(sed) = 2.54 V = 3.50 - 4.00 G(lava) = 2.72 V = 4.50 - 5.00	lavas and tuffs (local) (basalts) lavas (widespread)	some alkaline basic sills, volcanic necks, plugs, dykes and sills of basaltic and trachytic type	sandstone, mudstone, siltstone, coals marine limestone, ironstone, seatclays, shales, cementstone, cornstone, lavas and tuffs
			Middle coal measures		dc2					
			Lower coal measures		dc1					
		Millstone Grit Series	Passage group		dMc	350				
			Upper Limestone group		dM2	600				
			Limestone coal group		dM1	550				
		Carboniferous Limestone series	Lower Limestone group		dL4	230				
			Calciferous sandstone measures	U. oilshale Gr.	dL3	850				
				L. oilshale Gr.	dL2	1411				
				Cementstone Gr.	dL1	1100				
	Old Red Sandstone	Upper Old Red Sandstone			c^3	1000	G = 2.42			conglomerates, sandstone, marls, cornstone
		Unconformity								
		Lower Old Red Sandstone	Strathmore group Garvock group Arbuthnott group Crawton group Dunnottar group Stonehaven group		c^1	? 9000	G(sed) = 2.50 G(lava) = 2.66 V = 5.00 - 5.30	lavas (andesite)	volcanic necks, sills and major plutons	conglomerates, sandstone, mudstone, braccia siltstone, shales, agglomerates, lavas, basalts, andesites lavas
		Unconformity								
Lower Palaeozoic	Silurian	Wenlock series Llandovery series			b^{5-6}	>2000	G = 2.72 (sed. and volc.) V = 5.60 - 6.00	Spilitic lavas and tuffs	serpentine gabbro	greywackes, shales, mudstone, red sandstone, conglomerate, thin limestone cherts
	Ordovician	Ashgill series Caradoc series Llandeilo series			b^{1-4}					
		Unconformity								
		Arenig series								
		Unconformity								
Presumed Pre-Cambrian		Metamorphic crystalline rocks underlying the Midland Valley					G = 2.80 - 2.90 V = 6.40			

Table (1.1) Geological succession, rock type, thicknesses and relevant physical properties. G = density ($gmcm^{-3}$) V = P-wave velocity (kms^{-1})

1.2.3 Permian

About 600 or 700 m of sandstone and basalt in the Mauchline Basin lying south west of the area studied.

1.2.4 Permo-Carboniferous Sills and Dykes (Figure 1.2)

The most prominent exposures in the Bathgate - Harthill area are of quartz-dolerite sills which are up to 150 m thickness. They are extensively quarried and their main significance for this study has been in determining the seismic source sites available (Tamsloup, Kaimes, Craigpark, Cairney Hill, lavas, Sandstone conglomerate, coal, felsite, Lower Old Red Sandstone). The dykes, 20-30 m wide, form the transgressive links between sills at different horizons and presumably represent feaders.

These connections, principally seen west of Bathgate, suggest at least the possibility of a deeper, larger intrusive particularly in that area.

At shallow depths, within the Carboniferous sediments, it is unlikely that the dolerite sills are thick enough to affect the velocity of transmission of seismic waves in the 10-30 CPS waveband. (See further CH. 3).

1.2.5 Carboniferous (Figure 1.3)

The Carboniferous strata represent the principal screen below which lies the target of these investigations. Most of the recording sites and many of the source sites necessarily lie on its outcrop. The screening effect is a variable one with thickness and lithology contributing. Lateral depositional changes are as important as those variations imposed later by structure.

Above the HURLET or MAIN LIMESTONE which is widely correlated, thicknesses are well established from mining information and litho-logical variations are on a scale and of a type which is not resolved by the seismic refraction measurements. Below the Hurlet limestone

Fig. (1.2)

(After MacGregor and MacGregor, 1948)

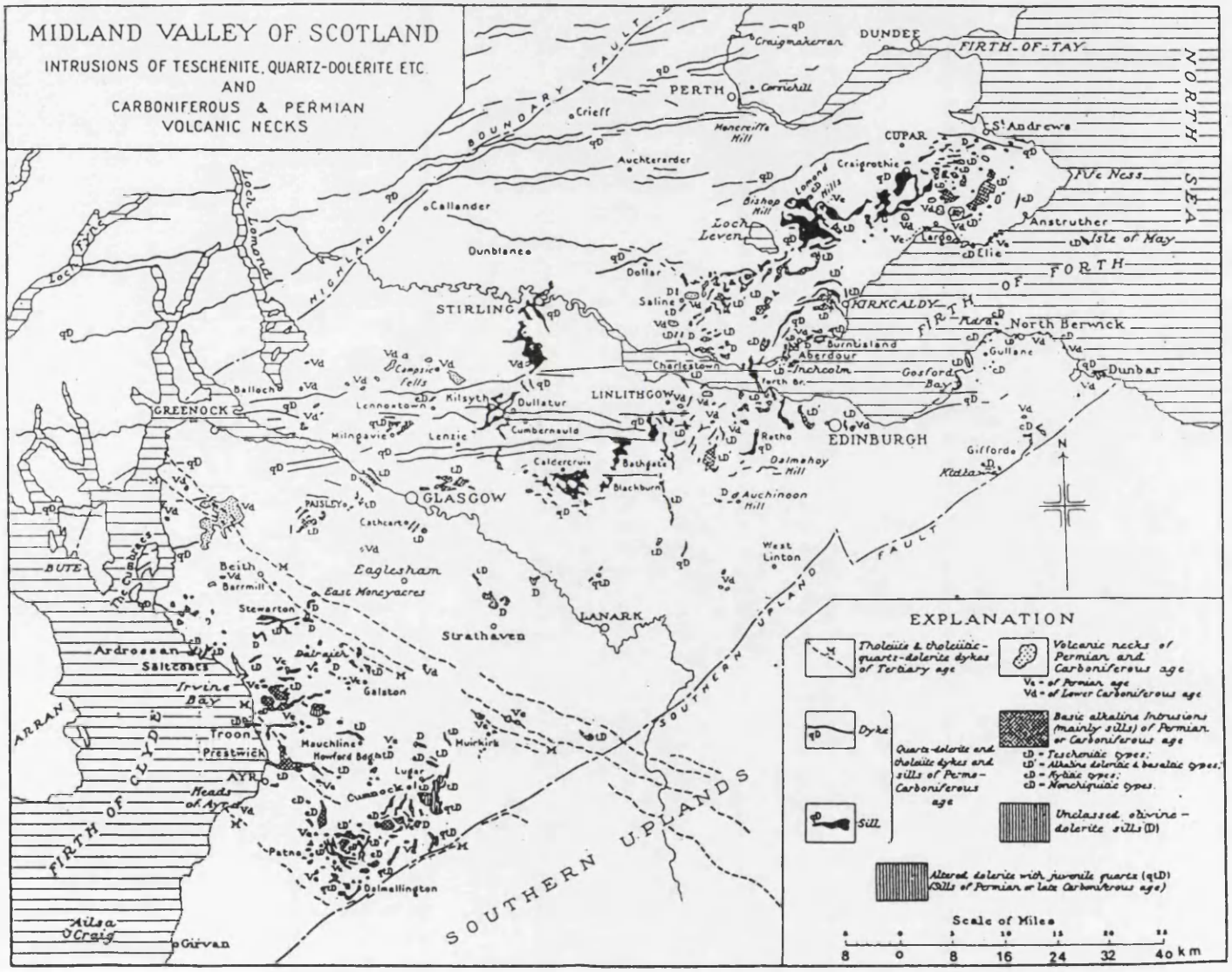

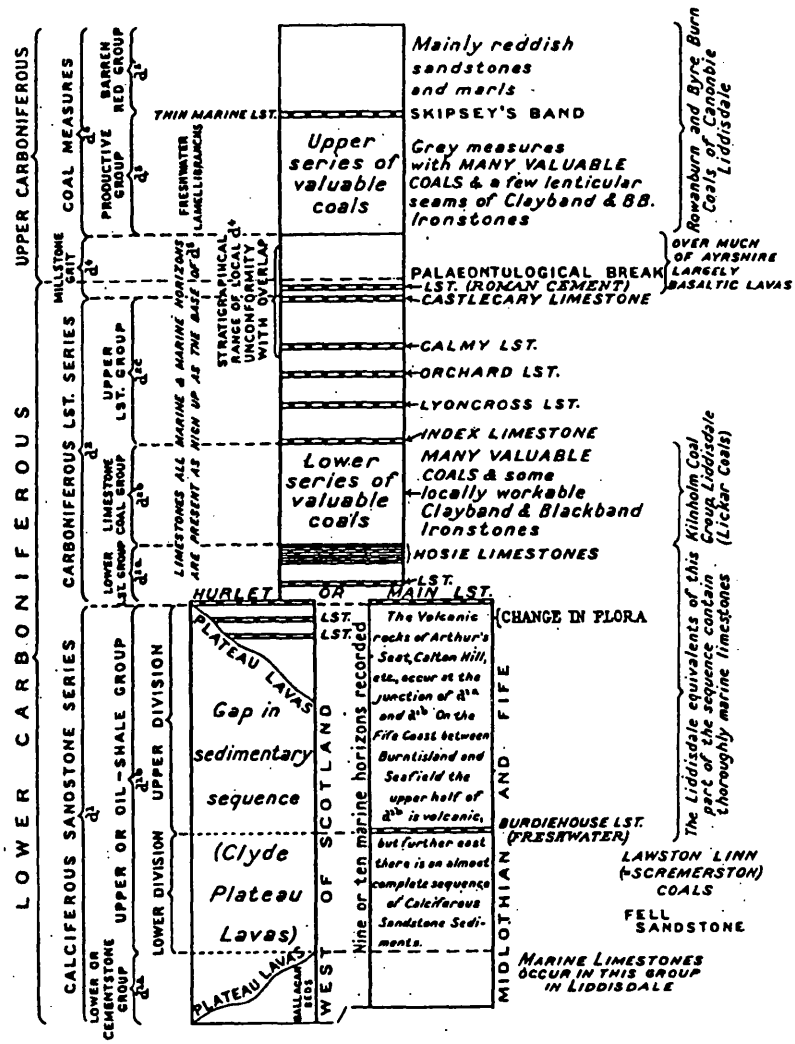

Fig. (1.3) Diagram showing general succession in the Carboniferous of the Midland Valley with subdivision and principal index horizons. (After MacGregor and MacGregor, 1948)

thickness information is relatively sparse and lateral changes of seismic significance are more important, especially the presence or absence of basalt lavas. (Fig. 1.3).

ABOVE THE HURLET

Stratigraphic and economic significance is attached to particular thin beds (limestones, marine bands, coals, ironstones) but shale and sandstone are dominant in thickness. Individual beds of even those dominant lithologies are rarely more than a few metres thick. Only gross physical property estimates are of significance in interpreting seismic travel or gravity effects.

The thickness variation picture of this group of rocks (Fig. 1.4) which shows deposition variation in thickness is primarily controlled by structure. Their preserved thickness is greatest in the Central Coalfield and Fife - Midlothian synclines (in so far as the latter are connected under the Forth) and the least on the intervening anticline where they are eroded completely south of the Forth (Fig. 1.1). The east - west Ochil Fault truncates the structures to the north. To the south the limit is more irregular due to the fold-fault structures parallel with the southern Uplands Fault. Most important of these, as far as this thesis is concerned, is the Pentland Fault near which the Carboniferous strata are strongly folded (Fig. 1.5B).

Lateral variations in succession are mainly thickness changes as measured between marker horizons rather than facies changes. There are some localised developments of volcanic rocks e.g. (Fig. 1.6). In so far as these are ashes, tuffs, agglomerates, they do not introduce contrasting velocity/density elements, (CH. 3 and Spilmersford Borehole Data). Where they are lavas then, as pointed out in connection with transmission by sills, a fairly continuous sequence of well over 200 m

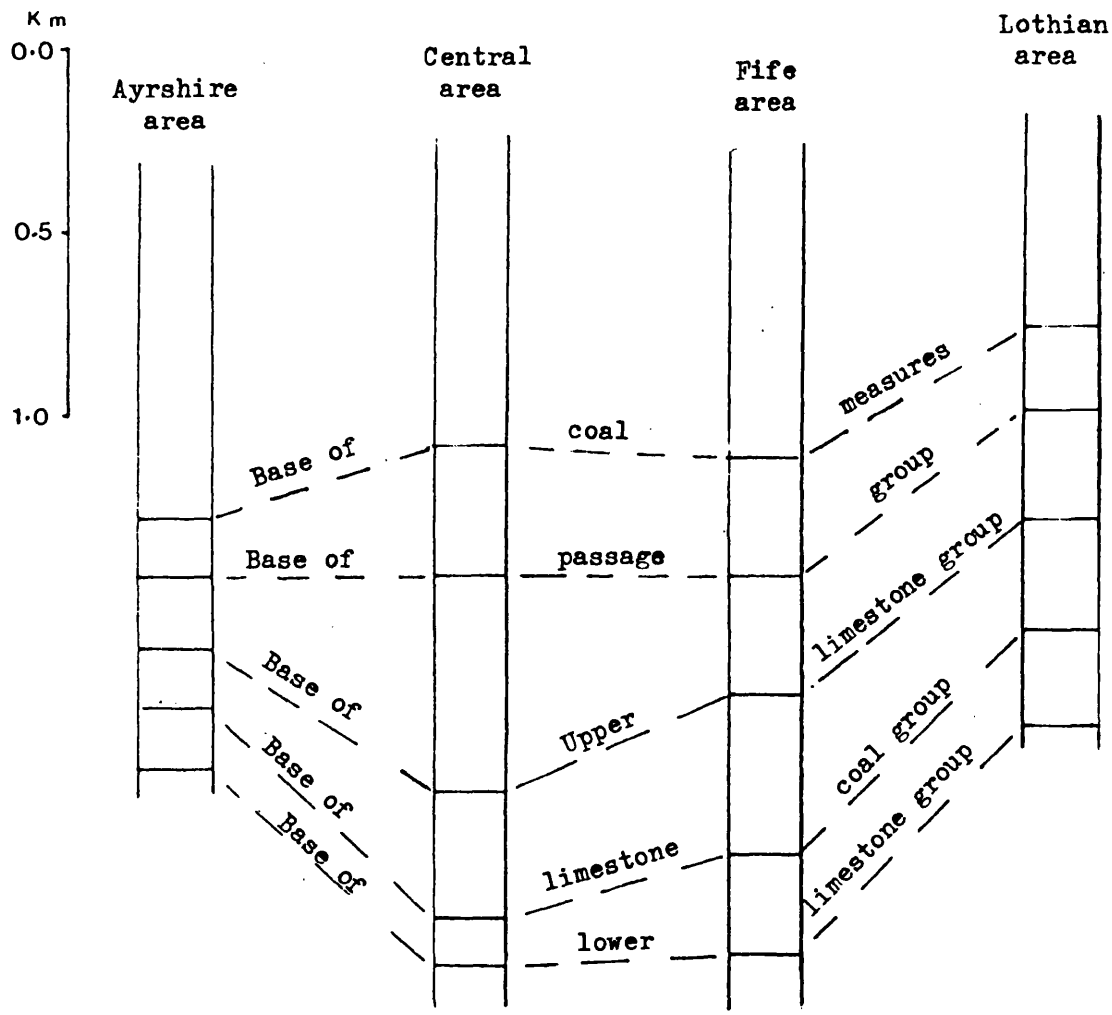

Fig. (1.4) Comparative vertical sections of the Carboniferous above the Hurlet limestone.

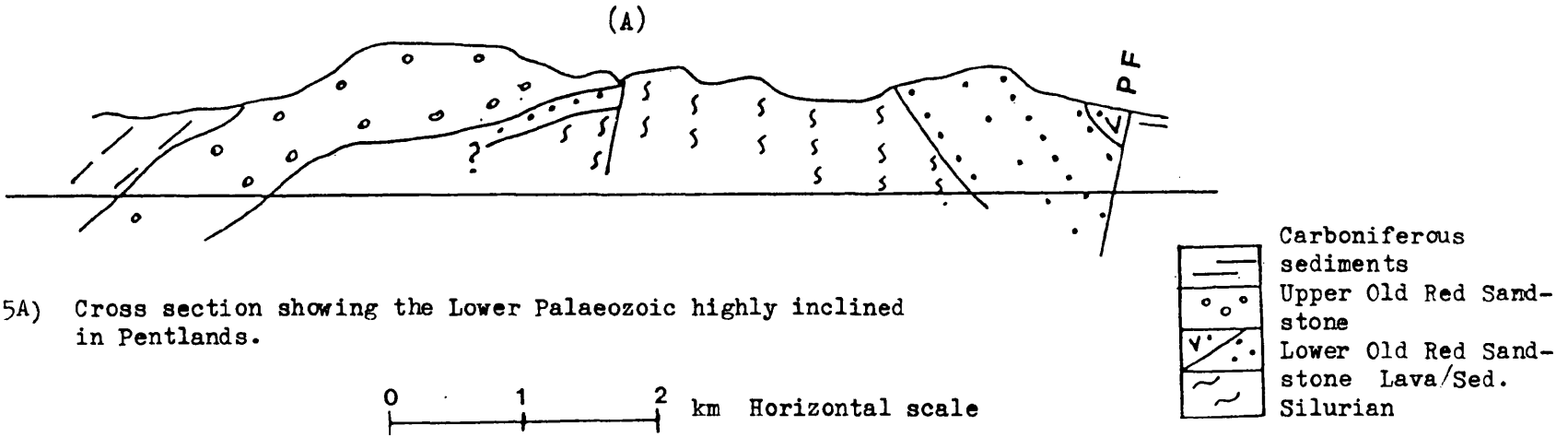

Fig.(1.5A) Cross section showing the Lower Palaeozoic highly inclined in Pentlands.

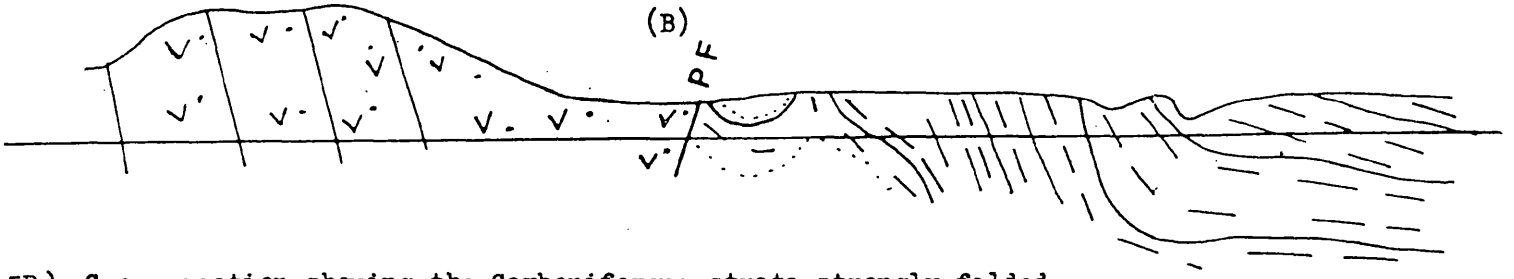

Fig.(1.5B) Cross section showing the Carboniferous strata strongly folded. (After IGS)

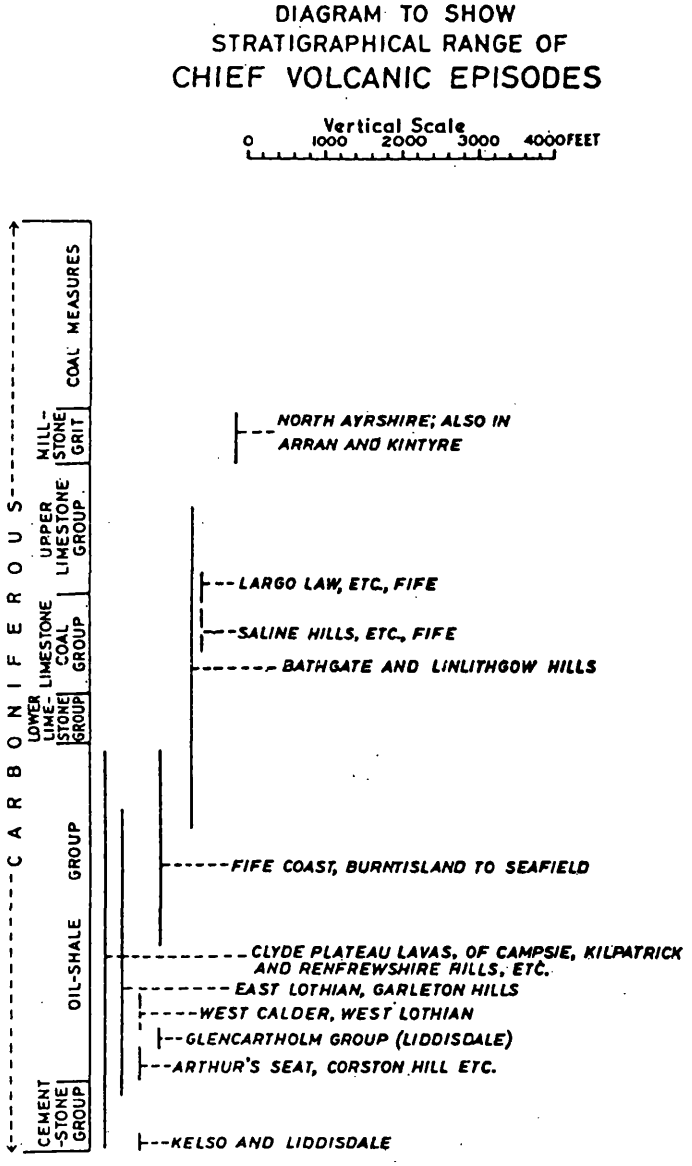

Fig. (1.6) Diagram showing stratigraphical range of chief volcanic episodes in the carboniferous of the Midland Valley and Southern Uplands.

(MacGregor and MacGregor, 1948)

would be necessary for seismic resolution (see CH. 3). The Bathgate lavas at outcrop in the Carboniferous Limestone series are not that thick. (Fig. 1.7 and 1.8B).

BELOW THE HURLET

The underlying Calciferous Sandstone Series is laterally and vertically more variable. This is mainly due to the great thickness of lavas in the west and the extent to which they broke up the area of deposition into several basins. The major change, from west to east across the Midland Valley, is that the Clyde Plateau lavas (consisting of up to 1 km of olivine-basalts) are completely replaced by the Oil-shale Groups of the Lothians (consisting of over 2 km of sandstone, shale and generally ashy volcanics). (Fig. 1.3 and 1.7).

The Clyde Plateau lavas have been proved by boring at Slamannan, Anderson (1963) to continue eastward from their outcrop beneath the Central coalfield basin to join with the Bathgate Hills volcanic rocks which are mainly younger (Fig. 1.8). Their combined thickness is about 1 km.

In the West Calder borehole, SSE of Bathgate, 850 m of oil-shale facies occurs with ashy volcanics but virtually no lavas.

To the north-east in Fife the Calciferous Sandstone and shale with thin lavas and tuffs.

The Calciferous Sandstone measures rest conformably upon the Upper Old Red Sandstone which has always presented a stratigraphic problem. Calcareous cementstones characterise carboniferous; whereas cornstones characterise Upper Old Red Sandstone. It is possible that at least some of the rocks at present mapped as Upper Old Red Sandstone are of Carboniferous age (Francis in Craig, 1983).

Geophysically this is unimportant since the physical properties

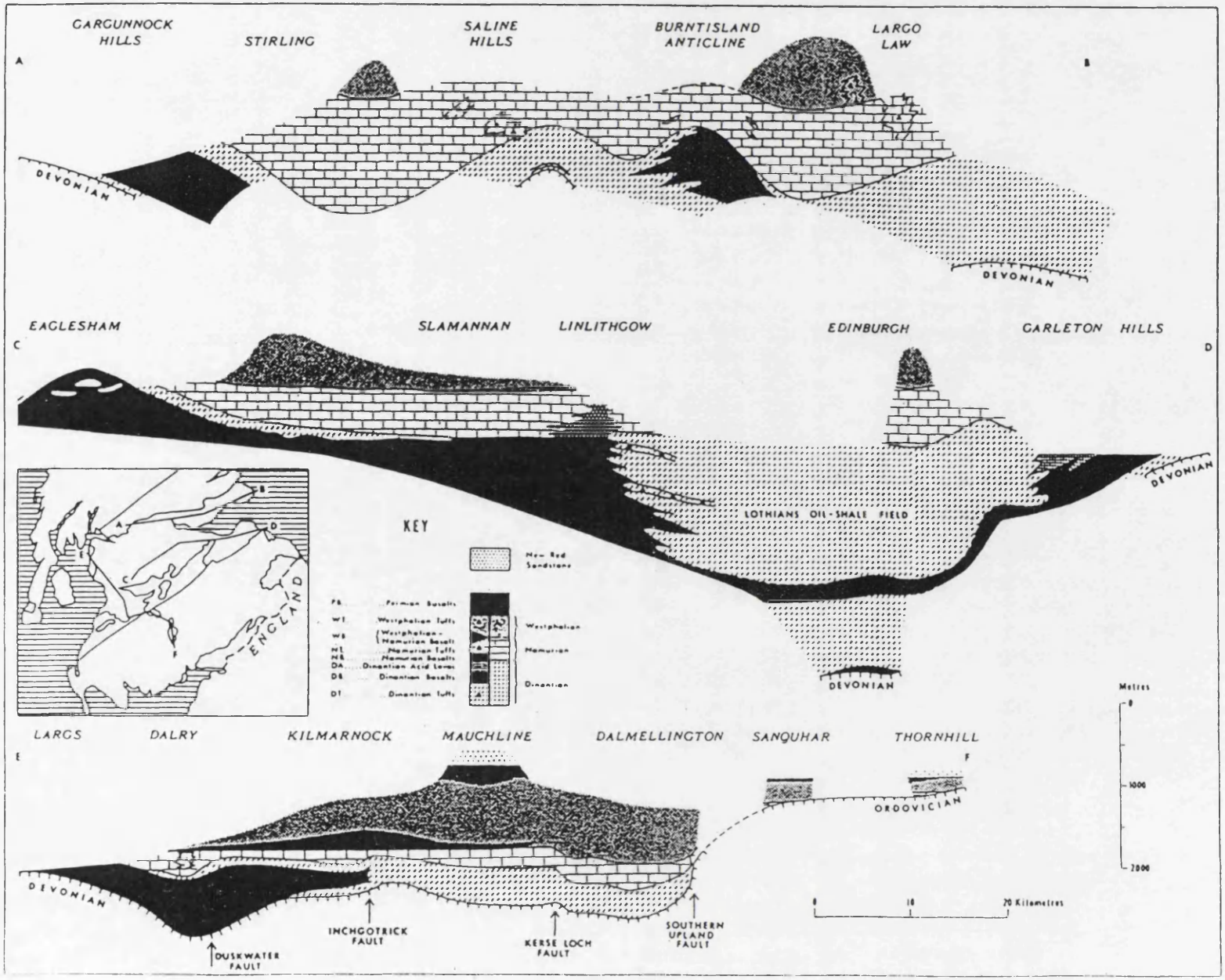

Fig. (1.7)

Horizontal section along the Midland Valley to show the stratigraphical position of the principal lavas and tuffs.

(Francis, 1983)

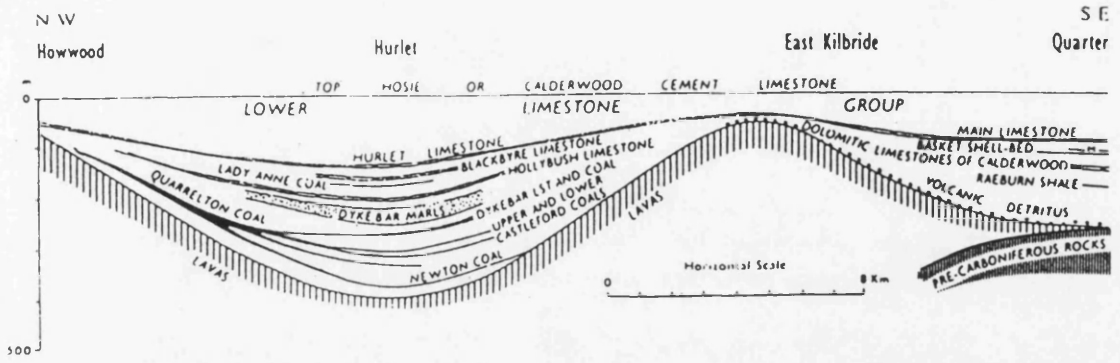

Fig (1.8A) Horizontal section across the southern part of the Central coalfield basin.

(Francis, 1983)

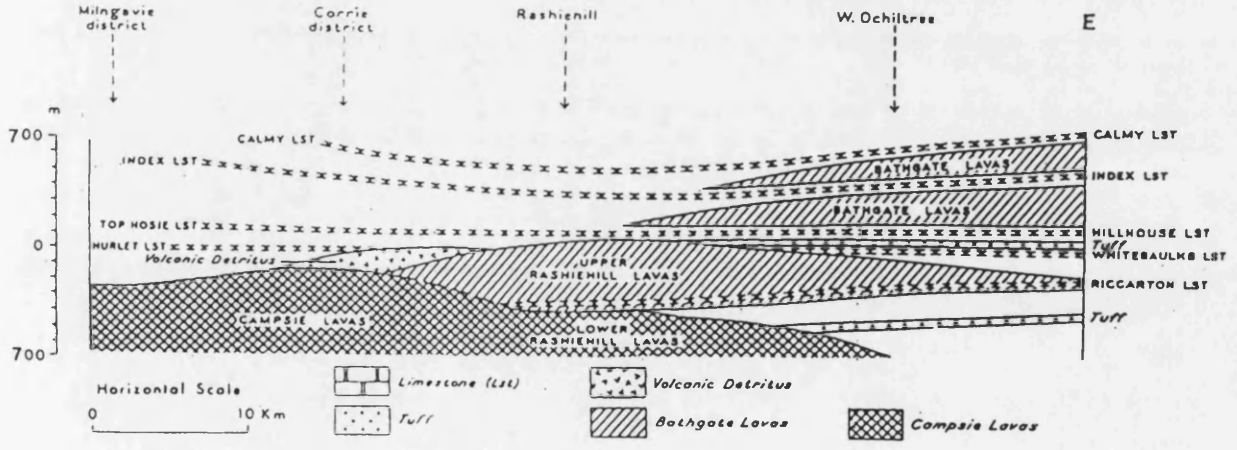

Fig. (1.18B) Horizontal section to show relationship between lavas of Clyde Plateau and of Bathgate Hills.

(Anderson, 1963, Fig. 3)

of both groups should be similar. At present the velocity of Upper Old Red Sandstone has to be judged from its densities and hence the porosities, (CH. 3).

1.2.6 Upper Old Red Sandstone

Forms two trending belts of outcrops within the Midland Valley, (Map 1.1). It consists of sandstone, marls, thin basal conglomerates and beds of cornstone which laid down unconformably on an irregular surface of older sediments and lavas.

The succession is most complete and thickest in the west where it is about 1 km (Bluck, 1978), thinning east (Pentlands, Fig. 1.5A about 0.3 km but 0.6 km to north) and missing in some places. South of Lanark the Carboniferous Limestone Series rests directly on Lower Old Red Sandstone (Fig. 1.1). The pattern of thickness change is not clear enough to project under the Central Coalfield.

1.2.7 Lower Old Red Sandstone

The Lower Old Red Sandstone sediments and lavas crop out along the northern and southern flanks of the Midland Valley (Fig. 1.1). The deposition of sediment was interrupted by one or more igneous episodes which resulted in thick sequences of andesite and basalt lavas in the Ochils and Pentlands. Sills and dykes of felsite and acid porphyrite were intruded. Cairngryffe/Cloburn quarries are in a felsite.

A plutonic complex (granodiorite and diorite) intrudes the Lower Old Red Sandstone sediments at Distinkhorn in SE Ayrshire. Its outcrop is from 2 to 5 km across and of a suite forming bodies ten times that size in the southern Uplands.

The Lower Old Red Sandstone has its main outcrop to the north and NE. Here it is about 30 km wide across the strike southward from the HBF, the asymmetric Strathmore syncline contains a very thick

5 km even 9 km (Armstrong and Paterson, 1970), series of sediments. These are conglomerates, sandstones, siltstones and shales which are stratigraphically equivalent to much of the lava sequence which has its outcrop in the complimentary anticline of the Ochils and Sidlaws (Fig. 1.1, Table 1.1, Appendix 2). Uncertainty about the thickness arises from correlation problems between delta facies in old beds and the amount of overlap against the underlying Highland Border Complex.

Thirty kilometres south of the Ochils the Lower Old Red Sandstone reappears as a 2 km thick sequence of mainly volcanic rocks around Edinburgh which rest unconformably on the Lower Palaeozoic vertical rocks of the Pentlands (Fig. 1.5 and appendix 2).

North and west from Tinto the Lower Old Red Sandstone is sedimentary, mainly sandstone (Mykura in Craig, 1983) and apparently conformable on Lower Palaeozoic (Fig. 1.9).

A speculative projection of this boundary is shown on Appendix 2 profile (CF - HX). Under the Central Coalfield the existence of Lower Old Red Sandstone rocks, whether sediments, lavas of even granodiorite intrusives is essentially unknown. A model proposing deposition in marginal basins has however been proposed (Bluck, 1983). (Fig. 1.10).

1.2.8 Lower Palaeozoic

The Lower Palaeozoic rocks in the Midland Valley graben are represented by inliers of Ordovician and Silurian age exposed along the southern region (Fig. 1.11)

They include greywacke, shale, conglomerate, sandstone, siltstone, limestone and igneous rocks. Several kilometres of thicknesses

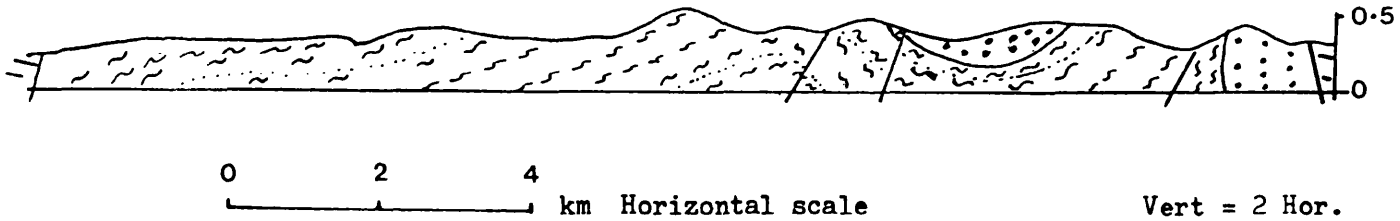

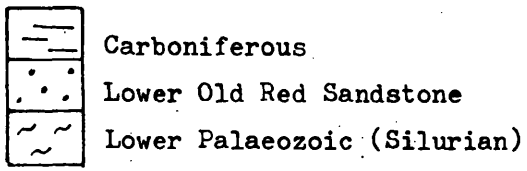

Fig. (1.9) Section across Lesmahagow and Hagshaw Hills Silurian inliers showing comparatively gentle folding of Silurian apparently conformable Lower Old Red Sandstone. (After MacGregor and MacGregor, 1948).

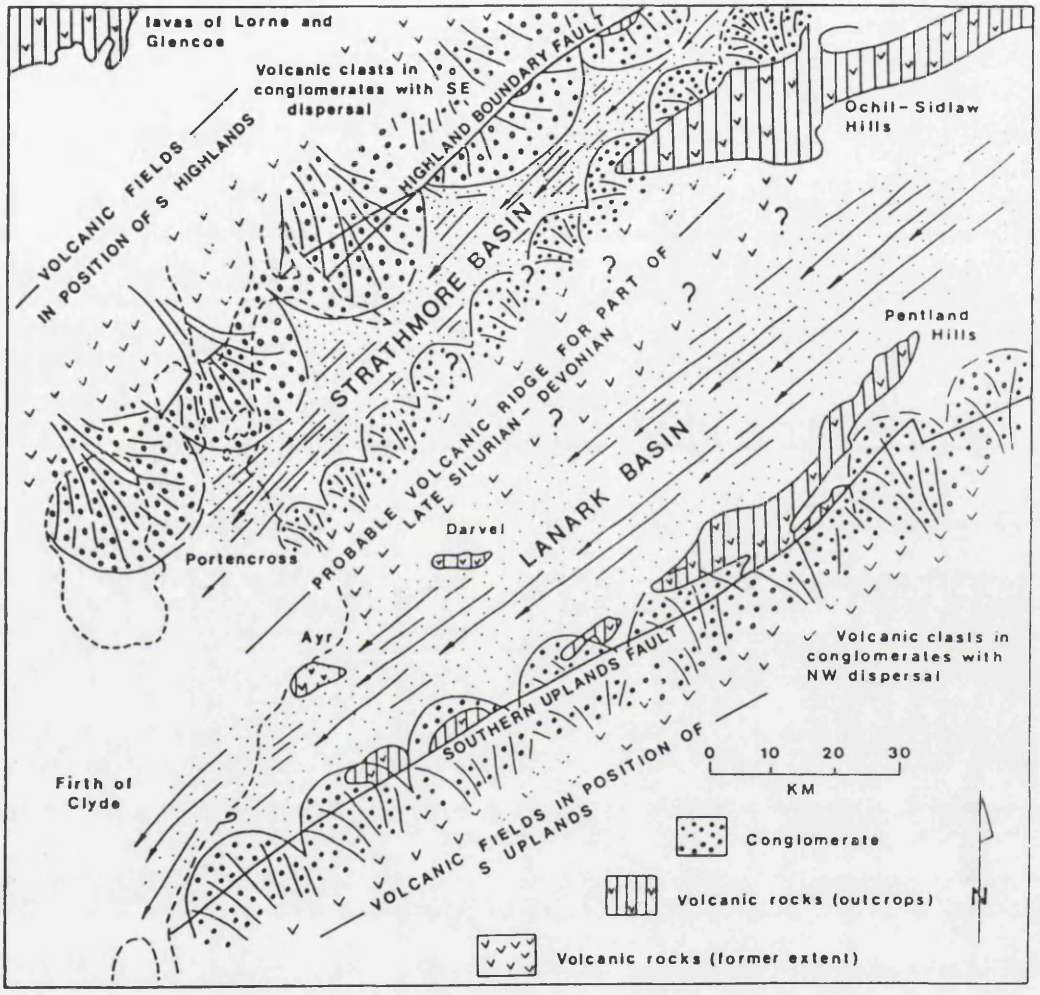

Fig. (1.10) Palaeogeography of Late Silurian-Early Devonian of W. Midland Valley. (After Bluck 1983).

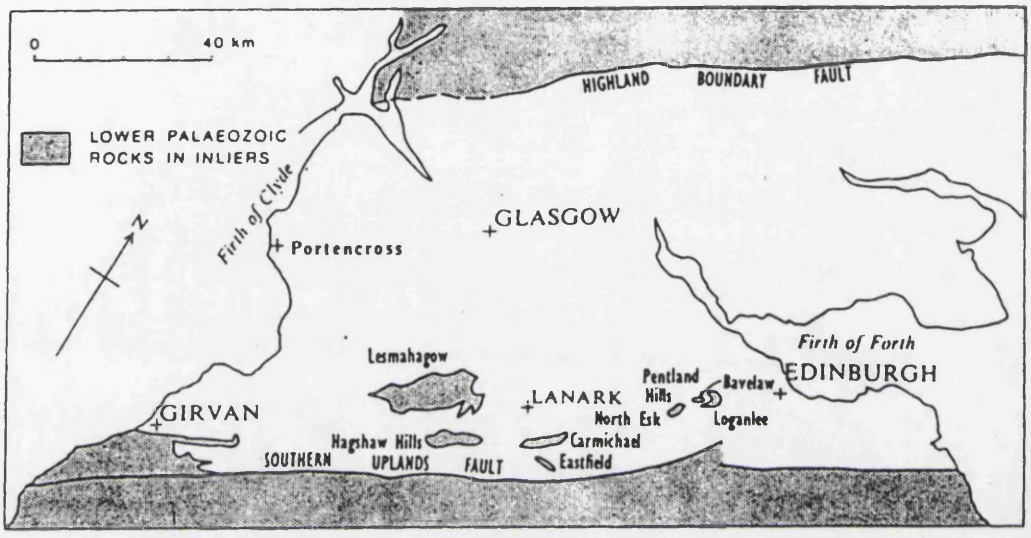

Fig. (1.11) Sketch map showing the lower palaeozoic inliers in the southern part of the Midland Valley.

(After Walton, 1983)

measured across vertical beds (Pentlands). (Fig. 1.5A). The upper Ordovician rocks unconformably overlie an ophiolitic complex (spilite lava, black shale, gabbro and serpentinite) of Arenig age south of Girvan. The complex may represent an obducted remnant of a volcanic island arc emplaced during the closure of the Iapetus Ocean.

The Highland Border Complex consists of a similar suite of rocks separated from the Dalradian by the Highland Boundary Fault and concealed on the Midland Valley side beneath the Sub Lower Old Red Sandstone unconformity (Curry et al, 1984). Limestone clasts in southerly derived Lower Old Red Sandstone conglomerates from the Stonehaven area suggest the possibility of a Lower Palaeozoic shelf carbonate facies within the Midland Valley (personal communication P. Haughton, 1984).

1.2.9 Crystalline Basements

Locally within the Midland Valley there may be a crystalline "basement" consisting of a Lower Old Red Sandstone granodiorite intrusion or, perhaps more widespread, obducted ophiolitic igneous rocks of Arenig age. Igneous, especially granite, pebbles in Ordovician conglomerates near Girvan indicate upper plutons now concealed close to the north (Longman et al, 1979). Southerly derived igneous and metamorphic pebbles are now recognised from Lower Old Red Sandstone conglomerates around Balmaha (personal communication Bluck, 1984).

Clasts in Palaeozoic conglomerates and Upper Palaeozoic volcanic vents indicate a crystalline basement of quartzofeldspathic gneisses and granulites under the Midland Valley (Upton, 1984).

1.3 Previous Geophysical Work

1.3.1 Magnetic field

The aeromagnetic map of Great Britain was compiled and published by the geological survey of Great Britain (1968). The part covering the Midland Valley is shown in Fig. (1.12).

The dominant feature is the high magnetic anomaly centred over the Central Coalfield Basin (Bathgate High) of about 500 nT, and about 20 km diameter, surrounded by smaller anomalies which lie over the Carboniferous lavas or dykes and sills outcrops.

Spectral analysis of the magnetic field over the area of the Midland Valley has shown the existence of two distinct groups of sources, one group of high frequency shallow sources and a second of low frequency and potentially much deeper origin, (R. Banks personal communication in Davidson et al, 1984). The high frequency anomalies are most intense in regions where Carboniferous basic lavas or sills outcrop, Hall & Dagley, (1970), for example north and south of Glasgow. Hall & Dagley map (Fig. 1.13) is an attempt to separate anomalies of different wavelengths, by filtering. Regular gradients with low frequency content are seen over the Lower Old Red Sandstone outcrop towards the Highland Boundary Fault and south of Lanark. Over the Lower Palaeozoic beyond the Southern Upland Fault both frequency and amplitude are generally low. Most of the lower frequency amplitude is to be associated with the dominant sub-circular pattern centred over the Central Coalfield Basin, the 500 nT Bathgate High. At half amplitude its diameter is about 20 km consequently that of a causative body reaching mid-crustal or shallower depths cannot be much less (see further under section 1.3.3)

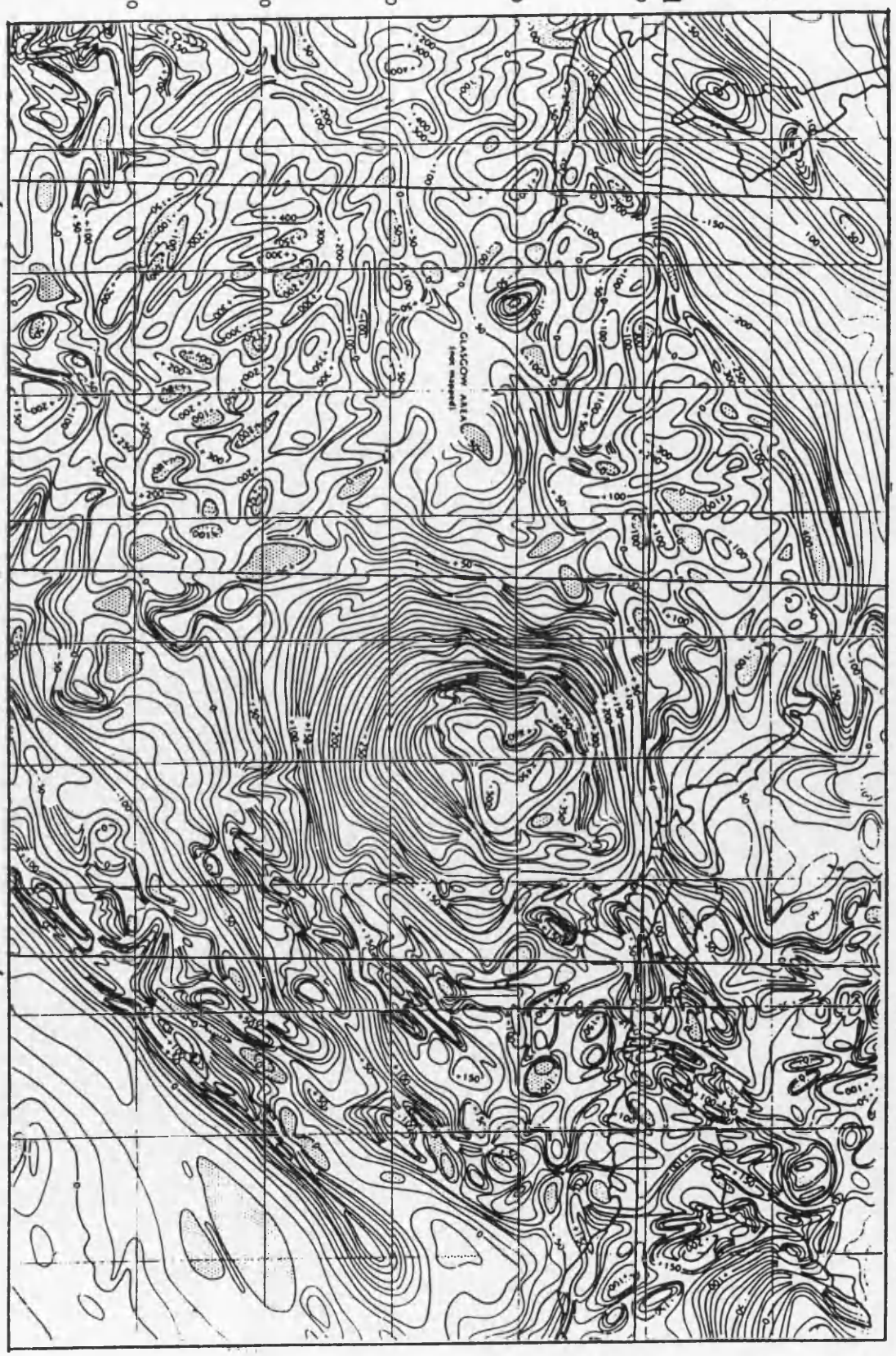

Fig. (1.12) Aeromagnetic anomaly map of the Midland Valley. (After IGS, 1968) CI = 10 nT.

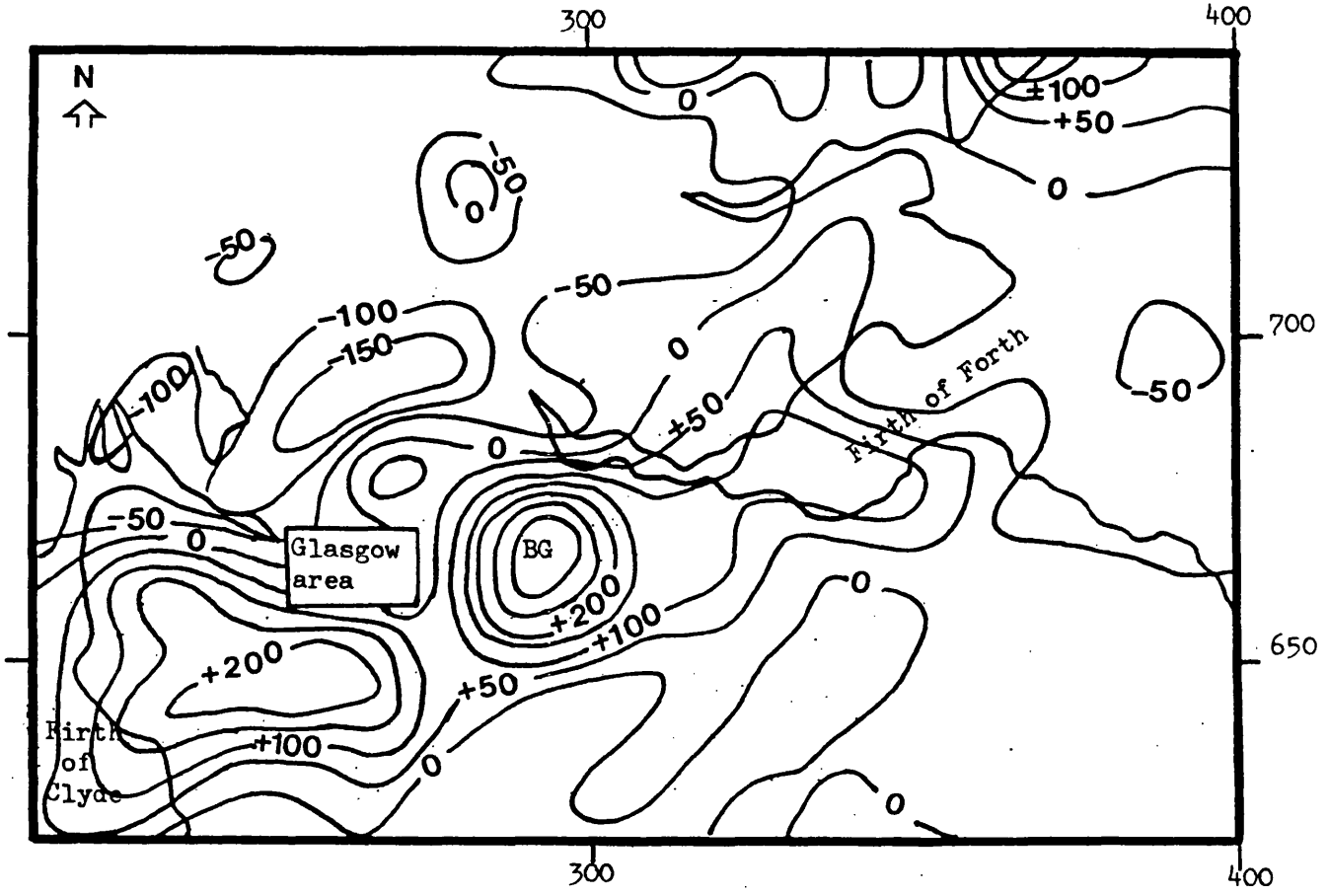

Fig. (1.13) Smoothed aeromagnetic map of the Midland Valley. (After Hall and Dagley, 1970).
Contour interval 50 nT. (BG) Bathgate area.

1.3.2 The Bouguer Gravity Field (Fig. 1.14)

The wavelength spectrum of this anomaly pattern differs from that of the aeromagnetic map. The shallow igneous bodies associated with the higher frequency elements on the latter have too small volumes to effect the gravity values at contrasts of 0.4 gm cm^{-3}. The gross effect of the lavas, (40 x 0.2 gm cm^{-3} x 1 km) about 8 mgals, is apparent on a broader scale.

Gravity minima occur over the coal basins (-8 mgal closure within the Fife field, -4 mgal within Clackmannan, -2 mgal within Lothian and Hamilton). Amplitudes are about 10 mgal indicating 2.5 km of thickness on Lower Old Red Sandstone (-0.1 gm cm^{-3}). Attempts have been made to strip the gravity effects of geologically established thicknesses of these lower density sediments (Hossain, Thesis, 1976, Al-omari, Thesis, 1980, Hussain and Hipkins, IGS Report, 1981). Their density is quoted to average 2.54 gm cm^{-3} from mine shaft gravity gradients (McLean, 1961). This density is too high to match reasonable amounts of sandstone (2.30 to 2.40 gm cm^{-3}), if the shale density is 2.55 gm cm^{-3} (Allsop 1974). All recognise that thickness below the Hurlet Limestone are too uncertain for estimation. Different choices of replacement density have been used. In the two notional Lower Old Red Sandstone at + 0.1 gm cm^{-3} has been substracted for Carboniferous. Hussain and Hipkins replace only the Upper Carboniferous using + 0.2 gm cm^{-3} for a Sub Lower Old Red Sandstone basement (Fig. 1.15).

Despite the problems of this approach, a gravity feature of about + 10 mgal seems certain to remain over the Central Coalfield and roughly co-entensive with the Bathgate Magnetic High. The range of possible models to account for these anomalies is discussed under 1.3.3.

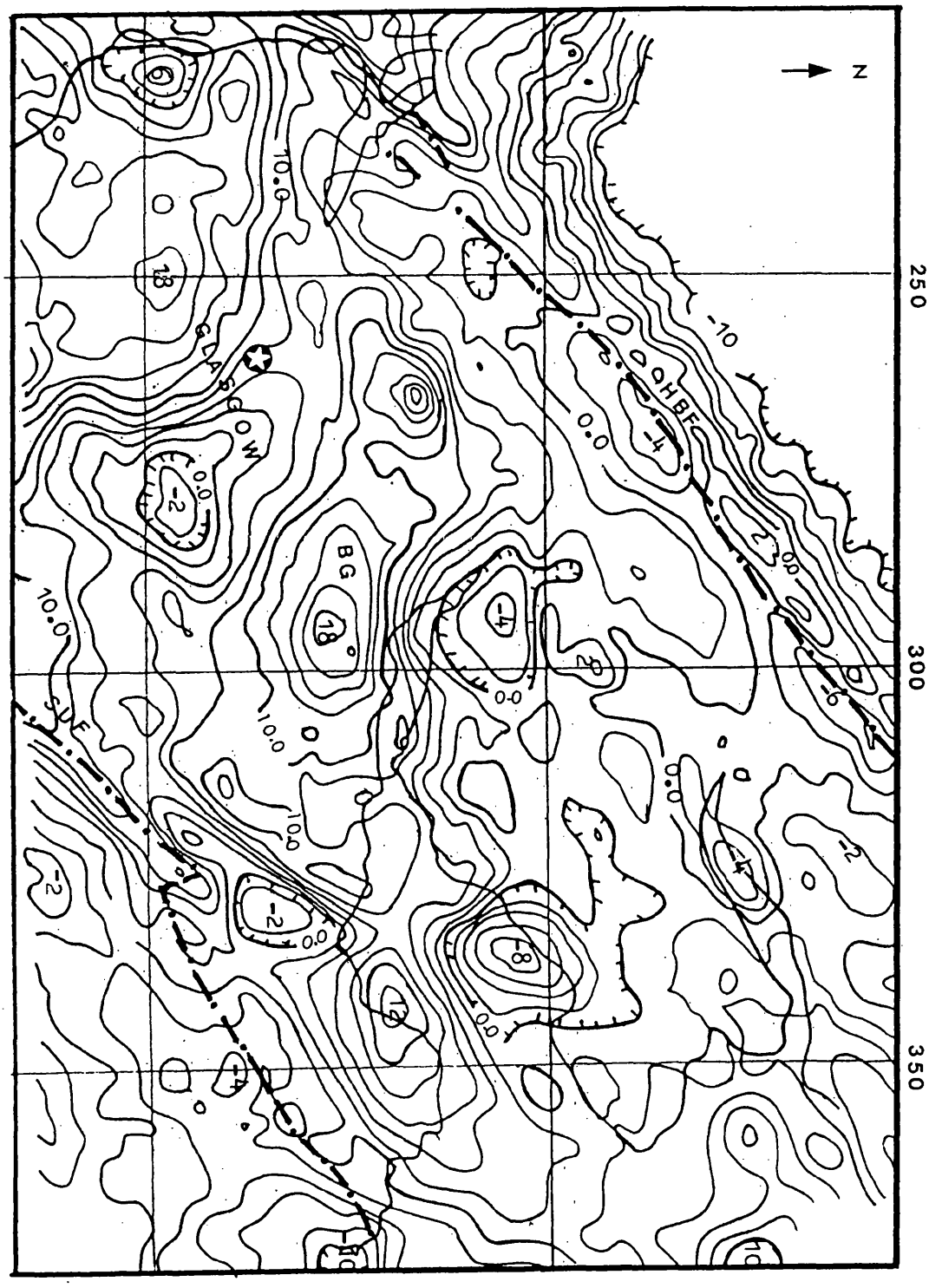

Fig. (1.14) Bouguer anomaly map of the Midland Valley. (After Hussain and Hipkin, 1981). CI = 2 mgal. BG = Bathgate.

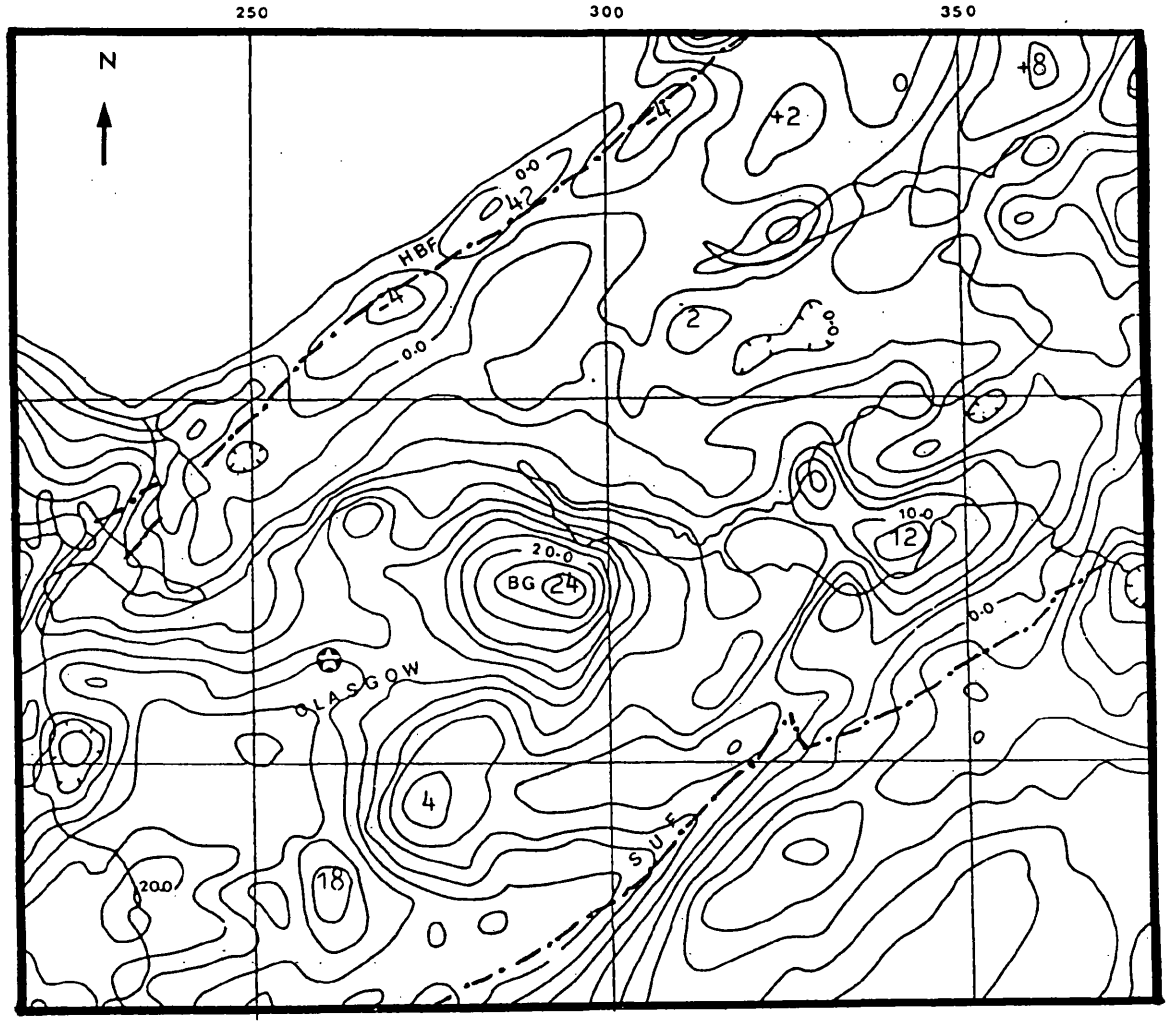

Fig. (1.15)

Bouguer gravity map of the Midland Valley.

Corrected for Upper Carboniferous thickness with + 0.20 gm cm^{-3}.

(After Hussain and Hipkin , 1981).

CI = 2 mgal

The gravity effects of Old Red Sandstone basins against the Highland Boundary Fault as far as Callander have been interpreted by Qureshi (1970) who shows 2 to 3 km thicknesses and for which he uses a density of 2.51 gm cm^{-3} rather than 2.64 gm cm^{-3} (McLean 1961). The main problem here lies in estimating a northerly falling regional gravity gradient which virtually nullifies that in the opposite direction due to the edge of the basin (Fig. 1.16).

REGIONAL GRAVITY ANOMALY ACROSS THE MIDLAND VALLEY

When a correction for the Upper Palaeozoic thicknesses on Lower Palaeozoic is made to the Bouguer anomalies the result, on a NNW - SSE profile from Loch Lomond to Sanquhar, is a central high approximated by McLean and Qureshi (1966) to a parabola. Their interpretation of a 5 to 6 km relative uplift of a denser (0.2 gm cm^{-3}) basement between the boundary faults is similar in form to that seismically deduced on a 6.40 km s^{-1} basement (LISPB, Fig. 1.20) on which Al-omari (1980) has based an extrapolation of the regional gravity.

Al-omari has attempted to distinguish, separate and interpret the components of the Bouguer gravity map for the western Midland Valley (Callander, Bathgate, Lanark line). About the Lower Old Red Sandstone thickness he concludes that there is a gradual increase into the Valley from the Southern Upland Fault making an average of 2.5 to 4 km. Depending upon the density used to correct for the magnetically derived Bathgate model (2.72 gm cm^{-3} as for Carboniferous lavas or 2.85 gm cm^{-3} as for gabbro), there may be zero to 2.5 km of Old Red Sandstone in their area. Close to the Highland Boundary Fault an Old Red Sandstone basin is up to 8 km thick. This, however,

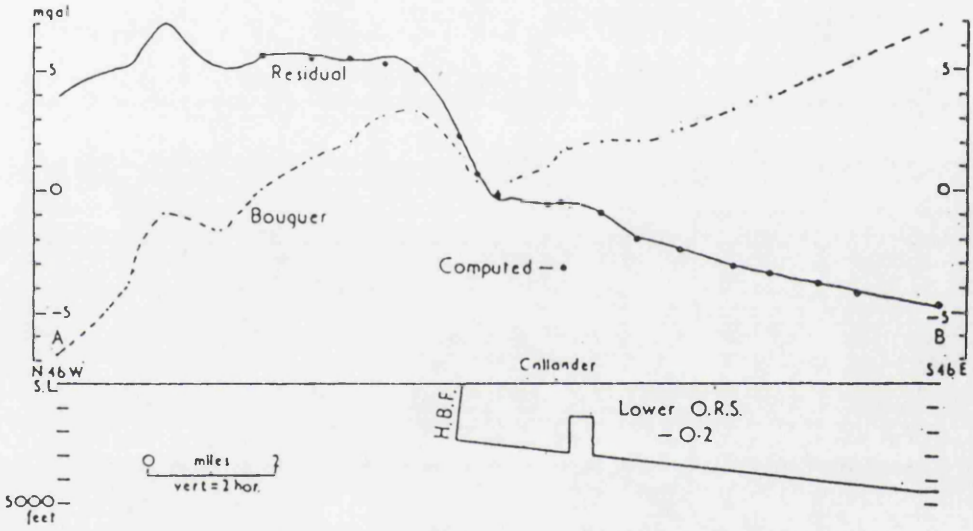

Fig. (1.16) section showing the Bouguer and the residual anomaly profiles and the computed gravity effect of the inferred distribution of rocks along the line of section and below the datum. Density contrast with respect to basement is given in g/cm³.

(After Qureshi, 1970)

is based on a-0.07 gm cm^{-3} contrast rather than -0.2 gm cm^{-3}. In connection with the Hamilton low, Al-omari points out that Downtonian sandstones from Lesmahagow area have a 2.54 cm cm^{-3} density.

Local gravity anomalies from Sub Old Red Sandstone sources exist. An acid igneous body is proposed by Al-omari to account for the Hamilton low. The Bathgate anomaly may fall into an intra-basement category. (There is no similar analysis for the eastern Midland Valley).

1.3.3 Magnetic and Gravity Interpretations of the Bathgate "High".

The magnetic and gravity anomalies centred over the Central Coalfield Basin (Bathgate High) indicating both due to the same source (Intrusion) which exhibits both density and magnetization contrasts with its surroundings.

Since it appears easier to isolate the magnetic anomaly and its possible components than it is the gravity, the primary modelling has been to fit the magnetic situation. Hossain (1976) considers two principal geological possibilities. The shallower, using a polarisation based upon Clyde Plateau Lava samples, takes the top of the magnetic model as the geologically expected top of those lavas (0.3 to 1.5 km sub-flight of the aeromagnetic measurements).

The shape which results from adjusting the base depth, is then a downward tapering cone reaching 4 km depth over 10 km width. This is three times the likely maximum lava thickness (shading on Fig. 1.17). It is concluded that this part of the model represents a necessary intrusion additional to the lavas and is the shallowest which is geologically possible. It would represent a body within Lower Old Red Sandstone (2.64 gm cm^{-3} density) country rocks. If of gabbro, it would have a contrast of at least +0.15 gm cm^{-3} and hence produce a gravity effect of at least +10 mgals.

A similar model on a smaller horizontal scale has been proposed by Cotton (1968) to explain a +12 mgal anomaly arising from beneath the Clyde Plateau Lava outcrop over the Campsie Fells. Here the base of the lavas outcrops nearby and their thickness is predictably small. The comparison, however, does not extend to the magnetic anomaly which is much less than over Bathgate.

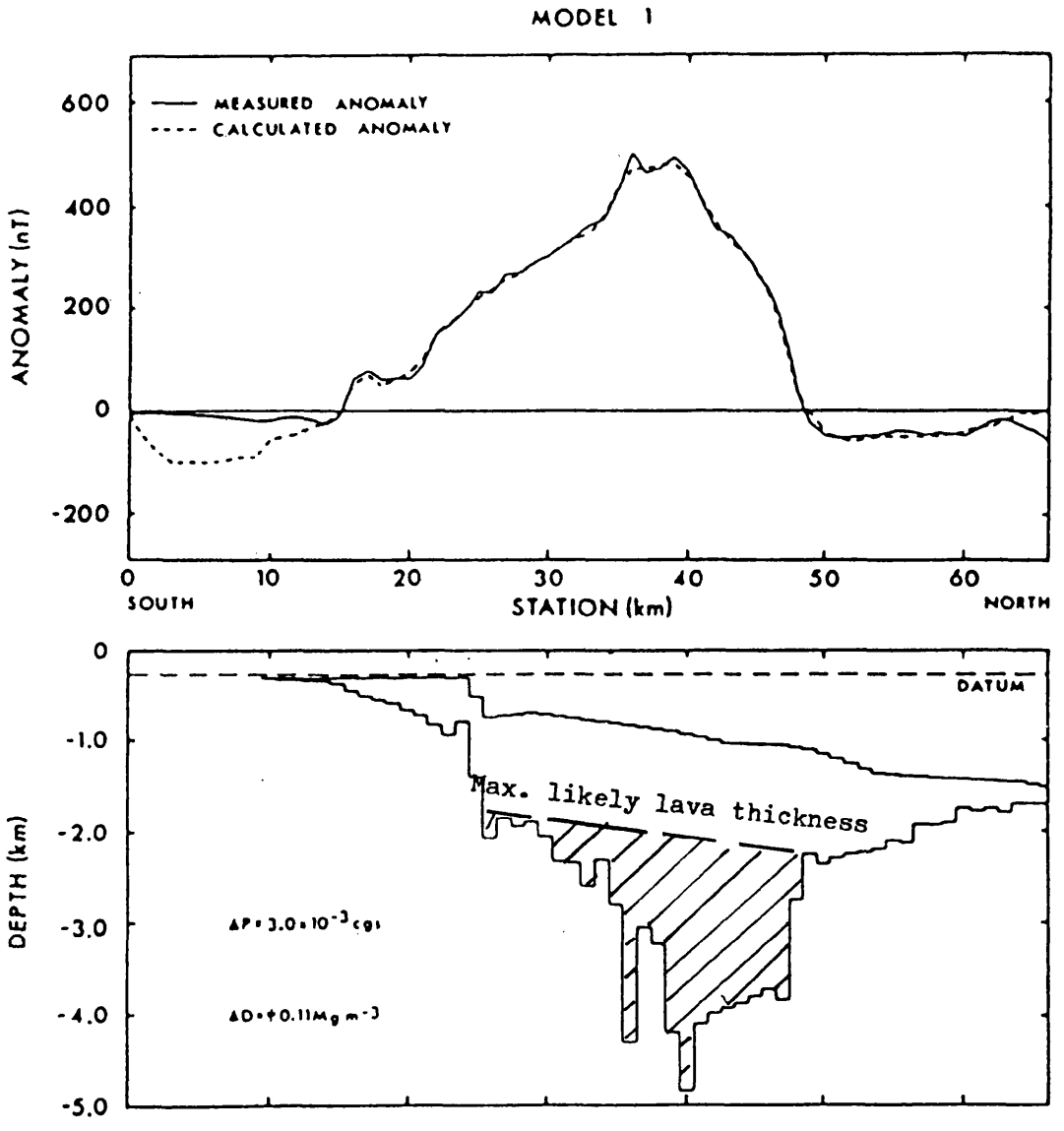

Fig. (1.17) shows model 1, the observed and calculated anomalies.

(After Hossain, 1976)

There are of course many deeper possible models quite separate from the lavas under Bathgate. All imply anomaly separation of shallow from deeper body components. Rather than attempt to specify the contributions from the shallow lavas and minor intrusions directly, Hossain reduced them by upward continuation of the anomaly field through 2 km. It is then possible to model the smoothed anomaly by a body within the Lower Crust (10 to 15 km depth range). It requires a polarisation about 3 times that for the lavas but not impossibly high (10% magnetite), Fig. (1.18). If, as seems likely, the associated gravity effect is +10 mgals the associated necessary density contrast becomes 0.45 gm cm^{-3} which, if the average Lower Crustal density is at least 2.85 gm cm^{-3} does seem extreme. This approaches the deepest geological possibility. Many intermediate possibilities exist which will equally satisfy the gravity and magnetic anomalies.

1.4 Seismological studies in the Midland Valley

Efforts have been made by seismologists to explain the crustal structure of the Midland Valley graben and to solve some geological problems.

1.4.1 The Lowlands seismological network (LOWNET)

A permanent radio-linked short period seismometer network has been operating in Central Scotland Midland Valley (Fig. 1.19A) since 1969. Recording is on analogue magnetic tapes which are stored at I.G.S., Edinburgh.

Crampin et al (1970) gave a detailed description of this LOWNET equipment, its sites and the results of a study of some explosions and natural events recorded on the network. Their travel time diagram (Fig. 1.19B) is mainly based upon observations of

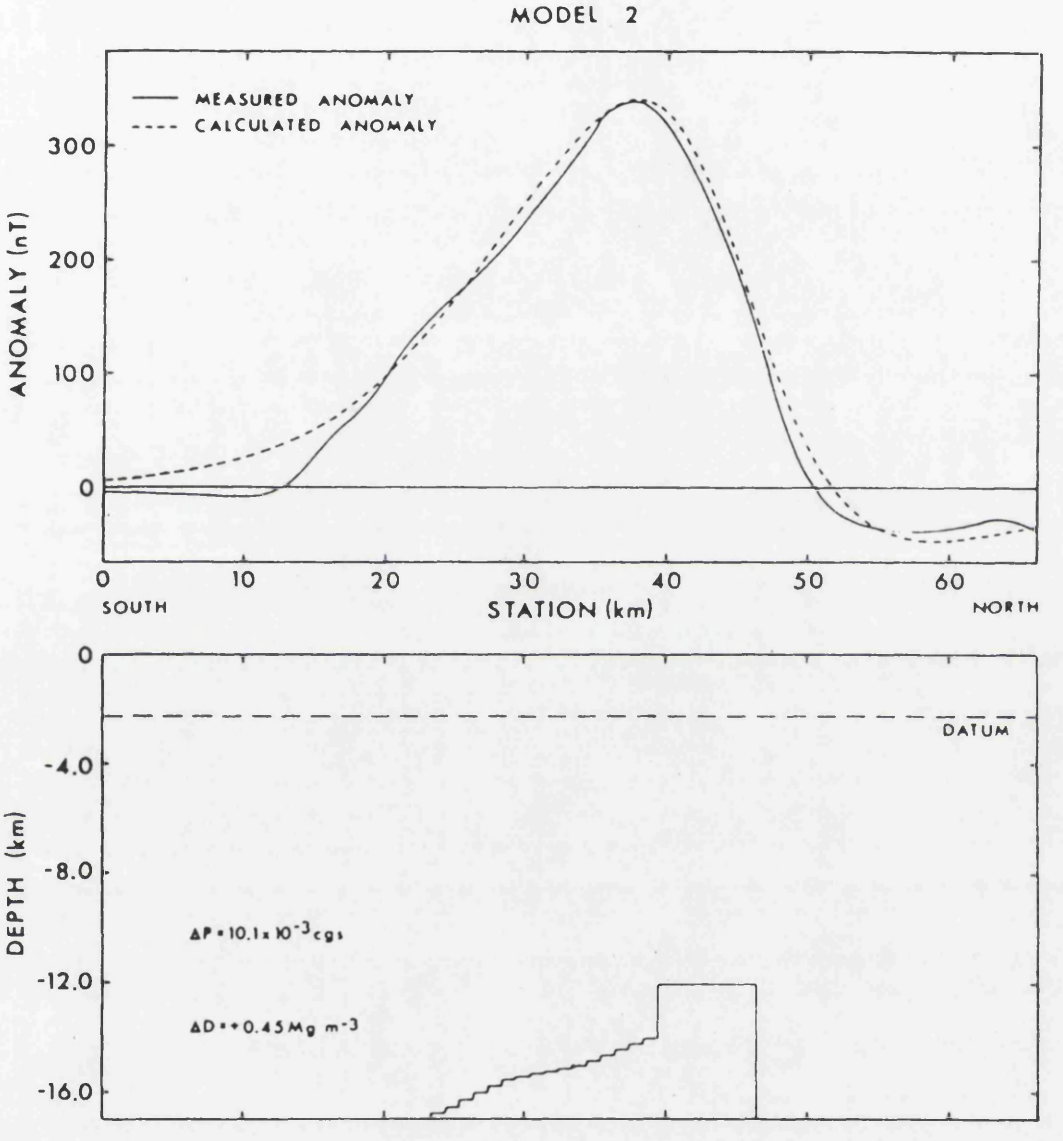

Fig. (1.18) shows model 2, the observed and calculated anomalies. (After Hossain, 1976)

(A)

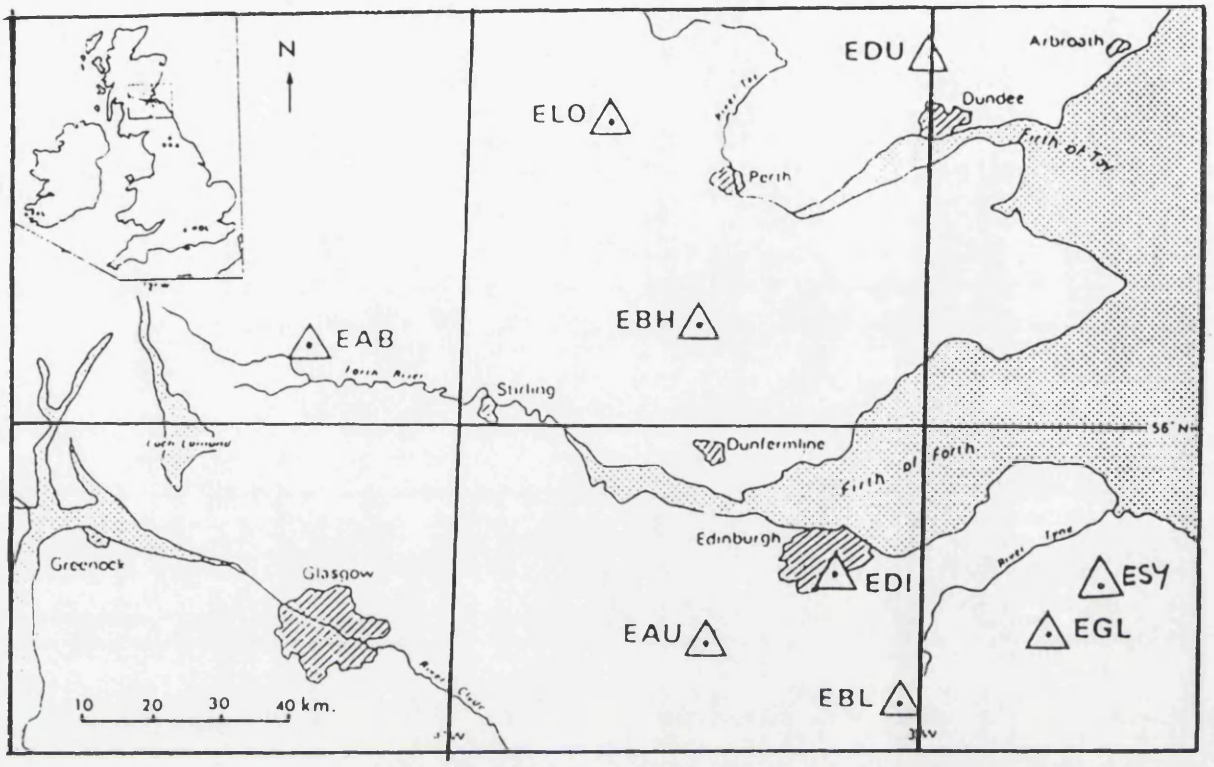

(B)

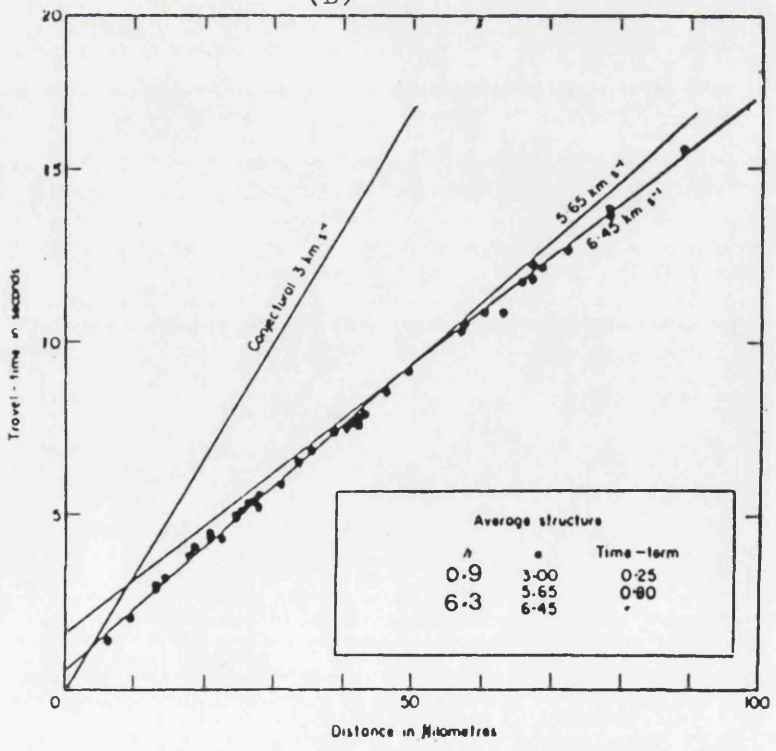

Fig. (1.19) (A) Map showing the eight LOWNET sites (After IGS) (B) Travel time diagram for explosions recorded on LOWNET (After Crampin, 1970).

commercial quarry blasts in the Midland Valley. It is represented by a three layer model. The thin top layer (3.00 km s^{-1}) is assumed. There are no direct arrivals from it. The middle layer (5.65 km s^{-1}) is 5.4 km thick and gives refracted arrivals out to 50 km where they are overtaken by a 6.45 km s^{-1} segment.

1.4.2 Lithospheric seismic profile in Britain (LISPB)

This experiment was designed to study the crustal and upper mantle structure of the British Isles. A detailed description and interpretation are given by Bamford et al (1976, 1977).

It crossed the Midland Valley on a north/south line centred on Edinburgh (Fig. 1.20A). Again a three layered upper crust was defined in the Midland Valley (Fig. 1.20B). The uppermost layer of velocity 4.00 - 5.00 km s^{-1} (and thickness 2.5 km) is related to Upper Palaeozoic, Old Red Sandstone and Carboniferous, sequences. Layer 2 of velocity (5.8 - 6.0 km s^{-1}) has been related to the Lower Palaeozoic rocks by comparison with the thicker layer between these velocity limits south of the Southern Upland Fault. Under the Midland Valley this layer is represented as 5 km rather than 10+ km thick. North of the Highland Boundary Fault, over the Dalradian outcrop, 6.0 km s^{-1} is attained near the surface but the velocity increase with depth down to 12 km is minimal.

Beyond 50 km within the Midland Valley, as into LOWNET, a 6.40 km s^{-1} segment is seen. The layer with this velocity, at 7 - 8 km depth, has been compared with that at shallower depths under the Caledonian Foreland where it is considered to be of Lewisian crystalline granulite facias rocks.

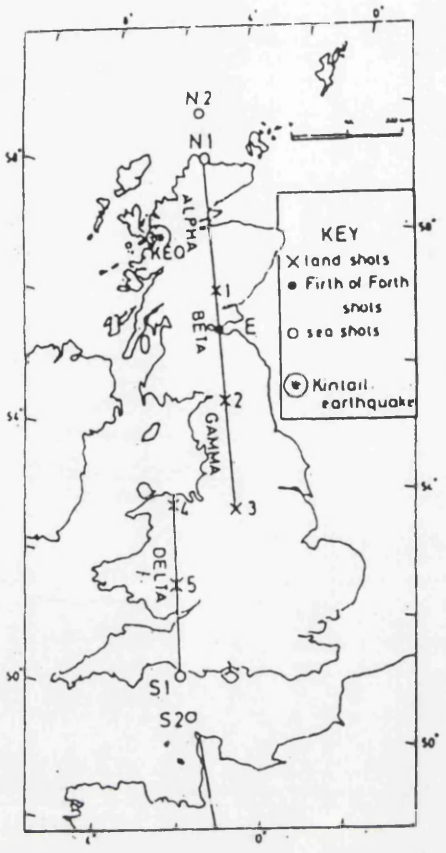

(A) Location of LISPB shots and profile, Northern Britain.

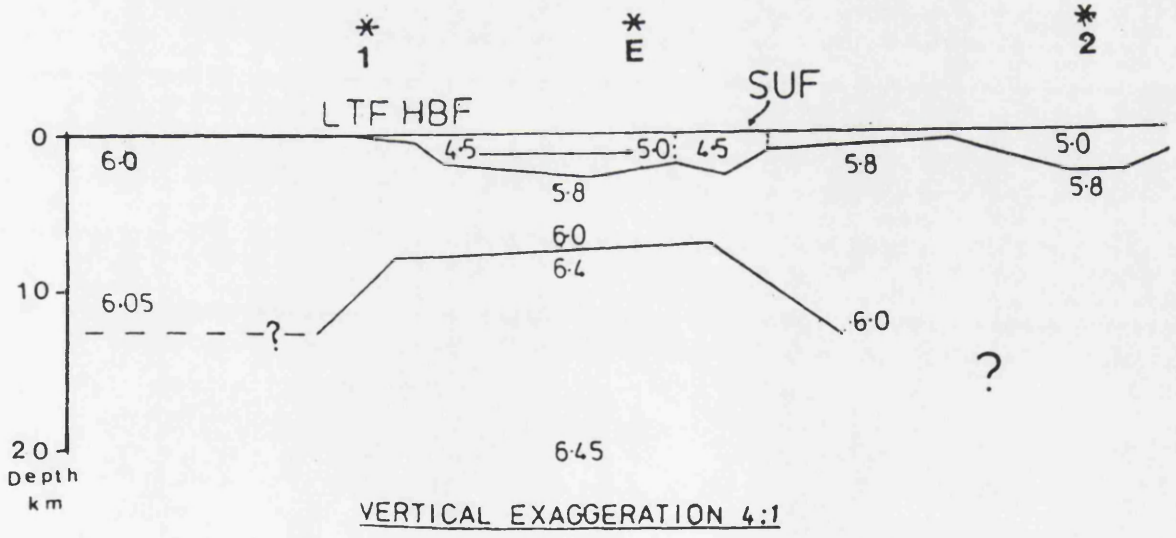

Fig. (1.20) (B) P-wave velocity distributions and upper crustal structure Midland Valley, Southern Upland and Highlands. (After Bamford et al, 1977).

1.4.3 Southern Upland Seismic Profile (SUSP) and associated results and discussions

The results from this profile running just within the Southern Uplands from Oxwellmains (DUNBAR) to SANQUHAR along the Ordovician outcrop of the North Belt have yet to be published in detail.

Warner (1982) proposed a velocity-depth model for the Upper Crust which consists again of 3 layers. The first, 5.7 - 5.8 km s^{-1}, about 1 km thick, presumably of Ordovician greywacke and possibly spilite lavas, is underlain by a middle 6.0 km s^{-1} layer which is 2 or 3 km thick and followed by a 6.30 km s^{-1} layer.

This result differs from the LISPB model where the lines cross. The LISPB travel time graph (E into B across the Southern Upland Fault) does however have a 6.4 km s^{-1} apparent velocity here. Similarly high apparent velocities were reported into an array on the Northern Belt (Broughton, near Biggar) from northerly sources at 25 to 50 km ranges (El-Isa, 1977).

It has been argued that the across strike measurements on LISPB barely resolve an alternation of higher and lower velocity blocks (Hall et al, 1983).

Adesanya (1982) has measured the velocities of greywacke cores over a range of pressures in the laboratory. From these it is argued that the higher velocity blocks in the Southern Uplands ($>$ 6.0 km s^{-1} at 3 to 4 km depth) are not Lower Palaeozoic greywacke but crystalline rocks (Hall et al, 1983).

1.4.4 Seismic Data on the Carboniferous Rocks in the Midland Valley

Drysdale (1955) from a shallow refraction survey in the Firth of Forth observed the following velocities:

	Velocity range (km s^{-1})
Superficial deposits	1.50 - 1.80
Boulder clay	2.00 - 2.20
Production Coal Measures to Calciferous Sandstone series at mean depth 0.18 km	2.50 - 3.51

Allsop (1974) presented velocity and density from geophysical logging and laboratory tests on cores from the Spilmersford borehole in East Lothian (Table 1.2). These have been used here (Fig. 3.5) in associating velocity with lithology and to support velocities inferred from densities in sandstones. Her values for Carboniferous tuffs and agglomerates compared with those for other sediments are given in (Table 1.2), these show:

1. shale, sandstone and siltstone velocities are similar to each other and also to tuffs and agglomerates.
2. the sandstone velocities and densities increases at depth indicate a greater degree of compaction.

Hall (1970) made a correlation of seismic velocities with formations in the Western Midland Valley and observed the following velocities:

	Velocity range (km s^{-1})
Millstone Grit	3.44 - 3.72
Upper Limestone Group	3.67 - 3.81
Limestone Coal Group	3.32 - 3.78
Lower Limestone Group	3.57 - 3.96
Clyde Plateau Lavas	3.35 - 4.69

TABLE 1.2

Depth Metres	Density log ρ_b g cm^{-3}	Lab. saturated ρ g cm^{-3}	Vel. from log km s^{-1}	Lab. vel km s^{-1}	Lithology
169	2.50	2.50	4.02	-	Siltstone
176	2.55	2.56	3.69	-	Shale
188	2.60	2.82	4.27	-	Calcareous sandstone
195	2.45	-	4.08	-	Sandstone
198	2.33	2.32	3.36	3.36V	Sandstone
220	2.30	2.33	-	-	Sandstone
285	-	2.54	3.90	-	Sandstone
292	-	2.59	4.09	3.97V	Tuff
293	-	2.52	4.09	4.12V	Tuff
295	-	2.48	3.51	-	Tuff
344	-	2.45	3.60	-	Agglomerate
345	-	2.49	3.39	3.54H	Tuff
546	2.75	2.68	4.70	-	Basalt
548	2.75	2.65	5.00	4.48V	Basalt
728	2.50	-	4.39	-	Sandstone
733	2.45	2.55	4.03	3.93H	Siltstone
734	2.45	2.47	4.03	3.60V	Siltstone
807	2.50	2.59	3.84	-	Siltstone
822	2.75	-	5.73	-	Basalt

The overlap of velocity ranges for different Carboniferous groups makes it impossible to distinguish between them seismically. Hall (1978) from a refraction line in Firth of Clyde observed three layers:-

Layer 1 of velocity 2.70 ± 0.05 km s^{-1} probably New Red Sandstone

Layer 2 of velocity 3.80 ± 0.05 km s^{-1} Carboniferous sediments

Layer 3 of velocity 5.00 ± 0.05 km s^{-1} Lower Carboniferous Lavas or Old Red Sandstone.

Hall (1974) concluded from seismic reflection survey in North Ayrshire and Renfrewshire that the Clyde Plateau Lavas form a 0.9 km thick pile along a NW to SE line following their main outcrop. Hall (1971) showed from a reflection adjacent to the Slamannan (Rashiehill) borehole that the lava thickness extended about 90 m below the borehole base making a probable total of 470 metres.

1.5 The purpose of the Seismic Refraction Survey

The first objective has been to test some of the model possibilities suggested to explain the Bathgate anomaly (Fig. 1.21).

It has been apparent from the outset that any body within the 6.4 km s^{-1} basement (Case 3) would be out of range of the planned measurements.

Shot-receiver distances up to 40 km would encompass bodies in Case 2, i.e. within the LISPB model 5.8 to 6.0 km s^{-1} layer considered as Lower Palaeozoic. A crystalline rock body, however, need not have a readily detectable velocity contrast within this layer. Granitic intrusions in similar surroundings have been considered invisible to LISPB (e.g. Weardale in the Alston block).

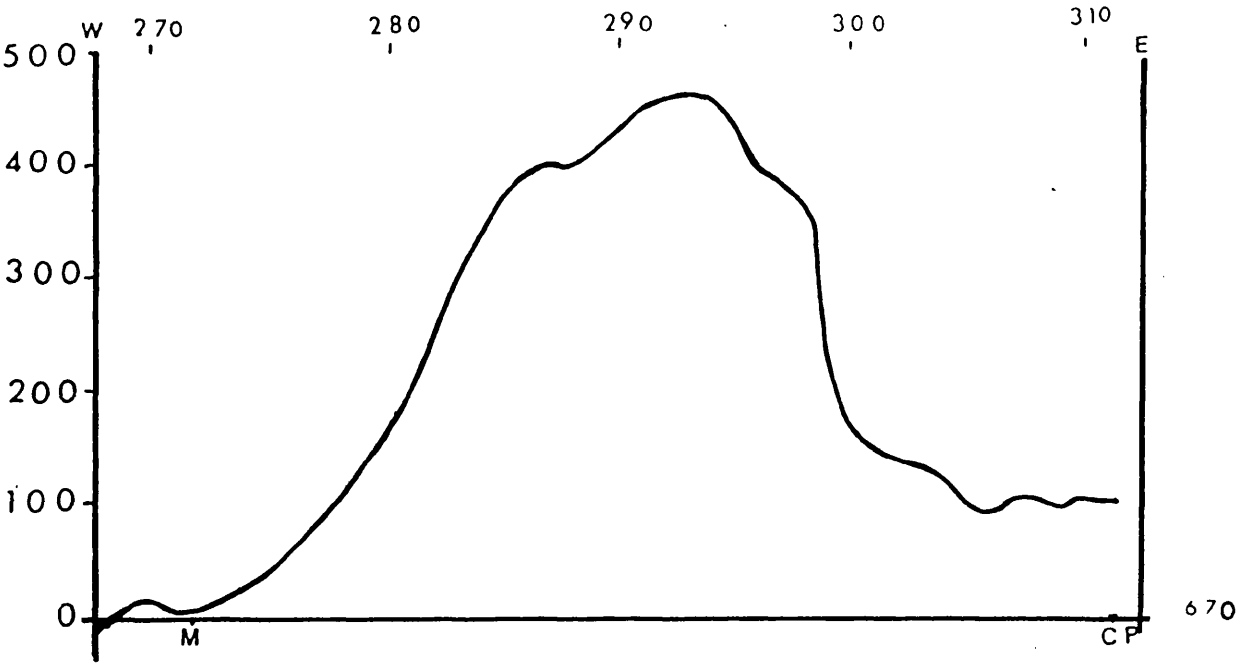

(A)

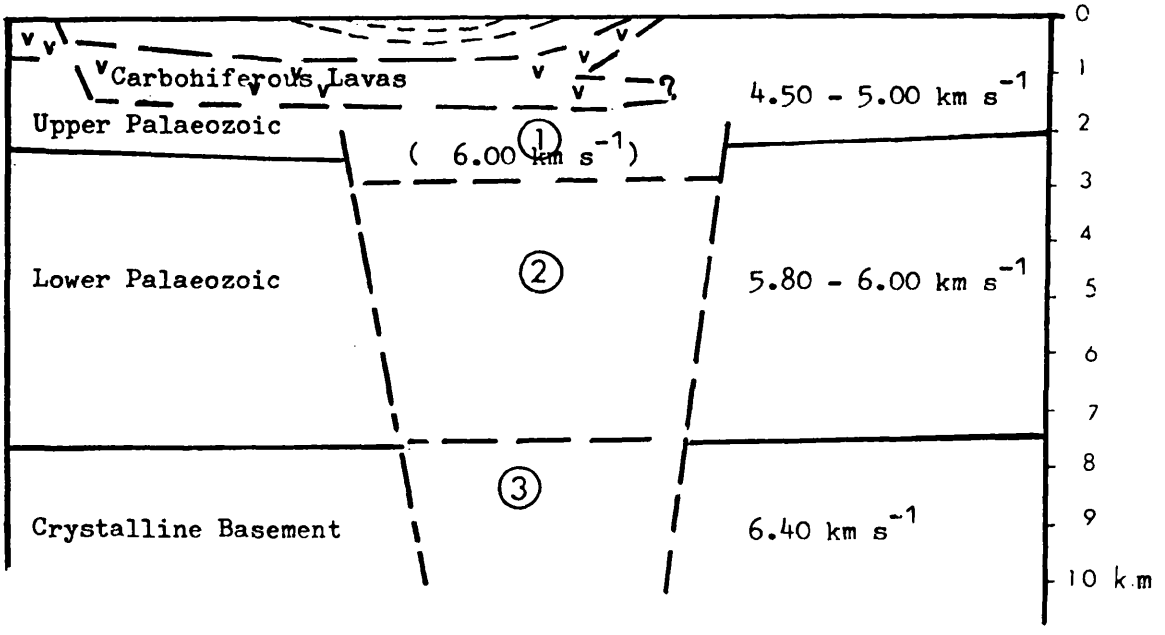

(B)

Fig. (1.21) (A) Magnetic anomaly across Bathgate High between Medrox quarry (M) west and Craigpark quarry (CP) east.
(B) 3 Possible magnetic models.

Recognition would depend upon demonstrating a locally different refractor velocity between the area under the magnetic anomaly compared with surrounding places. A situation in which the igneous target body penetrated the Upper Palaeozoic, 4.5 - 5.0 km s^{-1} LISPB model layer, offers the best chance of detection. The shallowest possibility envisages that the intrusion could occupy all the space in this layer below the Carboniferous Lavas (Case 1). Since its velocity may be similar to the Lower Palaeozoic layer, demonstration of a local shallowing of this (5.8 - 6.0 km s^{-1}) refractor could be the evidence for this model. This relief could be less than that associated with the magnetic body thickness if part of it was within the refractor (Intermediate Case between 1 and 2). Ambiguity between structural and "intrusive" relief seems inevitable. Despite this any results leading to a map of apparent Lower Old Red Sandstone thicknesses would be geologically valuable.

To achieve this the 4.5 - 5.0 km s^{-1} Upper Palaeozoic layer of the LISPB model needs subdivision.

Velocity contrasts between Carboniferous and Lower Old Red Sandstone sediments are already indicated by density contrasts (0.1 - 0.2 gm/cc). Substantial thicknesses of volcanic rocks in both systems may be seismically distinct. Evidence on these points is both of interest in its own right and a necessary preliminary to the main purpose of this study.

CHAPTER II

SEISMIC MEASUREMENTS

2.1 Introduction

To achieve the interpretational purpose of this study travel-times at ranges up to 40 or 50 km were required with an accuracy approaching 0.01 seconds. It was known that blasts from some of the quarries in the area had been received across the LOWNET array (Crampin et al 1970). Since then, however, many quarries have introduced more delays into their charge patterns and the gain settings on LOWNET have been reduced. At the outset the Glasgow University recorders were prototypes which were progressively improved and increased in number. Most of the work was conducted using quarries as sources and with six recorders.

2.1.1 Quarries as Seismic Sources (Fig. 2.1)

There are numerous quarries between Glasgow, Edinburgh and Stirling around the Bathgate anomaly area (Map 3.1).

The weight of explosive used for a single primary blast usually ranges from 500 to 2,500 kg distributed between 7 to 15 holes about 3 m apart in line behind the face. The hole depths range from 15 to 25 m. All quarries use delays of 7 to 10 ms, so that only about one tenth of the total charge is detonated simultaneously (Fig. 2.1). The pattern of delays both improves the fragmentation of the rock and reduces local damage from vibrations. Unfortunately, it also obscures the distribution of energy between different seismic phases and reduces the effective charge which determines the amplitude of the first arriving P-wave to that of the weight/delay.

(A)

(B)

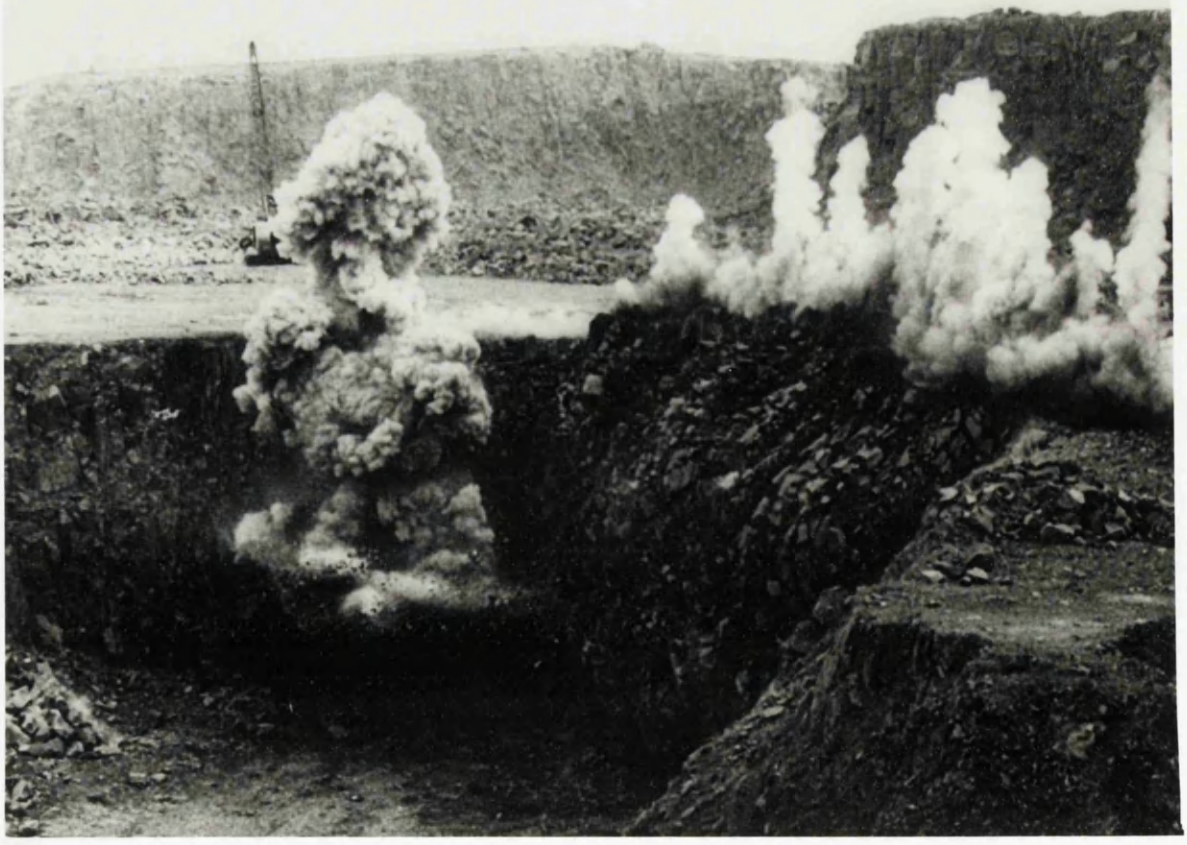

Fig. (2.1) shows Tamsloup quarry blast
(A) face before blast
(B) face during blast

Since only a few recorders were available, each travel-time graph has of necessity been built up in a piecemeal fashion from measurements on a number of occasions. It has, therefore, been important to choose quarries which blasted fairly frequently (the range is from weekly to six monthly intervals).

Beyond this, factors affecting one's ability to have the recorders on site with tapes running at the critical time should be mentioned. These are first communication of an intended day, and ultimately time of day of the event and secondly, reliability of the predicted time being the actual time. In many cases, these were regularly close to $\pm$ 5 minutes. The maximum recording window using cassette tapes is one hour. With some sets covered by one operator requiring manual switching, the effective window is narrowed by the travelling time around the sites.

2.1.2 Open cast blasting

An opencast coal site at Headless Cross, where blasting took place daily, sometimes twice a day, was also used as a source.

It was more difficult to record from the opencast than from a hard rock quarry because blasting took place as soon as the holes were drilled and loaded, limited only by two hour legal constraints (10 - 12 and 14 - 16 hours). The shotfires has limited discretion in the matter and a number of blasts were missed on this account.

In opencast coal working the quantity of explosives, the number of holes and the holes depth depend upon the depth to the coal seam, thickness and rock types between the coal seams to be removed, (Fig. 2.2).

Small delays are used in opencast workings as the intention is to break and lift the rocks covering the coal seam.

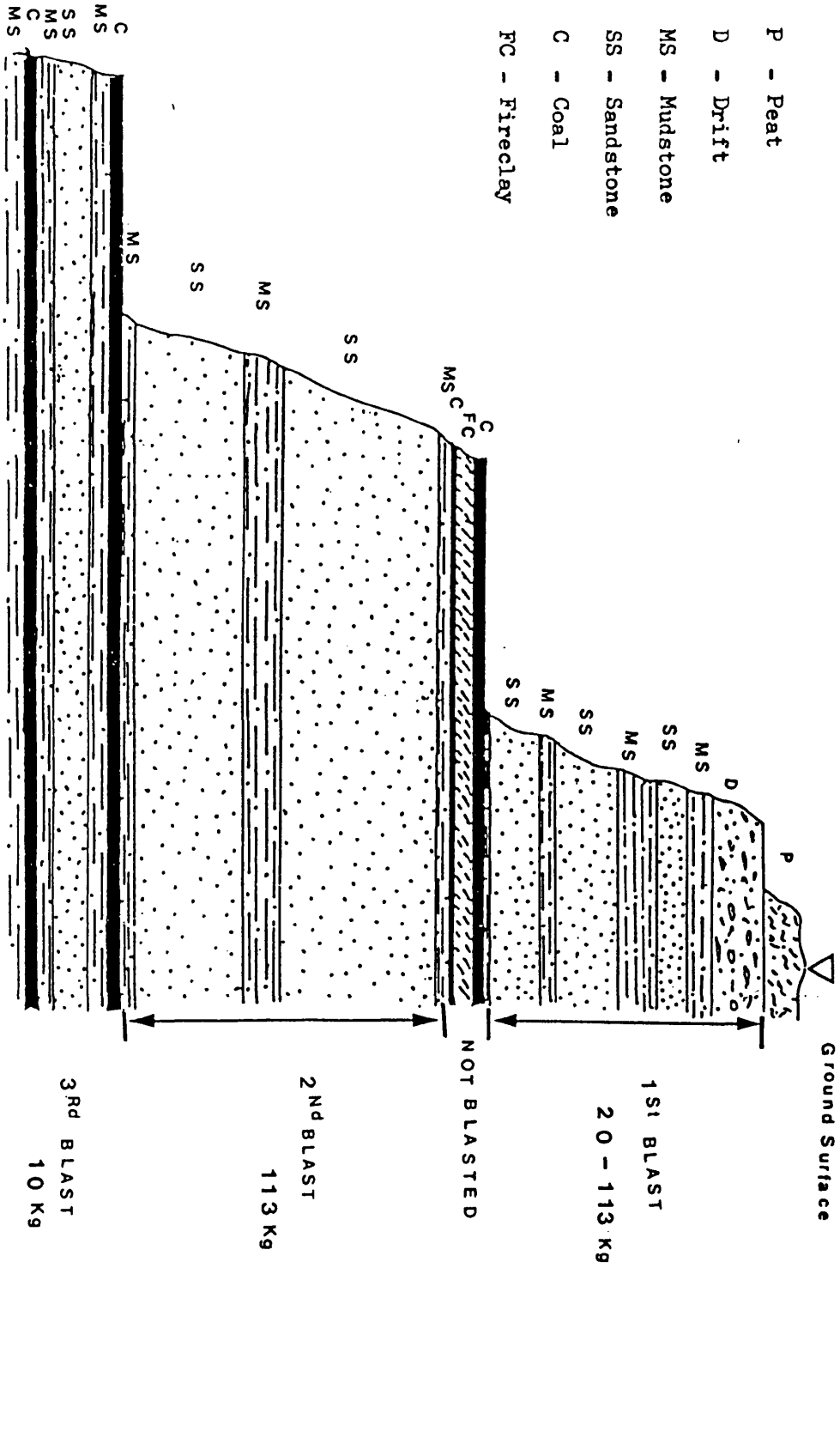

Fig.(2.2) Sketch section showing rocks to be removed on top of the coal beds. (Headless Cross opencast)

Successful recordings were made of these blasts to 21 km range. The only LOWNET site on which they registered was AU at 20 km.

2.2 Recording system (Figs. 2.3 and 2.6)

The system used in acquisition of the seismic data was the Glasgow FM seismic instrument designed and constructed by G. Gordon to specification stipulated by J. Hall.

During most of this study the apparatus was under development and subjected to modification and improvement. The work started in 1981 with one recording unit, together with an older shot instant recorder, ending with six recording units.

The recording equipment used (Figs. 2.3 and 2.6) consists of a seismometer, Amplifier - Modulator, cassette recorder and MSF radio time receiver.

2.2.1 Seismometer

The ground motion resulting from the arrivals of a seismic wave is detected by a seismometer and converted into oscillating electrical signals by a magnet moving relative to a coil.

Two types of plastic-coated, low resistance vertical geophones were used:-

a. Mark L15B 4.5 HZ and sensitivity 0.45 v/cm/s.

b. Mandrel EV22B 7.5 HZ and sensitivity 0.22 v/cm/s.

Both geophones are damped at 70% of critical damping.

2.2.2 Amplifier - Modulator (FM). (Fig. 2.7)

The signals from the geophones are selectively amplified to improve weak signals, filtered to exclude various unwanted frequencies, and then modulated and finally buffered before connection to recording head.

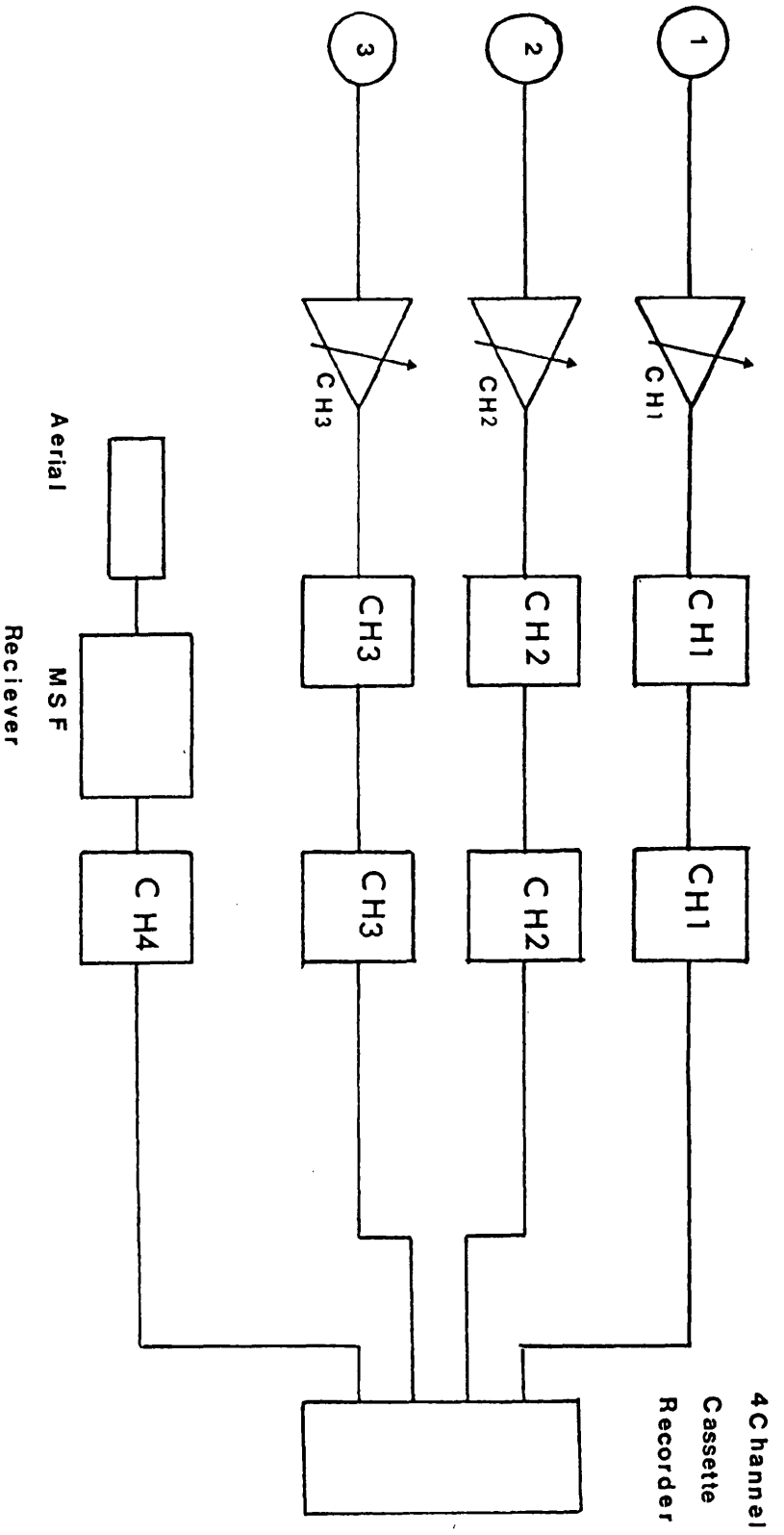

Fig.(2.3) Block diagram showing the complete recording arrangement.

By using a frequency-modulated (FM) recording system it is possible to obtain the bandwidth (2 - 60 HZ) needed without too much interference and noise. The amplifier has a variable gain control with a range of 46 - 112 dB divided into 6 dB steps.

The amplifier contains an active RC filter which attenuates at 6 dB/ octave the high frequency response above 60 HZ. (Fig. 2.4) shows the frequency response.

The amplified seismic signals are then frequency modulated at a centre frequency of 3 KHZ (ideal for tape recording). The carrier-frequency deviation is proportional to signal amplitude. The maximum amplified signal is 8 V. P-P and this produces $\pm$ 80% deviation.

System noise at maximum gain, dynamic range is amplifier limited to 52 dB increasing directly with gain reduction until limited to about 60 dB by modulator/demodulator noise.

The head electronics produces a current of 250 μA to saturate the magnetic recording tape.

2.2.3 MSF Radio Time

1. Transmission

The time signals are transmitted on a 60 KHZ carrier from MSF station in Rugby.

The MSF transmits second pulses with the start of each carrier break marking the start of the second.

2. Reception

A Cambridge kits beat-frequency receiver was used during this work with a separately mounted aerial, (Fig. 2.6). The aerial picks up the 60 KHZ signals. A 3 KHZ tone is produced by beating this against an internal oscillator. This tone is off during the second pulses which constitute the time code.

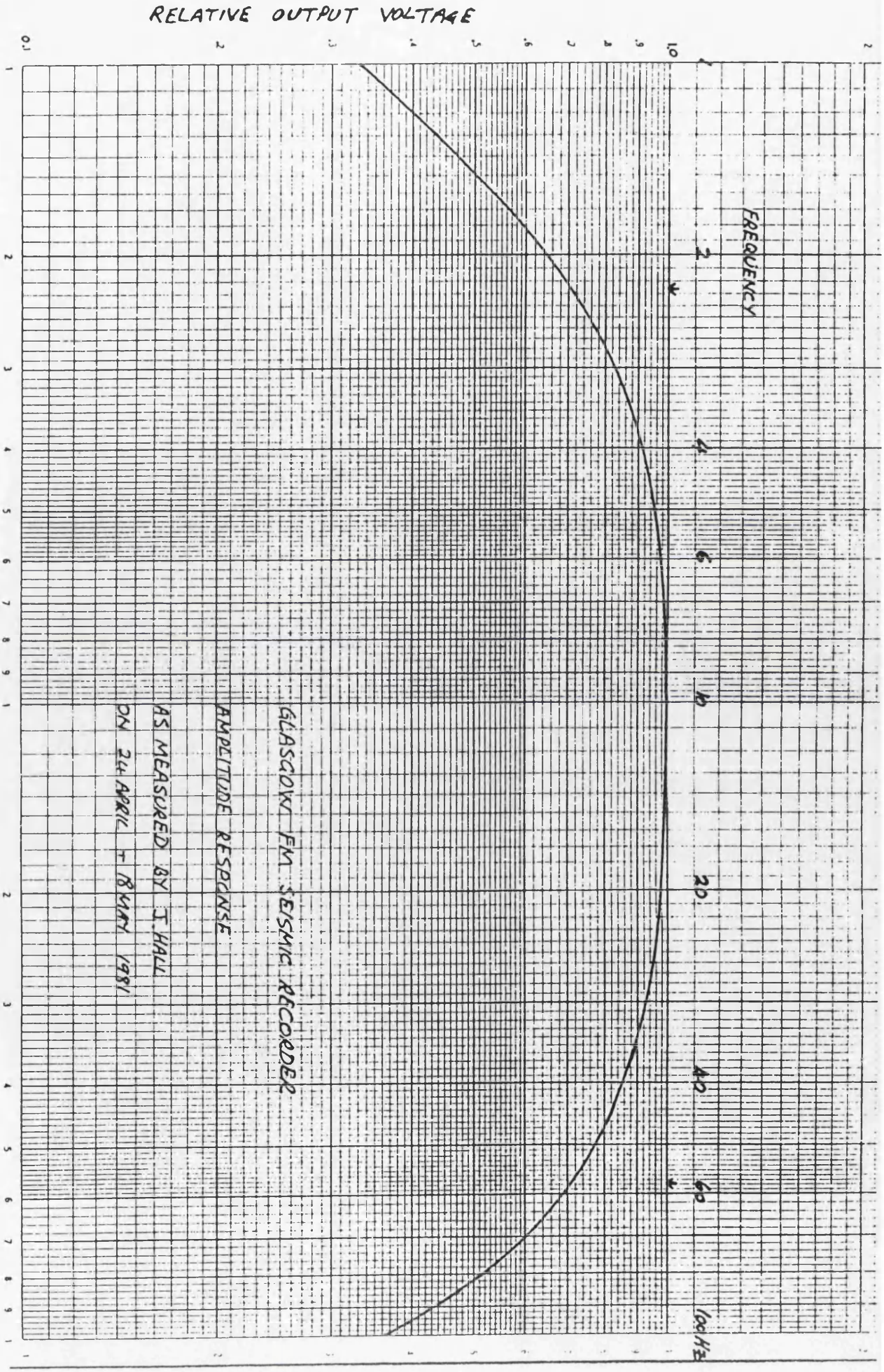

Fig.(2.4) Frequency response of the Amplifier

The code is sent by the length of the carrier break thus 100 ms break is equal to zero, (normal break) and the 200 ms break is equal to one. The pattern of these different pulses throughout a minute carries the information (time, date, identifier), (Fig. 2.5).

The quality (or lack of it) of MSF reception varied more than was expected from the location and position of the receiver and aerial orientation (see Field Operations). Many of the sets needed regular servicing. Interference was experienced near local radio/ TV transmitters.

The Rugby Radio station is off for maintenance between 10.00 - 14.00 GMT or longer on first Tuesday in each month.

2.2.4 Cassette recorder (Fig. 2.8)

The recorder used a commercial cassette tape mechanism fitted with a 4-track head built in a water-proof box. Three of the tracks could be used to record the FM signals on a 3 KHZ carrier from amplifier modulators and the fourth track was permanently connected to record MSF radio-time signals.

The duration of a recording was limited by the cassette to one hour. In the final versions of the sets a digital electronic clock was used to switch the recorder on up to 24 hours after deployment.

Power

The amplifier modulator uses 2 PP7, 9 volts batteries in series, and the recorder with the MSF receiver uses 2 PP9, 9 volts or re-chargeable Ni-Cd batteries in series.

The recorder is provided with a regulator to ensure a 12 v supply to run the tape motor at a constant speed.

An earphone can be used to test that the FM and the MSF signals are reaching the wires to the tape heads.

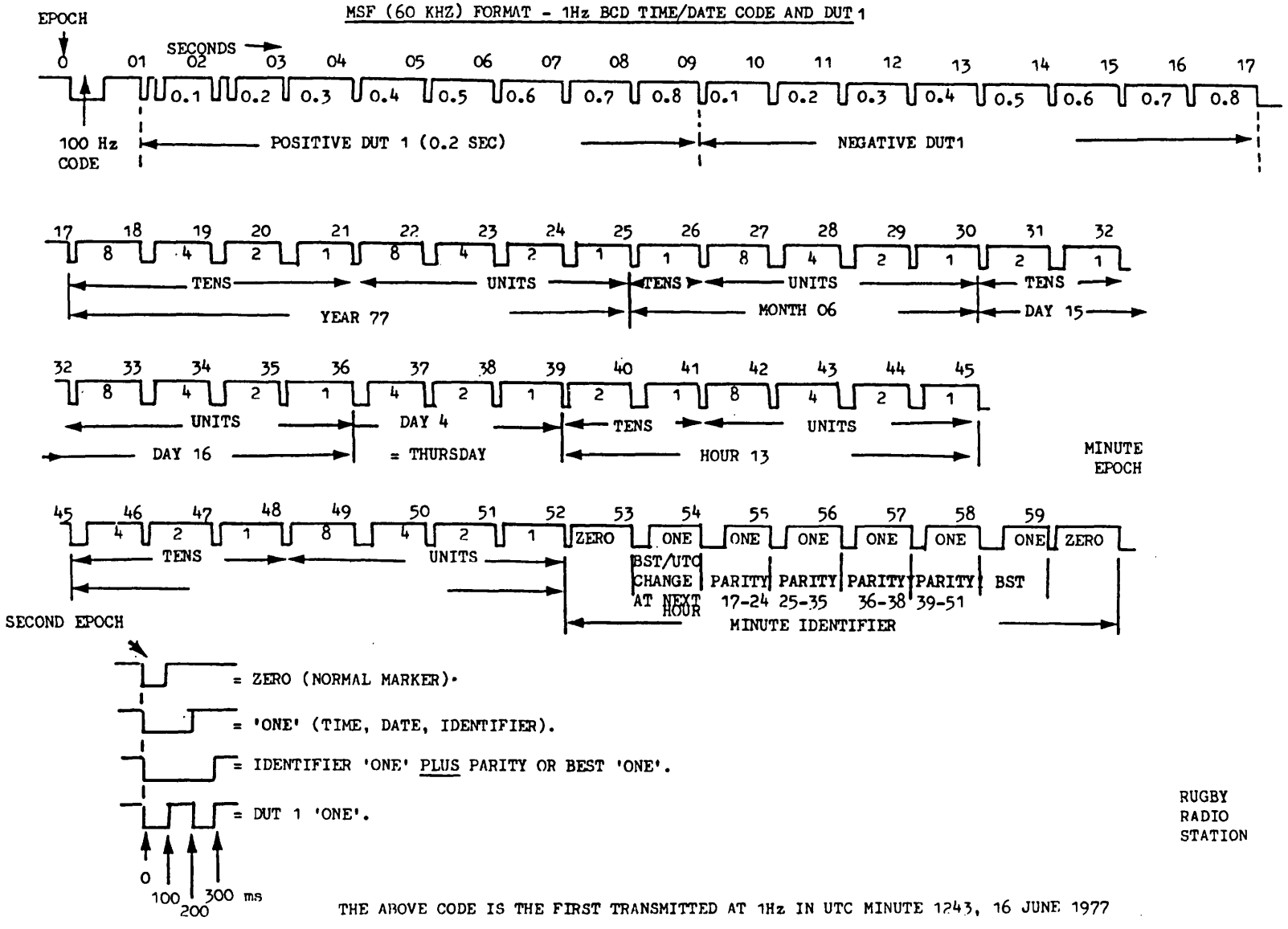

RUGBY RADIO STATION

THE ABOVE CODE IS THE FIRST TRANSMITTED AT 1Hz IN UTC MINUTE 1243, 16 JUNE 1977

Fig. (2.5) shows MSF slow code

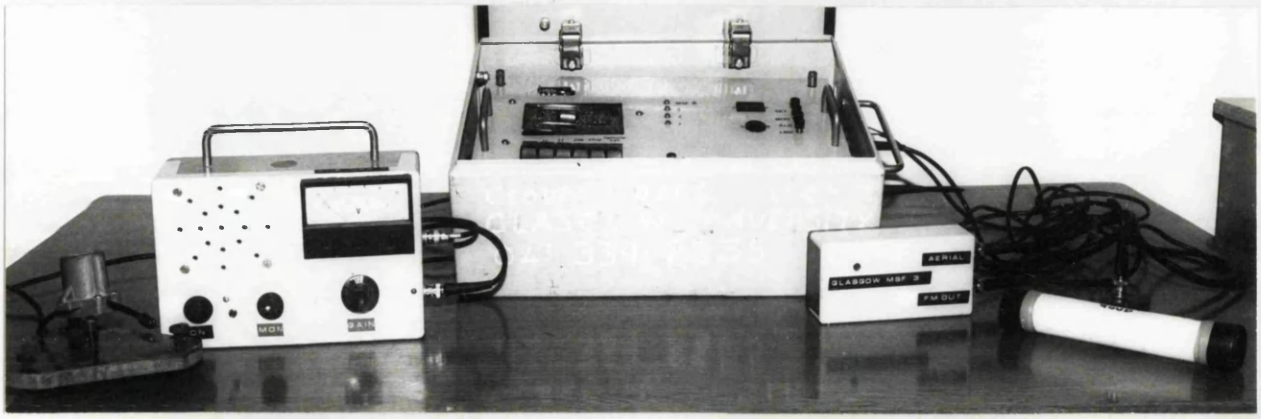

Fig. (2.6) Recording station

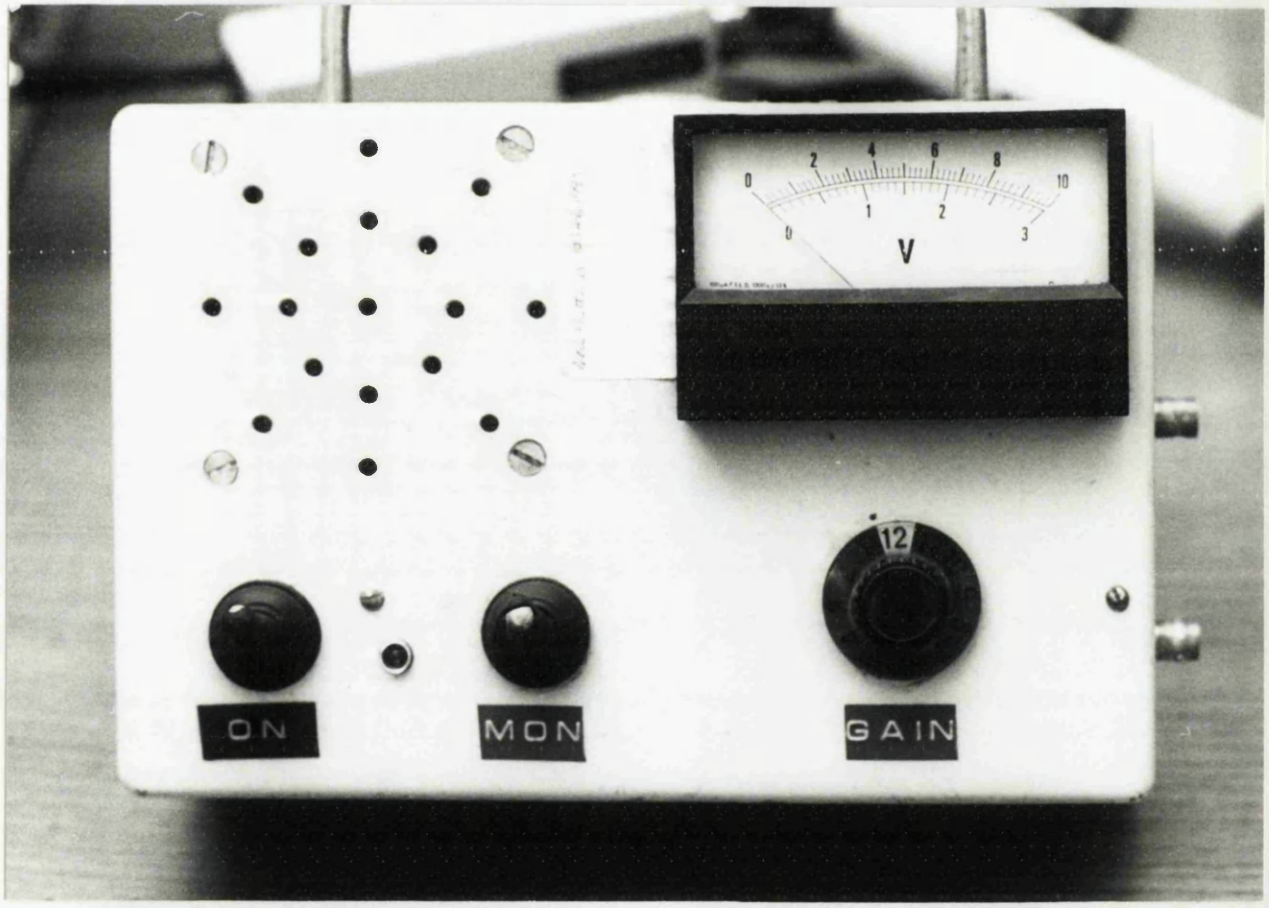

Fig. (2.7) Amplifier/Modulator

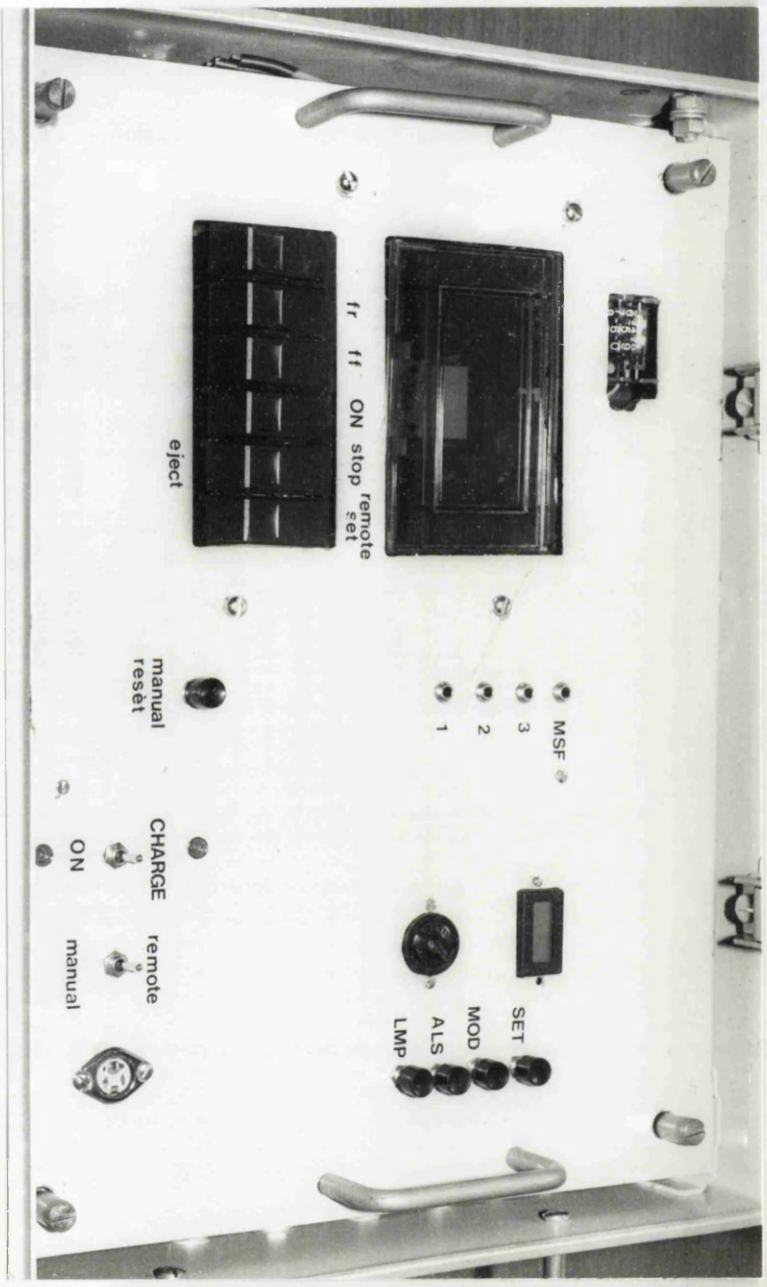

Fig. (2.8) The recorder see section 2.6 P 59

2.3 Playback System

The playback system consists of a cassette player, demodulator, filters and UV recorder, (Figs. 2.9, 2.10).

To recover the seismic signals, the FM recordings are played back in the laboratory at the Geology Department.

The cassette player has low wow and flutter so that it reproduces the FM signals free of instrument noise. The recovered FM signal is amplified and clipped to provide a suitable signal for demodulation.

The demodulator has a buffered input and is followed by a low pass filter to remove any residual FM signal from the demodulated seismic signal. The seismic signal may then be filtered using Kemo variable filters to remove high frequency ambient noise. Filtering was sometimes used between 10 - 30 HZ. Their accuracy is given as $\pm$ 5% of dial setting.

The demodulated seismic signal has a maximum amplitude of 1.5 volts and can now be amplified to a suitable level for driving the galvanometers on a Bryans Southern UV recorder series 40,000, with a selected speed. The speed accuracy is given as $\pm$ 5%.

The galvo-amplifier can amplify the seismic signals over the range 0.01 v/cm to 20 v/cm, and a hard copy of the seismic traces can be obtained.

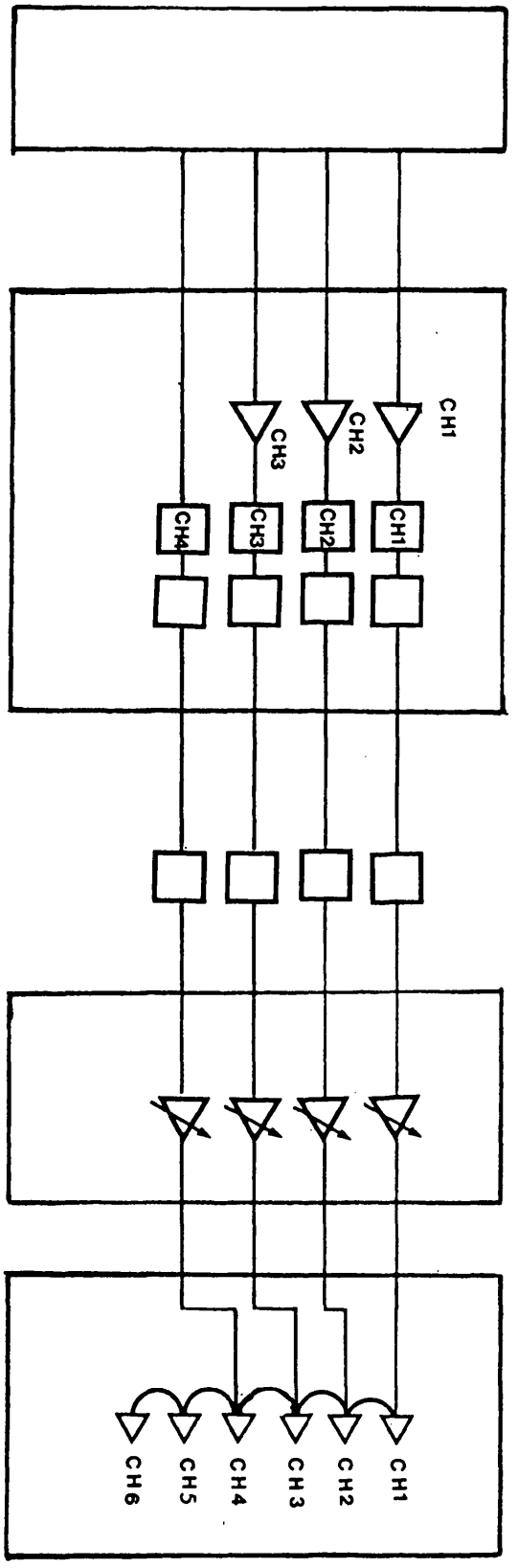

Fig.(2.9) Block diagram showing the complete playback arrangement

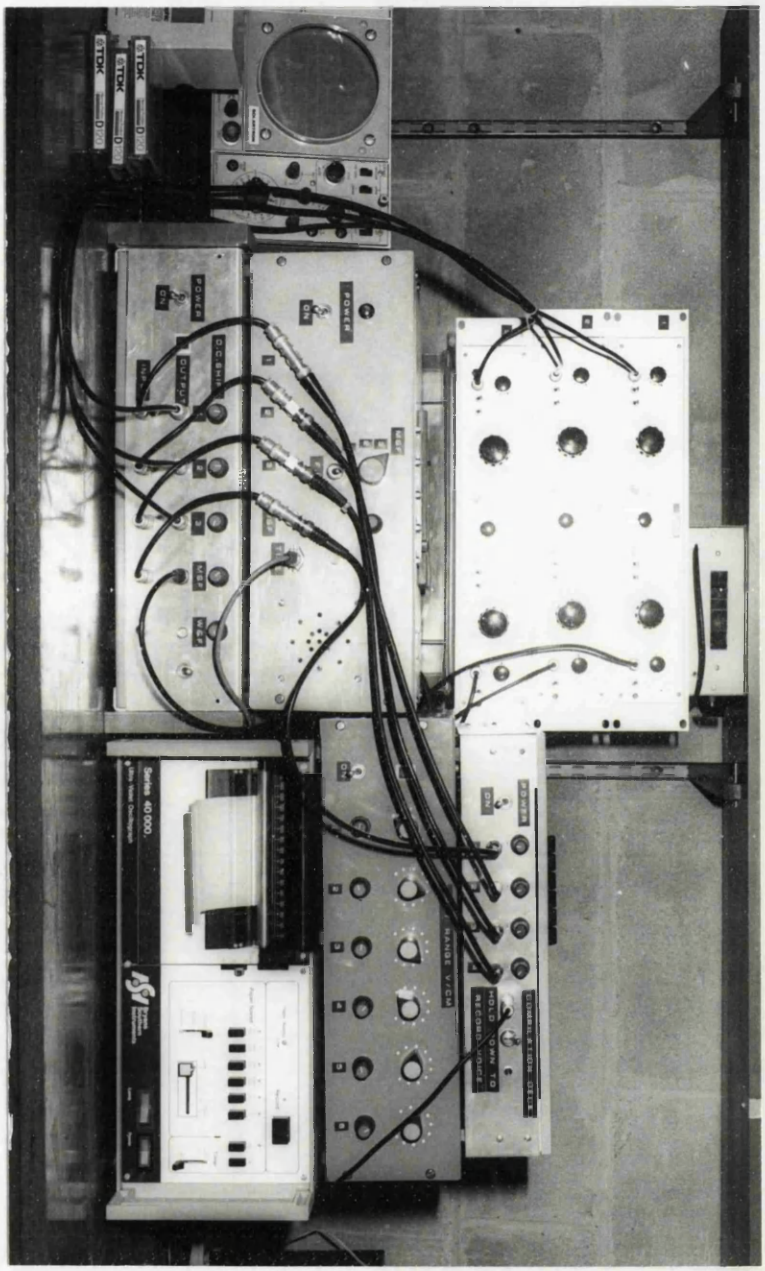

Fig. (2.10) Playback system

2.4 Practical problems in carrying out measurements

In carrying out field measurements, many difficulties may arise and over 25% of deployed sets gave no results, especially during the first year for the following reasons.

1. Quarries blast outside recording window.
2. Blast too small, either not recognisable event or insufficient for accurate picking of arrivals.
3. Local noise by traffic, farmers machines and livestock result as number 2.
4. Bad MSF reception on otherwise acceptable seismic records.
5. Failure of remote to start the recorder.
6. Battery failure, generally in recorder effecting number 4, 5.
7. Vandalism of unattended equipments.

Also quarries did not give advance notice, (recorder not deployed) and MSF transmitter servicing delayed the field work.

2.5 Accuracy of travel times

The overall accuracy has been assessed by repetition of recordings providing at least duplications of time differences. There are such repetitions indicated by (*) in Appendix 1.

Combining these indicates a standard error of $\pm$ 0.02 seconds. The known components of errors are assumed as follows:-

1. Picking onset time in an average signal/Noise ratio of 25 dB, with average filtering of 15 HZ will be in error of $\pm$ 0.017 seconds. (Appendix 3)
2. Interpolating time on same record effect on non-linearity between seconds based on uniformity of second pulses and spaces will give an error of $\pm$ 0.005 seconds.

3. Positional errors are mainly at quarry, movement of quarry face and hence line of shot holes which do not exceed $\pm$ 30 metres gives an error of $\pm$ 0.006 seconds.

2.6 Field operation

In the field layout (Fig. 2.6) the seismometer should be sited away from the noise sources like trees, telegraph poles, high fences, electric fences, falling water and anything that can induce noise in the ground through the effect of the wind upon them.

To maximise the signal/noise the seismometer should ideally be be situated on bedrock, or failing that, firmly planted in a pit about 50 cm deep.

After connecting the seismometer to the amplifier - modulator (AMP-MOD) input the power needs to be on for at least 20 seconds before the circuitry is sufficiently stabilised for the gain settings (in 6 db steps) to be judged; i.e. background noise is not more than 20% of full scale deflection of the amplifier - modulator meter. An audio-test of modulation is also available but the meter indication was found easier to interpret. (Fig. 2.7).

When the amplifier - modulator output is connected to the recorder cable continuity can be checked to a point just short of the tape heads.

MSF reception is checked both by 1 second flashes on LED indicator and by earphone. The aerial position needs to be adjusted to find the clearest (noise free when carrier off) reception.

It then remains to load a cassette and either start recorder manually or at pre-set time in advance from the alarm clock.

a. Manual start, switch the recorder power "on" and switch (remote/manual) to manual. Start the tape by pressing "on" button.

b. Electronic clock start (remote start). Switch power "ON" and (remote/manual) to remote. Set the alarm clock as follows:-

1. Press "ALS" twice within 3 seconds, then set alarm hours to desired time via (SET).

2. Press "ALS" once circuit returns to normal time display with "&" to show alarm signals is on. Depress "ON" button and leave to run 1 hour from alarm trigger, recorder will switch off automatically.

2.7 GLASGOW FM SEISMIC RECORDER SPECIFICATIONS

as used from (1981 - 1983).

Detector	:	Mark Products L15B 4.5 HZ geophones with 600 Ω coil, or alternative.
Amplifier Gain	:	adjustable 46 - 102 dB in 6 dB steps; clipped at 8V p-p (or less if required for better linearity). Input resistance of 4.7 K Ω for 0.65 of critical damping of L15B geophones.
Modulator	:	centre frequency is 3 KHZ; frequency deviation for 8V p-p input is ± 80%.
Recording	:	saturation.
Demodulator	:	produces 1.6V output for maximum modulator input (8V), 14 dB loss reduces overall system gain to the range 32 - 88 dB. Current output is 250μA.
Playback filters	:	Kemo VBF/3.
Oscillograph	:	Bryans 40000 6-channel.
System frequency response	:	these are for direct connection of modulator to modulator; 3 dB down points give approximate pass-band of 2 - 60 HZ.
System noise	:	at maximum gain, dynamic range is amplifier limited to 52 dB increasing directly with gain reduction until limited to about 60 dB by modulator/demodulator noise.
Distortion	:	less than 1% for input signal at 70% of clipping level.
Wow and flutter	:	less than 0.5% (combination of record and playback).
Power requirements for recording instruments	:	Amplifier - modulator 20 MA; 18V. Recorder (during recording) 100 MA; 18V.
Cassette recorder	:	Tape speed 4.75 cm/sec Maximum recording 1 hour Number of channels 4 Recommended tape TDK 120

After J. Hall
G. Gordon

CHAPTER III

TRAVEL TIME PROFILES
AND VELOCITY-DEPTH CURVES ASSOCIATED WITH GEOLOGICAL FORMATIONS

3.1 Introduction

New travel-time profiles have been measured from quarry sources around the Central Coalfield in order to provide a basis upon which to deduce the velocity structure especially that which may be associated with rocks beneath the Carboniferous Sedimentary sequence at outcrop. Some (short) profiles have been made beyond that outcrop to be over those rocks which are expected under the Coalfield. Some profiles and individual shot-receiver connections have been timed to inter-connect the main profiles.

Map (Fig. 3.1) locates the profiles together with pre-existing ones to which reference is made in interpretation and discussion. It also shows the related seismic sources and, for completeness, the detector arrays used to provide the time-term data set discussed in CH. 4. (Table 3.1) explains abbreviations used in (Fig. 3.1) and gives co-ordinates.

The following (Table 3.2) identifies the profiles on the map, gives the thesis locations of lists and figures presenting the travel-times and indicates their contributions to the components of the velocity structure as associated with geological formations which are later sections of this chapter. Inter-connecting profiles/ connections (Appendix 1) which principally contribute delay times relative to an assumed refractor are dealt with in CH. 4.

The LISPB line across the Midland Valley recording shots at Dunkeld (1) and Firth of Forth (E) is included in the same degree

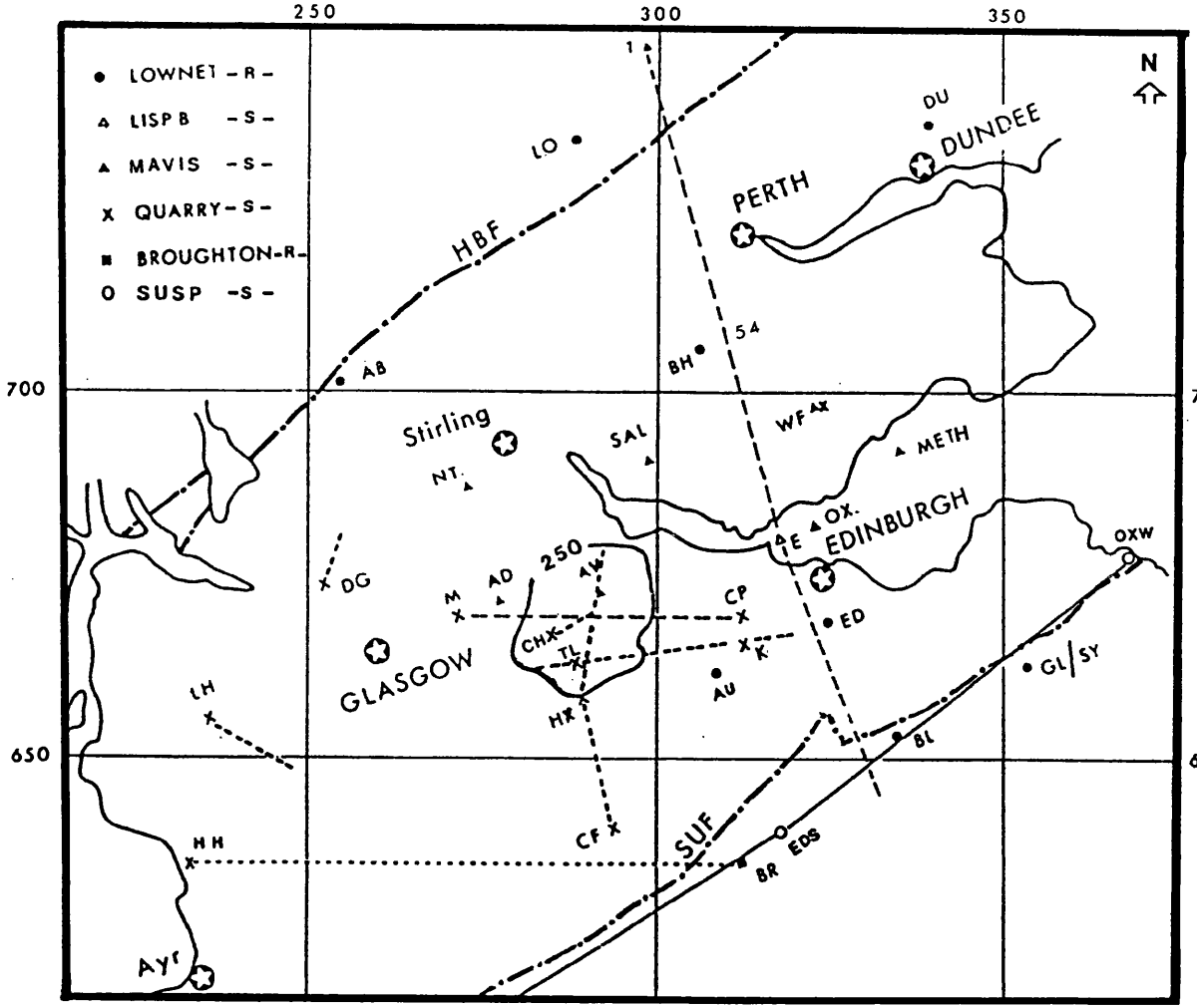

---- Central Midland Valley (CMV)

--- LISPB

···· Southern Midland Valley (SMV)

—— Southern Upland Seismic profile (SUSP)

Bathgate area shown by a 250 nT contour.

Fig. (3.1) Location map showing the seismic lines, sources (S) and receivers (R). See table (3.1) for source and receiver abbreviations and coordinates.

TABLE (3.1) Sources and receivers, co-ordinates and abbreviations.

	Quarry (sources)		Co-ordinates	
			E	N
	CP	Craigpark	312.900	670.400
	M	Medrox	272.895	669.790
	TL	Tamsloup	288.600	664.000
	K	Kaimes	313.800	666.600
	CH	Cairneyhill	284.950	666.550
	HX	Headless Cross	289.120	657.750
	CF	Cairngryffe	294.270	641.275
	DG	Douglasmuir	252.170	674.760
	LH	Loanhead	236.500	655.200
	WF	Westfield	321.260	699.280
	HH	Hillhouse	235.000	634.000
Midland Valley investigation by seismology	MAVIS (shots)		co-ordinates	
	METH	Methil	336.700	692.000
	OX	Oxcars	323.770	680.800
	WF	Westfield	321.110	698.900
	SAL	Saline	299.430	691.530
	NT	Norththird	274.930	688.190
	AV	Avonbridge	291.330	673.870
	AD	Airdrie	277.260	670.020
Lithospheric seismic profile in Britain	(LISPB) (shots)		co-ordinates	
	1	Dunkeld	296.750	747.050
	E	Forth	316.702	683.164

Southern upland seismic profile	(SUSP)	(shots)	co-ordinates E	N
	EDS	Edston	322.764	639.880
	OXW	Oxwellmains	372.271	675.566
Lowlands seismological network	LOWNET	(Receivers)	co-ordinates	
	ED	Edinburgh	325.887	670.659
	AU	Auchinoonhill	308.920	662.201
	AB	Aberfoyle	254.796	701.947
	BL	Broadlaw	334.539	653.824
	GL/SY	Gala Law	353.530	663.349
	DU	Dundee	337.653	739.948
	BH	Blackhill	306.324	707.313
	LO	Logiealmond	294.547	732.238
	BR	Broughton (Receiver)	312.710	635.340

Source line orientation	Appendix Table	Appendix Figure	Velocity components			
			$3.4 < V_d < 4.0$	$4.0 < V_{d(v)} < 5.0$	$5.0 < V_c < 5.7$	$5.7 < V_{b/x} < 6.4$
Tamsloup (TL) (E⟷W)	1 1	2 1,2	3.60±0.13	4.62±0.08	5.25±0.07	?6.07±0.30
Kaimes (K) (E⟷W)	1 2	2 1,2	3.70		4.75±0.06	5.85±0.12
Craigpark (CP) (E⟷W)	1 3	2 1,3	3.61±0.10		5.40±0.15	6.27±0.16
Medrox (M) (E⟷W)	1 4	2 1,3	3.31±0.03	4.21±0.19	5.13±0.17	6.28±0.12
Headless Cross (Hx) (N⟷S)	1 5	2 4,5	3.60±0.06		5.27±0.06	
Cairngryffe (CF) (N⟷S)	1 6	2 4,5			5.05±0.08	
Headless Cross ⟶ North	1 7	2 6,7	3.80±0.07		? 4.72±0.10	5.98±0.17
Tamsloup ⟶ North	1 8	2 6,7		4.20±0.07	4.97±0.08	
Douglasmuir (DG) ⟶ North	1 9	2 8,9		4.42±0.09		
Loanhead (LH) ⟶ SE	1 10	2 10,11		4.50	5.29±0.22	
Craigpark ⟶ East	1 11	2 12,13			4.91±0.13	
Kaimes ⟶ East	1 12	2 12,13			5.27±0.05	
Craigpark ⟶ SW (Near TL)	1 13	2 1,3				?5.85±0.28
Cairney Hill (CH) ⟶ ENE	1 14	2 6,14		4.40±0.12		
Interconnection	1 15					
LISPB Dunkeld (1)		2 15			~ 5.3	5.88±0.03
LISPB Firth of Forth (E) (N⟷S)					~ 5.3	5.98±0.04

as on IGS maps		
	d associates	Carboniferous sediment
	dv associates	Carboniferous lavas
	c associates	Lower Old Red Sandstone
	b associates	Ordovician and Silurian (greywacke shale type)
	x associates	Faster than above

Table (3.2) Identifies profiles on the map, gives Appendices, Tables, Figures and velocity components.

of detail as the new lines since it provides the only profiled basis for comparing the Bathgate/Central Coalfield area with another nearby but off the magnetic anomaly.

3.2 General Features

All the profiles are shown on (Figs. 3.2 and 3.3). In the former symbols distinguish lines, in the latter outcrop under source and receiver.

Initial velocities are seen to correlate with outcrop formations: thus about

4.0 km s^{-1} for d-d

4.5 km s^{-1} for v-v (See fig 3.3)

5.3 km s^{-1} for c-c

and 5.7 km s^{-1} for Dalradian.

Lateral changes can, therefore, be expected across some formation boundaries especially where large thicknesses are involved at faults. This is clearly seen across the Highland Boundary Fault (LISPB 1⟶E) because the lower velocity is more distant. It occurs in the opposite sense on the d-c lines, (Fig. 3.3).

Long enough profiles tend to an apparent velocity around 6.0 km s^{-1}. On d-d lines this is beyond 15-20 km. Where Lower Old Red Sandstone is involved it may be sooner (as south of Edinburgh but the lines are not long enough) or later (LISPB 1⟶E).

3.3 Velocity - depth values from WHB integrals

For the most part the slopes of the curves decrease rather regularly and are, therefore, as compatible with continuous as with discontinuous velocity functions. Where velocity increases only with depth and there are no loops in the time-distance graph due to sudden changes in the velocity-depth curve, the WHB integral

$$z(v) = \frac{1}{\pi}\int_0^{\Delta} \cosh^{-1}\left(v\,\frac{dt}{dx}\right) dx \quad \text{where } \frac{1}{v} = \left(\frac{dt}{dx}\right) \quad x = \Delta$$

(see Grant and West, 1965, p. 139)

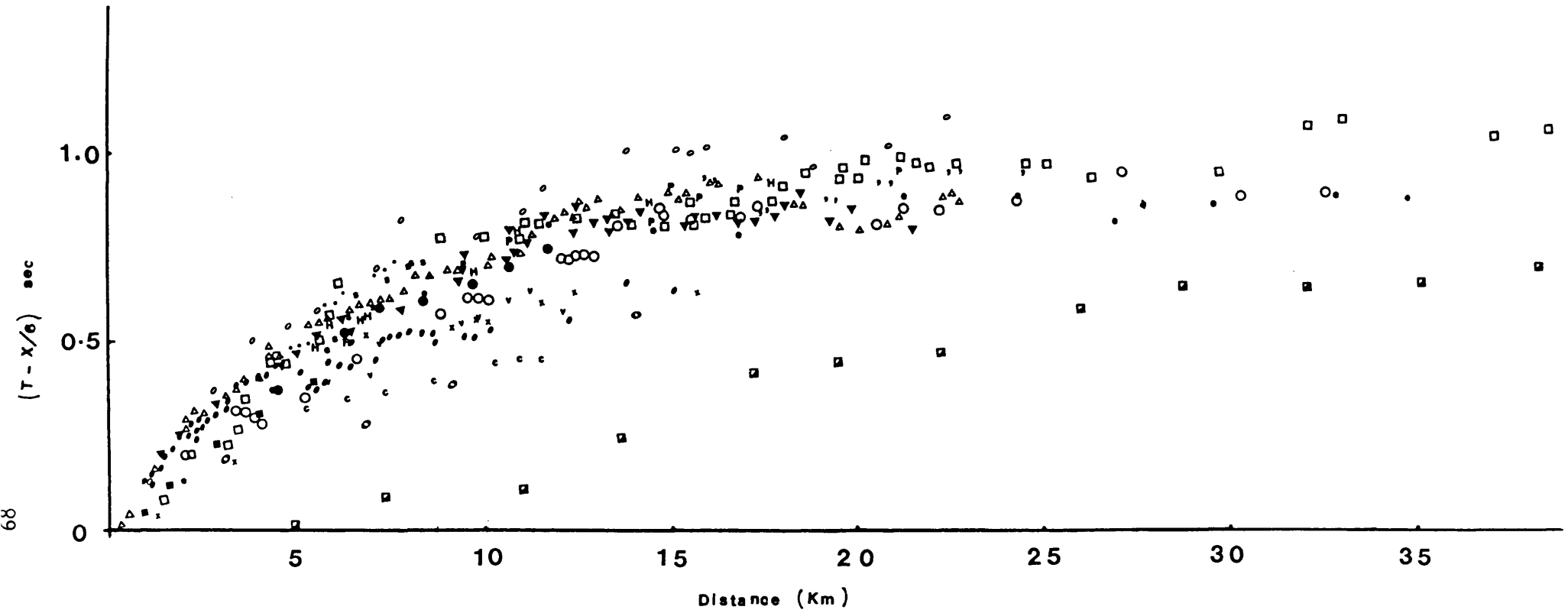

△	TL - East	•	HX - South	v	CP - East	,	CP - TL
○	K - West	o	CF - North	C	K - East	■	DG - North
□	CP - West	·	CH - North East	s	TL - Avonbridge	e	LISPB (E - 1)
o	M - East	●	TL - North	H	TL - Salsburgh	◪	LISP (1 - E)
▼	HX - North	x	LH - South East	P	HX - Salsburgh		

Fig. (3.2) Gross plot of the data related to different lines.

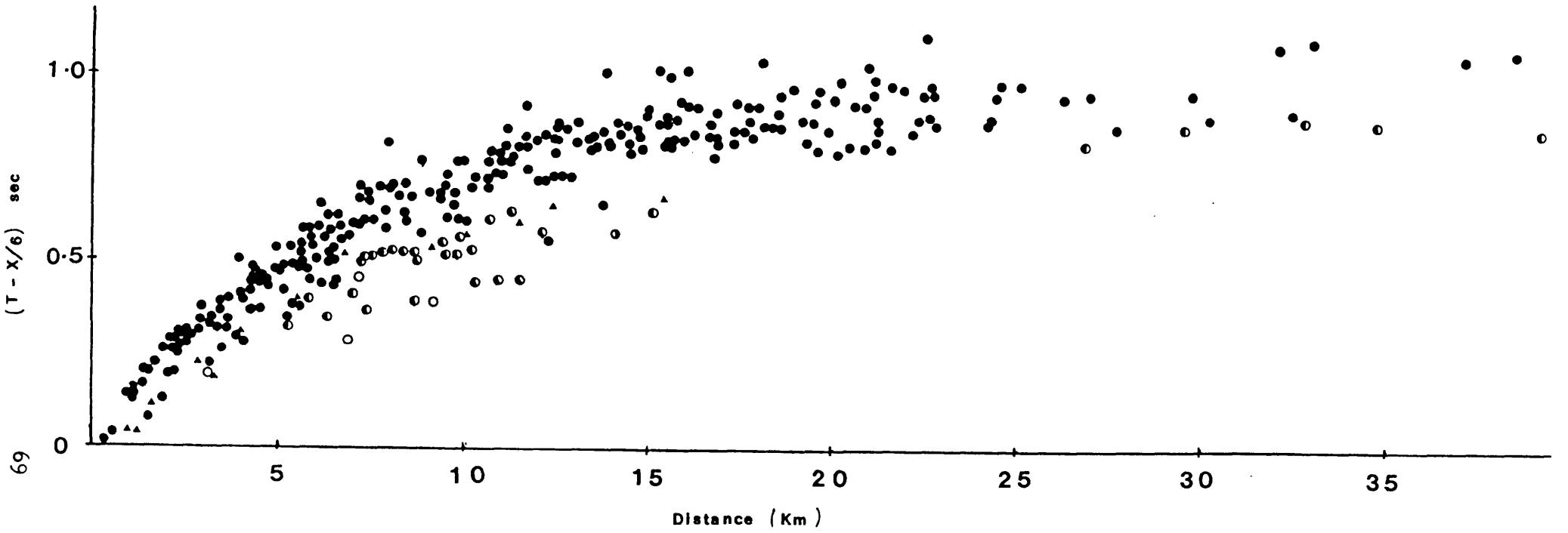

•	S/R over Carboniferous sediments	d — d
◐	S over Carboniferous sediments R over Lower Old Red Sandstone	d — c
◑	R over Carboniferous sediments S over Lower Old Red Sandstone	c — d
○	S/R over Lower Old Red Sandstone	c — c
▲	S/R over lavas	v — v

See Table 3.2 for abbreviation lett

Fig. (3.3) Gross plot of all the data related to outcrop under source (S) and receiver (R).

can be used to determine the depths at which a particular velocity is achieved by integration of the T - X graph.

These integrals have been calculated for ten profiles (Table 3.3) using a program, written by Dr.J . Hall, which takes as input an equispaced (here 1 km) sequence of T - X/6 values smoothed to ensure progressively decreasing differences.

In regard to smoothing, several lines (LH, DG, TL and CP) show a first time difference smaller than the succeeding few values. This has been removed by projecting to an assumed earlier origin time (-0.05 sec. at most). No single adequate explanation of this feature has been thought of. Both TL and CP are quarries in dolerite sills which may transmit energy faster than the surrounding Carboniferous sediments. At ranges beyond a few wavelengths, say 1 km, propagation of energy would involve a greater thickness of rock than the sill (itself less than a wavelength thick). The transmission velocity would then be reduced. LH and DG, however, are not in sills but show the same phenomenon. The shot instant might be recorded too late due to a distance estimate error because of the pattern of delays controlling the detonation between shot holes. The seismometer was generally placed about 20 m offset behind the face from the centre of the shot hole line. A 50 m error is very unlikely. Equally unlikely is a velocity of 1 km s^{-1} (for 0.05 sec.) even through fissured rock according to recordings near to single hole shots in such quarries (Al-Azzawi 1982, unpublished thesis).

Whilst LH combined with DG provide velocities below a Carboniferous lava outcrop and M, CP, TL, K and HX those below a Carboniferous sediment outcrop, only CF is directly available to follow Lower Old Red Sandstone velocities from the surface. The line from

(V_p Km s^{-1})

Depth (Km)	DG LH	M	CP	K	TL	HX N (L)	HX S (L)	E-1 (L)	1-E (L*)	CF
0	3.7	3.2	3.6	3.6	3.4	3.3	3.2	3.3	4.2	4.3
		3.6	3.6	3.5	3.5				4.2	
0.5	4.3	3.9	3.9	4.2	4.0	4.1	4.1	4.0	4.9	4.9
		3.6	3.6	3.6	3.8				4.5	
1.0	4.7	4.3	4.3	4.6	4.6	4.6	5.0	4.4	5.2	5.3
		4.5	3.7	5.3	4.6				4.8	
1.5	5.0	4.6	4.6	4.9	4.7	4.8	5.3	4.8	5.3	
		4.6	5.3	5.4	4.7				5.0	
2.0	5.2	4.9	5.0	5.2	4.9	5.2	5.7	5.2	5.4	
		5.3	5.3	5.4	5.3				5.2	
2.5	5.5	5.1	5.2	5.3	5.2	5.4	5.9	5.3	5.5	
		5.3	5.4	5.5	5.4				5.3	
3.0		5.4	5.4	5.5	5.6	5.6		5.5	5.6	
		5.3	5.4	5.6	5.5				5.4	
3.5		5.7	5.7	5.7	5.8	5.8		5.7	5.8	
		5.4	5.4	5.7	5.6				5.5	
4.0	5.9	5.9	5.9	6.2				5.9	5.9	
		5.5	6.0	6.1	6.1				5.6	
4.5			5.95					6.0		
		6.1	6.1							
5.0								6.1	6.0	
5.5									6.1	
6.0										
6.5									6.2	
7.0								6.2	6.2	
7.5										
8.0								6.3	6.3	
8.5								6.4		

L = lateral change probable
L*= correction for lateral velocity change

Table (3.3) results of WHB calculation with velocities interpolated at 0.5 km depth interval.

Ray traced tested values are underlined.

CF lacks detail (this quarry only blasts twice a year) and length (Carboniferous outcrop begins beyond 15 km).

It was thought that the LISPB recordings across the Lower Old Red Sandstone outcrop from the Dunkeld (1) might be used for this purpose. This requires that the ray paths to these receivers only diverge significantly after crossing into the Lower Old Red Sandstone i.e. that they have a virtually common 12 km path to a shallow point at the Highland Boundary Fault which can be treated as an effective origin. The published LISPB model has one condition which would favour this result i.e. a weak velocity gradient within the Dalradian ($\sim$0.1 km/s/km). It does not, however, have a sharp cut-off of the Sub-Old Red Sandstone refractor at the fault which is shown to dip gently south. A boundary with 5 km s^{-1} on 6 km s^{-1} dipping 45° S would spread the required emerging rays across it over a depth range of 2 km. A vertical or even north dipping boundary is, however, geologically predicted (Appendix 2, fig. 15) and should help to constrain the ray paths as required. On the other hand, a probably higher velocity unit (Highland Border Series) underlies the Lower Old Red Sandstone and may form a downward widening wedge more like the LISPB model velocity distribution.

Nonetheless, when a corrected origin is used, at $T - X/6 = 0.15$ and 12 km from actual origin, the LISPB and CF profiles begin similarly. The WHB results in (Table 3.3) relate to them. Since, however, the velocity of this result is doubtful a ray traced model based on it was devised to test it. It was found that the ray paths did diverge before crossing the fault and that the travel times were too fast.

Adjustment of the velocities to match the observed times resulted in the underlined figures in (Table 3.3). Ray trace velocities for other lines are similarly shown. They differ from the WHB results more because of step-like velocity-depth functions than because of lateral changes.

(Fig. 3.4A) shows the continuous velocity-depth functions from (Table 3.3) together with similar types of curve from other sources. The curves are labelled to indicate the geological formation to which they apply at their outset.

d-d is from M-CP 0 to 4 km depth

v-v is from LH/DG 0 to 1.5 km depth

c-c is from LISPB (1→E) ray traced 0 to 4.5 km depth

c'-c' is from CF 0 to 1 km depth

c* is from Lesmahagow applicable to Lower Old Red Sandstone 0 to 1 km depth (Davidson 1984)

b* is from Lesmahagow applicable to Silurian 0 to 1 km depth (Davidson 1984)

b is from EKA applicable to Silurian and underlying rocks 0 to 8 km depth (El-Isa 1977 and Jacob 1969).

The ray trace tested velocity-depth profiles from (Table 3.3) are plotted graphically in (Fig. 3.4B) together with other similarly derived results from other sources (LISPB model, SUSP model). The alternative LISPB result from (Fig. 3.4A) is included for comparison.

3.4 Velocity-depth fields for geological formations

The WHB velocity-depth values may be correlated with geological formations either certainly present (boreholes) or likely to be present (straightforward geological projection) in a depth interval

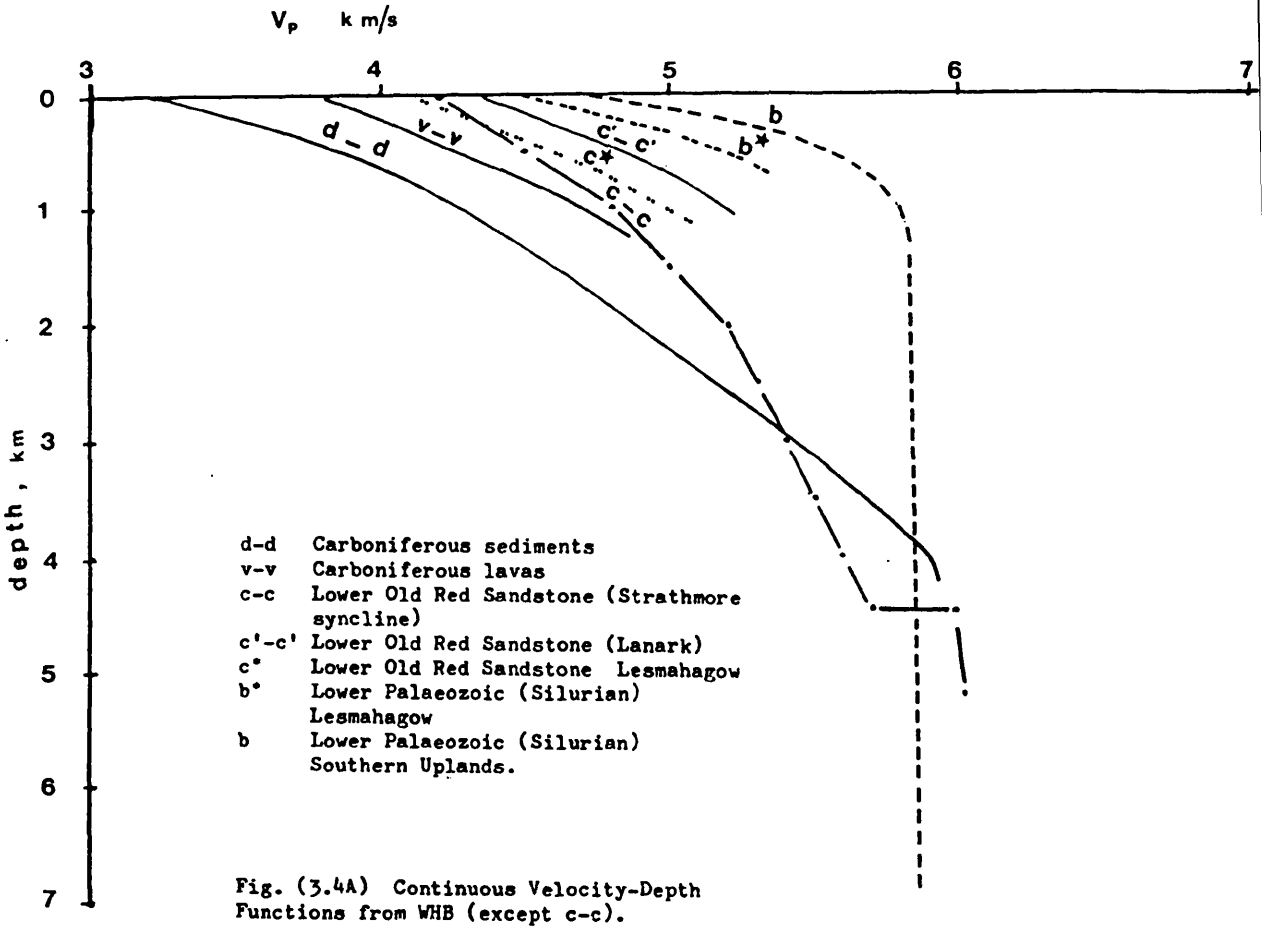

d-d Carboniferous sediments
v-v Carboniferous lavas
c-c Lower Old Red Sandstone (Strathmore syncline)
c'-c' Lower Old Red Sandstone (Lanark)
c* Lower Old Red Sandstone Lesmahagow
b* Lower Palaeozoic (Silurian) Lesmahagow
b Lower Palaeozoic (Silurian) Southern Uplands.

Fig. (3.4A) Continuous Velocity-Depth Functions from WHB (except c-c).

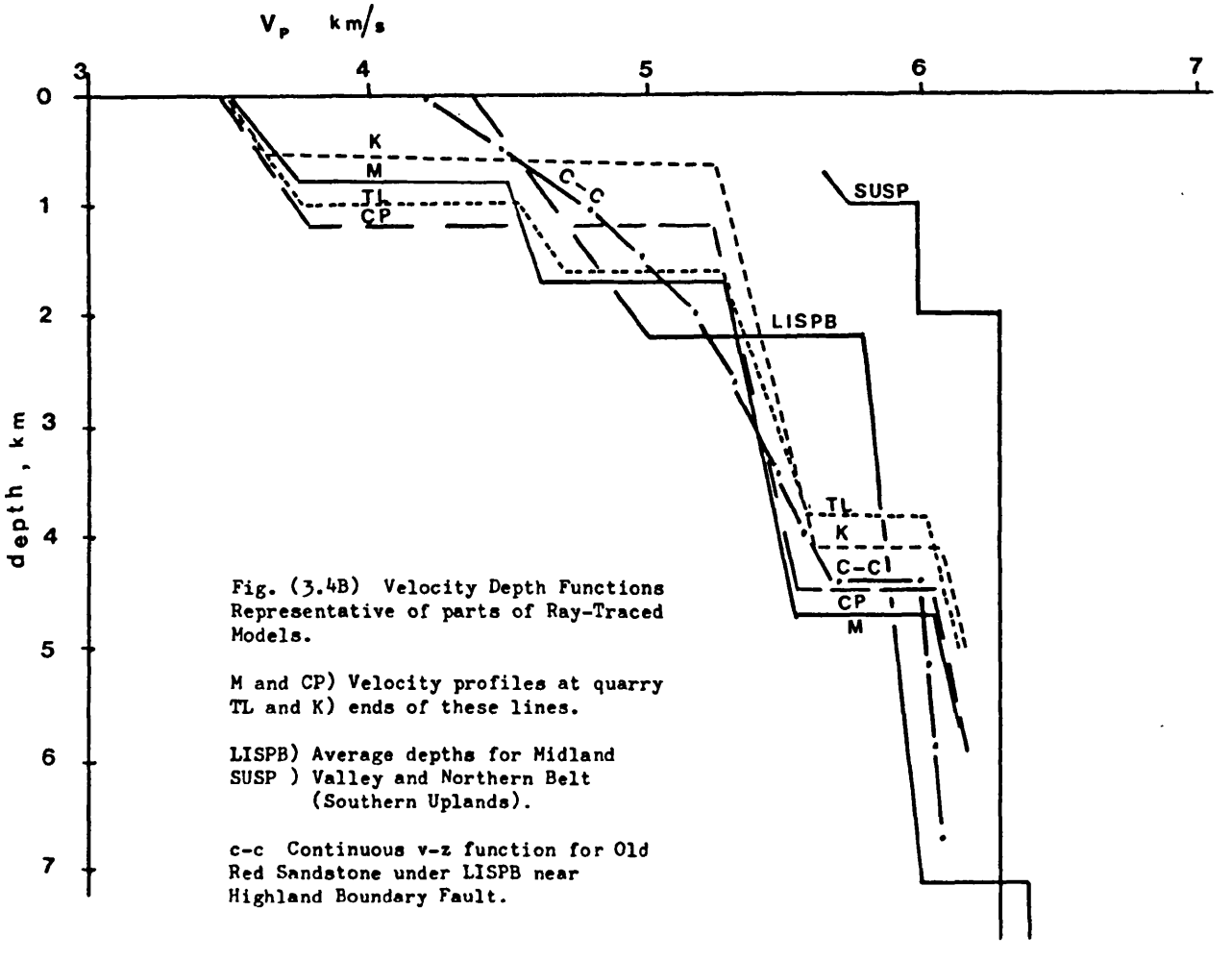

Fig. (3.4B) Velocity Depth Functions Representative of parts of Ray-Traced Models.

M and CP) Velocity profiles at quarry
TL and K) ends of these lines.

LISPB) Average depths for Midland
SUSP) Valley and Northern Belt (Southern Uplands).

c-c Continuous v-z function for Old Red Sandstone under LISPB near Highland Boundary Fault.

(see cross-sections in Appendix 2, embodying projections of varying degrees of probability).

On the velocity-depth plot of (Fig. 3.5) formations symbols (d,v,c,b) have been placed in appropriate positions to represent the correlation. Other symbols are explained in sub-sections which follow.

3.4.1 Carboniferous sediments (d)

The pattern of (d) symbols derives from profiles TL, M, CP, HX and K. The upper velocity boundary separates (d) from the (v) symbols derived from LH/DG. At 1 km depth between M and CP is the control point on the boundary determined by its depth in the Slamannan borehole (underlined). No deeper Carboniferous sediments are proved on any line but may exist within the area (Methil in Fife).

Treating the refraction model as one of constant velocity layers the set of profiles used for the WHB results gives 3.63 ± 0.08 km s^{-1} at a mean depth of 0.5 km. Hall (1970 and 1978) for similar data in the western Midland Valley and Firth of Clyde gives 3.61 ± 0.10 km s^{-1} and 3.80 ± 0.05 km s^{-1} respectively. The overall mean 3.68 ± 0.14 km s^{-1} is shown at a mean depth of 0.5 km (1 on Fig. 3.5). Drysdale (1955) in Firth of Forth observed a mean velocity of 3.12 ± 0.23 km s^{-1} at shallow depth 0.18 km (3 on Fig. 3.5). Seventeen Spilmersford borehole velocity log values for Carboniferous sandstone, siltstone, shale, tuff and agglomerate (Allsop 1974) (Table 1.2) give 3.78 ± 0.32 km s^{-1} at a depth of 0.34 ± 0.2 km (2 on Fig. 3.5).

3.4.2 Carboniferous lavas (v)

The (v) symbols on (Fig. 3.5) are derived from the WHB values from profiles DG/LH, TL and M. The lower boundary (underlined) is determined by the control point at 2 km depth from Slamannan borehole

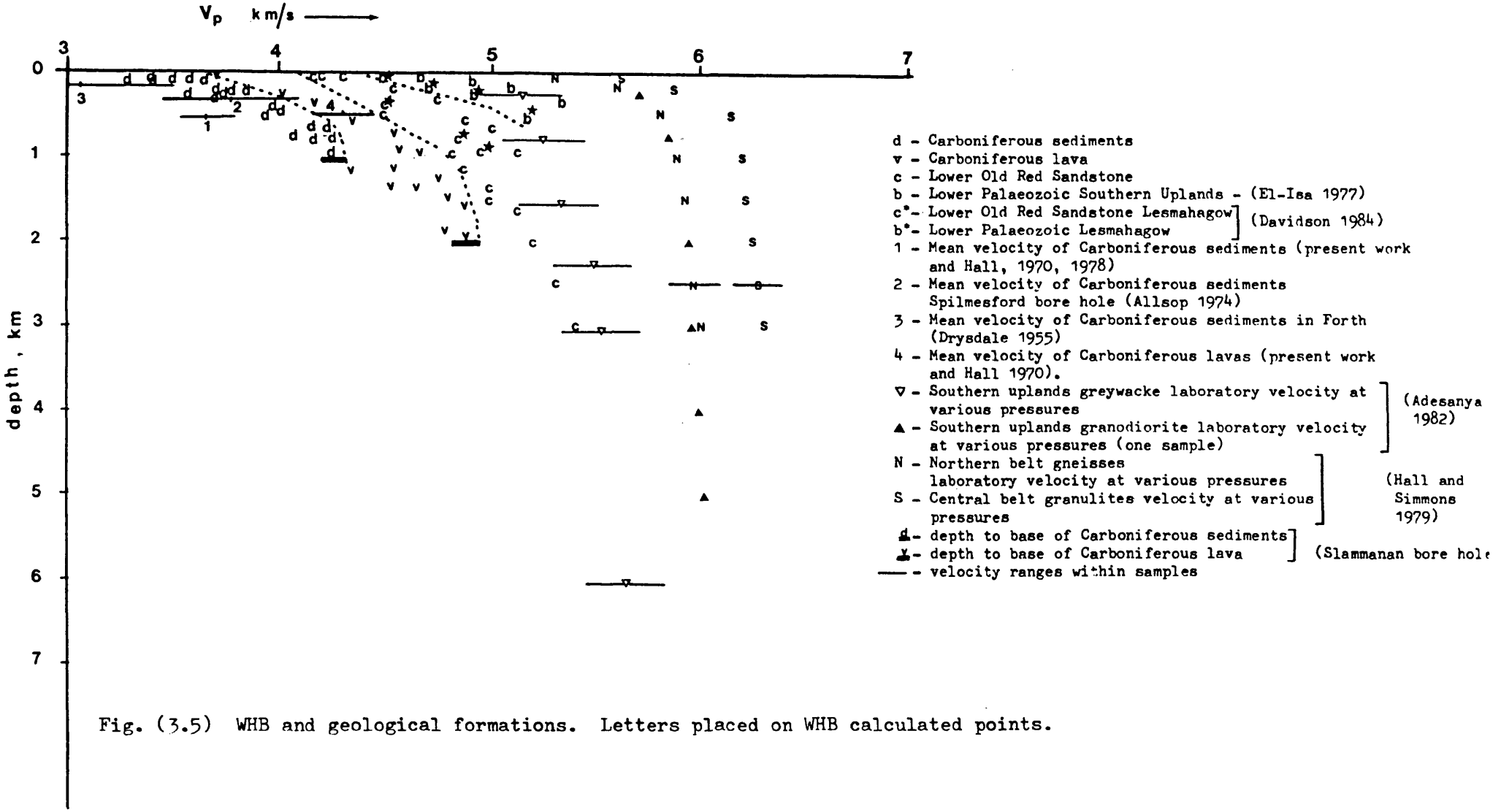

Fig. (3.5) WHB and geological formations. Letters placed on WHB calculated points.

near the M-CP line combined with a reflection survey interpreted as indicating the lava base (Hall 1974), treated as a constant velocity layer.

The combined DG/LH refraction profile gives a mean velocity of 4.46 ± 0.09 km s^{-1}. Hall (1970 and 1978) observed velocities of 4.14 ± 0.11 km s^{-1} and 5.00 ± 0.05 km s^{-1} respectively. Since the nature of the 5.00 km s^{-1} layer is unproven beneath a sedimentary layer under the Firth of Clyde it is not sufficiently direct evidence for inclusion here. The remaining two estimates provide a mean of 4.31 ± 0.14 km s^{-1} at an approximate depth of 0.5 km (4 on Fig. 3.5).

The Spilmersford borehole sonic log indicates velocities up to 4.70 km s^{-1} through a lava section (0.47 km deep). The lower 4.30 km s^{-1} refraction result is consistent with this since it represents a mean for several 100 m thickness of rock not all of which is lava. Thus within the "lava layer" in the Slamannan borehole basalt and sediment occur in the ratio 3 to 1 which would give around 4.30 km s^{-1} parallel to the bedding of a transversely isotropic model ($Vp1$ = 4.70 km s^{-1}, $Vp2$ = 3.60 km s^{-1} and normal Poisson's ratios and densities) (Postma 1955).

Refracted arrivals from the top of those lavas are indicated on 4 profiles (see Table 3.2).

3.4.3 Upper Old Red Sandstone (c3 with d)

No refraction measurements yet made on Upper Old Red Sandstone outcrop in the Midland Valley. The reddened sandstones and conglomerates towards the base of the Spilmersford borehole are similar to and may be of Upper Old Red Sandstone. These sandstones have a porosity about 10%, a bulk density of 2.54 gm cm^{-3} and a log velocity of 4.40 km s^{-1}. At higher levels within the Lower Carboniferous the corresponding values are 20%, 2.32 gm cm^{-3}

and 3.34 km s^{-1}.

A linear relationship between the reciprocal velocity and bulk density is commonly used in well log interpretations. There are different lines for different lithologies dependant upon the matrix (zero porosity) values of density and velocity. For quartz sandstones (2.66 gm cm^{-3} and 5.52 km s^{-1}) the line is:

$1/V$ km s^{-1} = 0.88 - 0.264 ρb gm cm^{-3} .

The Spilmersford sandstones plot 0.4 km s^{-1} slower over the density range on a line with 1.063 intercept and -0.329 slope indicative of matrix values 2.70 gm cm^{-3} and 5.74 km s^{-1}. This is towards the Limestone line (2.71 gm cm^{-3} and 6.44 km s^{-1}). The measured grain density is 2.70 gm cm^{-3} and calcite cement occurs in the rocks. Shale impurity is indicated by the nuclear logs.

The average densities measured on Upper Old Red Sandstone sandstones and fine conglomerates elsewhere are, however, about 2.41 gm cm^{-3} (McLean, 1961). This gives 3.70 km s^{-1} on the Spilmersford line and 4.10 km s^{-1} on the Sandstone line.

The densities and porosities of coarser conglomerates within the Upper Old Red Sandstone are not known. Porosities are likely to be less than for sandstones because of poorer sorting. Higher bulk densities and velocities can therefore be expected - though no higher than Lower Old Red Sandstone rocks of similar type.

Seismically the Upper Old Red Sandstone has been considered here as part of the Carboniferous velocity group with which it is conformable.

3.4.4 Lower Old Red Sandstone (c)

The (c) symbols on (Fig. 3.5) represent WHB based values from profiles CF, HX (south) and K (west) and also ray-trace tested

values for the velocity structure against the Highland Boundary Fault on the LISPB line. The depth ranges are based on geological projections (Appendix 2, Figs. 2,4,5 and 15). The c* symbols are for the Lesmahagow area (Davidson 1984). Only on CF is there a first segment representing an uncomplicated direct arrival through these rocks (5.05 ± 0.08 km s^{-1}).

None of these profiles distinguish Lower Old Red Sandstone lavas from sediments. Apparent velocities across the Pentlands' volcanic outcrop have been recorded from K and CP for this purpose (Appendix 2, Figs. 12 and 13). The asymmetry of the Carboniferous delays under the quarries which are missing under the recording sites precludes useful WHB analysis. The mean apparent velocity of second segments on these profiles is 5.09 ± 0.14 km s^{-1} indicating a velocity indistinguishable from the sediments. Davidson (personal communication) reaches a similar conclusion from measurements near Biggar. The similarity of densities between these sediments and lavas is further confirmation (Mclean 1961).

There are, however, density differences between the sediments from different areas from which velocity differences follow.

Area	Pb gm cm^{-3}	P grain gm cm^{-3}	V calculated 'Sandstone line' km s^{-1}	'Spilmersford line' km s^{-1}
S. Ayrs. (McLean) 1961	2.60	2.70	5.17	4.82
N. Ayrs. (Walker) 1969	2.52	2.59	4.65	4.27
Stirlings. (Qureshi) 1970	2.51	-	4.60	4.22

There is less basis for choosing one velocity column rather than the

other now than for the Upper Old Red Sandstone case. The conglomerate factor (3.4.3) is likely to apply.

The Lower density/Spilersford line values (4.2 - 4.3 km s^{-1}) are required within the top 0.5 km of the LISPB line model. The higher density/Sandstone line values, not attained until 2 km depth near the Highland Boundary Fault are found at half that depth in the south (CF). Under the Central Coalfield at depths of 2 or 3 km, a velocity of 5.3 km s^{-1} could be expected.

3.4.5 Lower Palaezoic (b)

No new measurements on Lower Palaeozoic outcrop have been made as part of this work. Measurements within the Midland Valley are restricted to Lesmahagow and provide line b* (Figs. 3.4A and 3.5) showing an increase from 4.00 to 5.50 km s^{-1} within a km from the surface (Davidson 1984).

In the Southern Uplands close (10 km range) shots into EKA provide line b (Fig. 3.4A and 3.5) showing an increase from 4.50 to 5.60 km s^{-1} within a km from the surface (El-Isa 1977). This extends back to the surface an inversion of apparent velocities from more distant shots in various azimuths (Jacob 1969), (Fig. 3.4A). Travel times across the Southern Uplands on LISPB (shots E and 2 into segment BETA) are the basis for the 5.80 - 6.00 km s^{-1} Lower Palaeozoic layer to over 10 km depth on that model (Bamford 1977, 1978). Higher along strike velocities on SUSP and into EKA suggest that the previous deep velocity projections are averages across unresolved structure (Hall et al 1983). The Lower Palaeozoic valuation of the same layer, 5.80 - 6.00 km s^{-1}, under the Midland Valley in the LISPB model (Fig. 1.20) is then subject to question also.

Laboratory velocity measurements at various pressures on

Lower Palaeozoic greywackes from the Southern Uplands (Adesanya 1982) do, however, provide a basis for extrapolation to depth (1 K bar) equivalent to 3 km, (Fig. 3.5 symbol ▽ through which the bars represent the range of values in the samples).

(Fig. 3.5) now suggests that velocities in Lower Old Red Sandstone and Lower Palaeozoic will overlap at depths between 1 and 3 km. (The greater depth applies to the Strathmore basin data from LISPB where the Lower Old Red Sandstone is considered at least that thick). Furthermore, it seems unlikely that the velocity of either group, whilst constituted of sandstone, conglomerate, greywacke and shale, will exceed 5.75 km s^{-1} at depths less than 5 km. Since (Fig. 3.4B) suggests velocities of 5.90 km s^{-1} or more at this depth possible lithologies are now considered.

3.4.6 Lithologies with velocities $\geq$ 5.90 km s^{-1} at 4 to 5 km depth

A. SEDIMENTARY ROCKS

Carbonate sediments come into this category,

for limestone; $\frac{1}{V}_{LST} = 0.155 + 0.462\phi$

and for dolomite $\frac{1}{V}_{DOL} = 0.143 + 0.474\phi$

where ϕ is the fractional porosity and V in km s^{-1}. Thus V $\geq$ 5.90 km s^{-1} in limestone for $\phi \leq 3.1\%$ and in dolomite for $\phi \leq 5.5\%$. Vuggy porosity is feasible and a km thickness of Cambro-Ordovician dolomite occur on the Caledonian foreland in NW Scotland.

B. IGNEOUS ROCKS

Plutonic rocks of intermediate composition have velocities

in this category. As an example laboratory measured values under confining pressures for a granodiorite (▲) are plotted on (Fig. 3.5) (from Adesanya, 1982). On a mineralogical basis he estimated a granite line close to upper greywacke limit and a diorite line close to the (s) symbols on (Fig. 3.5).

C. METAMORPHIC ROCKS

Dalradian. The travel-times on LISPB across the Dalradian outcrop have been modelled by a layer with velocities rising very slowly with depth to about 6.05 km s^{-1} at $\sim$ 10 km (Fig. 1.20)

Lewisian. Laboratory measurements on Lewisian gneisses (amphibolite facias) and pyroxene granulites from the Northern and Central Belt outcrops in N & S Scotland (Hall and Simmons, 1979) are shown in (Fig. 3.5), (N and S respectively).

Further discussion about the possible lithology at depth under the Midland Valley follows the evidence on structure in CH. 4.

CHAPTER 4

REFRACTOR VELOCITY, DELAYS AND DEPTHS (STRUCTURE)

4.1 Introduction

The reduced time graphs (Appendix 2) show progressive acceleration out to 15 or 20 km range and then become relatively linear at close to the reduction velocity of 6.00 km s^{-1} for the next 30 km. On the velocity-depth models (Fig. 3.4B) this straight segment transforms into a layer extending between 3 to 4 and 6 to 8 km in depth within which the velocity is quite constant. Its top represents the shallowest feasible crystalline basement (Fig. 3.5). Its local shallowness and/or velocity might indicate the Bathgate magnetic body (CH. 1.5).

For travel-times (T) over the range ($15 \leqslant x \leqslant 50$ km).

$Taj = Xaj/V + Da + Dj$

where a and j denote the source and receiver sites respectively. The site delay, Dj, equals $\sum_{n=1}^{n=m} Hn \sqrt{(V^2 - Vn^2)}/V.Vn$

for m layers having thicknessess Hn and velocities Vn.
It is assumed that any structure on the refractor is not so abrupt as to cause the refracted ray paths to depart from it. Shooting into a profile of receivers from both directions, distinguishes variations in the velocity of the refractor from those in its depth. Hence the MINUS TIME LINE (Figs. 4.1A, 4.1B)

$Taj - Tbj = (Xaj - Xbj)/V + (Da - Db)$ is independent of the receiver delays, has a slope dependent on V and an intercept

$\Delta Ti = Da - Db.$

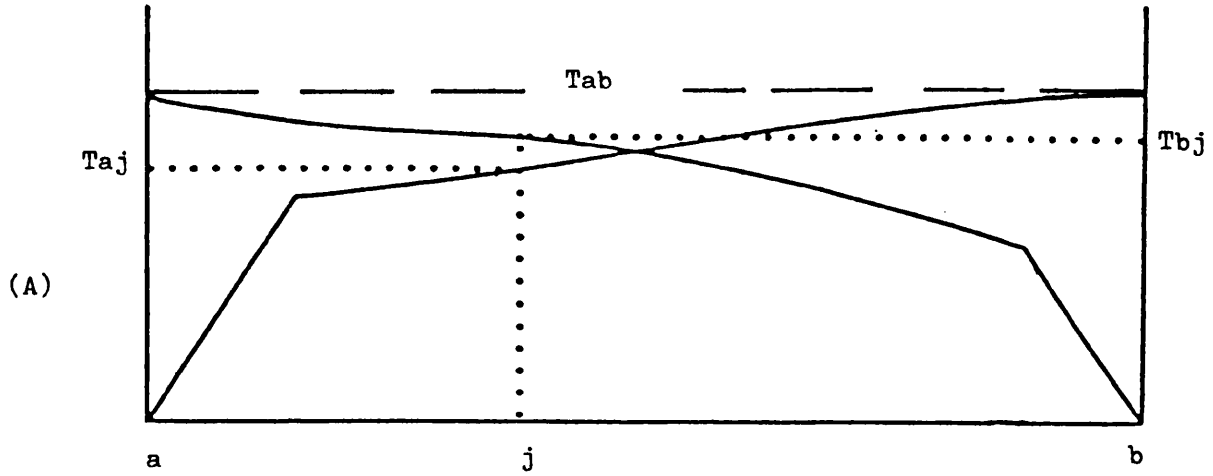

(A) reversed first arrival travel-time graph.

Fig. (4.1A, B) The plus-minus method of refraction interpretation (Hagedoorn, 1959)

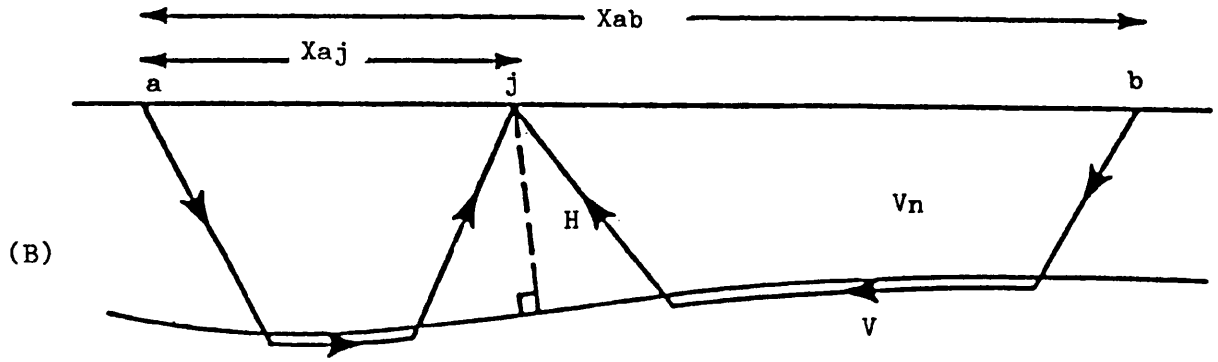

(B) Refracted ray paths from each end of a reversed seismic profile line to an intermediate receiver position.

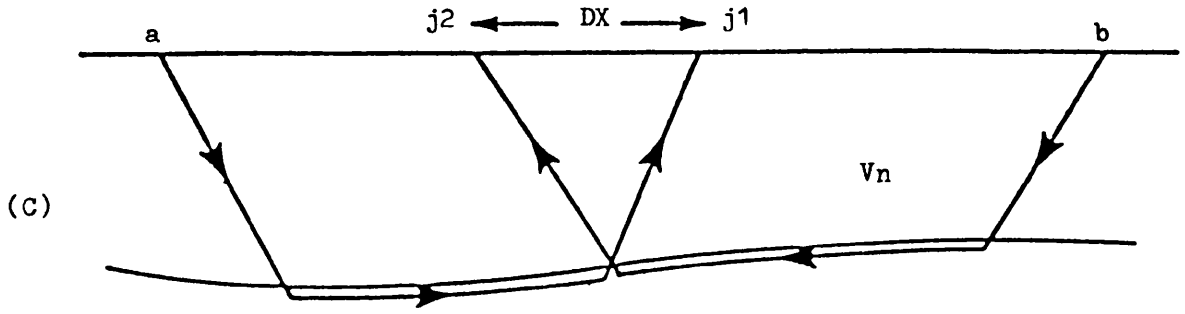

Fig. (4.1C) The generalised method of refraction interpretations. (Palmer, 1980).

The PLUS TIME LINE (Figs. 4.1A, 4.1B)

$$Taj + Tbj = (Xaj + Xbj)/V + (Da + Db) + 2Dj$$

can be reduced by subtracting the reciprocal time, Tab, which equals $Xab/V + (Da + Db) = (Xaj + Xbj)/V + (Da + Db)$

Hence $$Dj = \tfrac{1}{2} (Taj + Tbj - Tab)$$

$$Da = \tfrac{1}{2} (Tab - Xab/V + \Delta Ti)$$

$$Db = \tfrac{1}{2} (Tab - Xab/V - \Delta Ti)$$

By averaging between points on the refractor offset by $2Hj \tan ic$ (or the sum for separate layers) the PLUS-MINUS picture is smoothed. Receivers of rays with common refractor points may be found, (Fig. 4.1C). In general, paired segment slopes are affected similarly by refractor velocity changes and dissimilarly by structure on the refractor.

With critical distances of 15 to 20 km and 50 km, reversed coverage is, strictly, limited to 10 or 20 km when the sources are 50 km apart. On CP-M (40 km) this reduces to 10 km and is in fact 7 km due to not recording M beyond 22.5 km. For LISPB (1 - E, 70 km) reversal is extended to 30 km. The delays, however, are only known relative to Tab. The reciprocal time on this refractor cannot be observed beyond 50 km and must be obtained by extrapolation. No second arrivals extending this segment are apparent.

For network observations time differences from shots (i,j etc.) into a pair of receivers (a and b) yield a MINUS TIME line and $\Delta Ti = Da - Db$ intercept. If the shot instants are known PLUS TIMES are comparative of the site (i,j etc.) delays since (Da + Db), though undetermined, is a constant.

More stable solutions are obtained by treating the whole network simultaneously by TIME-TERM ANALYSIS.

$T_{ij} = X_{ij}/V + D_i + D_k + \delta_{ik}$ (Willmore and Bancroft, 1960)

where $\overline{V}$ is the average refractor velocity under the network and δ_{ik} the residuals (Observed-model times).

A solution is possible for a fully connected 4 site network (5 unknowns with 6 connections). At least one site must be both receiver and shot point. The present network (Fig. 4.2) is not fully connected. Even if it were many links would exceed 50 km. The number of unknowns (NSITES + $\overline{V}$) is, however, less than half the number of different connections. The number of observations is about half as many again due to repetitions. The number of equations used is then about doubled, by a weighting system based on SIGNAL/NOISE of arrivals (3, 2 or 1). As a result of being an overdetermined system of equations, error estimates are made on all the variables and for the whole solution

$$\text{S.E.} = \sqrt{\frac{\sum_{1}^{n} \delta_{ik}^2}{n}} \qquad \text{where n = NEQNS}$$

A computer program written by J. Mechie (1980) was used for calculating the Time-Term Analysis.

4.2 a_o velocities (Tables 4.1A, B and C), (Fig. 4.3) and Appendix 2. (Layer 2 of 1.4.2 P. 35)

On Fig. 4.3 the segments of the T - X graphs considered to represent arrivals refracted from a_o are shown by heavy lines. Their relationship in plan to the Bathgate magnetic body is indicated by the 250 nT ($\frac{1}{2}$ amplitude) contour.

On 2 (CP→west) there may be either one 5.78 km s^{-1} segment

USE TABLE 4.1A TO ASSOCIATE Appendix Figures with Text.

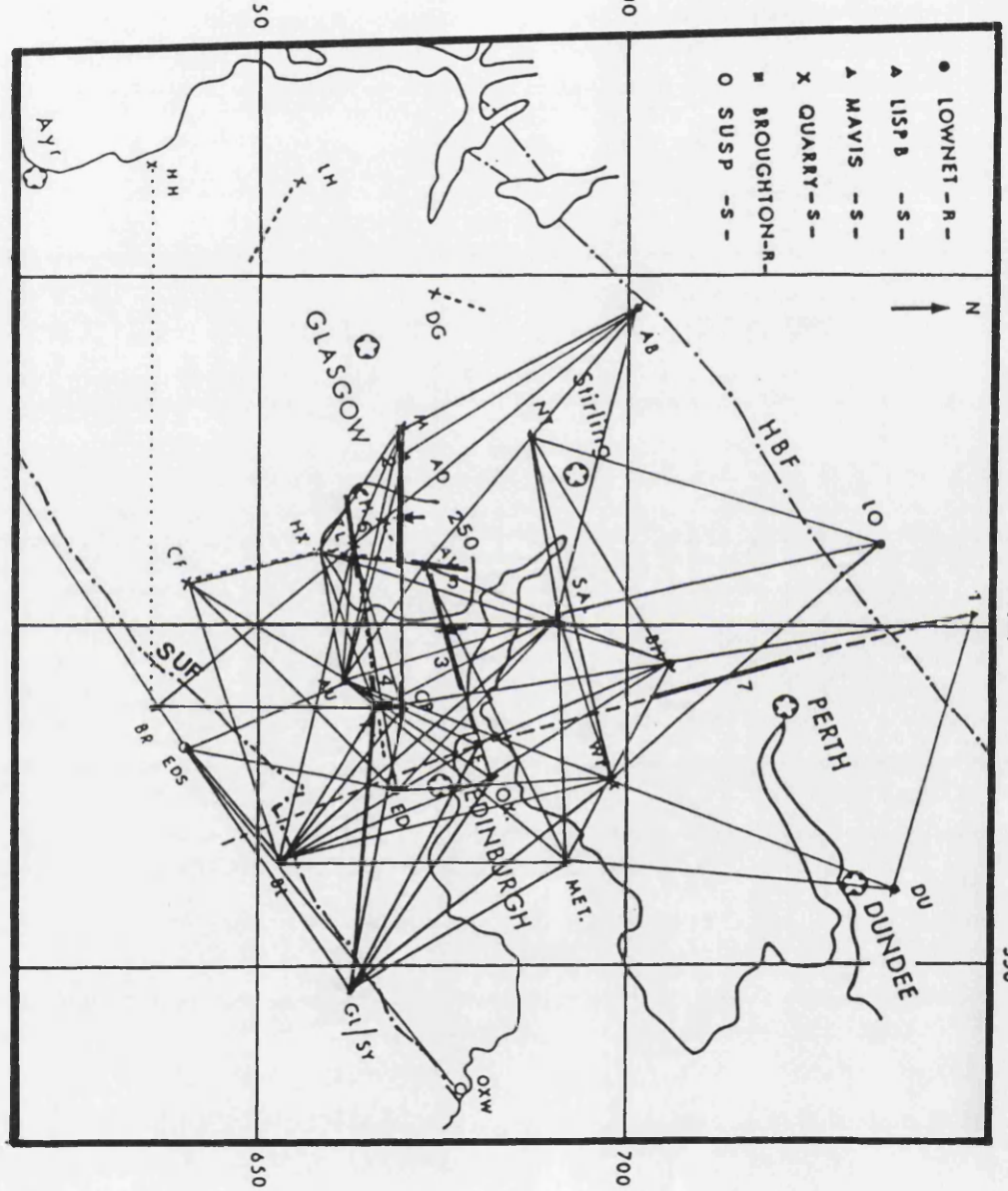

Fig. (4.2) shows the Network connections.

Table (4.1A) a_o Apparent velocities (heavy lines on Fig. (4.1) locates profile segments)

Appendix	Figure	Profile	Figure 4.3	X min km	X max km	n points	Va km s^{-1}	$\bar{V}$ km s^{-1}
2	3	CP → west	2	19.20	29.80	12	6.28 ± 0.12 [1]	
				32.22	38.53	4	6.11 ± 0.15 [2]	
				19.20	38.53	16	5.79 ± 0.06 [3]	6.07 ± 0.3
2	3	M → east	2	13.72	20.88	7	6.27 ± 0.16 [4]	
2	3	AD → east	3	19.95	30.12	7	5.96 ± 0.06 [5]	
2	2	K → west	6	14.80	24.20	9	5.93 ± 0.16 [5]	
				14.80	32.12	12	5.85 ± 0.12 [6]	
2	2	TL → east	4	17.40	22.85	10	6.07 ± 0.30 [6]	
2	7	HX → north	5	14.20	21.50	12	5.98 ± 0.17	
2	15	1 → south	7	26.00	46.50	7	5.88 ± 0.03	5.93 ± 0.05
2	15	E → north	7	21.30	45.60	9	5.98 ± 0.04	
							All	6.04 ± 0.06

Table (4.1B) a_o Minus Time velocities (using points receiving refracted arrivals from both sources

Profile	N from both sources	$\Sigma/\Delta K/$ km	$\Sigma/\Delta T/$ sec	$\bar{V}$ km s^{-1}
CP M	*4	16.66	2.78	6.04 ± 0.26
	**18	96.66	15.74	6.21 ± 0.11
E 1 (LISPB)	7	120.50	20.33	5.90 ± 0.10

Table (4.1C) Time-Term velocity network (Fig. 4.2) ($17 < x < 50$ km)

Area	Equation	Observation	Connection	Sites	St. error of solution	V km s^{-1}
CMV	68	36	20	10	0.03	6.01 ± 0.06
All data	266	137	93	35	0.08	6.02 ± 0.03
***	232	123	85	35	0.07	6.03 ± 0.03

1. Velocity from points before delay
2. Velocity from delayed points
3. Velocity from the whole points disregard the delay
4. AD from MAVIS to back up limited easterly propagation from Medrox
5. Last three points excluded (bad MSF/delay)
6. May be updip acceleration on 5.30 km s^{-1} refractor (a_{s2})

* See Table 4.2A

** Observed points from one direction combined with calculated times from the other direction to make reversed coverage Table 4.2A

*** All data less Southern Uplands - Forth connections.

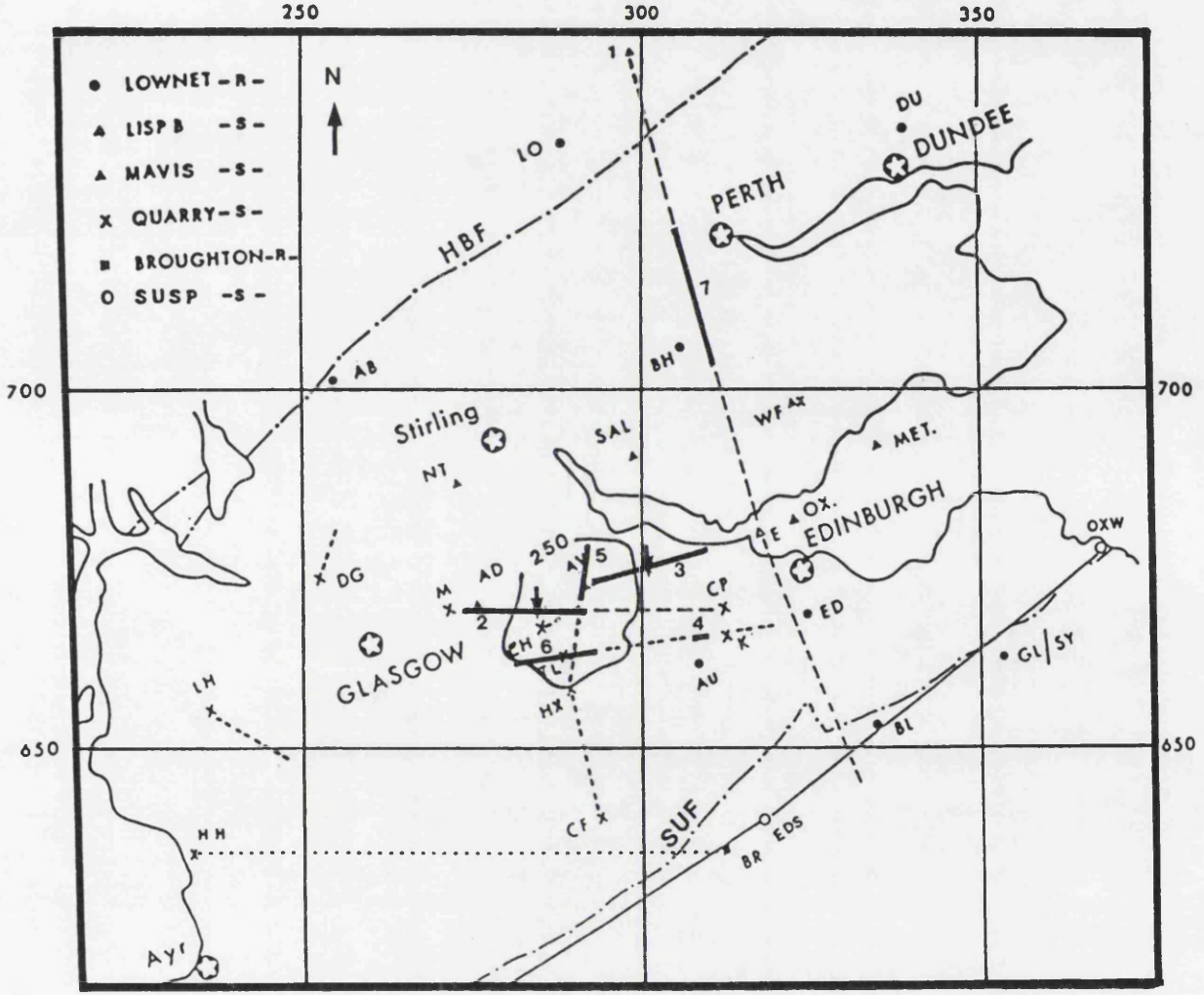

Fig. (4.3) shows refracted arrivals from a$_o$ (heavy lines)
6 from K, 2 from CP and M, 3 from AD, 4 from TL, 5 from HX and 7 from 1 and E.

from 19.20 to 38.53 km, or, preferably, 6.28 km s^{-1} separated by a 0.1 sec delay at 30 km (arrowed, see next section 4.3).

On 2 (M⟶east) the apparent velocity is similarly 6.27 km s^{-1} but the range covered is limited to 22.40 km (weak and discontinued source).

The sub-parallel line, 3, from AD re-inforces the value for shooting towards the east. It also is delayed beyond the magnetic outline.

On 6 (K⟶west) measurement has been extended beyond TL to improve the estimate of refractor velocity here. On 4 (from TL ⟶ east) the irregularity approaching K was originally interpreted as an updip acceleration on a 5.30 km s^{-1} refractor. Subsequent measurements on other lines suggest a_o arrivals are more likely. Extra range to the east is needed to improve this rather uncertain value ($\pm$ 0.3 km s^{-1}). From HX⟶north, 5, the value is close to those for both east and west directions nearby. See table 4.1A for these and LISPB line one-directional velocities and averages.

Reversed coverage for the refractor in the Central Midland Valley exists only on CP-M (Table 4.2A) and is strictly limited to 4 pairs of points spread over 7 km which give a minus time velocity of 6.04 $\pm$ 0.26. There are 10 additional but unpaired observations in the interval which have been used by interpolation and which then give a higher velocity. This minus time velocity line is:-

$$T = 0.00557 \pm 0.096\ \Delta x + 0.046 \pm 0.019$$

from which it appears that the delay time difference (DM-DCP) = 0.05 $\pm$ 0.02 s and the velocity is 6.21 $\pm$ 0.11 km s^{-1}.

Table 4.2A

CP - M Plus-Minus calculation on a_o (Average Reciprocal Distance 40.19 km)

N	XM km	t-x/6 (obs)s	t-x/6 (calc)s	X CP km	t-x/6 (obs)s	t-x/6 (calc)s	ΔX km	Minus s	Plus s
1	13.72	1.01	1.01	26.47		0.93	-12.75	0.08	1.94
2	13.89		1.02	26.30	0.95	0.94	-12.41	0.07	1.92
3	15.08	0.99	1.01	25.11		0.95	-10.03	0.04	1.94
4	15.11		1.00	25.08	0.98	0.94	- 9.97	0.02	1.98
*5	15.50	1.02	1.01	24.69		0.95	- 9.19	0.07	1.97
*6	15.66		1.00	24.63	0.99	0.95	- 8.97	0.01	1.99
7	15.91	1.01	1.00	24.28		0.95	- 8.37	0.06	1.96
8	17.44		0.98	22.75	0.99	0.96	- 5.31	-0.01	1.97
*9	18.07	1.02	0.99	22.12		0.96	- 4.05	0.06	1.98
*10	18.19		0.98	22.00	0.96	0.96	- 3.81	0.02	1.94
*11	18.53		0.98	21.66	0.97	0.97	- 3.13	0.01	1.95
*12	18.84	0.94	0.98	21.35		0.97	- 2.51	-0.03	1.91
*13	19.00		0.97	21.19	1.00	0.98	- 2.19	-0.03	1.97
14	19.88		0.97	20.33	0.99	0.98	- 0.47	-0.02	1.96
15	20.07		0.97	20.12	0.96	0.98	- 0.05	0.01	1.93
16	20.51		0.96	19.68	0.97	0.98	+ 0.83	-0.01	1.93
*17	20.57		0.96	19.62	0.95	0.99	+ 0.95	0.01	1.91
*18	20.88	0.97	0.96	19.21		0.99	+ 1.67	-0.02	1.96
									1.95

Observations underlined
Other times interpolated by linear regression lines.

Minus Line Columns 8, 9

EQUATION 1 t minus = (0.00557 ± 0.096) X + (0.05 ± 0.019)
(reduced)
Hence V refractor = 6.21 ± 0.11 km s^{-1}
Delay Difference = 0.05 ± 0.02 s
Line from Shots M (columns 2 and 4)

EQUATION 2 t reduced = (0.007 ± 0.0042) X + (1.11 ± 0.07)
(VRef = 6.27 ± 0.16 km s^{-1})
Line from Shots CP (columns 5 and 6)

EQUATION 3 t reduced = (0.007 ± 0.0031) X + (1.13 ± 0.07)
(VRef = 6.28 ± 0.12 km s^{-1})
Hence Intercept Times on Shots M 1.11 ± 0.07 s
on Shots CP 1.13 ± 0.07 s

and Observed Reciprocal Time at M from CP only 1.06

Average site delay at 18 receivers in Table
$[(1.95 \pm 0.03) - (1.06 \pm 0.05)] / 2$ = 0.45 ± 0.06s
Delay at M $(1.11 \pm 0.07) - (0.45 \pm 0.06)$ = 0.66 ± 0.09s
Delay at CP $(1.13 \pm 0.07) - (0.45 \pm 0.06)$ = 0.68 ± 0.09s
Delay difference M - CP from Plus Analysis = 0.02 ± 0.13s
Minus = 0.05 ± 0.02s

The Time-Term velocity for times between the sites in Central Midland Valley treated alone is closer to the unreversed line velocities. A weighted average for all the above gives 6.08 ± 0.03 km s^{-1}. (Weights proportional to number of points/ S.D.).

Velocities estimates for a_o outside the Central Midland Valley are dependent on LISPB. Here the reversed coverage is ten times as extensive (Table 4.2B). Bamford (1978) has mentioned 5.93 ± 0.10 km s^{-1} found here.

Enlarging the Time-Term data set to include the whole LOWNET area and LISPB 1—E as well as Central Midland Valley (Fig. 4.2) does not alter the resulting velocity. Nor does the removal of 8 connections (14 observations) affecting certain delays (see next section).

An overall weighted average a_o velocity is 6.04 ± 0.03 km s^{-1}. The only shred of evidence that the refractor velocity locally, over the Bathgate magnetic body, is any higher than average comes from using interpolated values in the MINUS time analysis. No interpretations significance can safely be read into it. On the other hand, nor can much significance be read into the failure of the local Central Midland Valley Time-Term data set to produce a higher velocity for this sub-region - about $\frac{1}{3}$ of the total line lengths lay within the 250 nT magnetic outline. The slightly lower than average LISPB line velocity is more firmly based but so marginal as to be discounted again for interpretation in what follows here.

Table (4.2B)

LISPB Line a_o between shots 1 and E PLUS-MINUS Calculation

Average Reciprocal distance 67.90 km (Times and Distances from Assumpcao thesis (1978)

N	X (From 1) km	T-X/6 s	X (From E) km	T-X/6 s	ΔX km	MINUS s	PLUS s
1	28.8	0.65	39.1	0.87	-10.3	-0.22	1.52
2	33.2	0.65	34.8	0.89	-1.6	-0.24	1.54
3	35.1	0.66	32.9	0.90	2.2	-0.24	1.56
4	38.3	0.70	29.6	0.87	8.7	-0.17	1.57
5	40.9	0.69	27.0	0.83	13.9	-0.14	1.52
6	43.6	0.71	24.3	0.86	19.3	-0.15	1.57
7	46.7	0.70	21.3	0.85	25.4	-0.15	1.55

Minus Line (Columns 6 and 7)

EQUATION 1 t minus = $(0.0029 \pm 0.0029)\ x - (0.21 \pm 0.03)$
(reduced)

Hence V Refractor = 5.90 ± 0.10 km s^{-1} (Bamford gives 5.93 ± 0.03 km s^{-1})

Delay difference = -0.21 ± 0.03 sec.

Line from shot 1 (columns 2 and 3)

EQUATION 2 t reduced = $(0.0037 \pm 0.008)\ x + (0.54 \pm 0.03)$ (V Refractor = 5.87 ± 0.03 km s^{-1})

Line from shot E (columns 4 and 5)

EQUATION 3 t reduced = $(0.0006 \pm 0.0012)\ x + (0.84 \pm 0.04)$ (V Refractor = 5.98 ± 0.04 km s^{-1})

Hence Intercept Times	ON shot 1	0.54 ± 0.03 sec
	ON shot E	0.84 ± 0.04 sec
and Reciprocal Times	AT E from 1	0.79 ± 0.06 sec
	AT 1 from E	0.88 ± 0.09 sec
	MEAN	0.84 ± 0.11 sec

Average site delay at 7 receivers in Table

$$\left[(1.55 \pm 0.02) - (0.84 \pm 0.11)\right] / 2 = 0.36 \pm 0.06\text{s}$$

Delay at site 1 $(0.54 \pm 0.03) - (0.36 \pm 0.06) = 0.18 \pm 0.07$ s

Delay at site E $(0.84 \pm 0.04) - (0.36 \pm 0.06) = 0.48 \pm 0.07$ s

Delay difference (1-E) from plus Analysis = -0.30 ± 0.10 s

minus = -0.21 ± 0.03 s

4.3 a_o delays

4.3.1 Derivation and tests

Tables 4.2A and B give the delays on the two reversed lines derived from the PLUS method.

There is trivial variation amongst the points at the centres of each line. The MINUS line intercepts show CP and M to have nearly identical delays whereas that at E exceeds 1 by 0.2 s.

The reciprocal time from CP is measured near M. From this the delays at CP and M appear 0.2 s greater than at the centre near Bathgate. The last four points beyond 30 km from CP suggest that this is achieved by an abrupt step in the refractor depth. From AD there is a similar feature stepping down this time to the east, (arrowed points on Fig. 4.3). These steps are too near the ends of the lines to be observed in the reversed directions.

The reciprocal time on a_o cannot be seen on LISPB as the shot points E and 1 are too far apart and the a_1 (6.4 km s^{-1}) segment begins at 50 km. The linear regression lines describing a_o have been extrapolated to give a mean reciprocal time of 0.84 ± 0.11 sec. The delays then decrease with increasing age of outcrop: E 0.48 ± 0.07 s on Carboniferous, Centre 0.36 ± 0.06 s on Lower Old Red Sandstone and 1 0.18 ± 0.07 s on Dalradian. The latter is too big to fit the near shot times going north which indicate an intercept time less than 0.1 s. Ray-tracing across the Highland Boundary Fault (Fig. 4.11) shows that the assumption that the rays follow the refractor over a distance approximated by the horizontal separation of the sites is unjustified here. The slope distance at 6.00 km s^{-1} from 1 to the base of the Highland Boundary Fault step accounts for the extra time

which the plus method assigns to the site delay.

The delay times at these and other sites (35 total) have also been calculated by the Time-Term calculation. The data include:

1.	Timed quarry blasts recorded over LOWNET	(Present work)
2.	Data from LISPB line between (1 - E)	Bamford (1976)
3.	LISPB shots (1 and E) recorded over LOWNET	Bamford (1976)*
4.	MAVIS shots recorded over LOWNET	(Hall personal communication 1984)*
5.	SUSP shots recorded over LOWNET	(Warner personal communication 1983)*
6.	Timed quarry blasts recorded over LOWNET and Broughton	El-Isa (1977)

* (3,4 and 5) Origin time and location only. Present work measures trial times.

A total of 266 equations, 137 observations, 93 connections between 35 sites (Fig. 4.2), form the basis of a data set, which produced a refractor velocity of 6.02 ± 0.03 km s^{-1} and standard error of solution 0.08 s.

Table 4.3 lists the delays. The higher Plus-Minus values at CP and M are due to the higher velocity by this method leaving an extra 0.13 s for each of the two delays. The lower mid - LISP line site 54 (near BH) plus - based value is more likely due to the reciprocal time projection which does not enter the Time-Term data set (over 50 km).

Six sites lie outside the Midland Valley on Lower Palaeozoic outcrop near the Southern Upland Fault (BR,BL,EDS,GL/SY), and Dalradian outcrop near the Highland Boundary Fault (1, LO).

At all of them delays are higher than expected. The expectation and probable reason have been mentioned for 1 and apply equally to nearby LO (but it is more loosely and distantly

Table (4.3) a_o delays

Site			Delays (s)				Standard Error		
			Time Term		(Plus)	Ray Trace			
Southern Upland Group	BL		0.37	0.24		0.07	±0.02	0.03	
	GL/SY		0.29	0.15			±0.03	0.05	
	BR		0.21	0.19			±0.06	0.05	
	EDS		0.20	0.22			±0.04	0.03	
Grampian Group	1 (LISPB)		0.25	0.22	(0.18)	0.05	±0.03	0.03	(0.07)
	LO		0.35	0.37			±0.04	0.04	
Lower Old Red Sandstone Group	BH		0.45	0.46			±0.02	0.03	
	LISPB	51	0.45	0.47			±0.05	0.05	
	between	52	0.45	0.47	Average		±0.05	0.05	
	(1-E)	53	0.44	0.46			±0.05	0.05	
	near	54	0.43	0.46	(0.36)	0.46	±0.05	0.05	(0.06)
	BH	55	0.46	0.49			±0.05	0.05	
		56	0.43	0.47			±0.05	0.05	
		57	0.40	0.42			±0.05	0.05	
		58	0.43	0.46			±0.05	0.05	
	DU		0.37	0.38			±0.04	0.04	
	ED		0.40	0.40			±0.03	0.03	
	AB		0.27	0.26		0.29	±0.03	0.03	
	CF		0.25	0.26			±0.03	0.03	
Carboniferous Group	CP		0.51	0.54	(0.68)	0.52	±0.02	0.02	(0.10)
	M		0.57	0.57	(0.66)	0.54	±0.02	0.02	(0.10)
	TL		0.43	0.43		0.45	±0.02	0.02	
	K		0.43	0.44		0.41	±0.02	0.02	
	AU		0.44	0.45			±0.02	0.02	
	HX		0.41	0.40			±0.02	0.02	
	AV		0.48	0.48			±0.03	0.02	
	BG	40	0.47	0.46	Average		±0.04	0.03	
		41	0.43	0.42	(0.45)	0.49	±0.04	0.03	(0.06)
		42	0.42	0.40			±0.04	0.03	
	SAL		0.63	0.64			±0.03	0.03	
	WF		0.58	0.51			±0.03	0.04	
	E (LISPB)		0.44	0.42	(0.48)	0.38	±0.02	0.02	(0.07)
	OX		0.53	0.49			±0.03	0.03	
	METH		0.96	0.93			±0.02	0.02	
	NT		0.40	0.38			±0.03	0.02	

$Va_o = 6.02 \pm 0.03$

$Va_o = \frac{6.03 \pm 0.03}{0.07\ s}$

Standard error of solution 0.085 s

(Underlined figures delays after omitting 8 connections).

(Bracketed figures from Plus-Minus Method Tables 4.2A and B)

interconnected). Warner's Southern Upland Line indicates delays of about 0.1 s along the Lower Palaeozoic outcrop of the Northern Belt. If the delays at these sites are fixed at such a value in the Time-Term calculation then refractor velocity becomes reduced to 5.85 km s^{-1} and the site delays within the Midland Valley are similarly reduced.

The connections EDS - BL and GL (along Warner's line) make it clear that both lower delays and a velocity of 6.00 km s^{-1} or more are needed.

The slow connections to these sites are from the Forth area, particularly across the Midlothian coalfield. When these eight (BL and GL from METH,OX,E and WF) are omitted some reduction in these delays occurs without affecting the refractor velocity (see Table 4.3, underlined figures).

As in the case of the Highland Boundary Fault, the LISPB line is the only profile across this structure (Fig. 15, Appendix 2). The Midlothian coalfield basin is bounded by opposing faults. A ray-traced solution again shows that the Time-Term site delays are too big because of time spent on obliquely upward paths within the basement from the base of the fault trough structure.

In the case of the Highland Boundary Fault model the ray-traced and Time-Term delays at site 54 (near BH) are similar. In the case of the Southern Upland Fault - E model the ray-traced delays at E and ED are 0.04 and 0.15 sec less than their Time-Term equivalents. The ray-traced delay times at CP,M,BG,K and TL are within the Time-Term delay error estimates at these sites.

It is concluded that the Time-Term delays are acceptable except for sites near to and connected across steep structures, such

as the Highland Boundary Fault and Southern Upland Fault. The ED LOWNET site is the only one within the Midland Valley apparently in this category.

4.3.2 Intra-Midland Valley Results

A total delay map (Fig. 4.4) reveals that the maximum delays occur over the Carboniferous outcrop especially towards the east (Clackmannan and Fife/Forth) i.e. where there is a corresponding gravity low (Fig. 1.14). The a_o delays at Carboniferous sites must be regarded as the sums of a_{s1} (Carboniferous/Upper Old Red Sandstone) and a_{s2} (Lower Old Red Sandstone) components with different delay/depth factors.

At stations situated on the Carboniferous, estimates of the a_{s1} delays (to the top of the Lower Old Red Sandstone) have been made from geological estimates of Carboniferous thicknesses (Table 4.4). The adjacent ray-traced values show that where the profiles exist the observed a_{s1} and a_{s2} segments can be matched using these thicknesses. The geological estimates are, however, subject to bigger uncertainty at some sites not on seismic profiles, METH is the worst case.

The thickness of the Lower Old Red Sandstone rocks have been estimated by converting the $(a_o - a_{s1})$ delays, i.e. that due to Lower Old Red Sandstone (a_{s2}) to thickness (see Table 4.4A). Where stations are situated on Lower Old Red Sandstone (Table 4.4B), the estimated thicknesses are got by direct conversion of the delays (a_{s2}).

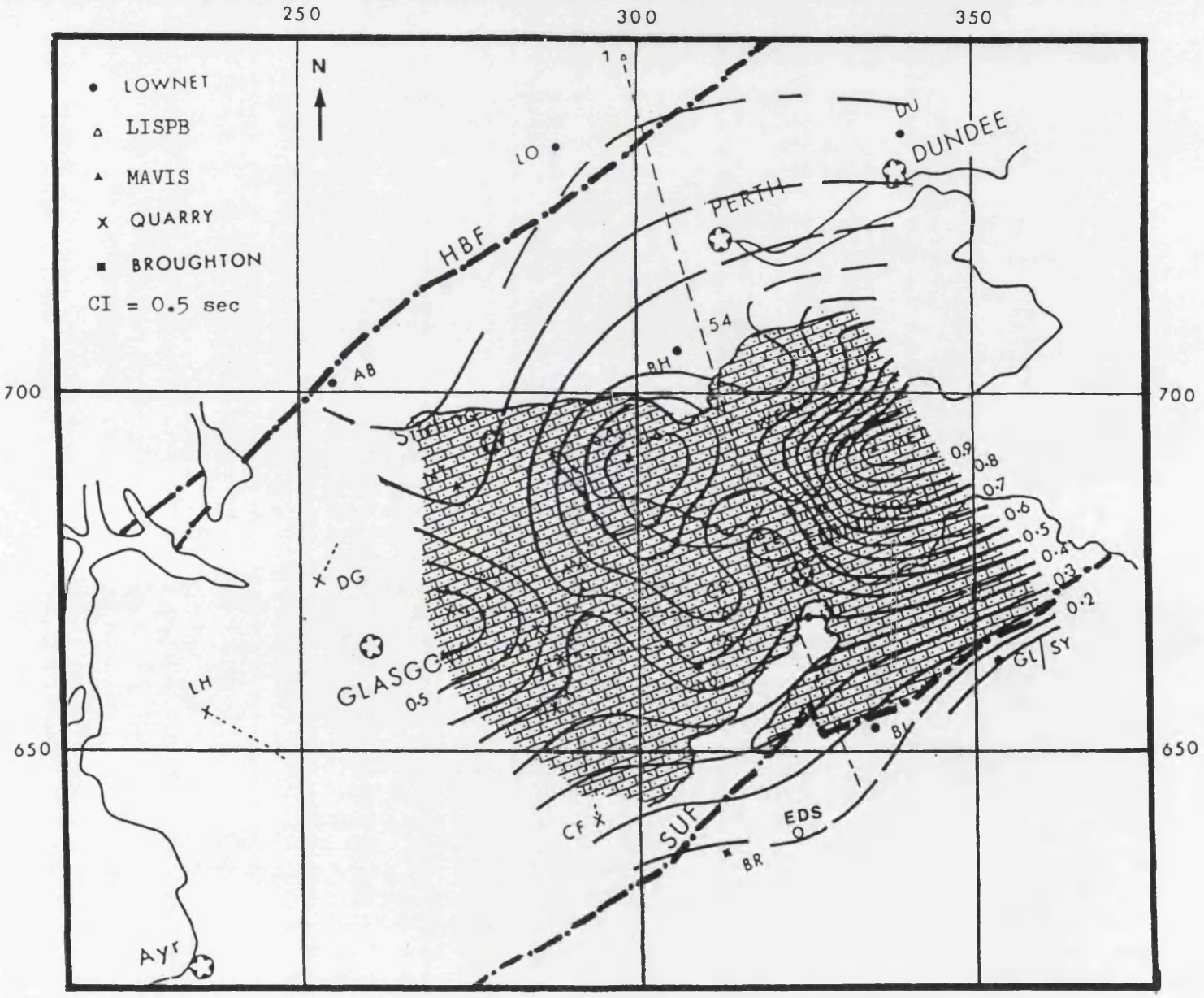

Fig.(4.4) Total delays map derived from Time-Term analysis (Carboniferous rocks shaded).

Table(4.4) Listing of a_o, a_{s1}, a_{s2} delays and thicknesses

Velocities used for calculations:

Va_{s1} = 3.70 km s^{-1}, Va_{x2} = 5.30 km s^{-1} and Va_o = 6.03 km s^{-1}

a - sites on Carboniferous outcrops

Site	Total delays (a_o) sec	Carboniferous thickness (km)		Carboniferous delays (a_{s1}) sec		Lower Old Red Sandstone delays (a_{s2}) sec		Lower Old Red Sandstone thickness (km)		Total depths to (a_o) km
CP	0.54±0.02	1.23±0.3	1.22	0.26±0.07	0.27	0.28±0.07	0.24	3.11±0.78	2.85	4.34±0.84
K	0.44±0.02	0.71±0.2	0.69	0.15±0.04	0.16	0.29±0.04	0.25	3.22±0.44	3.04	3.93±0.48
AU	0.45±0.02	1.00±0.2		0.21±0.04		0.24±0.04		2.67±0.44		3.67±0.48
SAL	0.64±0.03	1.43±0.4		0.30±0.09		0.34±0.09		3.78±1.00		5.21±1.08
WF	0.52±0.03	1.19±0.4		0.25±0.09		0.27±0.09		3.00±1.00		4.19±1.08
METH	0.93±0.02	2.29±1.0		0.48±0.21		0.45±0.21		5.00±2.33		7.29±2.54
E (LISPB)	0.42±0.02	0.81±0.3	0.99	0.17±0.07	0.18	0.25±0.07	0.21	2.78±0.78	2.50	3.59±0.84
HX	0.40±0.02	0.76±0.3		0.16±0.07		0.24±0.07		2.56±0.78		3.32±0.84
OX	0.53±0.03	1.00±0.5		0.21±0.11		0.32±0.11		3.56±1.22		4.56±1.33
NT	0.40±0.03	*0.93±0.1		0.14±0.02		0.26±0.04		2.89±0.44		3.82±0.45
TL	0.43±0.02	*1.60±0.3	1.62	0.28±0.07	0.28	0.15±0.07	0.17	1.67±0.78	1.95	3.27±0.84
M	0.57±0.02	*1.72±0.2	1.72	0.32±0.04	0.31	0.25±0.04	0.23	2.78±0.44	2.61	4.50±0.48
AV	0.48±0.02	*1.71±0.3		0.32±0.07		0.16±0.07		1.79±0.78		3.50±0.84
BG (40)	0.46±0.03	*1.70±0.3	1.71	0.30±0.07	0.32	0.16±0.08	0.17	1.79±0.89	1.99	3.49±0.94
BG (41)	0.42±0.03	*1.65±0.3	1.71	0.29±0.07	0.32	0.13±0.08	0.17	1.45±0.89	1.99	3.10±0.94
BG (42)	0.40±0.03	*1.60±0.3	1.71	0.28±0.07	0.32	0.12±0.08	0.17	1.35±0.89	1.99	2.95±0.94

b - sites on Lower Old Red Sandstone outcrops

Site	Total delays (a) sec		Lower Old Red Sandstone delays (a_{s2}) sec	Lower Old Red Sandstone thickness (km)	
AB	0.26±0.03		0.26±0.03	2.89±0.33	
ED	0.40±0.03	0.25	0.40±0.03	4.45±0.33	2.50
CF	0.26±0.03		0.26±0.03	2.89±0.33	
DU	0.38±0.04		0.38±0.04	4.22±0.44	
BH	0.46±0.03		0.46±0.03	5.11±0.33	
LISPB - 51 (between 1 and E)	0.47±0.05		0.47±0.05	5.22±0.55	
52 "	0.47±0.05		0.47±0.05	5.22±0.55	
53 "	0.46±0.05		0.46±0.05	5.11±0.55	
54 "	0.46±0.05	0.46	0.46±0.05	5.11±0.55	5.00
55 "	0.49±0.05		0.49±0.05	5.45±0.55	
56 "	0.47±0.05		0.47±0.05	5.22±0.55	
57 "	0.42±0.05		0.42±0.05	4.67±0.55	
58 "	0.46±0.05		0.46±0.05	5.11±0.55	

Carboniferous delays calculated from geology estimation.
*Lavas delays calculated by using V lavas = 4.50 km s^{-1} for (NT = 0.47 km, TL = 0.88 km and M, AV, BG = 0.9 km) and included in Carboniferous.
Underlined figures (delays and thicknesses) calculated from Ray trace models.

The relevant formulae are

$$\Delta ta_s = ha_s \frac{\sqrt{Va_o^2 - Va_s^2}}{Va_o \, Va_s}$$

by using $Va_{s1} = 3.70$ km s^{-1}, $Va_{s2} = 5.30$ km s^{-1} and $Va_o = 6.03$ km s^{-1}.

$$\Delta ta_{s1} = 0.21 \, ha_{s1}$$ (for Carboniferous/Upper Old Red Sandstone)

ans $$\Delta ta_{s2} = 0.09 \, ha_{s2}$$ (for Lower Old Red Sandstone)

Lower Old Red Sandstone delays/thicknesses (Table 4.4 and Fig. 4.5)

The best substantiated result is the doubling of the Lower Old Red Sandstone thicknesses between Bathgate (2.0 km) and Perth (5.0 km). It is less well established whether this change is fairly evenly distributed (see WF and SAL) or abrupt at the Ochil Fault. Ray-tracing on LISPB (Fig. 4.11) suggests that the 'Perth' basin extends up to the Highland Boundary Fault and, therefore, wider than the Strathmore syncline. Geologically anticipated thinning to the south west is supported by NT and AB values (< 3 km).

The modest increase to 3 km (CF) south from Bathgate at least distinguishes this area (E,CP,K,AU,CF) from the 'Perth' basin. East of these sites the pattern is quite uncertain. Depending upon the Carboniferous component the thickness at METH could match either the 'Perth' basin or 'Bathgate' high. The Time-Term estimate for ED is probably too high. It is a 'noisy' station and onsets may have been judged systematically late. The ray-traced model on LISPB south from E (Fig. 4.12) indicates 0.25 s (2.5 km) delay

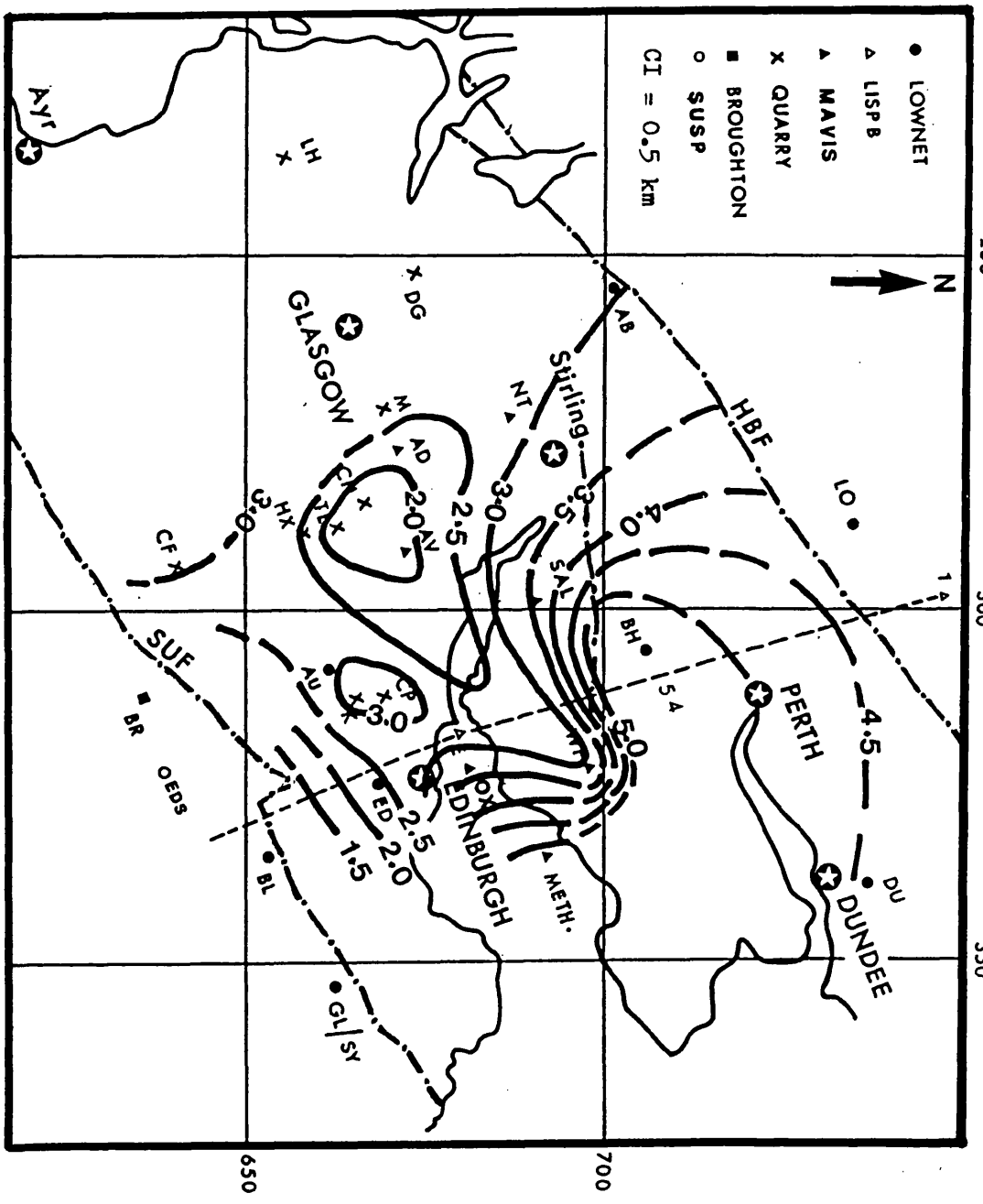

Fig. (4.5) Map showing Lower Old Red Sandstone thickness.

Ochil Fault east of Stirling

(thickness) under the Pentlands near Lower Palaeozoic outcrop. Between the Pentland and Southern Upland Faults under the Midlothian coalfield the Old Red Sandstone thickness may be 1.5 km.

4.4 Structure (depths to a_o)

Interpretation bearing on this to be found in:-

Table (4.4)
Map (Fig. 4.6)
Ray-traced diagrams

4.7B	M - CP
4.8B	CP - M
4.9B	TL - K
4.10B	K - TL
4.11B	1 - near BH (LISPB)
4.12B	E - near BL (LISPB)

Midland Valley seismic based section
4.13B 1 - BH - SAL - BG - CF - BR

see Appendix 4
Velocity Distribution for ray traced models

The contour patterns (Fig. 4.6) of depth to a_o are similar to those of Lower Old Red Sandstone thickness alone (Fig. 4.5). Addition of Carboniferous thicknesses south of the Ochil Fault reduces the change across it.

Around the Bathgate area the structure is detailed by ray-tracing method, using a program written by Cerveny and Psencik (1981).

The ray-traced models (Figs. 4.7B,4.8B,4.9B and 4.10B) on the reversed lines CP - M and TL - K for which the agreement between observed and calculated travel times are shown (Figs. 4.7A,4.8A, 4.9A and 4.10A).

The two models are very similar for both lines and incorporated four layers:

Layer 1	Carboniferous sediments/ Upper Old Red Sandstone	of velocity 3.50-3.80 km s^{-1}
Layer 2	Carboniferous lavas	of velocity 4.50-4.70 km s^{-1}
Layer 3	Lower Old Red Sandstone/ Lower Palaeozoic	of velocity 5.20-5.50 km s^{-1}
Layer 4	Crystalline/Lower Palaeozoic (a_o)	of velocity 6.00-6.15 km s^{-1}

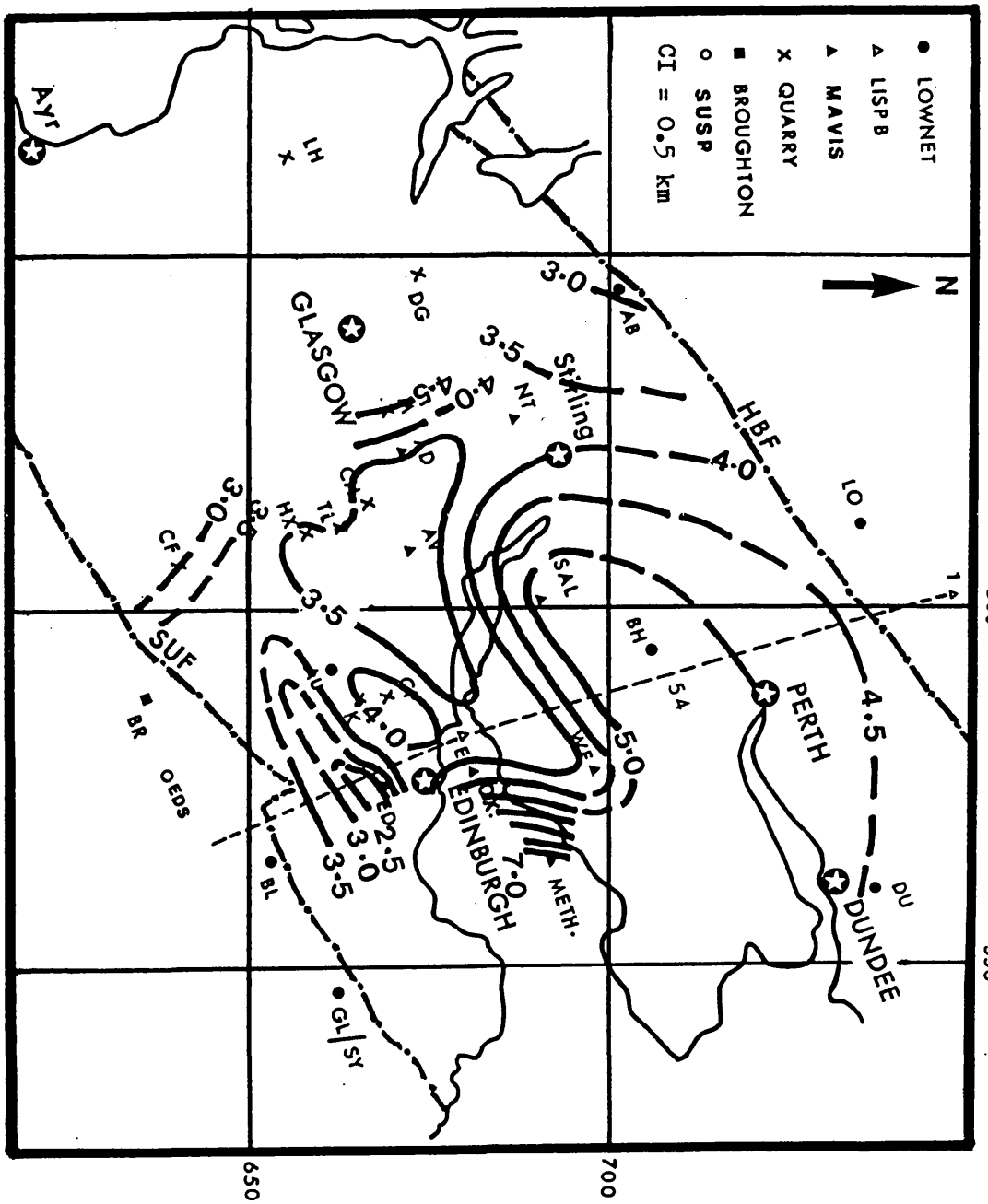

Fig. (4.6) Depth map of the Central and Eastern Midland Valley to a_o basement derived from Time-Term analysis.

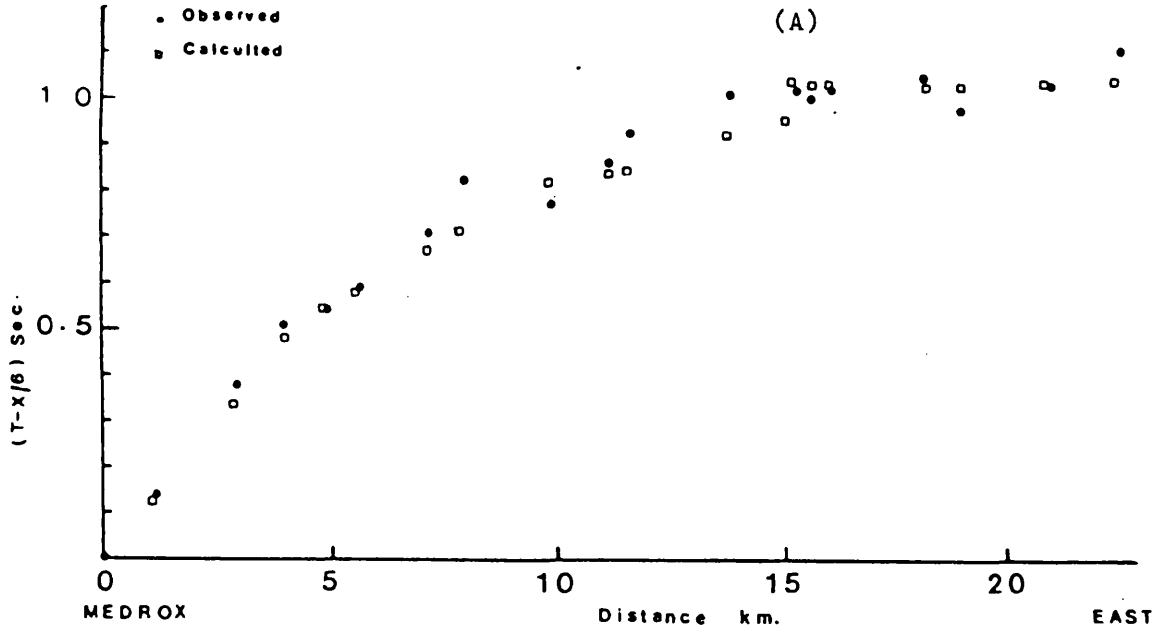

Formations and velocities of the ray-tracing model (see Appendix 4).

1. Carboniferous sediments/ Upper Old Red Sandstone	3.50-3.80 km s^{-1}
2. Carboniferous lavas	4.50-4.70 km s^{-1}
3. Lower Old Red Sandstone/ Lower Palaeozoic	5.30-5.50 km s^{-1}
4. Crystalline/Lower Palaeozoic a_o refractor	6.00-6.15 km s^{-1}

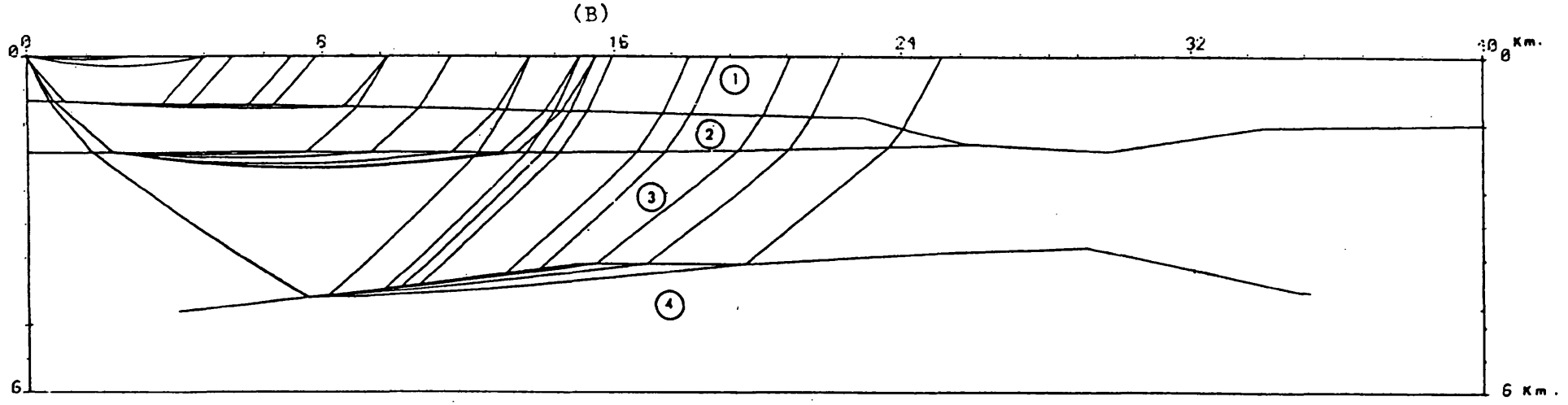

Fig. (4.7) Medrox-east (A) Reduced T-X/6 graph shows the observed and calculated travel times
(B) Ray tracing model for M-CP line.

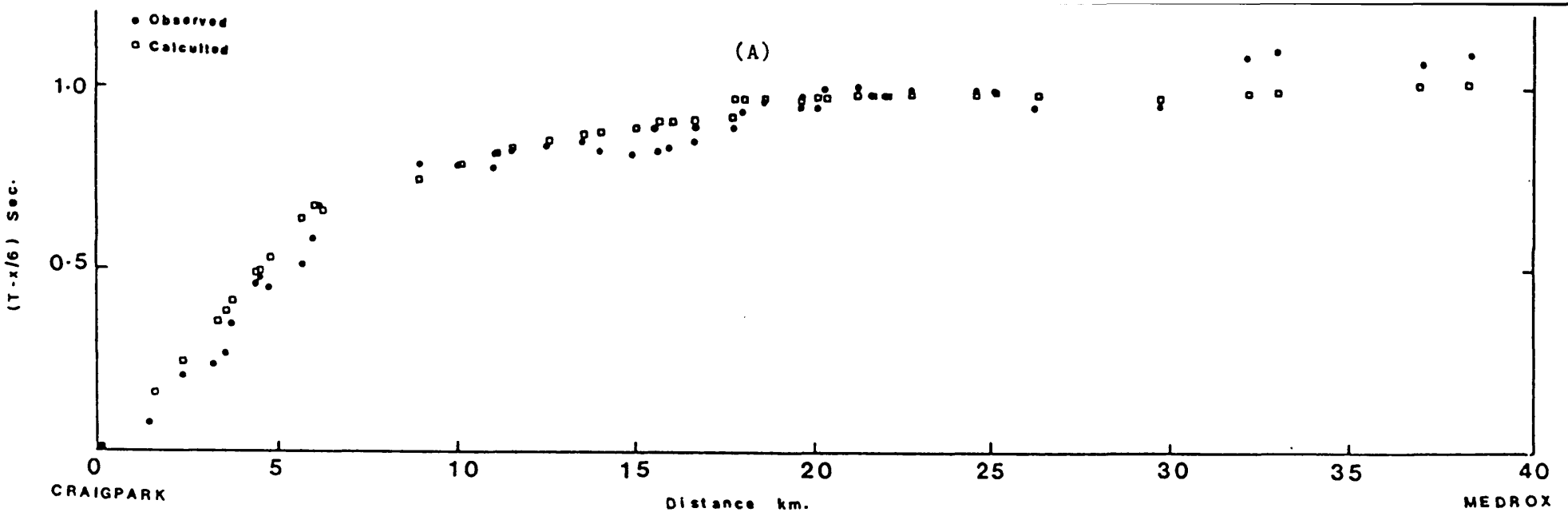

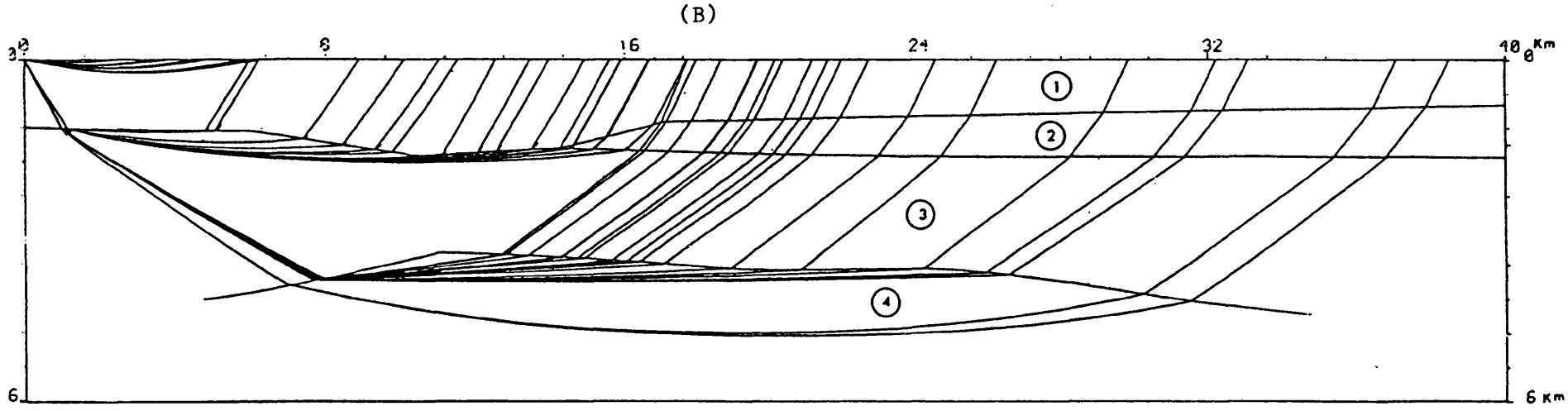

Fig. (4.8) Craigpark-west (A) Reduced T-X/6 graph shows the observed and calculated travel times
(B) Ray tracing model for CP-M line (same model as Fig. 4.7).

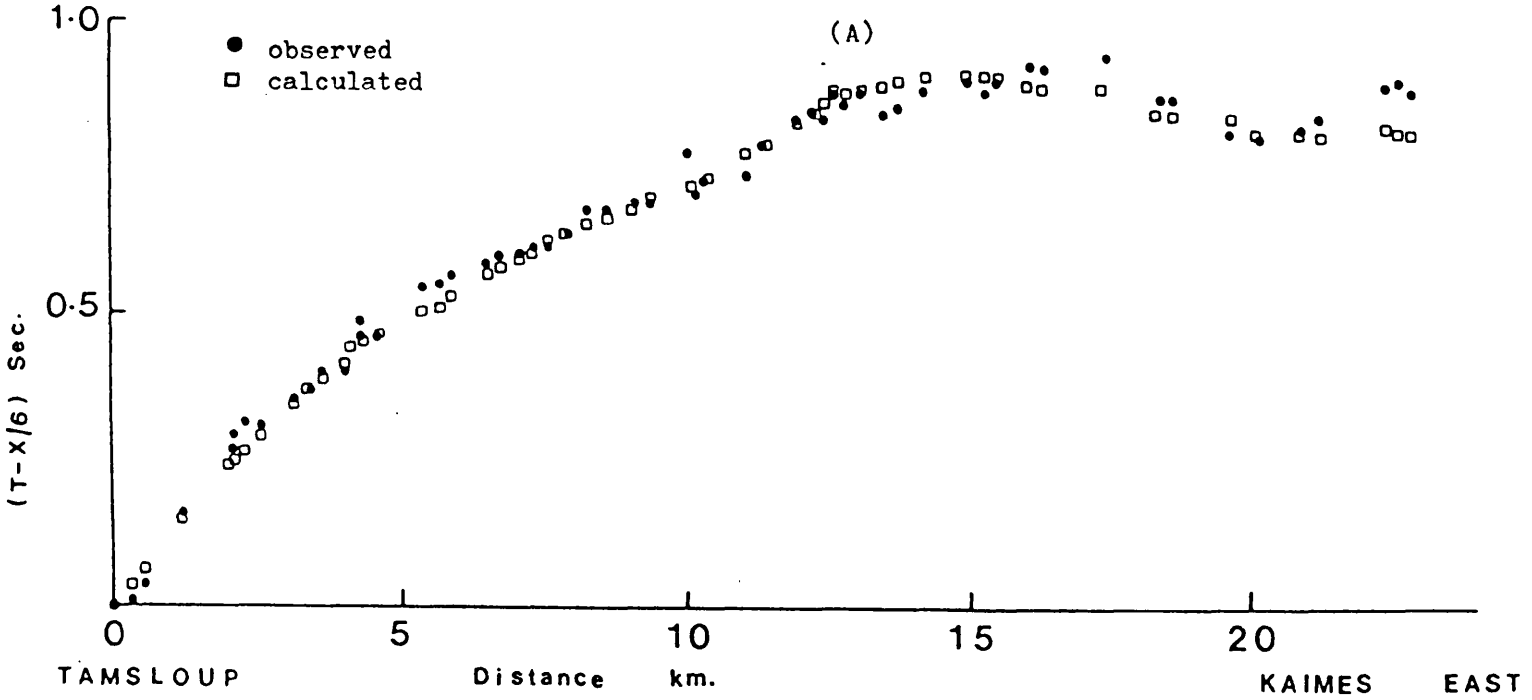

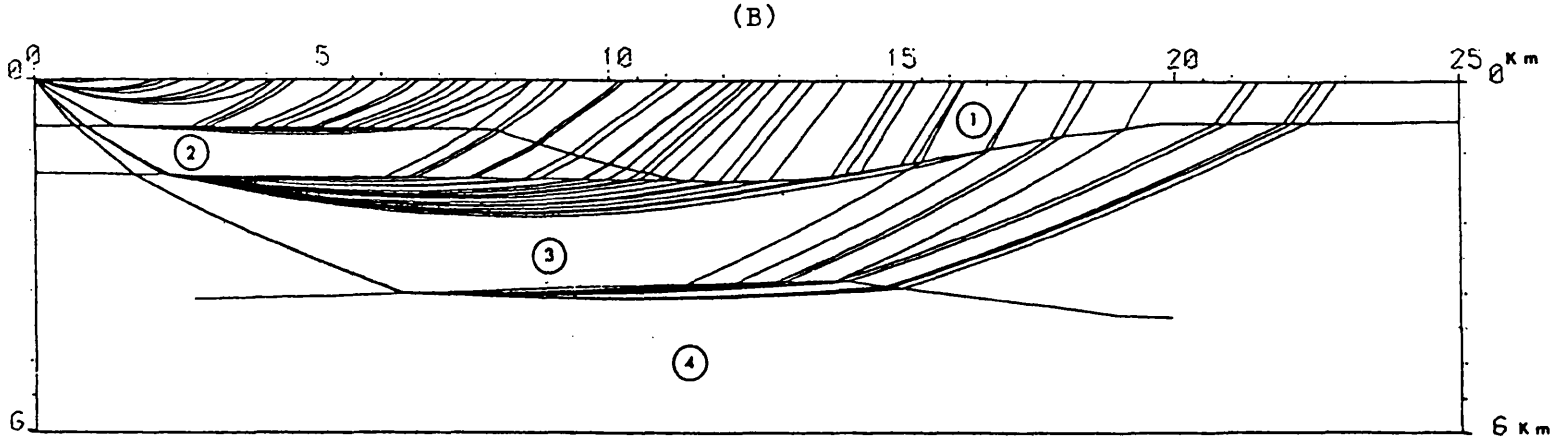

Fig. (4.9) Tamsloup-east (A) Reduced T-X/6 graph shows the observed and calculated travel times
(B) Ray tracing model for TL-K line (formations and velocities as Fig. 4.7)

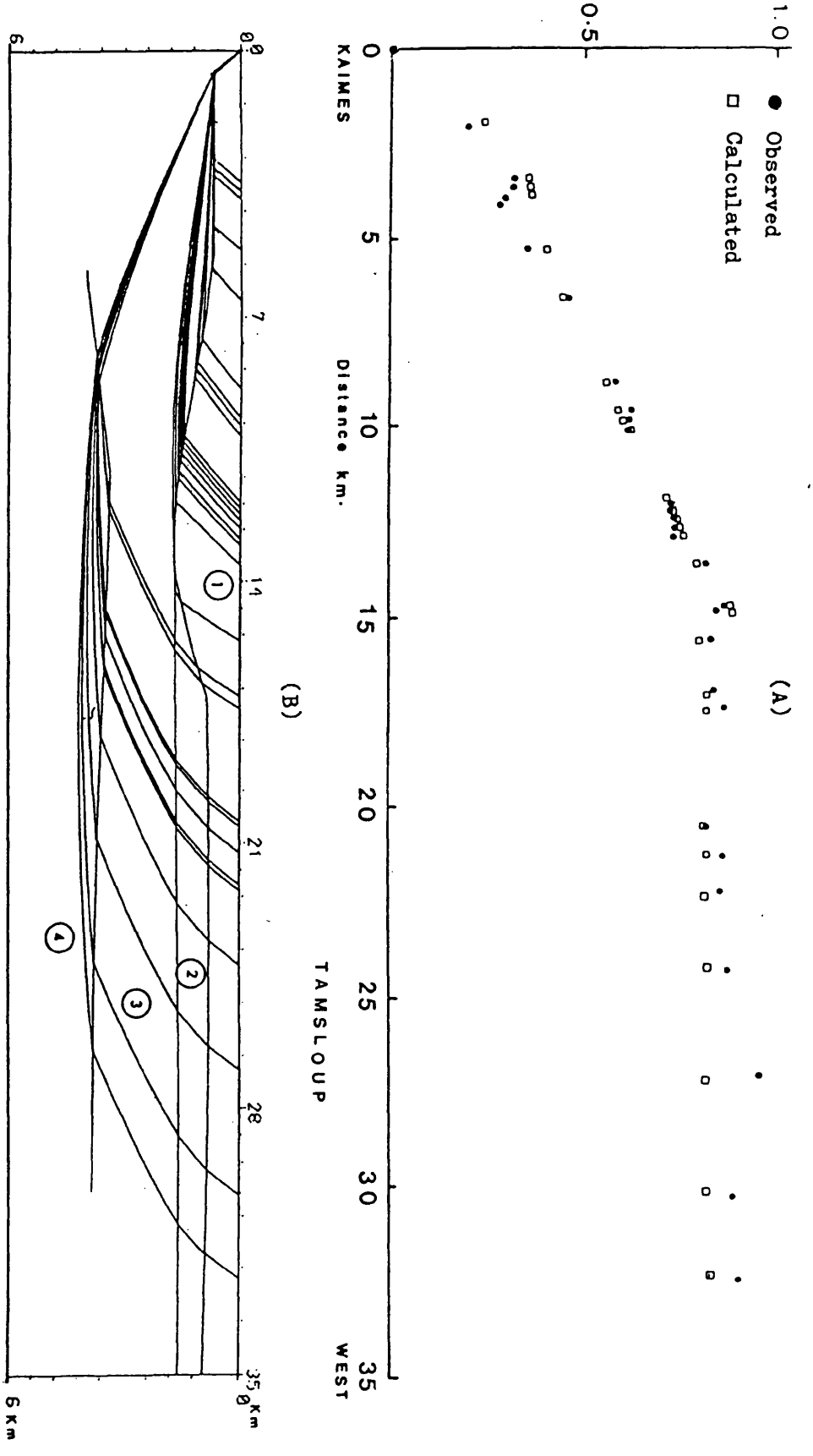

Fig. (4.10) Kaimes-west (A) Reduced T-X/6 graph shows the observed and calculated travel times
(B) Ray tracing model for K-TL line (formations and velocities as Fig. 4.7)

The models show the shallowest depth of the (a_o) refractor 3.00 km to occur underneath the Central Midland Valley (Bathgate) deepening both east and west under the quarries, confirming the results obtained from the Plus-Minus method and the Time-Term analysis.

Both models show Layer 1 and Layer 2 each of $\sim$ 1 km thick, correlates well with Rashiehill, Salsburgh boreholes and the known geology. Also show the Carboniferous lavas wedge out and that the sediments sequences thickens eastward.

The ray-traced model of structure across the Highland Boundary Fault (Fig. 4.11) was necessary to explain the too large Time-Term delay at shot point site 1 near Dunkeld (sec. 4.3). It is also the best basis for the velocity gradient with depth within the Lower Old Red Sandstone (Fig. 3.4 and 4.11).

The section is compatible with revised geological estimates for Lower Old Red Sandstone thickness against the Highland Boundary Fault in the Strathmore syncline (personal communication Bluck, 1984) (Appendix 2, Fig. 15).

A deepening of this basin near to the Highland Boundary Fault and a shallowing of it further south towards BH would be in better agreement with the geology and, no doubt, could be accommodated by the travel times on Fig. 4.11. Deductions from the delay under BH would then require compensating delays on rays to it from the south. These could arise in a similar manner to those crossing basement steps in Figs. 4.11 and Fig. 4.12. The Ochil Fault has already been suggested as a structure across which a sudden change in Lower Old Red Sandstone as well as Carboniferous thickness is possible (previous section). Unfortunately it is not clear on the LISPB line north from E whether the direct arrivals through the

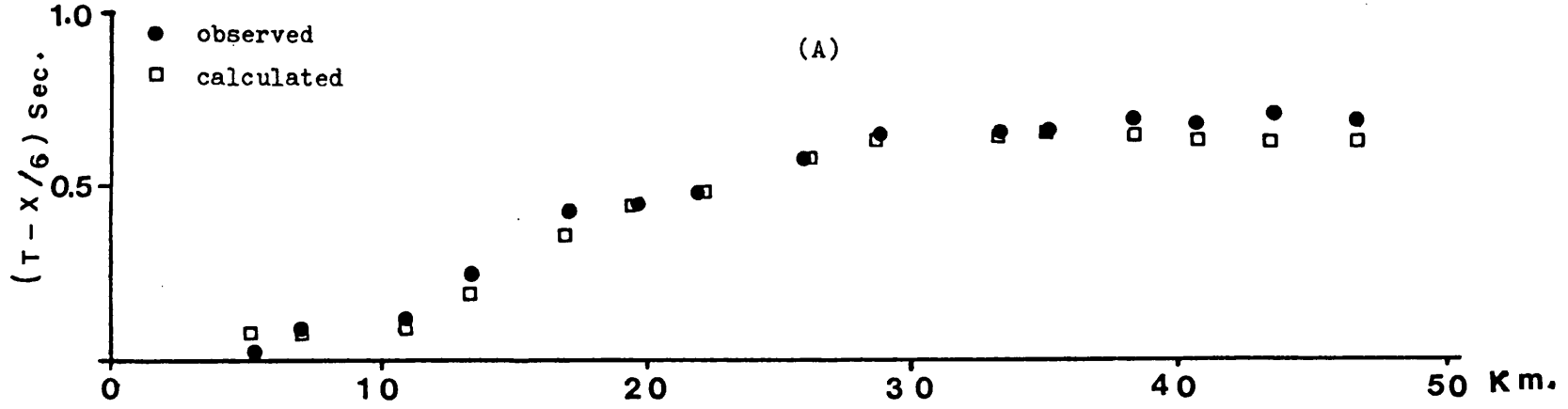

Fig. (4.11A) Reduced T-X/6 graph shows the observed and calculated travel times

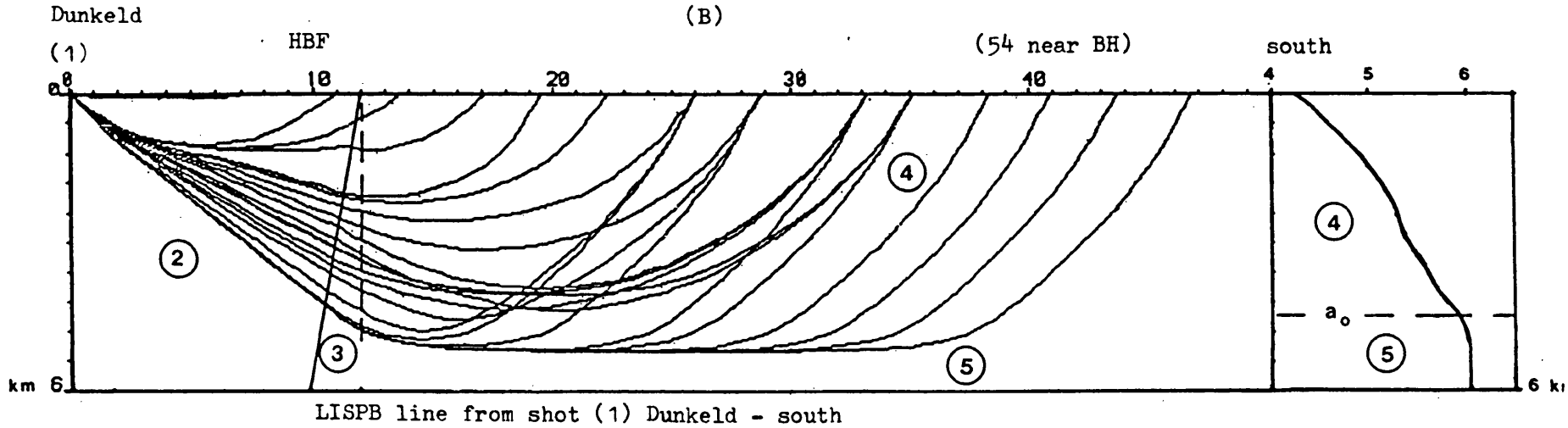

Fig. (4.11B) Ray-tracing model for LISPB (from shot 1 - south) and WHB model for Lower Old Red Sandstone
2 Dalradian (velocity 6.00-6.05 km s^{-1}) 3 Highland Boundary series (velocity 5.80-6.00 km s^{-1})
4 Lower Old Red Sandstone 5 a_o refractor. (see Appendix 4)

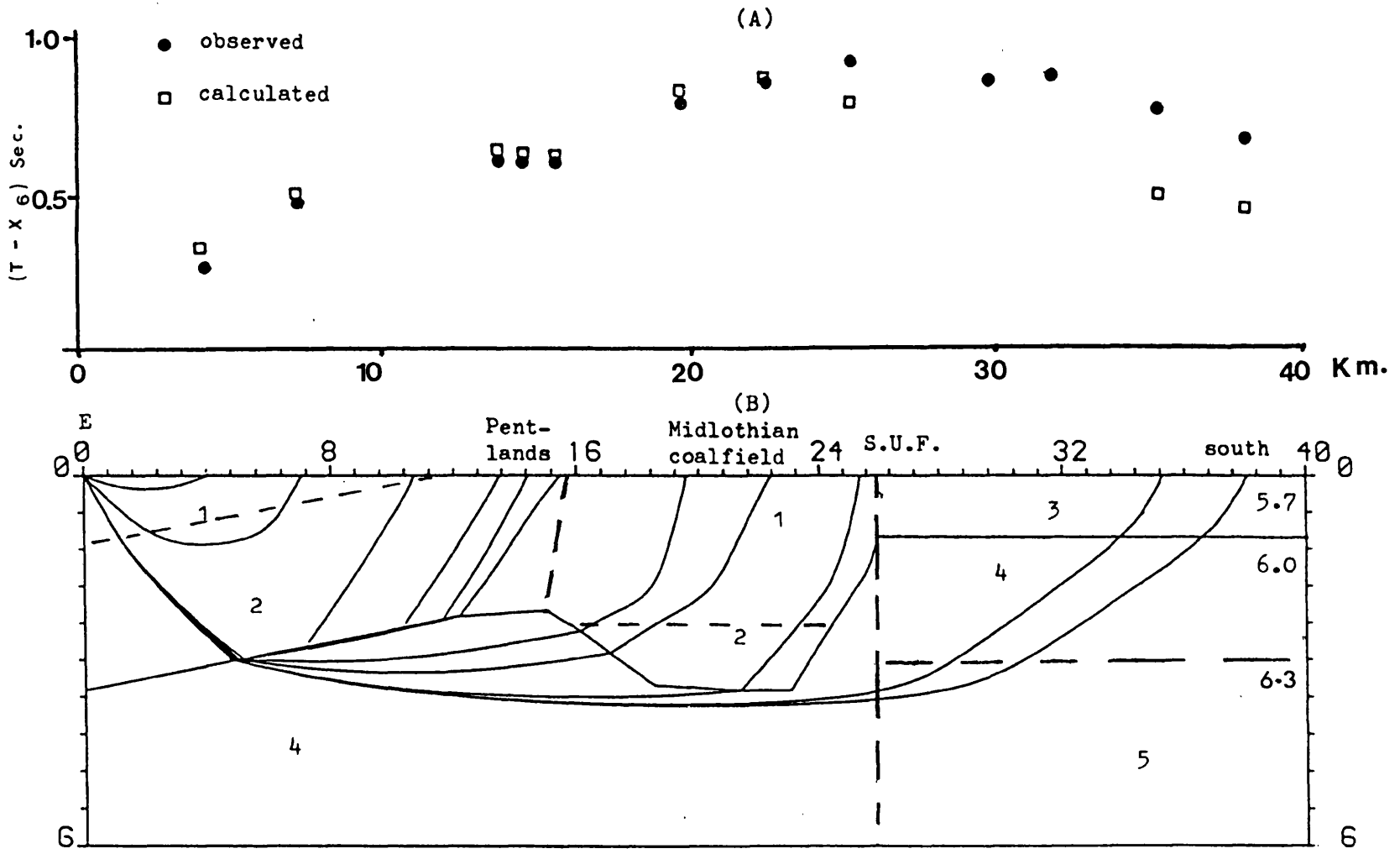

Fig. (4.12) LISPB line from shot E - south. (A) Reduced T-X/6 graph shows the observed and calculated travel times. (B) Ray-tracing model for LISPB (from shot E - south)
1 Carobinferous rocks 2 Lower Old Red Sandstone 3 Lower Palaeozoic
4 a_o refractor 5 6.30 km s^{-1} refractor. (see Appendix 4).

Carboniferous are overtaken by refraction from below or by a lateral change across this fault (Appendix 2, Fig. 15). I.G.S. did make recordings north from WF (close to the fault) along the LISPB line (W. B. Jacob, personal communication) which, could they be found, would constrain a model of this structure.

The ray-traced model across the Pentlands and Southern Upland Faults south from E (Fig. 4.12) is a more reliable indication of structure (and Lower Old Red Sandstone thickness) than the only Time-Term site result in that area. The a_o refractor under the Pentlands is probably as shallow as it is under Bathgate. This estimates the Lower Old Red Sandstone thickness agrees with a geological one (Mykura, 1983). Under the Midlothian coalfield its depth (3.5 km) is still short of matching the 'Perth' basin and the Lower Old Red Sandstone thickness (2.5 km) is even closer to nearby sites (K, CP, AU, CF).

4.5 Conclusions from Seismic Interpretation

A north-south section from the Highland Boundary Fault near Dunkeld, through BH in the Ochils, across the Bathgate area to CF near Biggar and the Southern Upland Fault (Fig. 4.13) represents the most reliable seismically established conclusions made here about the Bathgate area in relation to the broader Midland Valley structure.

Between the boundary faults the major change takes place at and/or just south of the Ochil Fault where the northerly truncation of the Carboniferous overlies a southerly thinning of Lower Old Red Sandstone. When the Lower Old Red Sandstone thickness changes are distributed linearly between the control points then the thinnest development corresponds fairly closely

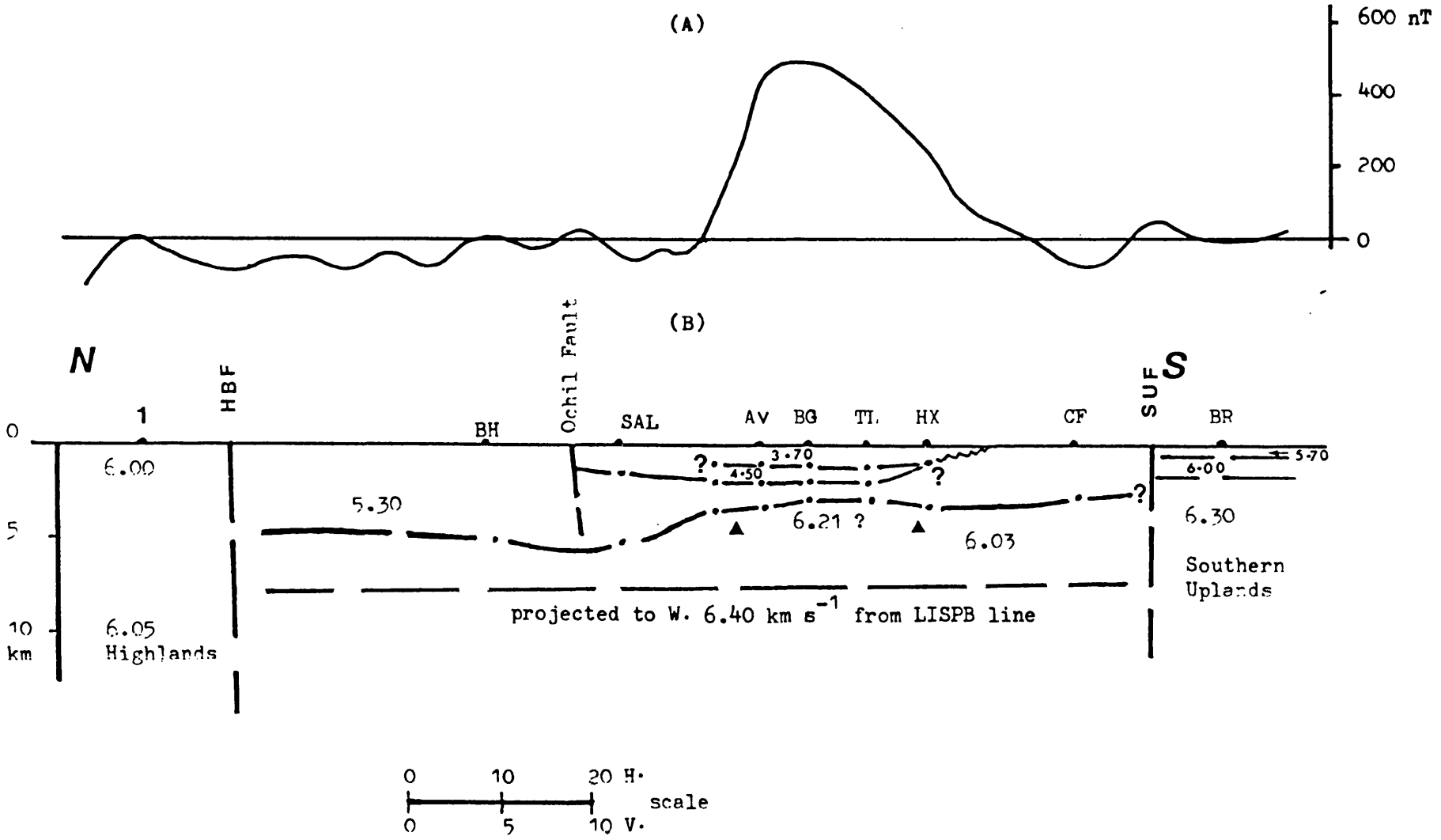

▲ showing the 250nT contour on the cross section

Fig. (4.13) (A) Magnetic anomaly across the Midland Valley.
(B) N-S cross section across the Midland Valley showing the Upper Crustal model.

to the extent of the magnetic body (Fig. 4.13A). The breadth of coverage is less in an east-west direction but the degree of detail over Bathgate rather more (Fig. 4.13B). The crystalline basement (a_o) depth may, on this line, step down by $\sim$ 1.0 km near the bounds of the magnetic body.

These sections show that the magnetic body, expected to be several kilometres thick, lies principally below the a_o refractor surface which is itself likely to be a regional crystalline basement surface. They show, however, that although the relief on this basement is insufficient to explain the magnetic anomaly, the magnetic body underlies its shallowest part and could even form part of the sediment/crystalline rock interface there.

It is not known from this study what form the deeper 6.40 km s^{-1} refractor does under Bathgate. At its average depth on LISPB (7 - 8 km) there is space above it for the magnetic body.

In so far as the 6.40 km s^{-1} refractor relief determines a regional gravity high across the Midland Valley, more information about it in the Bathgate area is determined from the seismic delays in conjunction with Bouguer anomalies in the next section.

4.6 Relationship between seismic delays and Bouguer anomalies

The Bouguer anomaly map (Fig. 1.14) shows a closed gravity high sufficiently near the Bathgate magnetic anomaly to suggest that the magnetic body is also denser than its surroundings. This Bouguer map is, of course, known to be the sum of various components. Subtraction of any that are calculable is a simplifying step towards interpretating what remains.

Such anomaly stripping has been applied to the Carboniferous sediments, or rather some of them, in the Midland Valley. Its extent has been limited by knowledge of formation thicknesses. Hussain and Hipkin (1981) have corrected for Upper Carboniferous only with respect to an assumed basement density of 2.70 gm cm^{-3}. Their map (Fig. 1.15) continues to show a closed positive Bathgate anomaly. Hossain (1976) and Al-Omari (1980) carried the process slightly deeper (Hurlet Limestone) but with respect to a Lower Old Red Sandstone density and with a similar result. As was found when trying to separate Carboniferous from Lower Old Red Sandstone seismic delays, the Lower Carboniferous thicknesses east of Bathgate are both uncertain yet necessary to assess the problem.

Along a line across the Midland Valley to the west, McLean and Qureshi (1966) have applied this type of correction to the whole of the Upper Palaeozoic with respect to a Lower Palaeozoic density of 2.72 gm cm^{-3}. Although their correction were of necessity imprecise their corrected profile showed an unambiguous central gravity high. It is still unclear whether in the Central Midland Valley the Bathgate high is part of the same regional feature or a more localised one connected with the magnetic anomaly. It is to this

question particularly that the seismic delays, by controlling and extending the stripping process, can most pertinently be applied.

The densities of the formations above the a_o basement are given in Table (1.1) and discussed again in CH. 3.4. The velocity of the basement itself has been used to infer that it consists of crystalline rocks of intermediate composition (of granodiorite and Laxfordian - CH. 3, Fig. 3.5). This tends to confirm a basement density about 2.75 gm cm^{-3}.

The expected contrasts (Δp) will then be:

Carboniferous sediments & Upper Old Red Sandstone	-0.2 gm cm^{-3}
Clyde Plateau basalts	0 to -0.05 gm cm^{-3}
Lower Old Red Sandstone	-0.10 to -0.15 gm cm^{-3}
Lower Palaeozoic	0 to -0.05 gm cm^{-3}

It is clear that the delay time (Δt) formula and that for the gravity effect of a slab (Δg) can be equated to convert 'seconds' into 'milligals'

$$h = \frac{\Delta t \; Vao \; Vs}{(Vao^2 - Vs^2)^{\frac{1}{2}}} = \frac{\Delta g}{2\pi G \, (ps - pao)}$$

hence $\Delta g = F(v,p)\,\Delta t$ where

$$F(v,p) = 2\pi G \Delta paos \; Vao \; Vs \; / \; (Vao^2 - Vs^2)^{\frac{1}{2}}$$

where G is the gravitational constant

$\Delta paos$ the density contrast

and Vao, Vs the velocities (ao basement) (s sediment)

Taking the basement to have

Vao = 5.95 km s^{-1} and pao = 2.75 gm cm^{-3} the graph Fig. (4.14) shows F(V,p) over a range of Vs and p s.

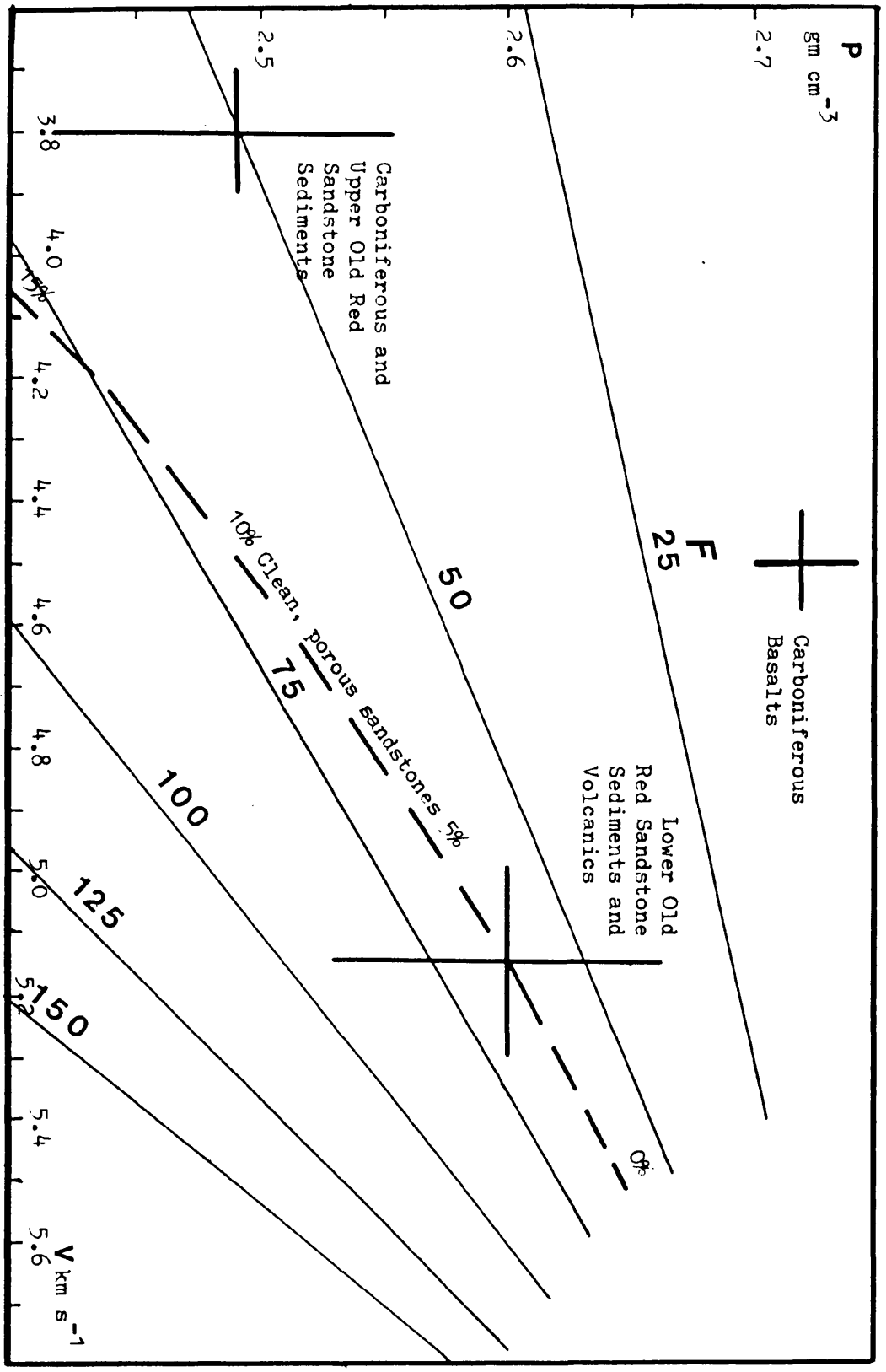

Fig. (4.14) shows F(V, P) plot.

From the time-term solution the total delays on a_o and their errors are known. Each total delay is the sum of components which, by and large, are not known though they could, in principle, be measured or at least estimated on a V - Z model fitted to a T - X profile. The gravity effect could then follow from a matching specification of P - Z (Density).

There are, however, places where considering only two components (Carboniferous with Upper Old Red Sandstone and Lower Old Red Sandstone with ? Lower Palaeozoic) is difficult (e.g. METH) because the top layer thickness is not known. This problem has been avoided by transferring all the uncertainty onto the physical properties. These have already been discussed (CH. 3.4). Averages and their uncertainties for the principal component groups are plotted against lines of constant F (Fig. 4.14). In addition the porous sandstone line relationship between V and P is shown. These plots show that F is unlikely to change between the two principal groups as much as either V or P and that $50 < F < 60$ is within the uncertainties. The gravity effect of the total delays (of Fig. 4.4) has been obtained by using a constant F = 50. The contoured values have been added to the Bouguer gravity contours (Fig. 1.14) to produce a gravity map (Fig. 4.15) corrected for sediments above a_o basement. A small modification has been made to produce (Fig. 4.15) since the Clyde Plateau lavas are considered to contribute to the seismic delays but not, significantly, to the gravity effect (Fig. 4.14 V-D plot) i.e. the seismic delays have been reduced at 5 stations (Table 4.5). The contouring has been done by interpolation on the two contoured maps rather than around the site values alone. No correction has been added to gravity

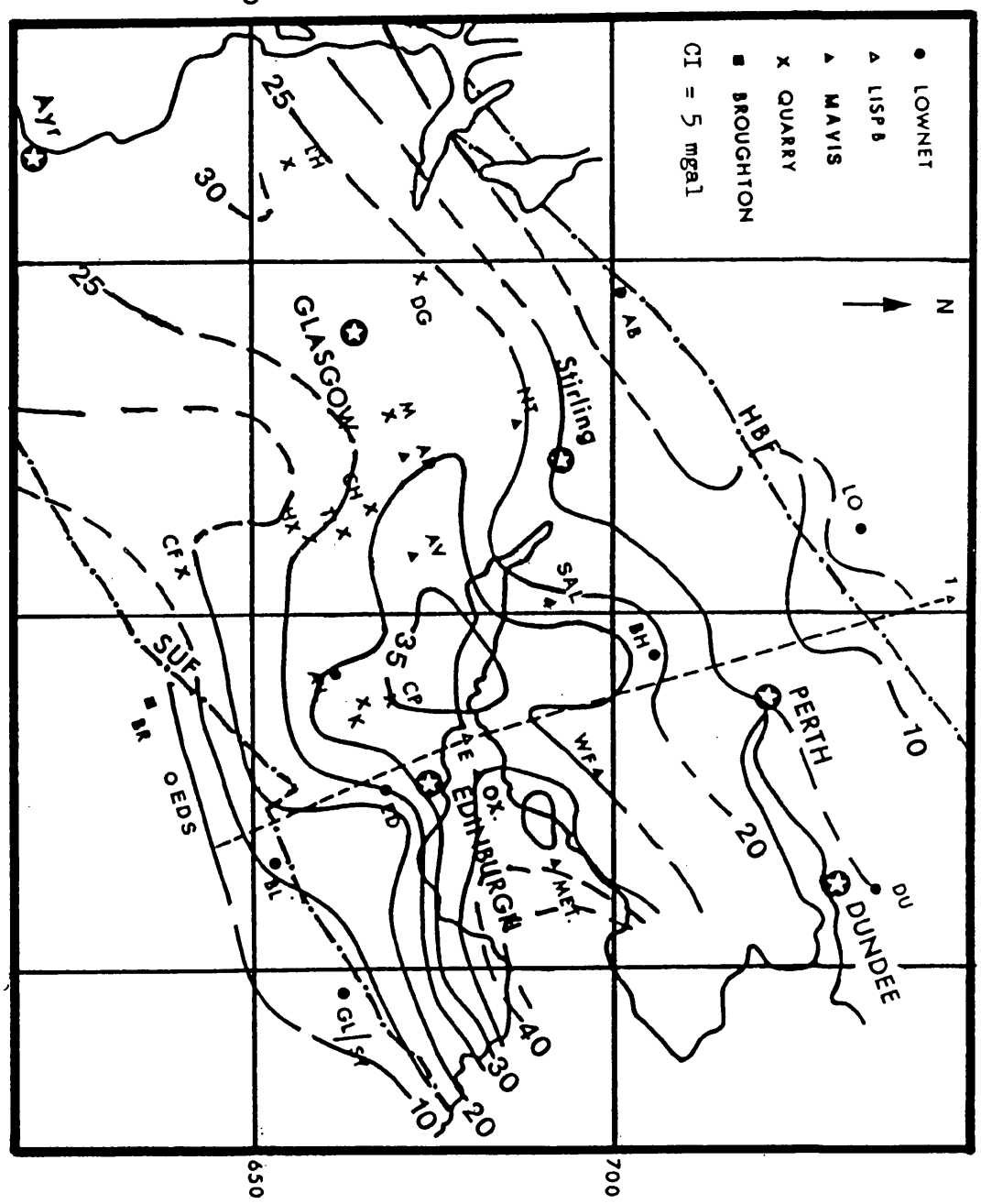

Fig. (4.15) Regional gravity map. Calculated from the delay times.

Table (4.5) GRAVITY EFFECTS ATTRIBUTED TO DELAYS

a - sites on Carboniferous sediments no lavas expected

site	Delay on a_o (s)		Bouguer value at site (mgal)	Gravity effect F=50	g = Delays xF F=60	Corrected gravity value (mgal)
CP	0.54	-	+9	27.0	32.4	36.5
K	0.44	-	+9	22.0	26.4	31.0
AU	0.45	-	+9	22.8	27.0	31.5
SAL	0.64	-	-2	32.0	38.4	30.0
WF	0.52	-	+1	26.0	31.2	27.0
METH	0.93	-	-8	46.0	55.8	38.0
E	0.42	-	+8	21.0	25.2	29.0
HX	0.40	-	+4	20.0	24.0	24.0
OX	0.53	-	+7	26.5	31.8	33.5

b - sites on Carboniferous sediments and Clyde Plateau Lavas

site	Delay on a_o (s)	Delay in Lava (s)	Delay in sediments (s)	Bouguer value at site (mgal)	Gravity effect F=50	F=60	Corrected (mgal)
NT	0.40	0.07	0.33	+9	16.5	19.8	25.5
TL	0.43	0.13	0.30	+8	15.0	18.0	23.0
M	0.57	0.14	0.43	+8	21.5	25.8	29.5
AV	0.48	0.14	0.34	+16	17.0	20.4	33.0
BG	0.42	0.14	0.28	+18	13.5	16.2	31.5

c - sites on Lower Old Red Sandstone

site	Delay on a_o (s)	Bouguer value at site (mgal)	Gravity effect F=50	F=60	Corrected gravity value (mgal)
BH	0.46	0	23.0	27.6	23.0
AB	0.26	0	13.0	15.6	13.0
ED	0.40	+10	20.0	24.0	30.0
CF	0.26	+10	13.0	15.6	23.0
DU	0.38	0	19.0	22.8	18.5

d - sites on Lower Palaeozoic (Southern Uplands) and Dalradian (Highlands)

site	Delay on a_o (s)	Bouguer value at site (mgal)	Gravity effect F=50	F=60	Corrected gravity value (mgal)
LO	-	-4	-	-	-4
1	-	-4	-	-	-4
BL		+1	-	-	+1
GL/SY		-1	-	-	-1
BR		+6	-	-	+6
EDS		-2	-	-	-2

values at sites outside the Midland Valley even though they have positive delays.

If, as the plotted means suggest, F = 50 is closer to an appropriate Carboniferous delay conversion but too low for a Lower Old Red Sandstone factor (F = 60 perhaps) then the results will underestimate the gravity results in proportion to 10 times the Lower Old Red Sandstone component of the delay. Over the Lower Old Red Sandstone outcrop this amounts to less than a contour interval. The main interpretive issues, however, concerns the effect along the ENE - WSW central 'FORTH AXIS' where with F = 50 the Methil site high at +40 mgal has already overtaken that of Bathgate (+35 mgal) and both, incidentally, the western profile peak of +30 mgal (McLean and Qureshi, 1966). Any uncounted Lower Old Red Sandstone effect would cause an inversion of the original easterly decrease in Bouguer gravity along this axis.

4.6.1 Discussion of and conclusions from Gravity Map, corrected for layers above a_o (including McLean and Qureshi line)

Fig. 4.15

1. Gravity stripping of the low density layers (essentially Upper Palaeozoic sediments) reveals a central regional high from Forth to Clyde.
2. Its continuity has still to be confirmed through the Glasgow area but its axis appears slightly oblique to the Midland Valley bounding faults (N 70^{o}E rather than N 45^{o}E).
3. Its origin must lie deeper than the top of the a_o basement. McLean and Qureshi deduced a mid-crustal origin. Al-Omari calculated the gravity effect of the LISPB structure on the 6.4 km s^{-1} basement to be similar to McLean and Qureshi curve 70 km to the SW.

4. The Bathgate high is still a 5 to 10 mgal culmination on the regional high axis (measured between control points AV,CP,E,OX and METH. The extra 10 mgal contoured extrapolates the high Methil correction). Since the Methil high is comparable but without an associated magnetic anomaly with deep seated characteristics, an intra-crystalline basement magnetic body divorced from any significant density contrast becomes more likely under Bathgate.

CHAPTER 5

CONCLUSIONS

1 The velocity layering in the area is represented as follows:

Seismic layer	velocity range (km s^{-1})	geological interpretation
1	3.40 - 3.80	Carboniferous sediments/ volcanic ash, tuffs and Upper Old Red Sandstone
2	4.50 - 5.00	Carboniferous lavas (CPL)
3	5.00 - 5.50	Lower Old Red Sandstone (sediment and lavas)/Lower palaeozoic
4	5.95 - 6.15	Crystalline basement/Lower palaeozoic (igneous or medium grade meta-morphic)

See Figures (3.4, 3.5) and table (4.1)

2 Layer (1) consists of Carboniferous and Upper Old Red Sandstone sediments and, in the former, ashy volcanics. On profiles across Bathgate area these rocks are about 1.0 km thick. They may be thicker around Methil but the seismic data here are insufficient to distinguish their effects from those of Lower Old Red Sandstone sediments.

3 Layer (2) consists of Clyde Plateau lavas about 1.0 km thick west of Bathgate but thinning to the east Figures (4.7 - 4.10). Upper Old Red Sandstone could be concealed beneath them by velocity reversal.

4 Layer (3) consists of Lower Old Red Sandstone and underlying Lower Palaeozoic greywacke and shale. Under the northern half of the area (Ochils and Highland Boundary Fault) these rocks are about 5.0 km thick whereas south of the Forth they are less than 3.0 km /

/reducing to 1.5 km thick around Bathgate. The transition between these areas is not well controlled and may be either gradual or abrupt (at the Ochil Fault). Figures (4.5, 4.13) and Table (4.4).

5 Layer (4) is Layer (2) of LISPB. Its top is the a_o refractor and has an average velocity of 6.08 ± 0.03 km s^{-1}. Local variations are still to be substantiated. This velocity is too high for sediments unless carbonates. Intermediate composition metamorphic and igneous rocks are more likely. Its depth ranges from 3.0 to 5.0 km under the area Figure(4.6)shallowest under Bathgate. The structure on N-S line through Bathgate is shown on Figure (4.13). Local relief over Bathgate is insufficient to explain the magnetic anomaly.

6 Regional gravity derived by stripping seismic delays from the Bouguer Map shows (Figure 4.15) that the Bathgate high is part of a broader axial feature (Ayrs - Forth). Consequently no need for magnetic body to be denser than surroundings, not seismically distinct either since a magnetic contrast depends only on accessory minerals, i.e. the basis for the seismic search outlined in Chapter 1. (Introduction) was mistaken.

Suggestions for further work

1 More refraction work needed to define the a_o refractor thickness, and to find what form the deeper LISPB (a_1) refractor (of 6.40 km s^{-1} velocity) does under Bathgate.

2 More refraction work over the Lower Old Red Sandstone outcrops (sediments and lavas).

REFERENCES

ADESANYA, O. (1982). Seismic velocities of the Upper Crust of the Southern Uplands. Unpublished Ph.D. Thesis, Glasgow University.

AL-AZZAWI, M. M. (1982). A seismological study of the rock quality behind a quarry face. Unpublished M.Sc. Thesis, Glasgow University.

ALLSOP, M. Jennifer. (1974). Geophysical surveys at the Spilmersford Borehole, East Lothian, Scotland. Bulletin of the Geological Survey of Great Britain. No. 45, 63 - 73.

ALOMARI, M. I. (1980). Geological interpretations of the gravity field of the western Midland Valley of Scotland. Unpublished Ph.D. Thesis, Glasgow University.

ANDERSON, F. W. (1963). The Geological Survey bore at Rashiehill, Stirlingshire. Bull. geol. surv. U.K. 20, 43 - 106.

ARMSTRONG, M. and PATERSON, I. B. (1970). The Lower Old Red Sandstone of the Strathmore region. Rep. No. 70/12, Inst. Geol. Sci.

ASSUMPCAO, M. (1978). Studies of crustal shear waves and poisson's ration. Unpublished Ph.D. Thesis, Edinburgh University.

BAMFORD, D., FABER, S., JACOB, B., KAMINSKI, W., NUNN, K., PRODEHL, C., FUCHS, K., KING, R. and WILLMORE, P. (1976). A Lithospheric Seismic Profile in Britain - 1, Preliminary Results. Geophys. J. R. Astron. Soc. 44, 145 - 160.

BAMFORD, D., NUNN, K., PRODEHL, C. and JACOB, B. (1977). LISPB-111. Upper crustal structure of Northern Britain. J. Geol. Soc. 133, 481 - 488.

BAMFORD, D., NUNN, K., PRODEHL, C. and JACOB, B. (1978). LISPB-IV. Crustal structure of Northern Britain. Geophys. J. R. Astron. Soc. 54, 43 - 60.

BLUCK, B. J. (1978). Sedimentation in a late orogenic basin: the Old Red Sandstone. In Bowes, D. R. and Leake, B. E. (Eds.). Crustal Evolution North Western Britain and adjacent Region Geol. J. Special Issue No. 10.

BLUCK, B. J. (1983). Role of the Midland Valley of Scotland in the Caledonian orogeny. Trans. R. Soc. Edinburgh Earth Sci. 74, 119 - 136.

COTTON, W. R. (1968). A Geological Survey of the Campsies and Kilpatrick Hills. Unpublished Ph.D. Thesis, Glasgow University.

CERVENY, V and PSENCIK, I., (1981). 2-D Seismic Ray Package, Research Report, Institute of Geophysics, Charles University, Prague.

CRAMPIN, S., JACOB, A. W. B., MILLER, A. and NEILSON, A. (1970). The LOWNET radio-linked seismometer network in Scotland. Geophys. J. R. Astron. Soc. 21, 207 - 216.

CURRY, B. G., BLUCK, B. J., BURTON, C. J., INGHAM, J. K. SIVETER, J. D. and WILLIAMS, A. (1984). Age, evolution and tectonics history of the Highland Border Complex, Scotland. Trans. R. Soc. Edinburgh Earth Sci. Vol. 75 part 2, 113 - 134.

DAVIDSON, K. A. S., SOLA, M., POWELL, D. W. and HALL, J. (1984). Geophysical model for the Midland Valley of Scotland. Trans. R. Soc. Edinburgh Earth Sci. Vol. 75, part 2, 175 - 182.

DRYSDALE, W. S. (1955) Firth of Forth seismic Refraction Survey. Transaction of the Institution of Mining Engineers. Vol. 115 part 6, 435 - 454.

EL-ISA, Z. H. M. (1977). Seismic studies of local events received at three arrays in Southern Central Scotland. Unpublished Ph.D. Thesis, Glasgow University.

FRANCIS, E. H. (1983). Carboniferous in Craig, G. Y. (edt). Geology of Scotland (2nd edn). chapter 9, 253 - 296.

FRANCIS, E. H. (1983). Carboniferous. Permian igneous rocks, in Craig, G. Y. (edt.). Geology of Scotland (2nd edn). chapter 10, 297 - 324.

GRANT, F. S. and WEST, C. F. (1965). Interpretational theory in applied geophysics, McGrah-Hill, New York.

HAGEDOORN, J. G., (1959). The Plus-Minus method of interpreting seismic refraction sections. Geophys. Prospect. 7, 158 - 162.

HALL, J. (1970). The correlation of seismic velocities with Formations in the southwest of Scotland. Geophys. Prospect. 18, 134 - 148.

HALL, J. (1971). A preliminary seismic survey adjacent to Rashiehill borehole near Slamannan, Stirlingshire. Scott. J. Geol. 7. 170 - 17.

HALL, J. (1974). A seismic reflection survey of the Clyde Plateau Lava in N. Ayrshire and Renfrewshire. Scott. J. Geol. 9, 253 - 279.

HALL, J. (1978). "LUST" - a seismic refraction survey of the Lewisian basement complex in N. W. Scotland. J. geol. soc. London; 135, 555 - 563.

HALL, J. (1978). Seismic refraction studies in Firth of Clyde. pp 43 - 48 in MCLEAN, A. C. and DEEGAN, C. E. (Editors). The solid Geology of Clyde Sheet ($55^{o}N/6^{o}W$) Rep. Inst. Geol. Sci., No. 78/79.

HALL, D. H. and DAGLEY, P. (1970). Regional magnetic anomalies: An analysis of the smoothed Aeromagnetic map of Great Britain and Northern Ireland. Rep. Inst. Geol. Sci., No. 70/10.

HALL, J., POWELL, D. W., WARNER, M. R., EL-ISA, Z. M. H., ADESANYA, O. and BLUCK, B. J. (1983). Seismological evidence of shallow crystaline basement in the Southern Uplands of Scotland. Nature 305, 418 - 420.

HALL, J. and SIMMONS, G. (1979). Seismic velocities of Lewisian metamorphic rocks at pressures to 8 kbar: relationship to crustal layering in North Britain. Geophys. J. R. Astron. Soc. 58, 337 - 347.

HIPKIN, R. G. and HUSSAIN, A. (1983). Regional gravity anomalies 1 Northern Britain. Rep. Inst. Geol. Sci. 82/10.

HOSSAIN, M. J. A. (1976). Analysis of the major gravity and magnetic anomalies centred about Bathgate, Central Scotland. Unpublished MS.c. Thesis, Glasgow University.

HUSSAIN, A. and HIPKIN, R. G. (1981). Regional gravity Map of the British Isles, Northern Sheet. (University of Edinburgh).

JACOB, A. W. B. (1969). Crustal phase velocities observed at the Eskdalemuir Seismic Array, Geophys. J. Roy. Astr. Soc., V. 18, 189 - 197.

LONGMAN, C. D., BLUCK, B. J. and VAN BREEMEN, O. (1979). Ordovician conglomerate and the evolution of the Midland Valley. Nature 280, 578 - 81.

MACGREGOR, M. and MACGREGOR, A. G. (1948). The Midland Valley of Scotland, Mem. Geol. Surv, U.K., Edinburgh

McLEAN, A. C. (1961). Density measurements of rocks in southwest Scotland. Proc. R. Soc. Edinb. 68, 103 - 111.

McLEAN, A. C. and QURESHI, I. R. (1966). Regional Gravity. Anomalies in the Western Midland Valley of Scotland, Trans. R. Soc. Edinburgh, V. 66, 267 - 283.

MECHIE, J. 1980. Program to calculate Time-Term Anisotropy. Dept. of Geological Sciences, University of Birmingham.

MYKURA, W. (1983). Old Red Sandstone, in Craig, G. Y. (edt). Geology of Scotland (2nd edn). chapter 8, 205 - 242.

PALMER, D. (1980). The generalised reciprocal method of seismic refraction interpretation. Tulsa, Society of Exploration Geophysicists.

POSTMA, G. W. (1955). Wave propagation in a stratified medium. Geophysics 20, 780 - 806.

QURESHI, I. R. (1970). A gravity survey of a region of the Highland Boundary Fault in Scotland. Q. J. geol. Soc. Lond. Vol. 125, 481 - 502.

UPTON, B. G. J., ASPEN, P. and HUNTER, H. R. (1984). Xenoliths and their implications for the deep geology of the Midland Valley of Scotland and adjacent regions. Trans. R. Soc. Edinburgh Earth Sci. Vol. 75 part 2, 65 - 70.

WALKER, J. H. D. (1969). Geophysical and geological measurements in the Upper Firth of Clyde. Unpublished Ph.D. Thesis, Glasgow University.

WALTON, E. K. (1983). Lower Palaezoic - stratigraphy in Craig, G. Y. (edt). Geology of Scotland (2nd edn). chapter 5, 105 - 160.

WARNER, M. R., HIPKIN, R. G. and BROWITT, C. W. A. (1982). Southern Uplands Seismic Refraction Profile - Preliminary Results. Geophys. J. R. astr. soc. 69, 279.

WILLMORE, P. L. and BANCROFT, A. M., (1960). The time-term approach to refraction seismology, Geophys. J. R. astr. soc. 3, 419 - 432.

APPENDIX 1

List of P travel time

Quarry and site co-ordinates. Distances are in km.

The travel times are given in total and reduced

(in seconds) with reduction velocity of 6.0 kms^{-1}.

* indicating repetition.

APPENDIX 1 Table 1

Quarry: Tamsloup Grid Reference: 288.600/664.000

Station	Grid Reference		Distance (km)	Time (sec)	T - x/6 (sec)	
1	288.832	663.895	0.367	0.07	0.01	
2	289.074	663.980	0.594	0.13	0.03	
3	289.737	664.179	1.270	0.37	0.16	
4	290.563	664.137	2.088	0.62	0.27	
5	290.600	664.126	2.140	0.65	0.30	
6	290.810	664.210	2.340	0.70	0.31	
7	291.084	664.210	2.610	0.74	0.31	
8	291.596	663.990	3.174	0.88	0.35	*
9	291.850	663.990	3.427	0.94	0.37	
10	292.090	664.010	3.667	1.01	0.40	
11	292.589	664.126	4.111	1.09	0.41	
12	292.789	664.221	4.315	1.20	0.48	*
13	293.032	664.284	4.561	1.22	0.76	
14	293.853	664.211	5.377	1.44	0.54	
15	294.105	667.305	5.633	1.49	0.55	
16	294.337	664.337	5.867	1.54	0.56	
17	294.910	663.780	6.792	1.67	0.59	
18	295.025	663.555	6.619	1.70	0.60	
19	295.537	664.695	7.091	1.79	0.61	
20	295.737	664.832	7.305	1.83	0.61	
21	295.958	664.958	7.539	1.87	0.62	*
22	296.315	664.789	7.875	1.95	0.64	

Station	Grid Reference		Distance (km)	Time (sec)	T - x/6 (sec)	
23	296.642	665.053	8.230	2.05	0.68	
24	297.000	665.147	8.597	2.11	0.68	
25	297.737	665.030	9.060	2.20	0.69	
26	297.779	665.032	9.314	2.24	0.69	*
27	298.084	665.126	9.670	2.44	0.78	
28	298.590	664.958	10.155	2.40	0.71	
29	298.711	664.842	10.266	2.44	0.73	
30	299.505	664.852	11.058	2.58	0.74	
31	299.742	664.895	11.298	2.67	0.79	
32	300.126	665.211	11.872	2.81	0.83	
33	300.200	665.190	11.903	2.84	0.86	
34	300.474	665.126	12.157	2.87	0.85	*
35	300.674	665.168	12.413	2.90	0.83	
36	300.957	665.294	12.544	2.97	0.88	
37	301.189	665.368	12.782	2.99	0.86	
38	301.421	665.450	13.022	3.05	0.88	
39	301.821	665.495	13.425	3.08	0.84	
40	302.053	665.442	13.650	3.13	0.86	
41	302.568	665.558	14.174	3.25	0.89	
42	303.379	665.547	14.979	3.39	0.89	
43	303.610	665.737	15.240	3.42	0.88	*
44	304.432	665.558	16.028	3.60	0.93	
45	304.642	665.684	16.249	3.63	0.92	*
46	305.779	665.400	17.356	3.83	0.94	
47	306.705	665.674	18.302	3.92	0.87	
48	306.947	665.790	18.554	3.96	0.87	

Station	Grid Reference		Distance (km)	Time (sec)	T - x/6 (sec)
49	308.011	665.710	19.606	4.08	0.81
50	308.568	665.716	20.161	4.16	0.80
51	309.370	665.905	20.977	4.32	0.81
52	309.582	666.026	21.199	4.35	0.82
53	310.770	662.250	22.403	4.63	0.90
54	310.940	666.370	22.585	4.66	0.90
55	311.200	666.450	22.852	4.69	0.88

APPENDIX 1 Table 2

Quarry: Kaimes Grid Reference: 313.800/666.600

Station	Grid Reference		Distance (km)	Time (sec)	$T - x/6$ (sec)
1	311.185	666.440	2.028	0.59	0.25
2	309.815	666.148	3.418	0.88	0.31
3	309.582	666.026	3.665	0.91	0.30
4	309.370	665.905	3.893	0.94	0.29
5	309.180	666.630	4.032	0.95	0.28
6	308.011	665.716	5.264	1.23	0.35
7	306.705	665.674	6.563	1.55	0.46
8	304.400	665.543	8.867	2.03	0.58
9	303.614	665.725	9.631	2.22	0.62
10	303.392	665.624	9.861	2.26	0.67
11	303.153	665.561	10.105	2.29	0.61
12	301.426	665.442	11.863	2.69	0.71
13	301.200	665.468	12.034	2.72	0.71
14	301.095	665.358	12.173	2.75	0.72
15	300.905	665.232	12.375	2.79	0.73
16	300.674	665.168	12.612	2.83	0.73
17	300.421	665.126	12.868	2.87	0.73
18	300.200	665.190	13.081	2.89	0.71
19	299.742	664.895	13.550	3.07	0.81
20	298.632	664.853	14.676	3.30	0.85

Station	Grid Reference		Distance (km)	Time (sec)	T - x/6 (sec)	
21	298.495	664.968	14.800	3.32	0.86	
22	297.737	665.053	15.545	3.42	0.83	
23	296.315	664.789	16.986	3.55	0.72	
24	295.958	664.958	17.325	3.74	0.85	
25	292.789	664.221	20.553	4.23	0.81	*
26	292.090	664.010	21.272	4.40	0.85	
27	291.063	664.242	22.243	4.54	0.85	*
28	289.158	663.842	24.204	4.90	0.87	
29	286.100	665.200	27.016	5.49	0.95	
30	282.925	664.340	30.240	5.93	0.89	
31	280.650	664.400	32.504	6.32	0.90	

APPENDIX 1 Table 3

Quarry: Craigpark Grid Reference: 312.900/670.400

Station	Grid Reference		Distance (km)	Time (Sec)	T - x/6 (Sec)	
1	311.400	670.650	1.500	0.31	0.06	
2	310.600	670.345	2.320	0.59	0.20	
3	309.653	670.753	3.272	0.78	0.24	
4	309.410	670.705	2.500	0.83	0.25	
5	309.179	670.610	3.730	0.88	0.26	
6	308.516	670.663	4.395	1.18	0.45	
7	308.411	670.653	4.499	1.22	0.47	
8	308.158	670.621	4.750	1.24	0.45	
9	306.168	670.632	5.730	1.47	0.51	
10	306.916	670.632	5.991	1.58	0.58	
11	306.700	671.150	6.220	1.67	0.63	
12	304.000	671.225	8.918	2.28	0.79	
13	302.850	671.110	10.075	2.46	0.78	
14	301.910	670.570	10.990	2.62	0.79	*
15	301.875	670.725	11.025	2.64	0.80	
16	301.400	670.425	11.500	2.65	0.74	
17	300.380	670.360	12.521	2.92	0.83	
18	299.410	670.063	13.494	3.08	0.83	
19	298.885	670.370	14.015	3.13	0.79	*

Station	Grid Reference		Distance (km)	Time (Sec)	T - x/6 (Sec)
20	297.947	670.421	14.953	3.35	0.86
21	297.300	670.175	15.602	3.41	0.85
22	296.984	670.200	15.922	3.45	0.79
23	296.968	670.200	15.935	3.54	0.88
24	296.263	670.095	16.640	3.67	0.89
25	296.200	670.100	16.700	3.54	0.75
26	295.210	670.421	17.690	3.86	0.91
27	294.900	670.200	18.002	3.93	0.93
28	294.250	670.375	18.650	4.04	0.93
29	293.265	670.850	19.618	4.22	0.95
30	293.225	670.850	19.677	4.25	0.97
31	292.788	670.820	20.115	4.31	0.96
32	292.539	670.835	20.333	4.38	0.99
33	291.714	670.714	21.188	4.53	1.00
34	291.243	670.540	21.657	4.58	0.97
35	290.958	670.148	22.002	4.63	0.96
36	290.150	670.600	22.750	4.78	0.99
37	288.275	670.238	24.625	5.10	0.99
38	287.825	671.000	25.078	5.16	0.98
39	286.600	670.100	26.302	5.28	0.90
40	283.105	669.475	29.795	5.85	0.88
41	280.685	670.525	32.215	6.46	1.09
42	279.850	671.350	33.064	6.61	1.09

Station	Grid Reference		Distance (km)	Time (Sec)	T - x/6 (Sec)
43	275.812	669.612	37.100	7.24	1.05
44	274.375	670.200	38.525	7.51	1.08

APPENDIX 1 Table 4

Quarry: Medrox Grid Reference: 272.895/669.790

Station	Grid Reference		Distance (km)	Time (sec)	T - x/6 (sec)
1	273.950	669.725	1.057	0.31	0.13
2	275.700	669.775	2.805	0.84	0.37
3	276.700	670.480	3.867	1.16	0.52
4	277.290	671.700	4.790	1.34	0.54
5	278.350	670.825	5.556	1.52	0.59
6	279.825	671.358	7.108	1.89	0.71
7	280.684	670.526	7.824	2.14	0.84
8	282.684	670.221	9.798	2.41	0.78
9	283.850	670.850	11.008	2.69	0.86
10	284.400	670.453	11.530	2.86	0.94
11	286.611	670.116	13.720	3.30	1.01
12	287.968	670.095	15.081	3.53	0.99
13	288.392	670.233	15.503	3.60	1.02
14	288.394	670.450	15.914	3.66	1.01
15	290.958	670.148	18.068	4.03	1.02
16	291.714	670.714	18.843	4.08	0.94
17	293.737	671.000	20.877	4.45	0.97
18	295.210	670.421	22.423	4.80	1.06
19	297.947	670.421	25.060	5.22	1.04

APPENDIX 1 Table 5

Quarry: Headless Cross Open Cast Grid Reference: 289.120/657.750

Station	Grid Reference		Distance (km)	Time (sec)	T - x/6 (sec)	
1	290.105	656.989	0.949	0.30	0.14	
2	290.316	656.947	1.133	0.32	0.13	*
3	289.463	656.390	1.155	0.34	0.15	
4	289.474	656.210	1.355	0.39	0.17	
5	289.316	656.063	1.487	0.44	0.19	
6	289.337	656.842	1.706	0.51	0.23	
7	289.010	655.663	1.930	0.58	0.26	
8	289.063	655.379	2.198	0.62	0.25	
9	289.695	655.400	2.279	0.63	0.25	
10	289.137	655.263	2.302	0.67	0.29	*
11	290.253	655.625	2.303	0.66	0.28	
12	290.095	655.337	2.434	0.70	0.29	
13	289.695	655.137	2.541	0.70	0.28	*
14	289.863	655.137	2.578	0.71	0.28	
15	289.632	655.032	2.655	0.74	0.30	
16	289.389	654.979	2.701	0.75	0.30	
17	289.053	654.821	2.870	0.79	0.31	
18	288.737	654.600	3.144	0.84	0.32	
19	288.789	654.495	3.236	0.88	0.34	
20	289.105	654.210	3.471	0.97	0.39	
21	289.221	653.000	3.672	1.02	0.41	

Station	Grid Reference		Distance (km)	Time (sec)	T - x/6 (sec)	
22	289.400	653.632	4.048	1.09	0.42	
23	289.463	653.421	4.259	1.13	0.42	
24	288.937	653.253	4.484	1.17	0.42	
25	288.947	653.105	4.630	1.20	0.43	
26	288.979	652.853	4.878	1.26	0.45	
27	289.000	652.589	5.137	1.28	0.42	
28	289.200	652.463	5.251	1.26	0.39	
29	289.200	652.121	5.414	1.26	0.36	
30	289.210	652.200	5.514	1.30	0.38	
31	289.126	651.895	5.643	1.30	0.36	
32	289.168	651.947	5.768	1.36	0.70	
33	289.126	651.653	5.885	1.35	0.37	
34	288.937	651.811	5.919	1.43	0.44	*
35	288.905	651.578	6.153	1.47	0.44	
36	288.884	651.305	6.428	1.51	0.44	*
37	288.821	651.284	6.445	1.51	0.43	
38	288.695	651.042	6.554	1.60	0.51	
39	288.874	650.442	7.110	1.61	0.49	
40	288.968	650.221	7.324	1.63	0.51	
41	289.070	650.025	7.539	1.77	0.51	
42	289.030	649.790	7.775	1.82	0.52	
43	288.935	649.555	8.015	1.86	0.52	
44	288.810	649.150	8.428	1.93	0.53	
45	288.690	648.950	8.637	1.97	0.53	
46	288.750	648.850	8.707	1.95	0.50	

Station	Grid Reference		Distance (km)	Time (sec)	T - x/6 (sec)
47	288.190	648.100	9.511	2.10	0.52
48	288.070	647.880	9.745	2.14	0.52
49	292.510	647.940	10.200	2.24	0.54
50	293.050	645.910	12.288	2.61	0.56
51	293.800	644.540	13.822	2.97	0.67
52	294.050	643.310	15.069	3.16	0.65

APPENDIX 1 Table 6

Quarry: Cairngryffe Grid Reference: 294.270/641.275

Station	Grid Reference		Distance (km)	Time (sec)	T - x/6 (sec)
1	293.400	644.290	3.140	0.70	0.18
2	292.510	647.940	6.890	1.41	0.26
3	291.650	650.100	9.206	1.92	0.39
4	290.100	655.350	14.680	3.00	0.55

APPENDIX 1 Table 7

Quarry: Headless Cross Open Cast Grid Reference: 289.120/657.750

Station	Grid Reference		Distance (km)	Time (sec)	T - x/6 (sec)	
1	289.842	658.568	1.438	0.45	0.21	
2	289.590	659.137	1.946	0.59	0.26	
3	289.900	660.020	2.840	0.82	0.34	
4	290.550	661.750	4.693	1.23	0.44	
5	289.895	662.779	5.021	1.31	0.47	
6	289.890	662.770	5.592	1.46	0.53	
7	289.990	663.400	6.228	1.61	0.57	
8	289.758	664.253	6.473	1.61	0.53	
9	290.337	665.500	7.825	1.89	0.59	
10	290.790	666.490	9.258	2.23	0.67	
11	290.525	667.115	9.400	2.23	0.66	*
12	290.525	667.115	9.450	2.33	0.73	
13	290.350	668.320	10.577	2.49	0.73	
14	291.337	667.830	10.666	2.58	0.80	*
15	290.350	668.320	11.160	2.63	0.77	
16	290.500	669.320	11.588	2.78	0.85	
17	290.737	669.875	12.353	2.85	0.80	
18	290.980	670.580	12.897	2.95	0.82	
19	290.926	670.905	13.260	3.04	0.80	
20	290.695	671.558	13.830	3.12	0.81	*
21	290.695	671.558	13.835	3.12	0.81	

Station	Grid Reference		Distance (km)	Time (sec)	T - x/6 (sec)	
22	290.550	672.225	14.164	3.21	0.85	
23	290.700	672.875	15.334	3.36	0.81	
24	290.758	673.253	15.625	3.44	0.84	
25	290.325	673.725	16.154	3.54	0.85	
26	290.421	674.453	16.793	3.62	0.82	
27	290.260	675.260	17.250	3.71	0.83	*
28	290.260	675.460	17.788	3.81	0.85	
29	290.350	676.125	18.051	3.88	0.87	
30	290.480	676.160	18.500	4.00	0.91	
31	290.550	676.700	19.138	4.02	0.83	
32	290.160	677.530	19.850	4.17	0.86	
33	289.275	679.300	21.500	4.38	0.80	

APPENDIX 1 Table 8

Quarry: Tamsloup Grid Reference: 288.500/644.000

Station	Grid Reference		Distance (km)	Time (sec)	T - x/6 (sec)
1	290.135	668.080	4.395	1.10	0.37
2	290.884	672.020	8.367	2.00	0.61
3	290.820	673.326	9.610	2.25	0.65
4	290.158	674.442	10.575	2.47	0.71
5	290.326	675.442	11.587	2.68	0.75

APPENDIX 1 Table 9

Quarry: Douglasmuir Grid Reference: 252.170/674.760

Station	Grid Reference		Distance (km)	Time (sec)	T - x/6 (sec)
1	253.010	675.190	0.944	0.19	0.03
2	253.150	675.990	1.585	0.37	0.11
3	253.940	676.940	2.810	0.70	0.23
4	254.580	677.930	3.980	0.97	0.31
5	255.520	679.020	5.420	1.29	0.39

APPENDIX 1 Table 10

Quarry: Loanhead Grid Reference: 236.500/655.200

Station	Grid Reference		Distance (km)	Time (sec)	T - x/6 (sec)
1	237.600	654.560	1.300	0.18	0.04
2	239.330	653.500	3.300	0.73	0.18
3	242.060	651.300	6.790	1.65	0.52
4	244.050	650.170	9.072	2.05	0.54
5	245.600	651.400	9.862	2.20	0.56
6	244.520	648.220	10.028	2.22	0.55
7	245.700	648.220	11.550	2.54	0.61
8	247.800	650.200	12.377	2.70	0.64
9	250.600	648.600	15.680	3.24	0.63

APPENDIX 1 Table 11

Quarry: Craigpark Grid Reference: 312.900/670.400

Station	Grid Reference		Distance (km)	Time (sec)	T - x/6 (sec)
1	317.200	666.950	5.839	1.37	0.40
2	318.250	667.010	6.921	1.57	0.42
3	319.330	667.130	7.214	1.71	0.51
4	321.670	667.070	9.381	2.12	0.56
5	322.230	667.110	9.893	2.22	0.57
6	323.180	667.550	10.668	2.39	0.61
7	323.830	667.540	11.298	2.52	0.64
8	324.550	667.230	12.074	2.61	0.60

APPENDIX 1 Table 12

Quarry: Kaimes Grid Reference: 313.080/666.600

Station	Grid Reference		Distance (km)	Time (sec)	T - x/6 (sec)
1	318.250	667.010	5.186	1.19	0.33
2	319.330	667.130	6.272	1.40	0.36
3	320.350	667.330	7.305	1.59	0.37
4	321.670	667.070	8.603	1.84	0.41
5	323.180	667.550	10.145	2.15	0.46
6	323.830	667.540	10.791	2.26	0.46
7	324.550	667.230	11.487	2.37	0.46

APPENDIX 1 Table 13

Quarry: Craigpark Grid Reference: 312.700/670.300

Station	Grid Reference		Distance (km)	Time (sec)	T - x/6 (sec)
1	297.737	665.053	15.856	3.61	0.97
2	297.500	665.053	16.080	3.65	0.97
3	296.305	664.674	17.333	3.81	0.92
4	296.105	664.567	17.555	3.85	0.92
5	294.305	664.242	19.367	4.14	0.91
6	294.053	664.126	19.642	4.18	0.91
7	293.032	664.284	20.568	4.38	0.95
8	292.789	664.221	20.818	4.44	0.97
9	291.084	664.210	22.458	4.73	0.99
10	289.084	663.990	24.444	5.07	0.99

APPENDIX 1 Table 14

Quarry: Cairney Hill Grid Reference: 284.950/666.550

Station	Grid Reference		Distance (km)	Time (sec)	T - x/6 (sec)
1	289.520	667.920	4.870	1.29	0.48
2	289.760	667.965	5.113	1.34	0.49
3	290.010	668.020	5.370	1.38	0.49
4	290.455	668.218	5.850	1.57	0.60
5	290.678	668.300	6.087	1.62	0.60
6	290.915	668.385	6.338	1.68	0.63
7	291.735	668.770	7.139	1.86	0.67
8	291.980	668.890	7.409	1.93	0.69
9	292.160	669.030	7.625	1.98	0.71

APPENDIX 1 Table 15

INTERCONNECTIONS

Quarry: Headless Cross Grid Reference: 289.120/657.750

Station	Grid Reference		Distance (km)	Time (sec)	T - x/6 (sec)
1	281.895	665.440	10.552	2.53	0.77
2	282.660	664.590	9.408	2.37	0.80
3	284.395	671.275	14.327	3.20	0.81
4	283.250	672.250	15.643	3.48	0.87
5	282.712	673.287	16.807	3.71	0.91
6	280.932	670.312	14.995	3.42	0.92
7	271.775	669.775	21.106	4.47	0.95

Quarry: Tamsloup Grid Reference: 288.600/664.074

1	291.547	657.790	6.941	1.74	0.58
2	289.787	658.675	5.556	1.42	0.50
3	281.895	665.440	6.842	1.73	0.58
4	282.660	664.590	5.962	1.56	0.55
5	275.557	670.230	14.423	3.33	0.88
6	283.250	672.250	9.771	2.32	0.69
7	282.712	673.287	10.934	2.63	0.80
8	286.556	670.125	6.389	1.57	0.51
9	271.775	669.775	17.765	3.89	0.93
10	291.714	670.714	7.455	1.91	0.67
11	290.958	670.148	6.627	1.73	0.63
12	291.243	670.540	7.096	1.78	0.60
13	293.325	670.900	8.408	2.07	0.71

Station	Grid Reference		Distance (km)	Time (sec)	T - x/6 (sec)
14	292.885	670.850	8.076	2.03	0.71
15	292.575	670.850	8.016	2.01	0.70
16	287.968	670.095	6.435	1.64	0.57
17	288.392	670.233	6.208	1.55	0.53
18	288.794	670.450	6.087	1.52	0.52

APPENDIX 2

Geological maps with recording sites

Reduced travel time plots with geological cross sections.

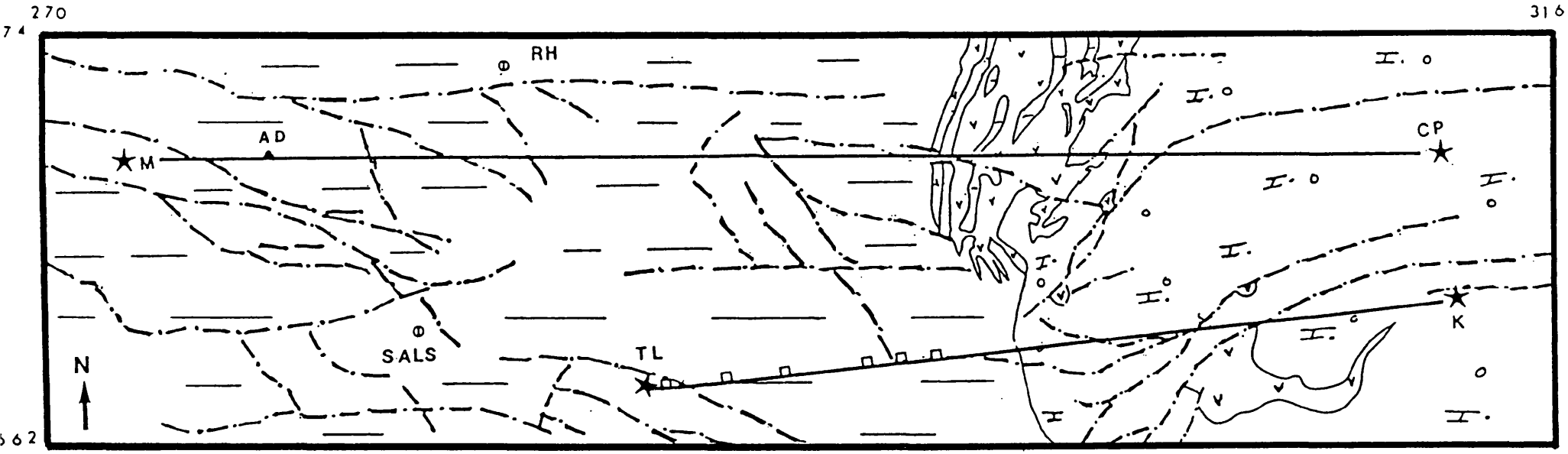

Φ Borehole (RH) Rashiehill, (Sals) Salsburgh.

□ (CP) Recording Site Harthill

—— Recording Line

Scale 1:170000

C.Sed

C.Lava

C.Sed/UORS

Fig. (1) Geological map showing the recording profiles between (K) Kaimes, (TL) Tamsloup and (CP) Craigpark, (M) Medrox (After IGS 1" Geological Map)

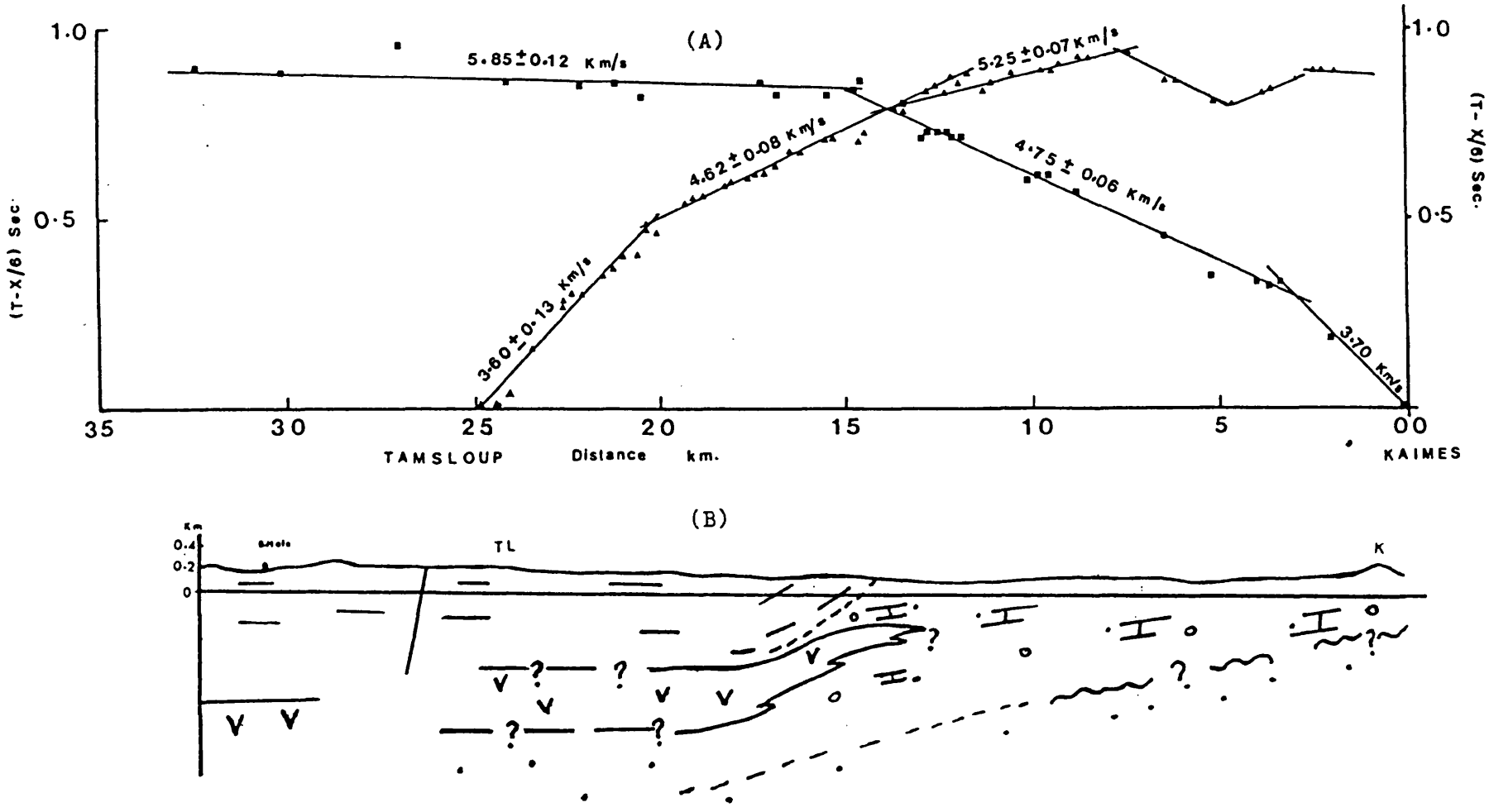

Fig. (2) Tamsloup (TL) - Kaimes (K) line. (A) reduced travel time plot of the first arrival. (B) cross section based on geological evidence and Salsburgh borehole. Vert = 3 Hor.

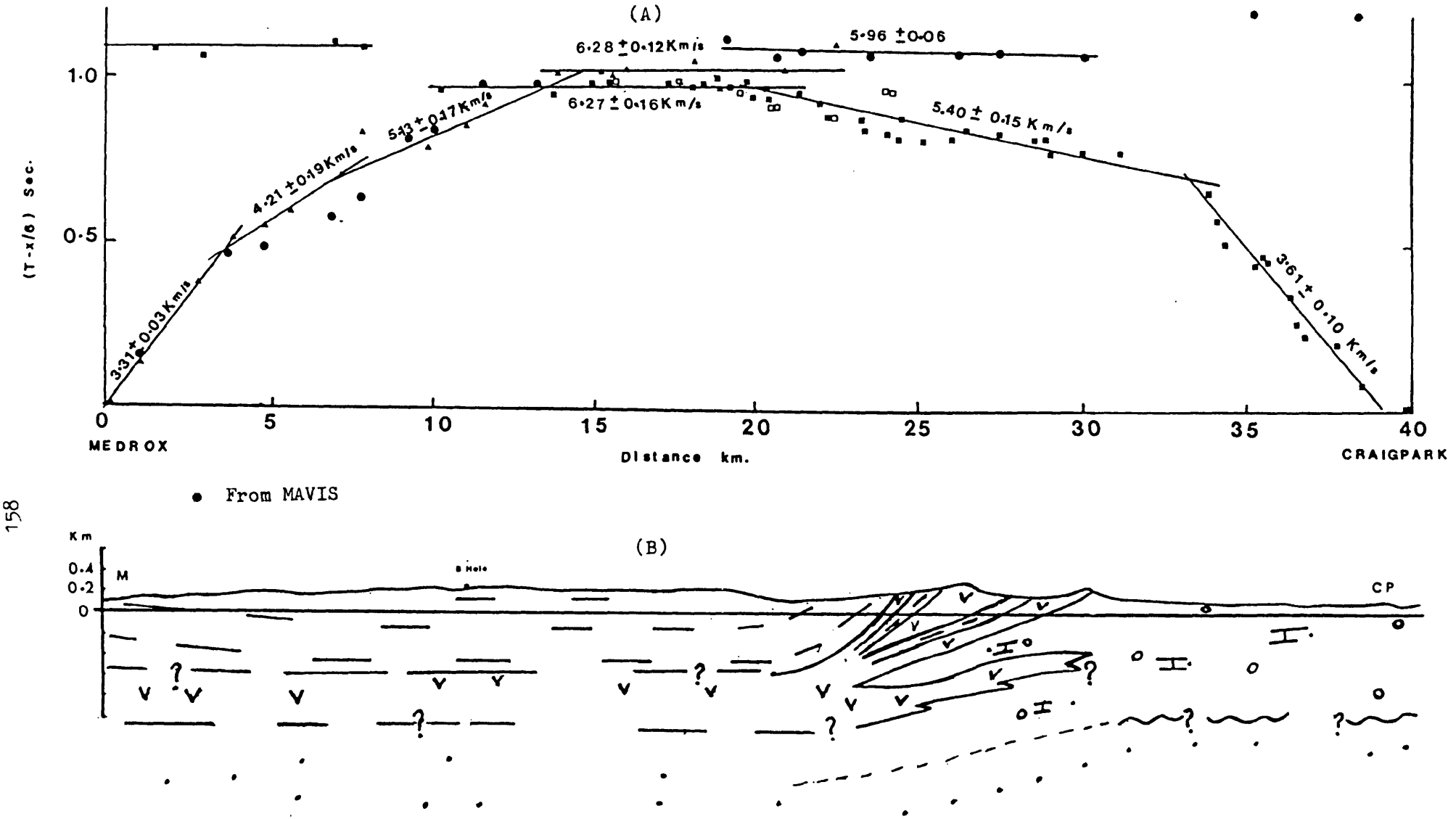

Fig. (3) Medrox (M) - Craigpark (CP) line. (A) reduced travel time plot (B) cross section based on geological evidence and Slamannan borehole control. Vert = 3 Hor.

Fig. (4) Geological map showing sites recorded from Headless Cross (HX), Cairngryffe (CF) (After IGS 1" Geological map)

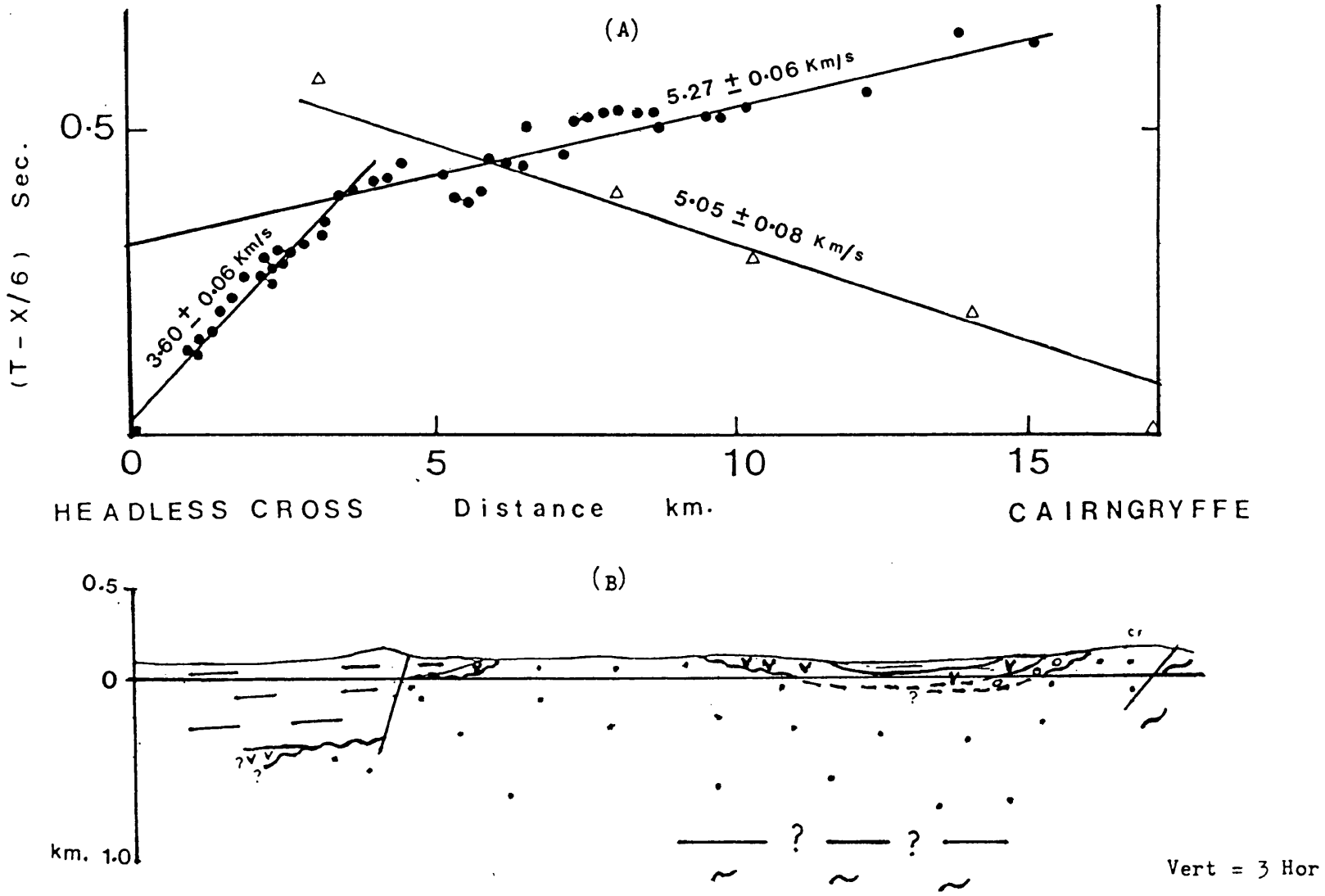

Fig. (5) Headless cross (HX) - Cairngryffe (CF) line. (A) reduced travel time plot of the first arrival. (B) cross section based on geological evidence. Lower Old Red Sandstone thickness projected from southwest where underlain by silurian and ordovician rocks.

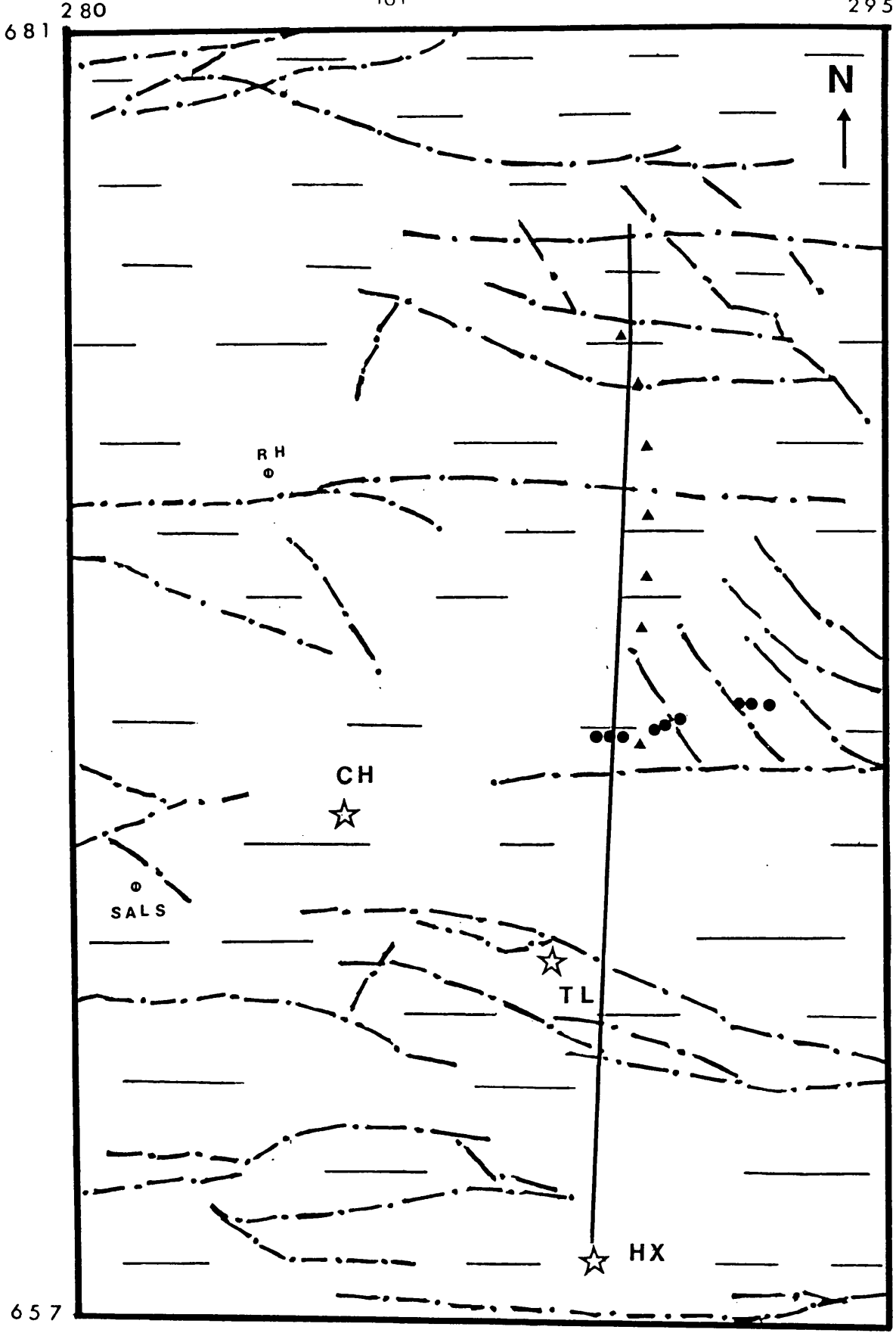

C. Sed.

Scale 1:104000

Recording Line (HX)

⊕ borehole (RH) Rashiehill
(Sals) Salsburgh

▲ (TL) recording sites

● (CH) recording sites

Fig. (6) Geological map showing sites recorded from (HX) Headless Cross, (TL) Tamsloup and Cairneyhill (from IGS 1" Geological map)

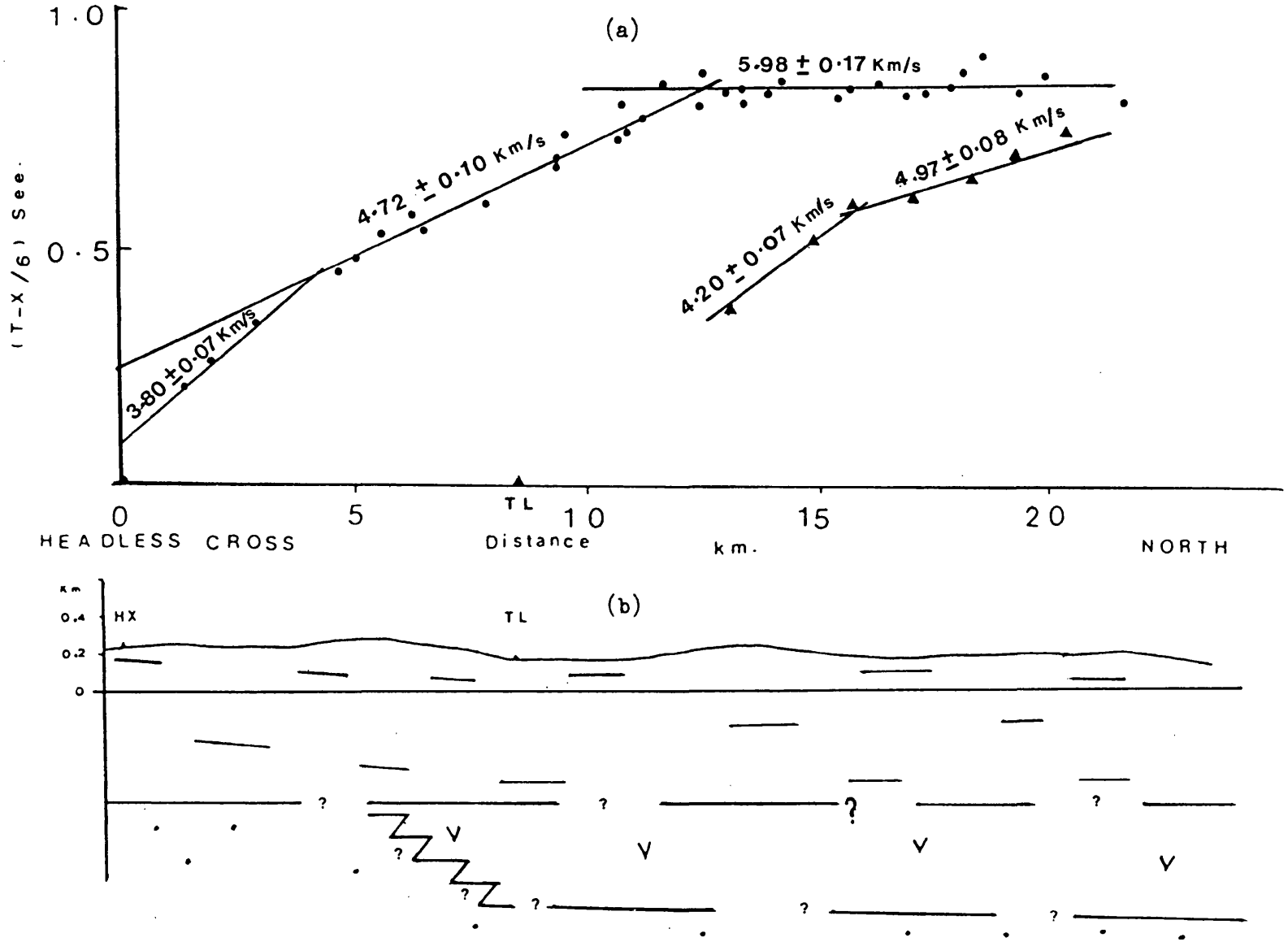

Fig. (7) Headless Cross (HX) Tamsloup (TL) North lines. (a) reduced travel time plot of first arrival (b) cross section based on geological evidence. Carboniferous sediments and lava thicknesses projected from Slamannan bore hole. Vert = 4 Hor

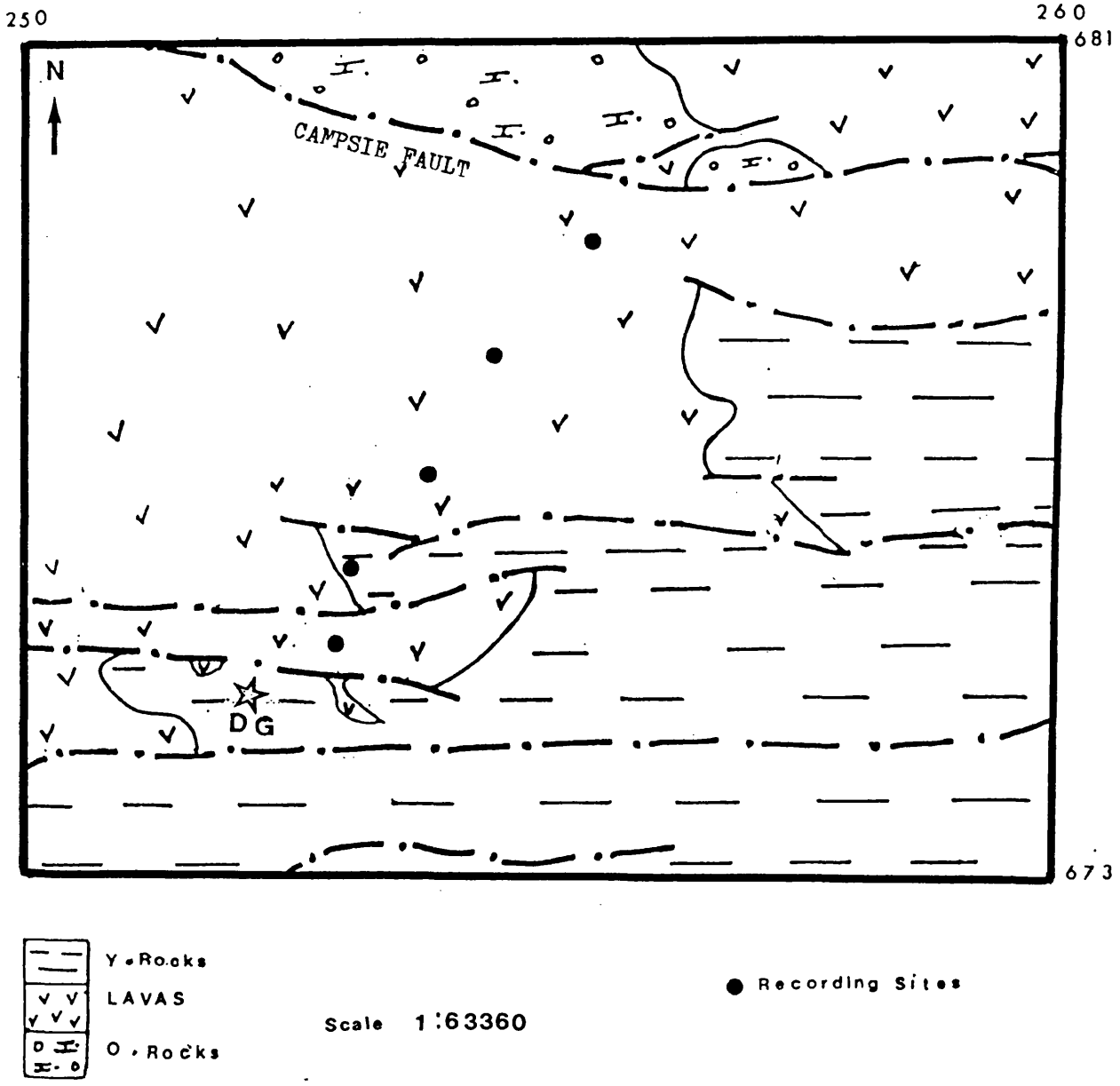

Fig. (8) Geological map showing sites recorded from Douglasmuir (DG) quarry (from IGS 1" Geological map)

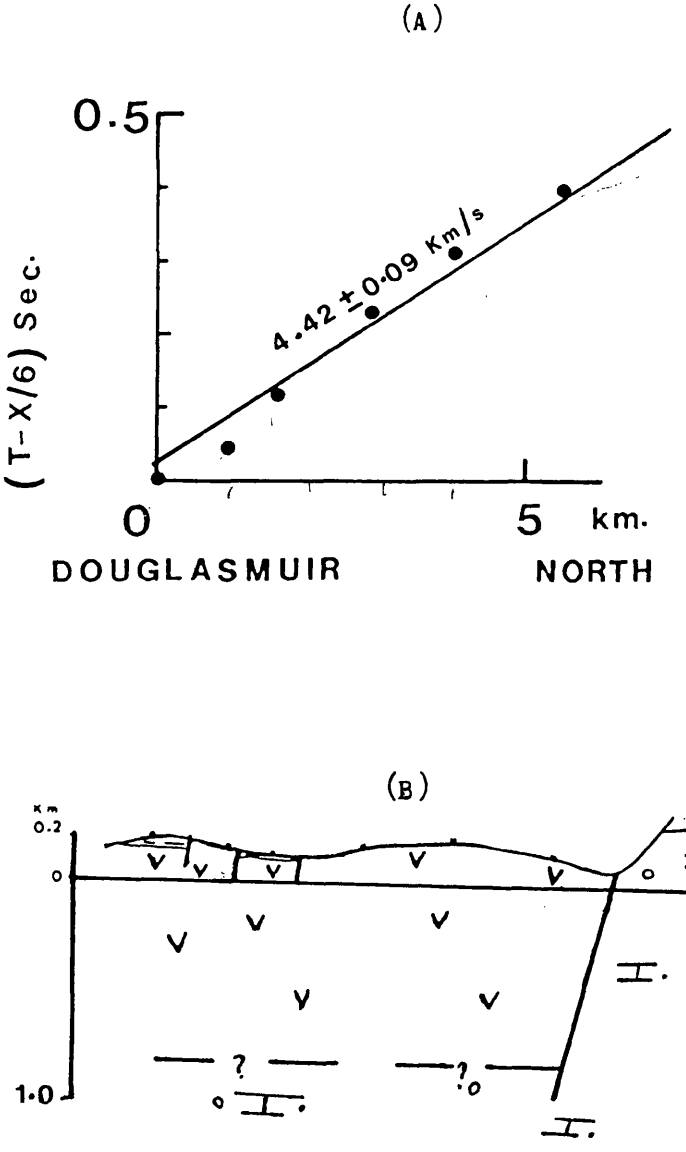

Fig. (9) Douglasmuir line
(A) reduced travel time plot of the first arrival
(B) cross section based on geological evidence. The base of lavas projected from SW (near Dumbarton) at 5^{o} dip from its outcrop 12 km. Vert = 3 Hor.

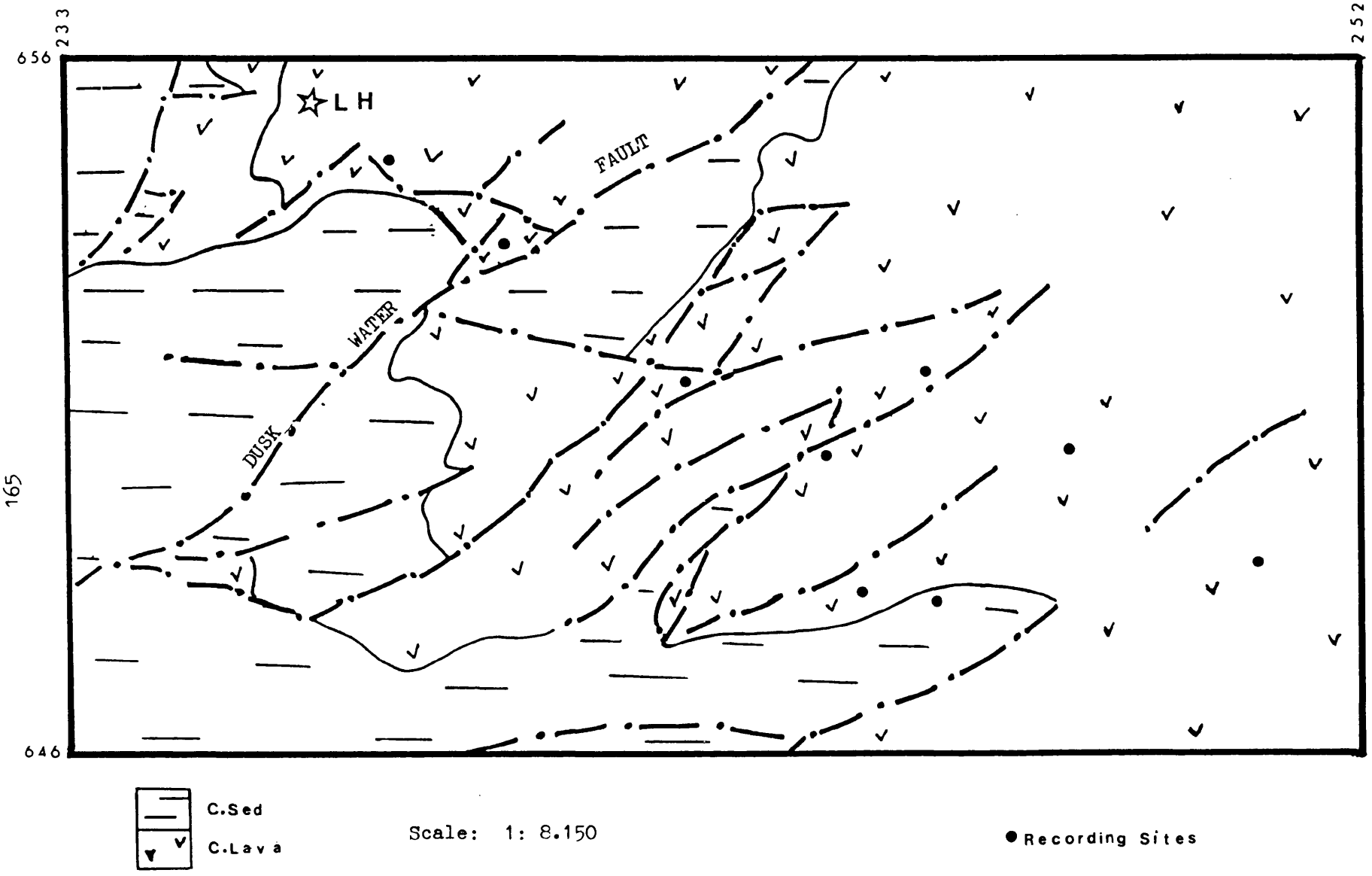

Fig. (10) Geological map showing sites recorded from (LH) Loanhead quarry (After IGS 1" Geological map)

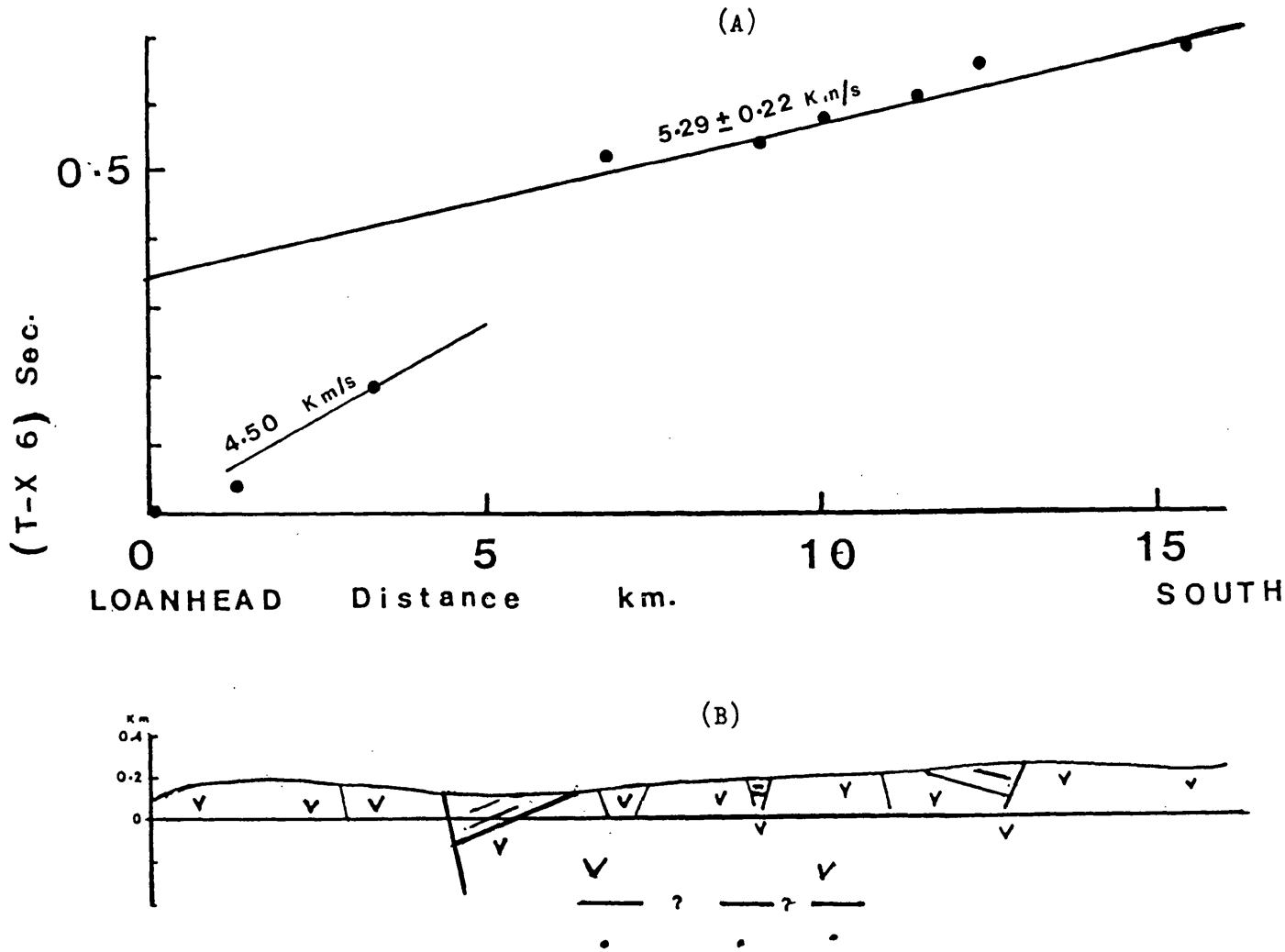

Fig. (11) Loanhead (LH) line. (A) reduced travel time plot of first arrivals. (B) cross section from Loanhead East based on geological evidence. Lavas thickness based on reflection survey. Vert = 3 Hor.

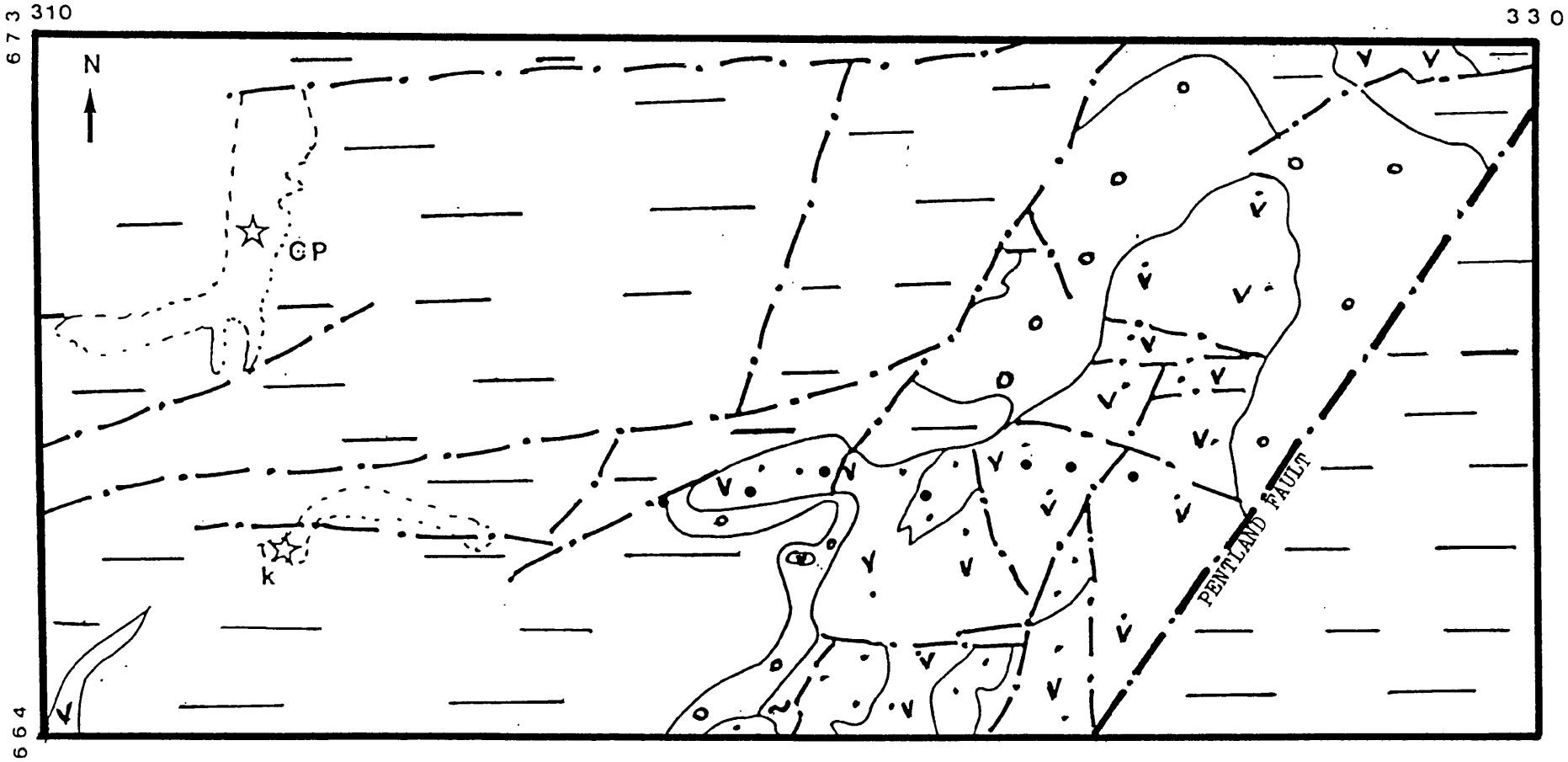

Fig. (12) Geological map showing sitesrecorded at Pentland Hills from (K) Kaimes and (CP) Craigpark (from IGS 1" Geological map).

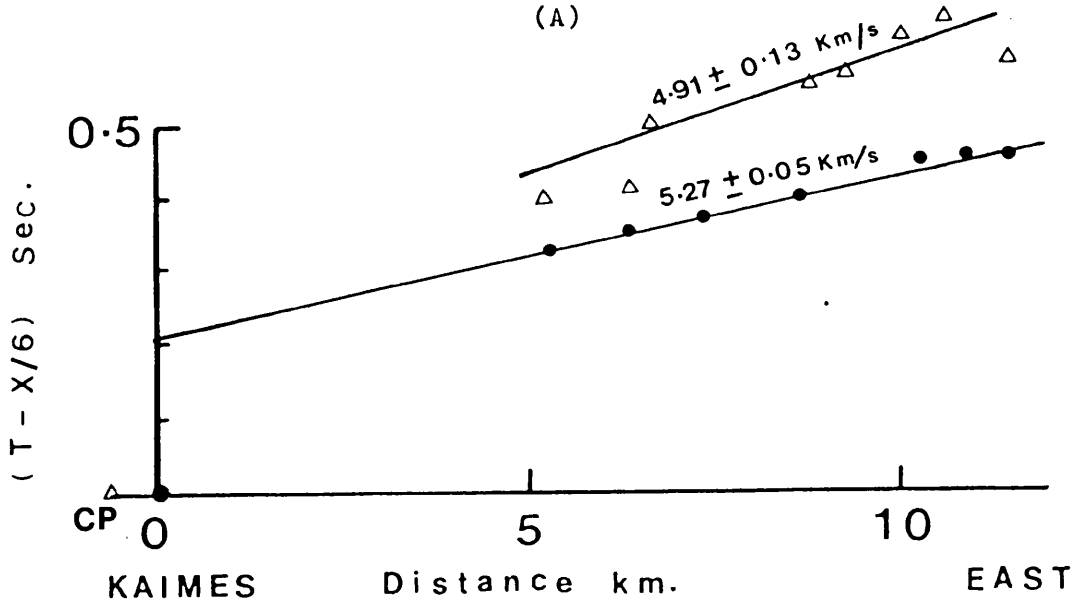

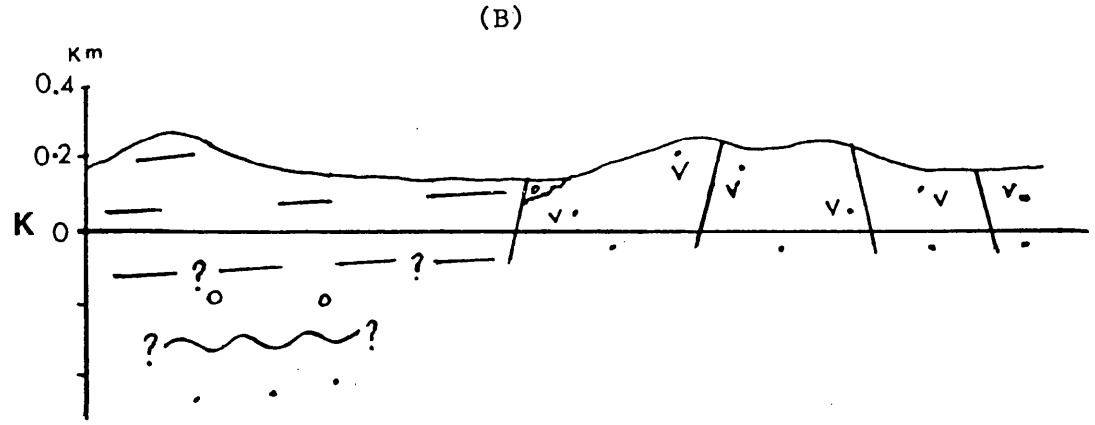

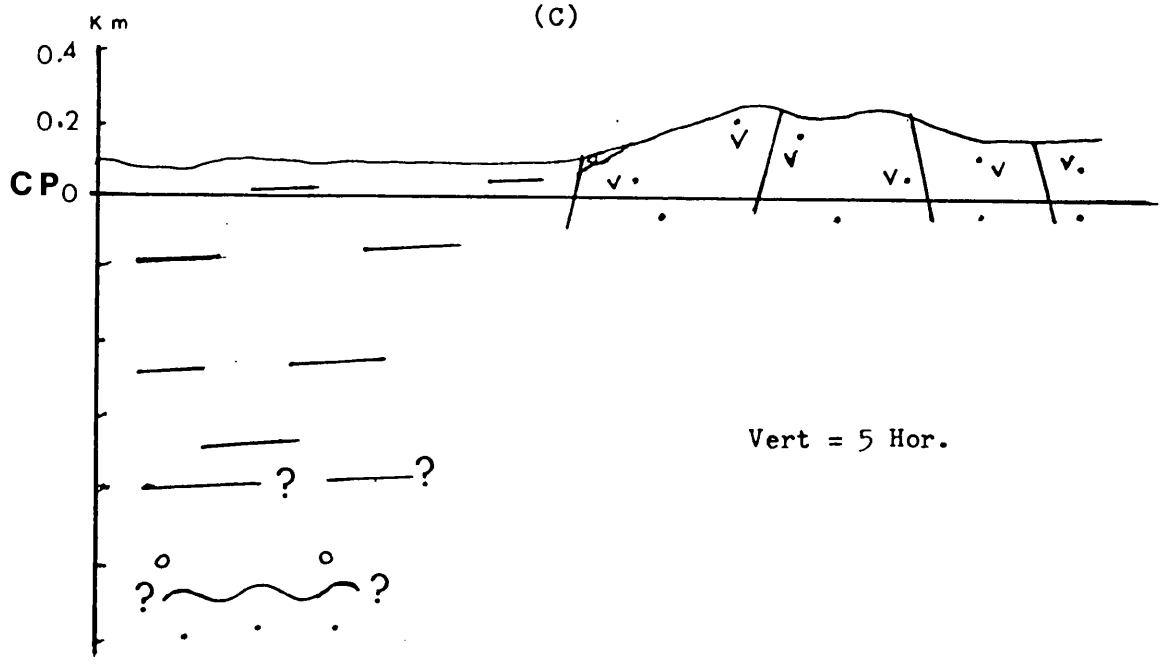

Fig. (13) Kaimes (K) and Craigpark (CP) - Pentlands line
(A) reduced travel time plot of first arrivals (B) (K) cross-section based on geological evidence (C) (CP) cross section based on geological evidence. The cross sections show the difference in carbon-

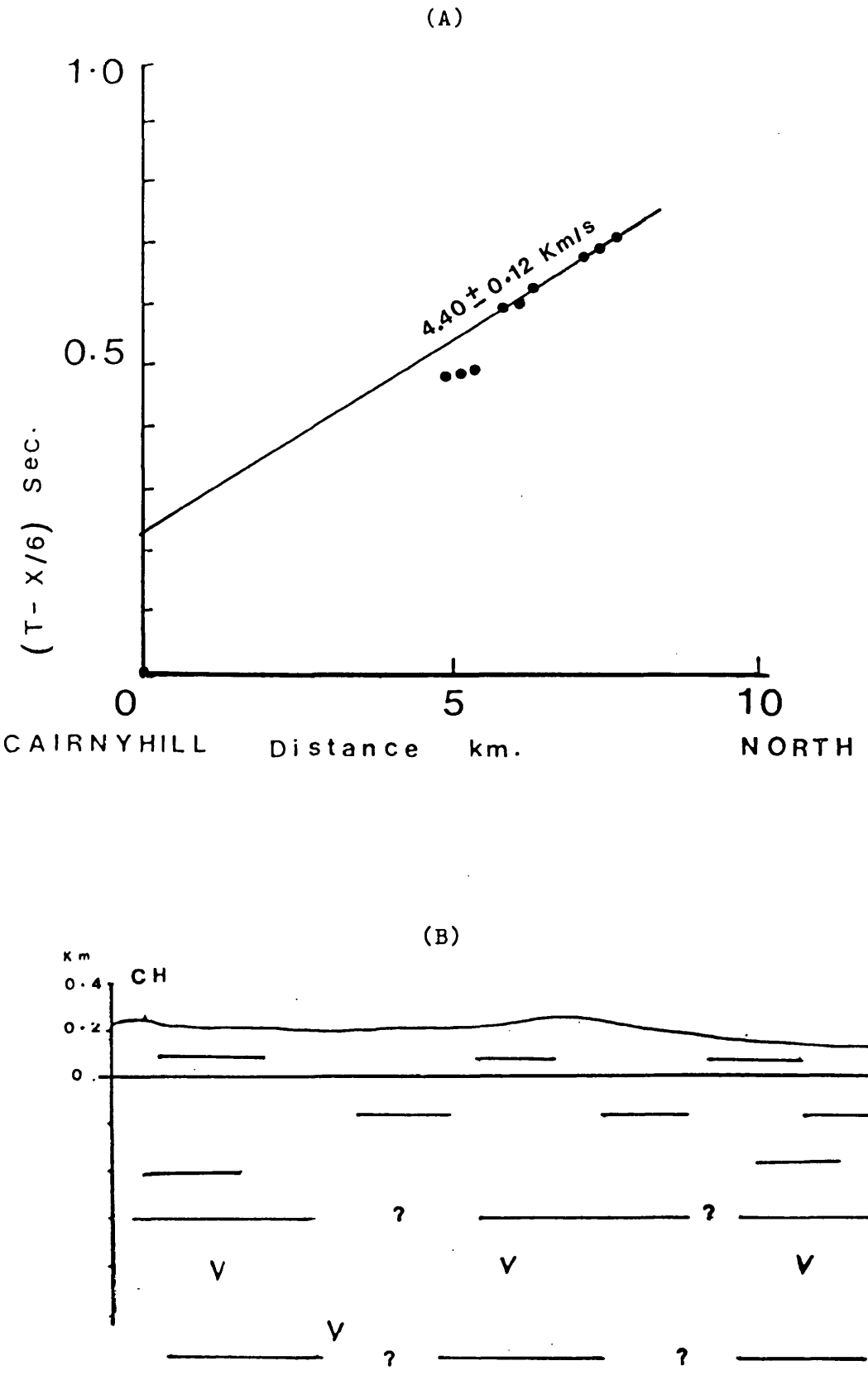

Fig. (14) Cairney Hill (CH) line. (A) reduced travel time plot of the first arrival. (B) cross section based on geological evidence. Carboniferous sediment and lava thicknesses projected from Slamannan borehole. Vert = 4 Hor.

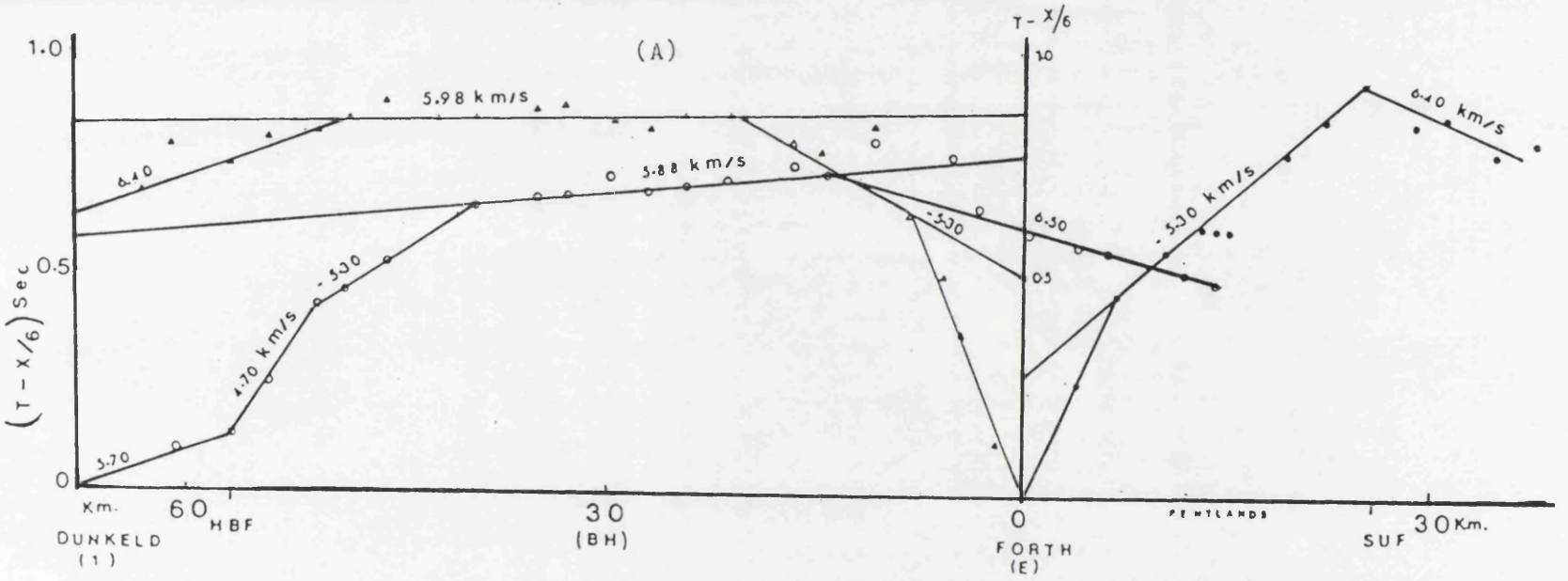

Fig. (15A) Reduced travel time plot of LISPB line

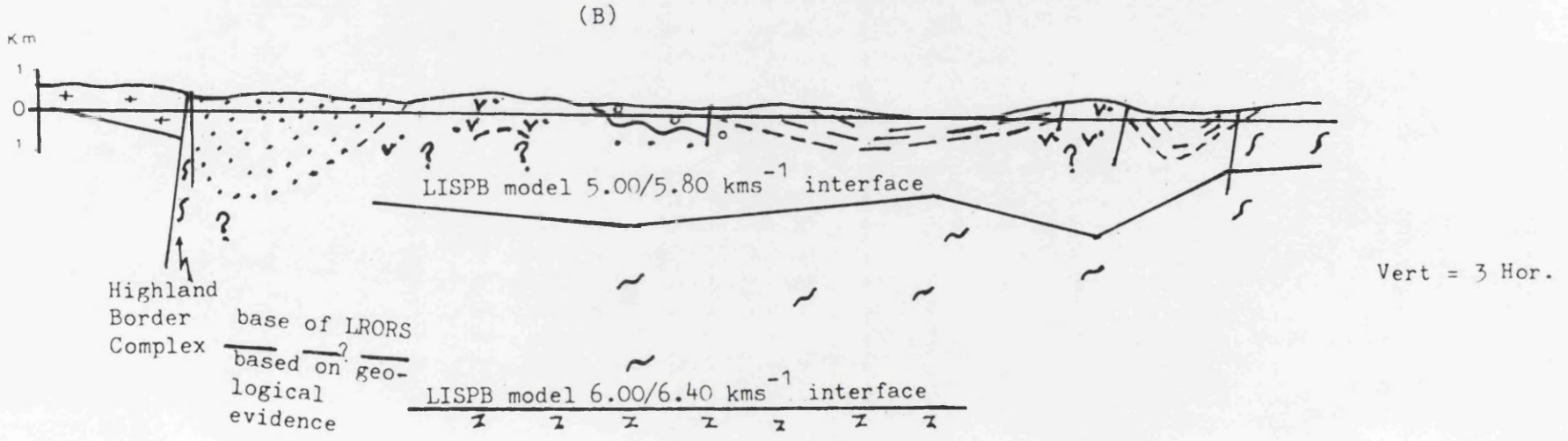

Fig. (15B) Cross section across the Midland Valley based on LISPB results and geological evidence.

APPENDIX 3

Reduced record sections.

Appendix 4. VELOCITY DISTRIBUTION of ray traced model for Fig.4.12

ISOLINES CONSTRUCTED FROM 3.40000 TO 6.40000 WITH INCREMENT 0.30000

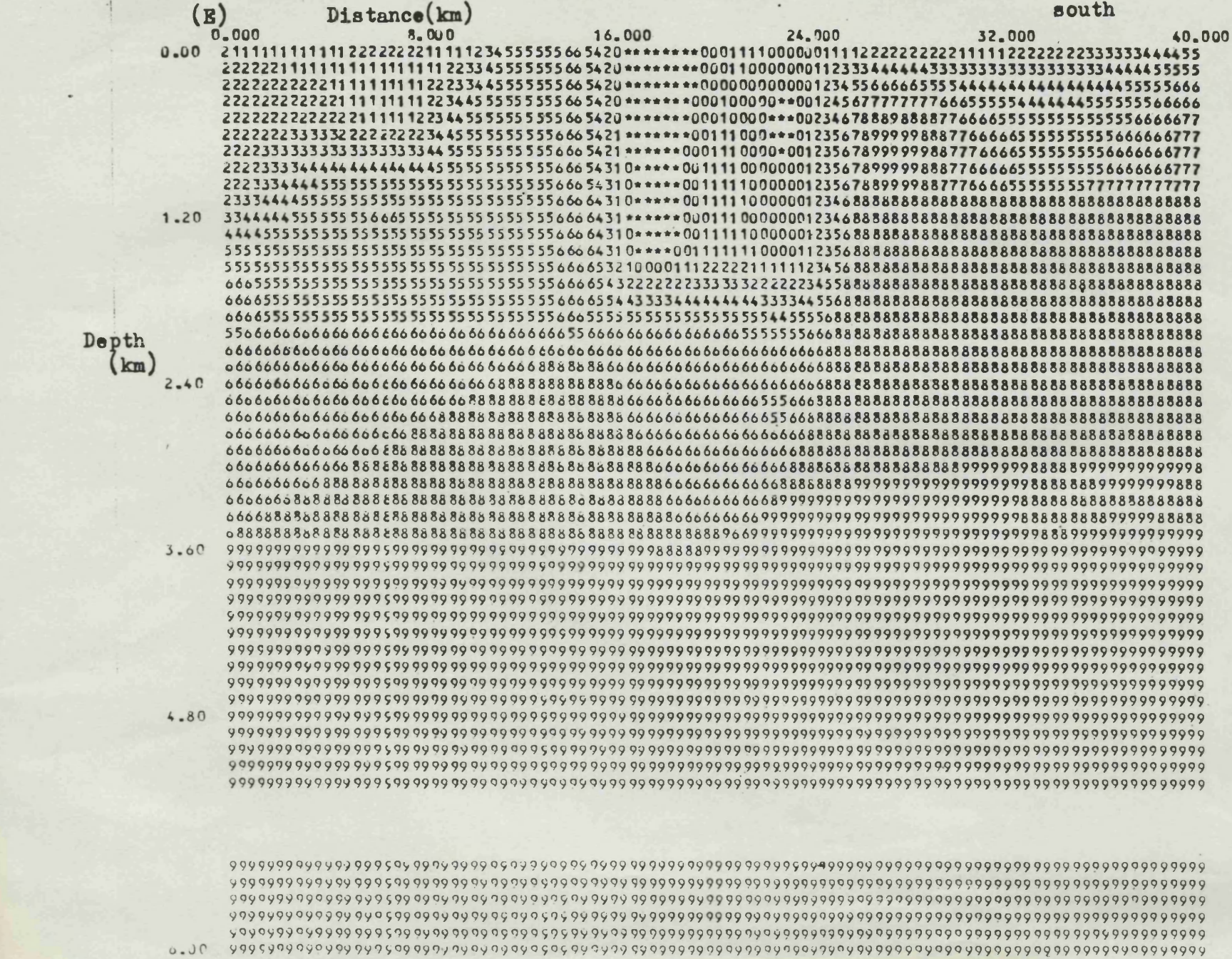

Appendix 4 . VELOCITY DISTRIBUTION of ray traced models for Figs 4.7 & 4.8

ISOLINES CONSTRUCTED FROM 3.40000 TO 6.40000 WITH INCREMENT 0.30000

Appendix 4

VELOCITY DISTRIBUTION of ray traced model for Fig.4.11

ISOLINES CONSTRUCTED FROM 3.40000 TO 6.40000 WITH INCREMENT 0.30000

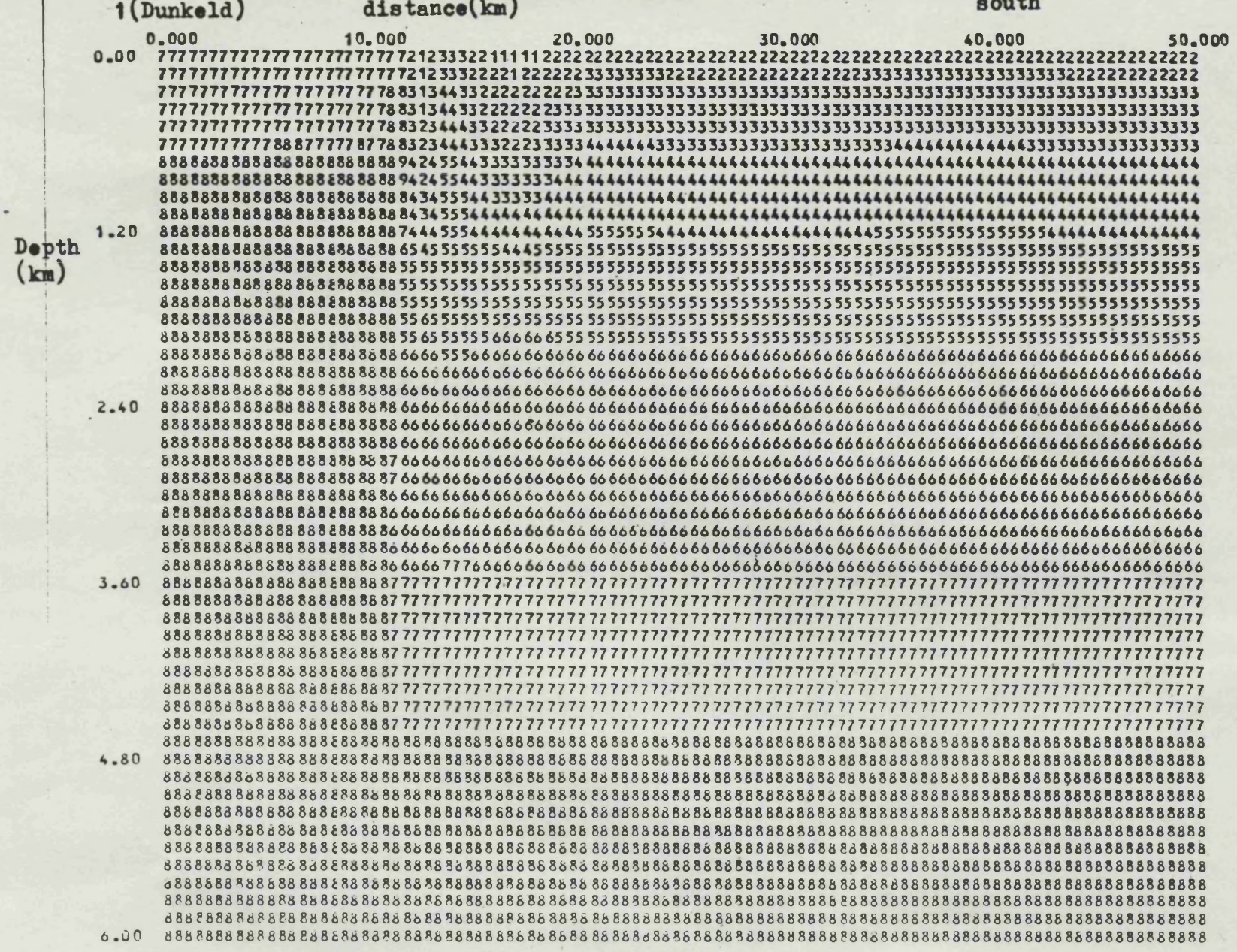

Appendix 4

VELOCITY DISTRIBUTION of ray traced models for Figs 4.9 & 4.10
ISOLINES CONSTRUCTED FROM 3.40000 TO 6.60000 WITH INCREMENT 0.32000

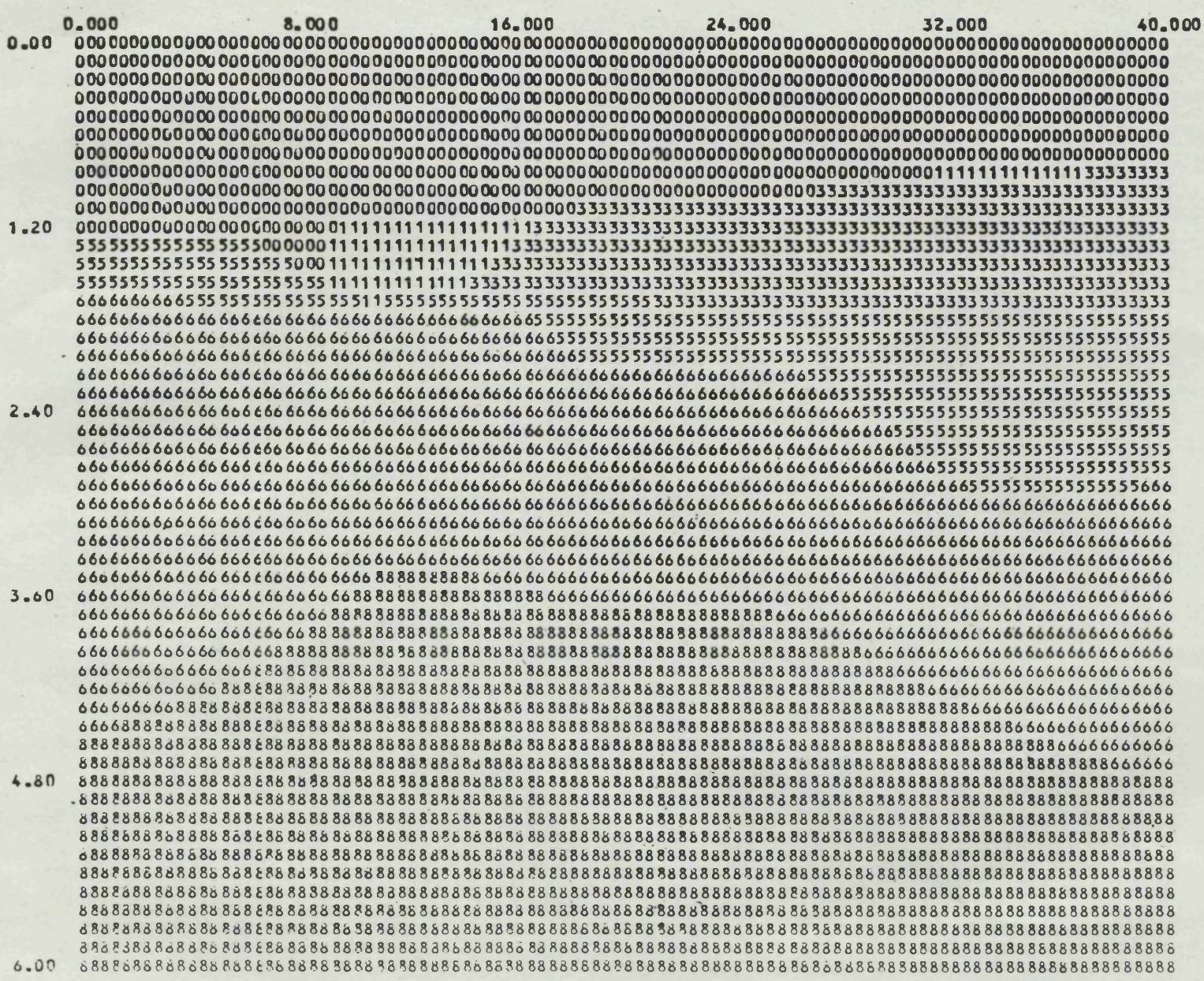

Appendix 4

VELOCITY DISTRIBUTION of ray traced models for Figs 4.9 & 4.10
ISOLINES CONSTRUCTED FROM 3.40000 TO 6.60000 WITH INCREMENT 0.32000

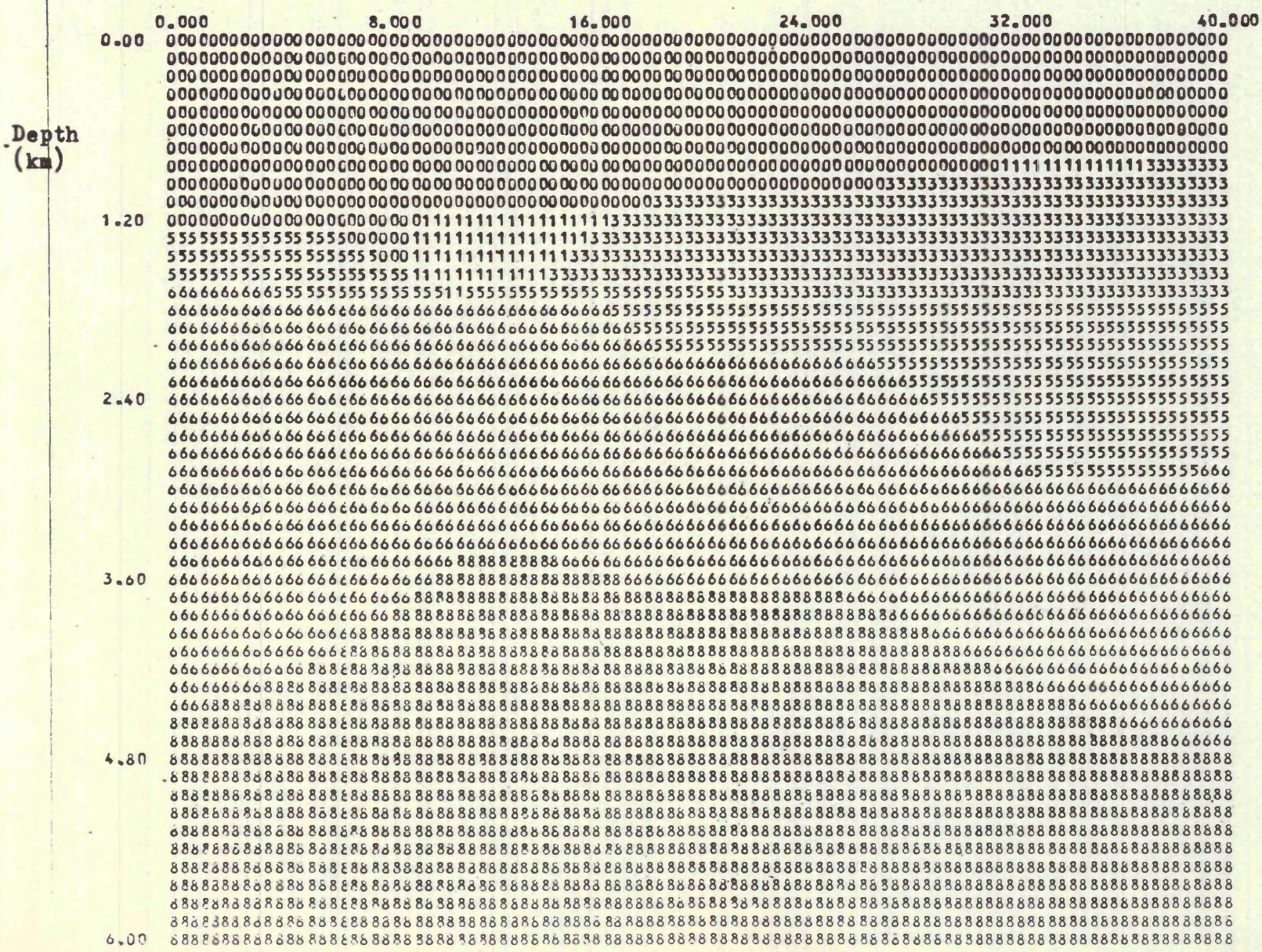

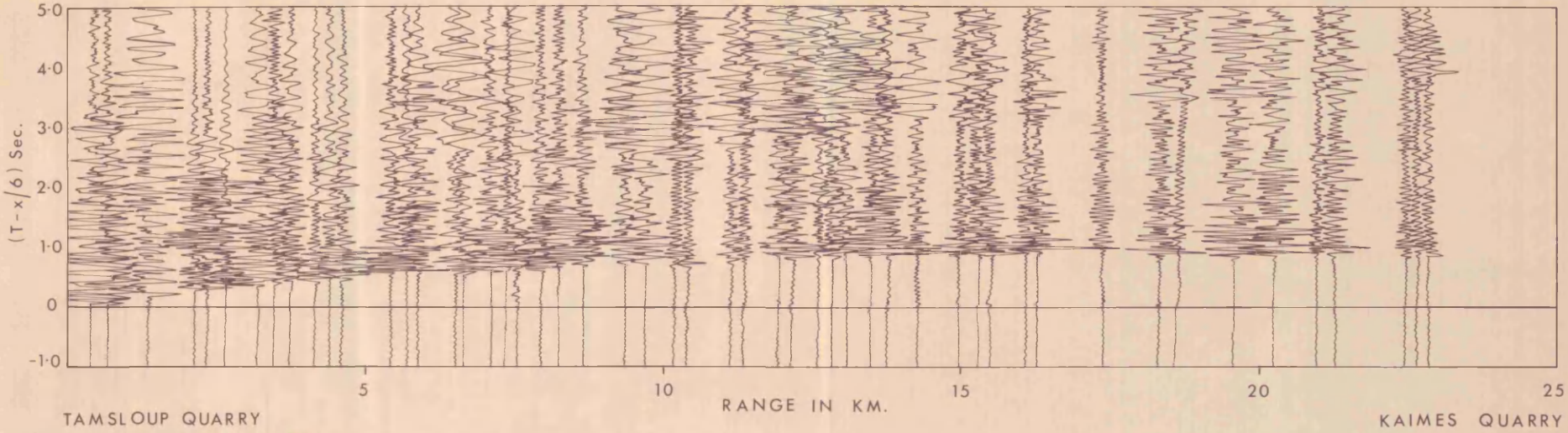

Appendix 3 (Fig. 1) Reduced record section from Tamsloup Quarry east to Kaimes Quarry.

Appendix 4

VELOCITY DISTRIBUTION of ray traced model for Fig.4.11

ISOLINES CONSTRUCTED FROM 3.40000 TO 6.40000 WITH INCREMENT 0.30000

1(Dunkeld) distance(km) south

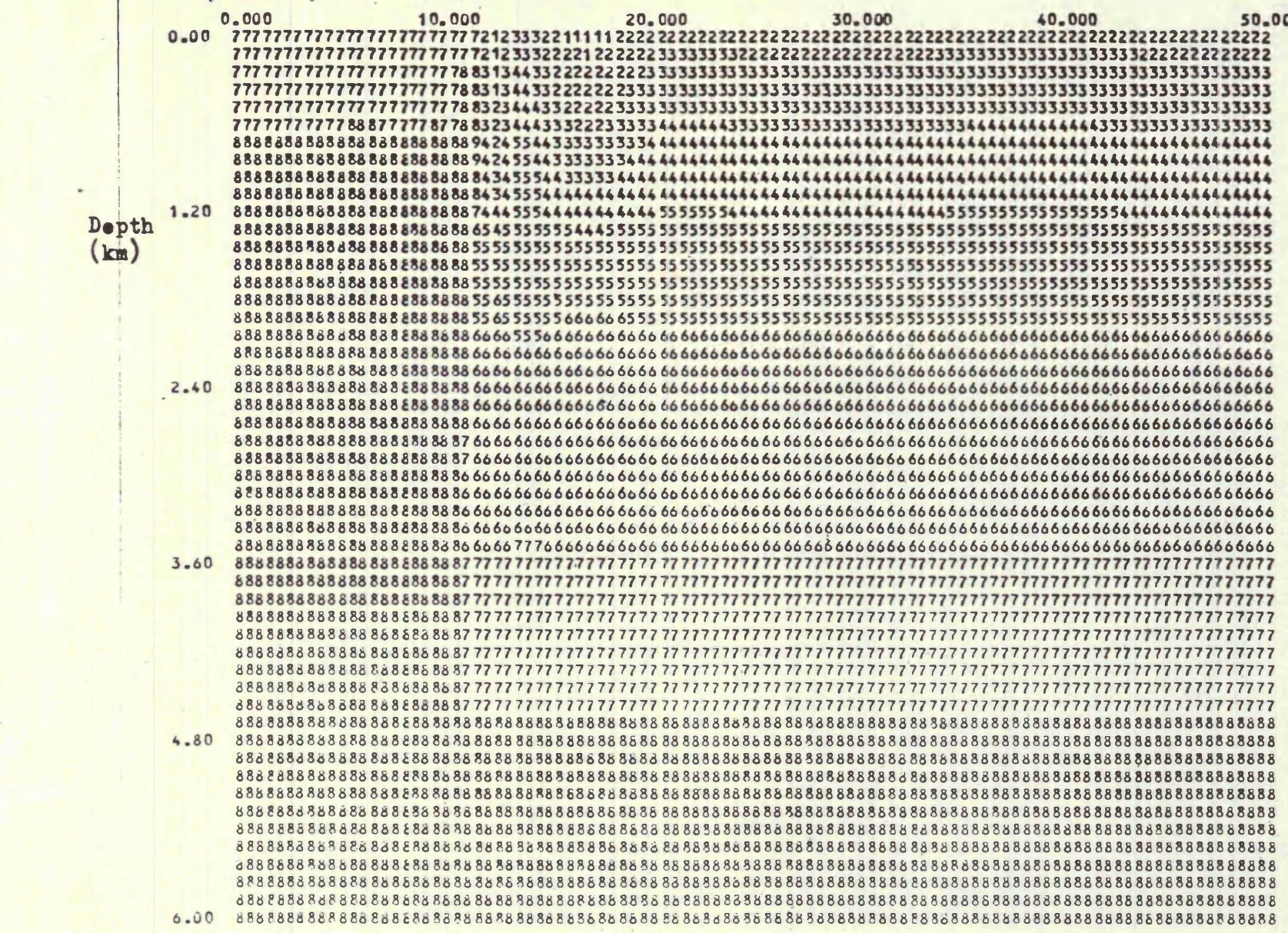

Appendix 4 VELOCITY DISTRIBUTION of ray traced models for Figs 4.7 & 4.8

ISOLINES CONSTRUCTED FROM 3.40000 TO 6.40000 WITH INCREMENT 0.30000

Kaimes distance(km) Tamsloup

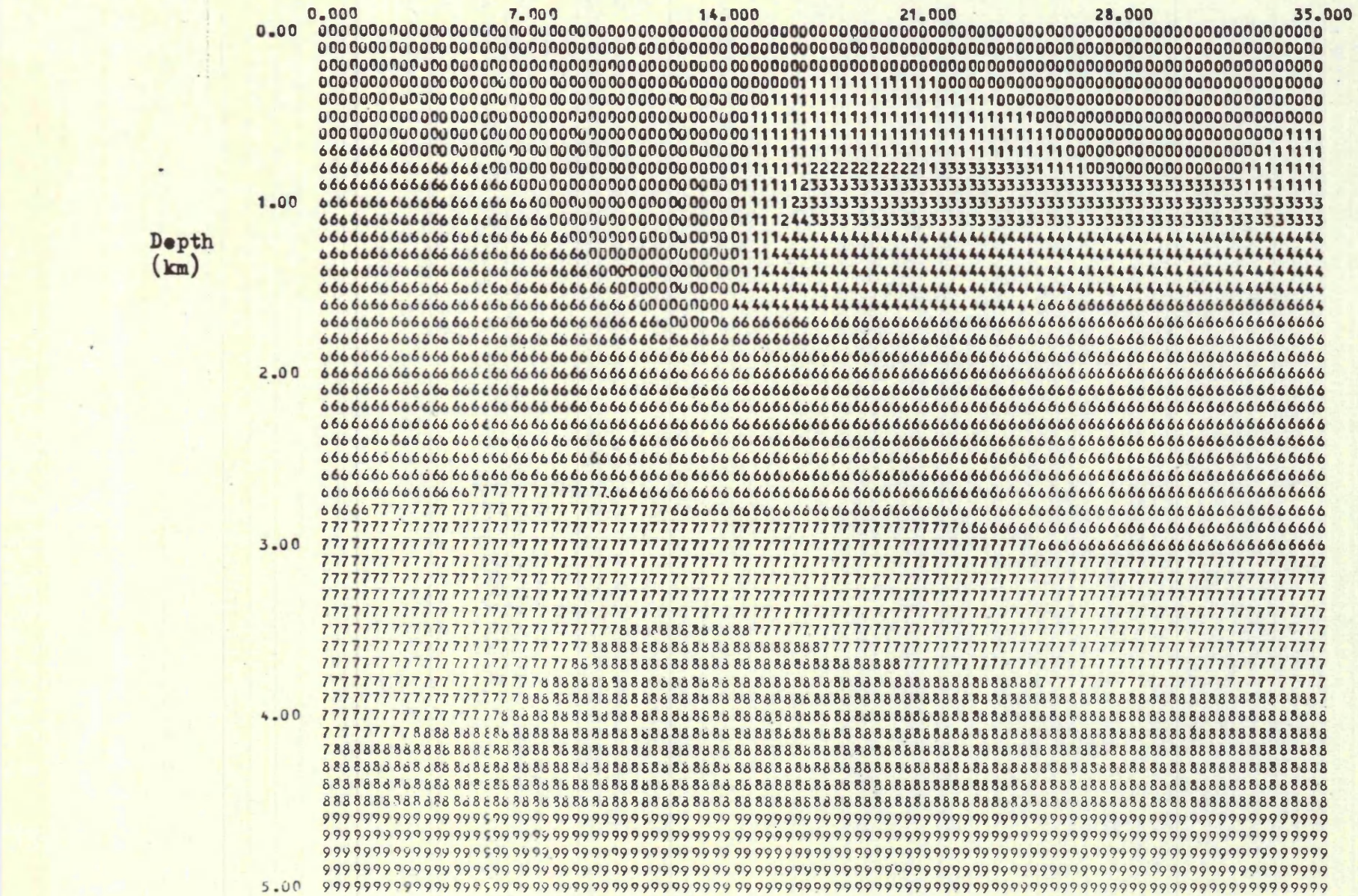

Appendix 4. VELOCITY DISTRIBUTION of ray traced model for Fig.4.12

ISOLINES CONSTRUCTED FROM 3.40000 TO 6.40000 WITH INCREMENT 0.30000

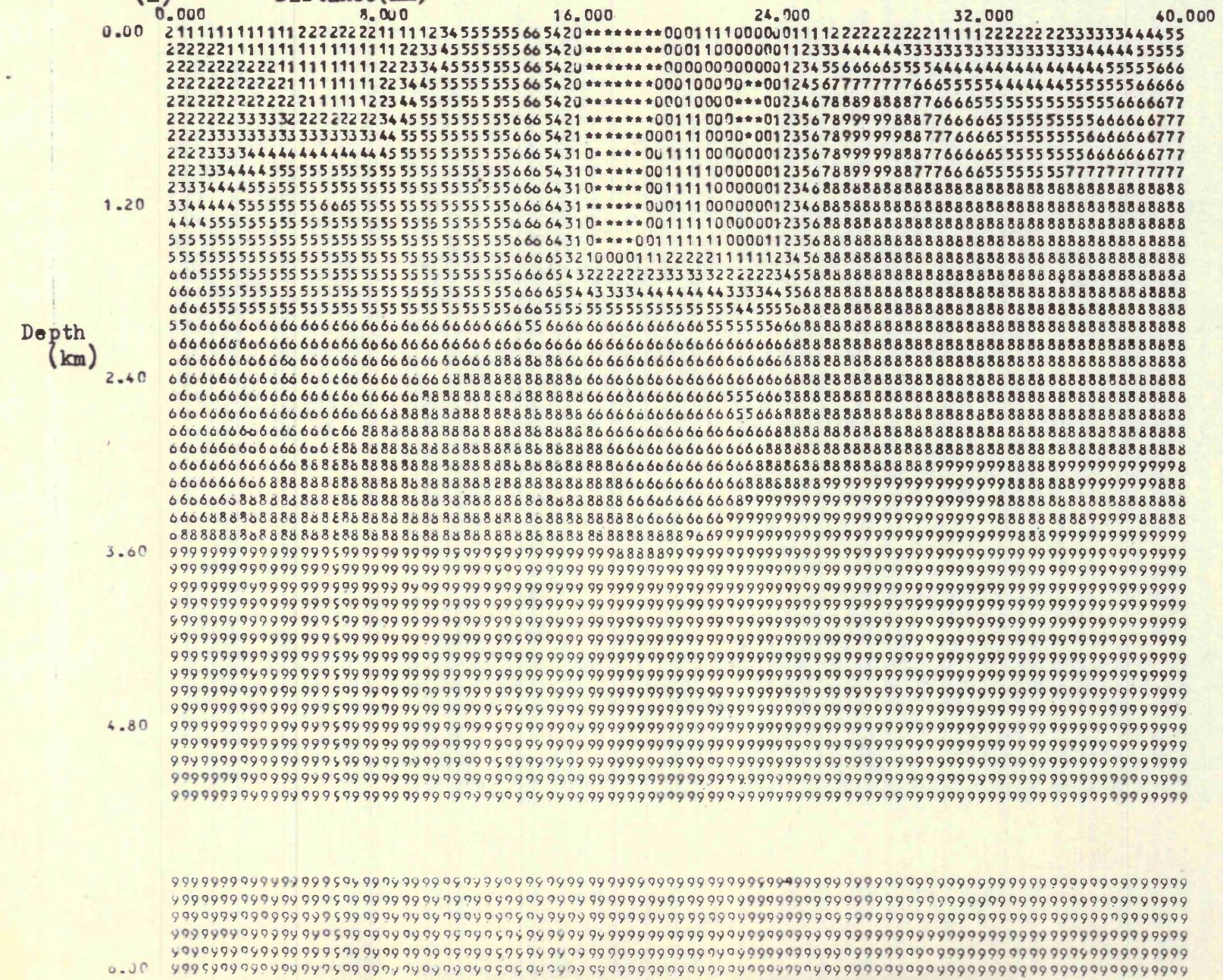

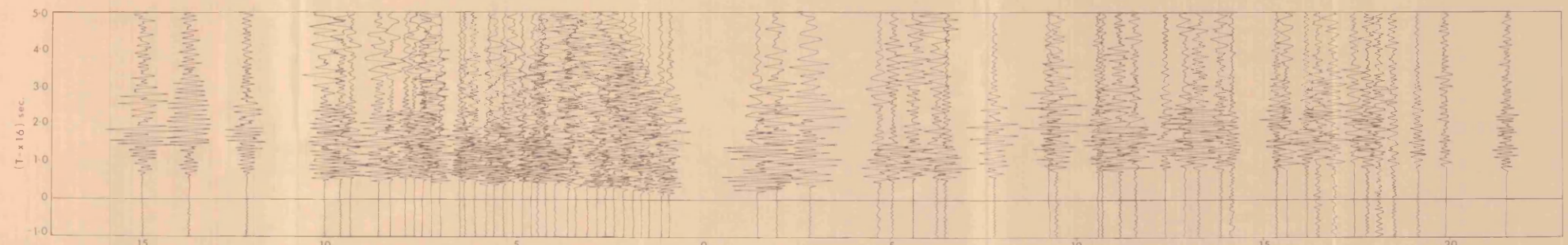

Appendix 3 (Fig. 5) Reduced record section for Headless Cross Open east north and south.

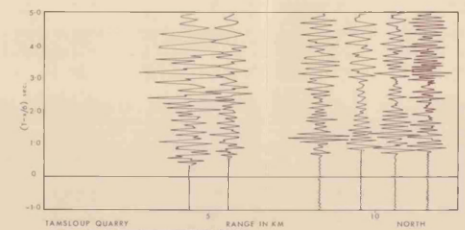

Appendix 3 (Fig. 6) Reduced record sections for: Tamsloup quarry north, Caingryffe quarry south, Douglasmuir quarry north, Loanhead quarry south east

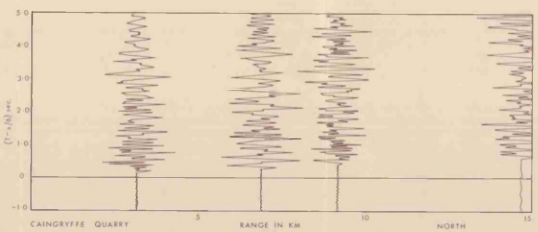

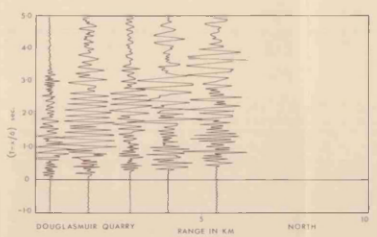

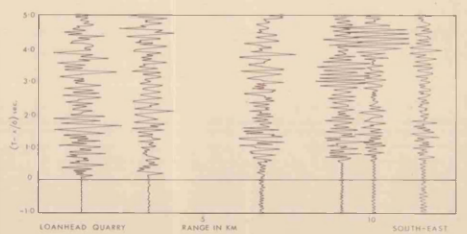

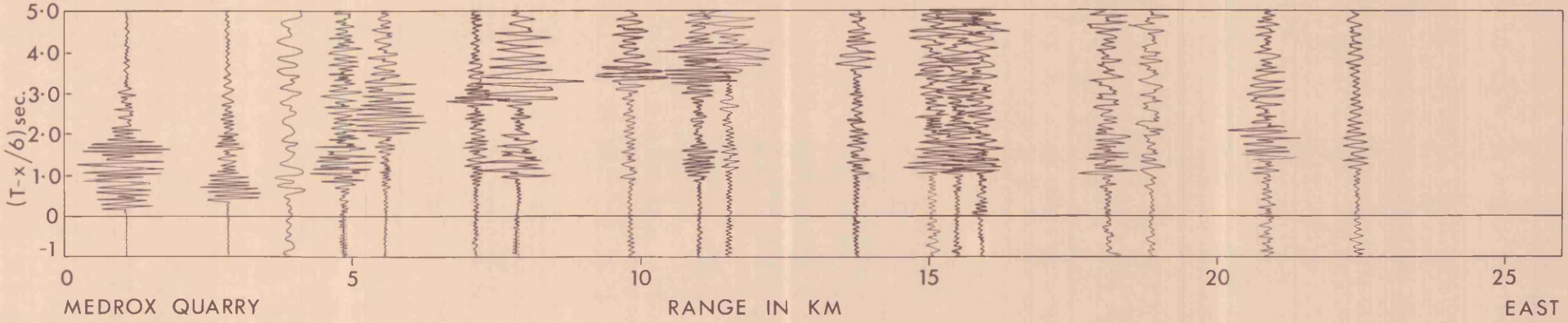

Appendix 3 (Fig. 4) Reduced record section for Medrox Quarry east.

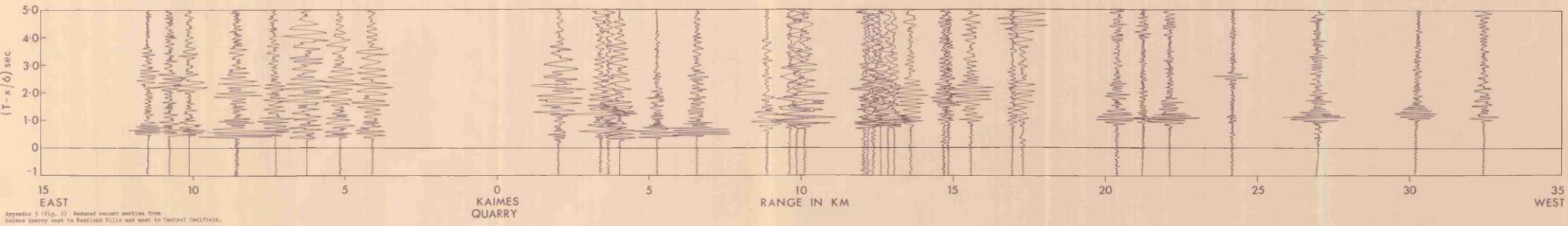

Appendix 3 (Fig. 2) Reduced record section from Kaimes Quarry east to Pentland Hills and west to Central Coalfield.

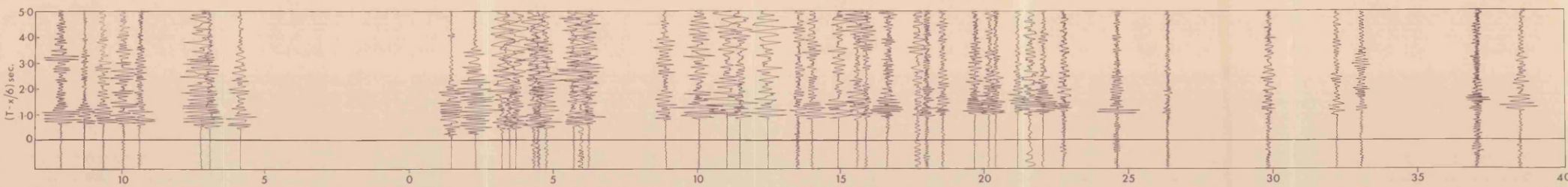

Appendix 3 (Fig. 3) Reduced record section from Craigpark Quarry east to Pentland Hills and west to Redrox Quarry.

Appendix 4

VELOCITY DISTRIBUTION of ray traced models for Figs 4.9 & 4.10
ISOLINES CONSTRUCTED FROM 3.40000 TO 6.60000 WITH INCREMENT 0.32000

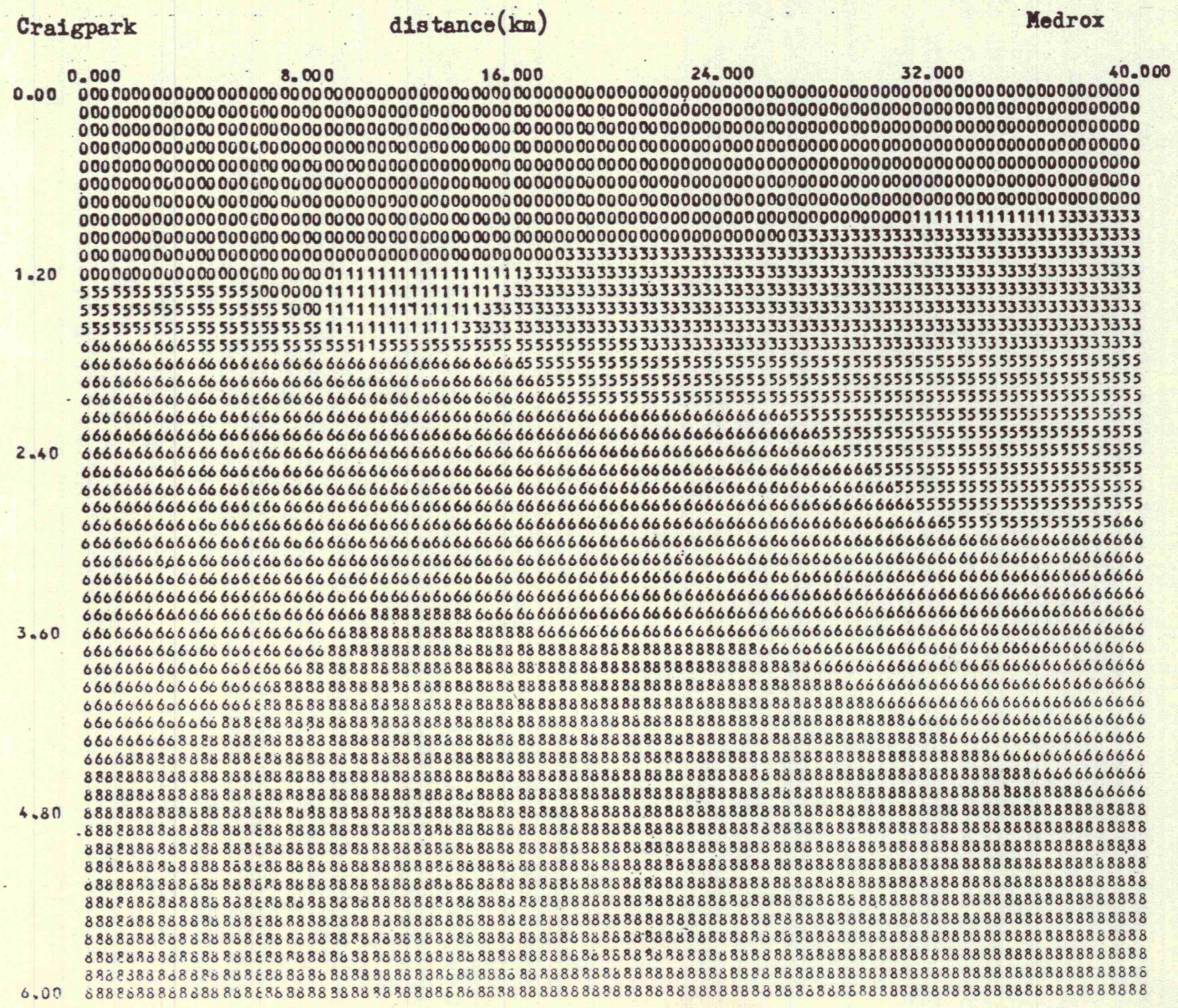

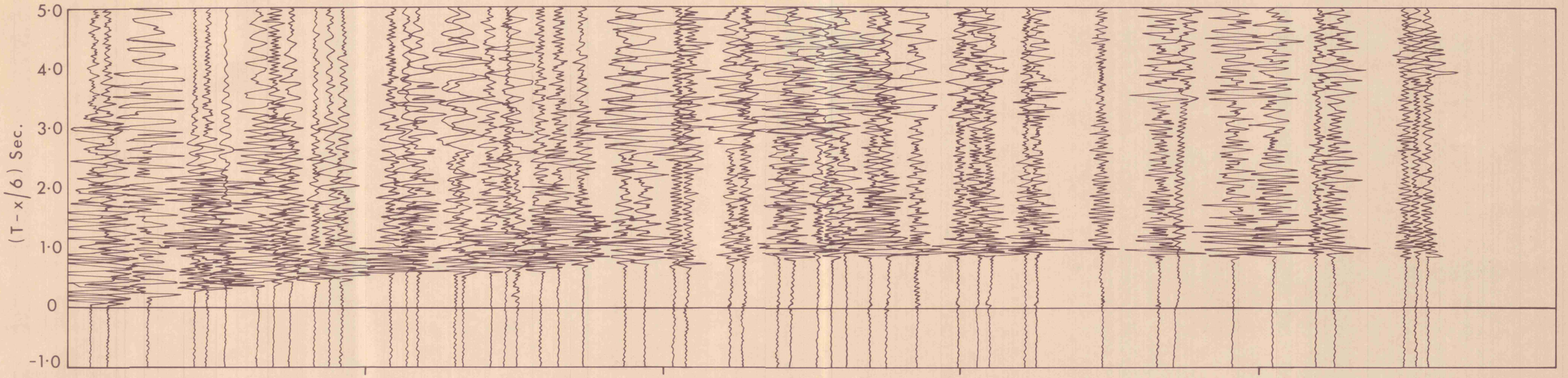

Appendix 3 (Fig. 1) Reduced record section from Tamsloup Quarry east to Kaimes Quarry.

Appendix 4

VELOCITY DISTRIBUTION of ray traced model for Fig.4.11

ISOLINES CONSTRUCTED FROM 3.40000 TO 6.40000 WITH INCREMENT 0.30000

1(Dunkeld) distance(km) south

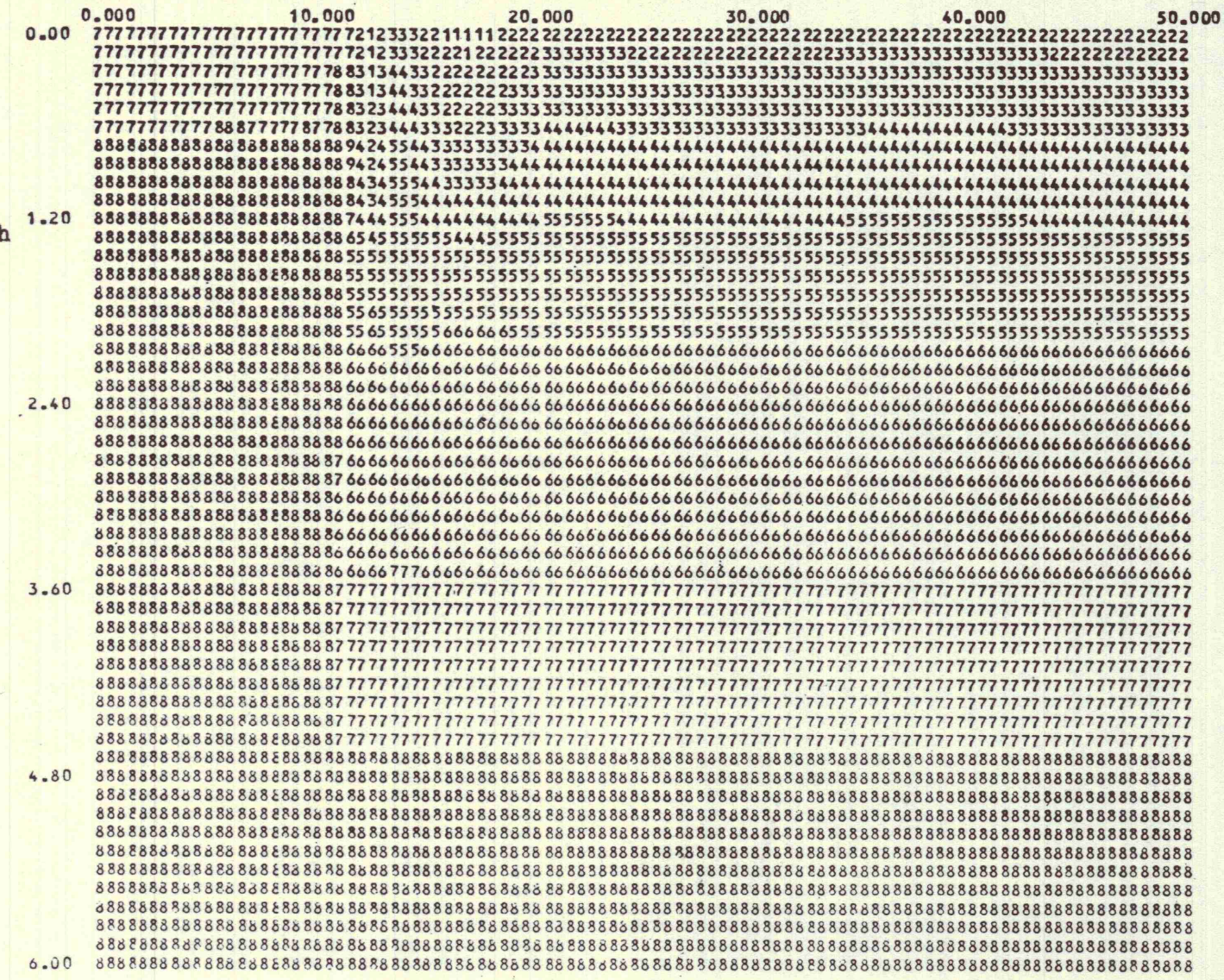

Appendix 4 VELOCITY DISTRIBUTION of ray traced models for Figs 4.7 & 4.8

ISOLINES CONSTRUCTED FROM 3.40000 TO 6.40000 WITH INCREMENT 0.30000

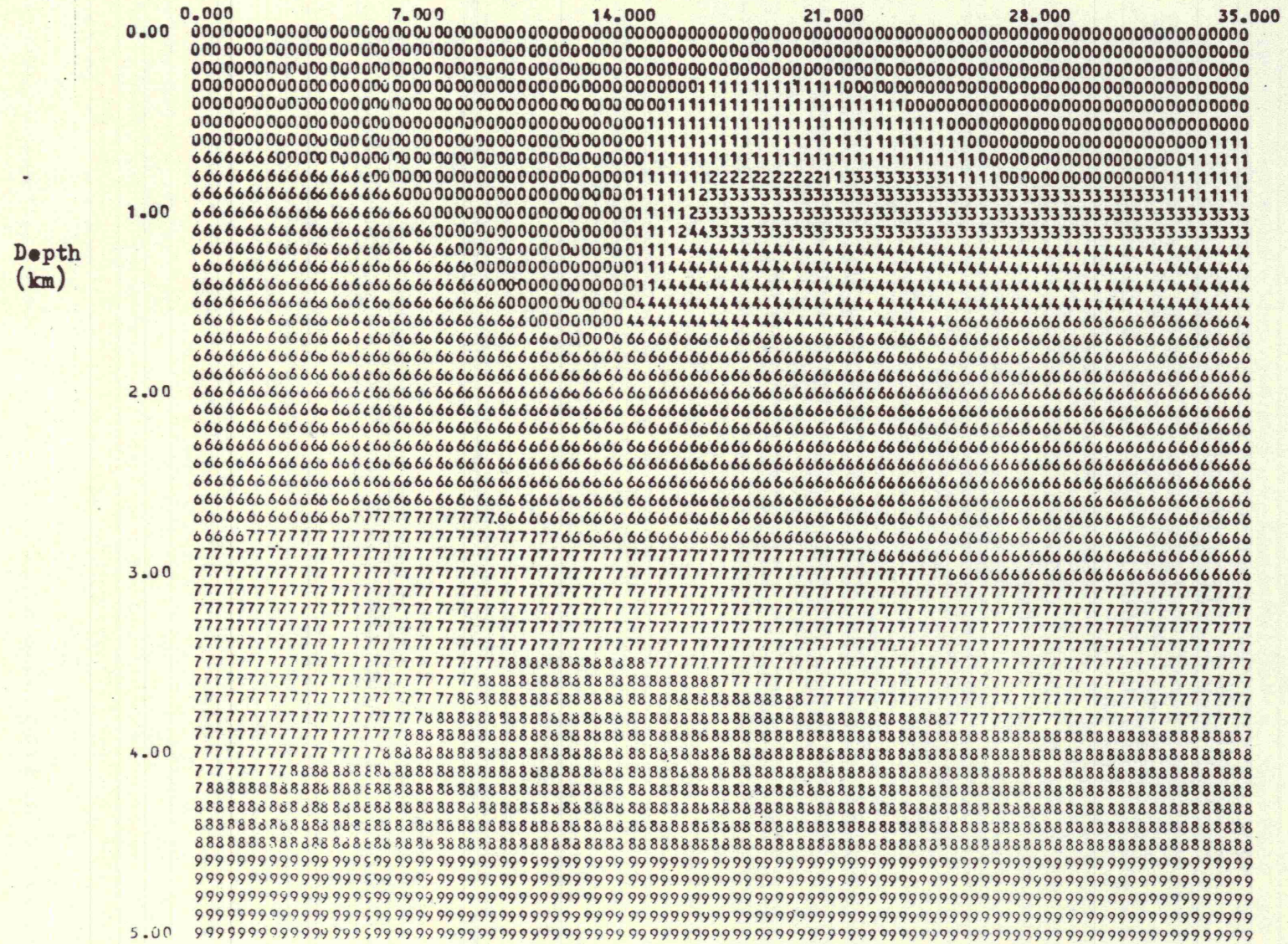

Appendix 4. VELOCITY DISTRIBUTION of ray traced model for Fig.4.12

ISOLINES CONSTRUCTED FROM 3.40000 TO 6.40000 WITH INCREMENT 0.30000

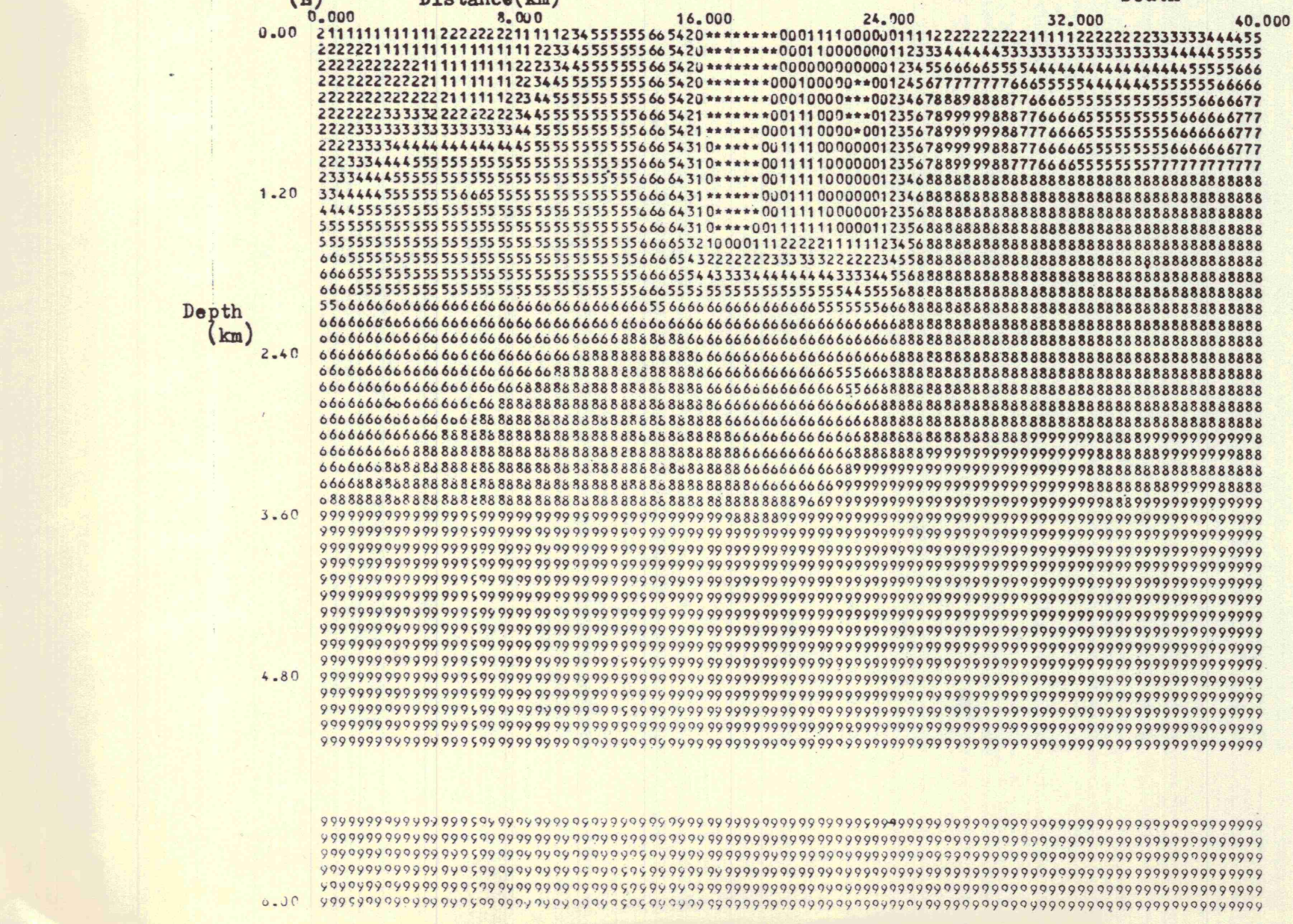

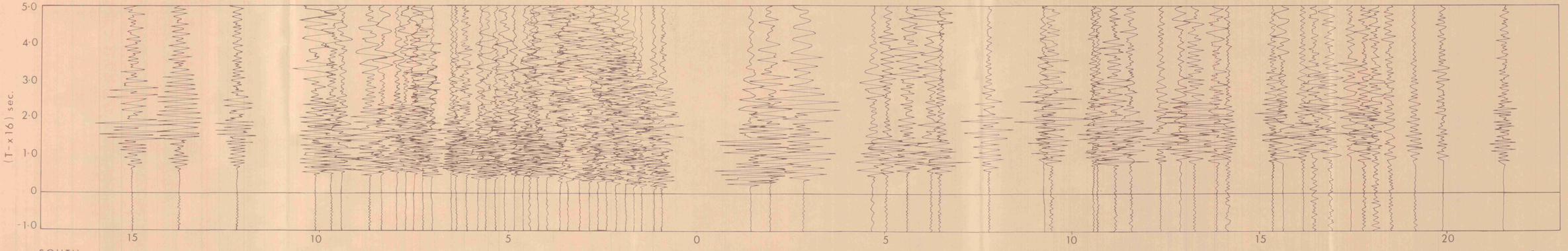

Appendix 3 (Fig. 5) Reduced record section for Headless Cross Open east north and south.

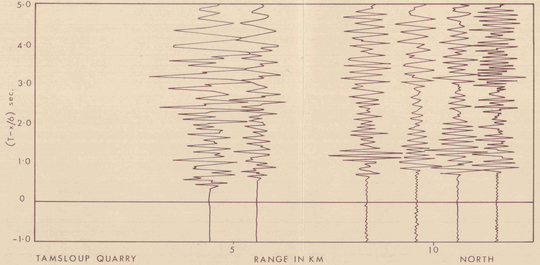

TAMSLOUP QUARRY

Appendix 3 (Fig. 6) Reduced record sections for: Tamsloup quarry north, Cairngryffe quarry north, Douglasmuir quarry north, Loanhead quarry south east

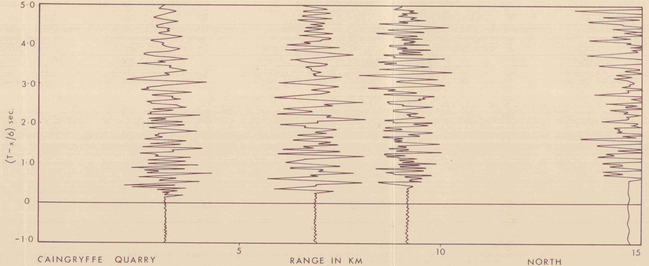

CAINGRYFFE QUARRY

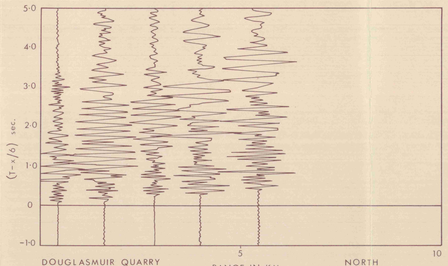

DOUGLASMUIR QUARRY

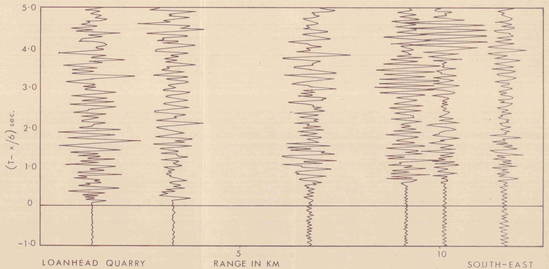

LOANHEAD QUARRY

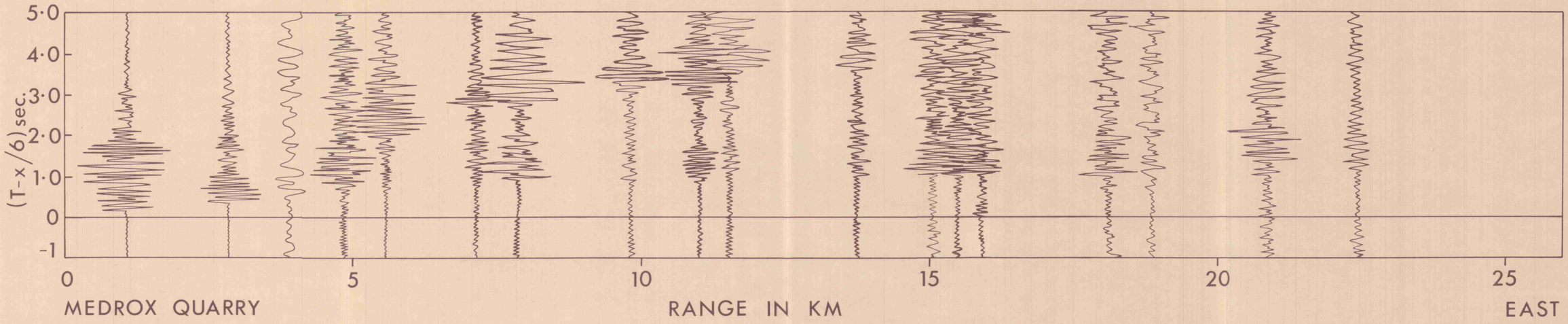

Appendix 3 (Fig. 4) Reduced record section for Medrox Quarry east.

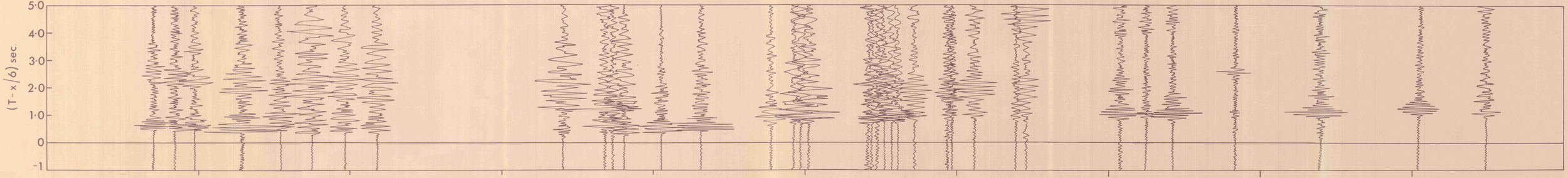

Appendix 3 (Fig. 2) Reduced record section from Kaimes Quarry east to Pentland Hills and west to Central Coalfield.

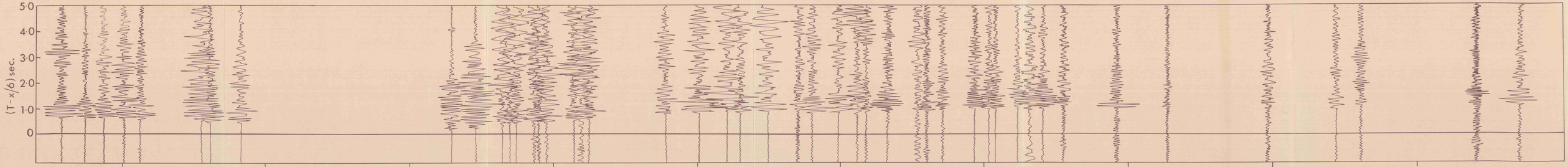

Appendix 3 (Fig. 3) Reduced record section from Craigpark Quarry east to Pentland Hills and west to Medrox Quarry.